Developing Various Design Strategies for Poly (ethylene oxide) (PEO) Based Dry Polymer Electrolytes (SPEs)

by

Recep Bakar

A Dissertation Submitted to the
Graduate School of Sciences and Engineering
in Partial Fulfillment of the Requirements for
the Degree of

Doctor of Philosophy

in

Material Science and Engineering

KOÇ ÜNİVERSİTESİ

December 2022

Developing Various Design Strategies for Poly (Ethylene Oxide) (PEO) Based Dry Polymer Electrolytes (SPEs)

Koç University

Graduate School of Sciences and Engineering

This is to certify that I have examined this copy of a doctoral dissertation by

Recep Bakar

and have found that it is complete and satisfactory in all respects,
and that any and all revisions required by the final
examining committee have been made.

Committee Members:

Assist. Prof. Dr. Erkan Senses (Advisor)

Assist. Prof. Dr. Umut Aydemir

Prof. Dr. Adem Levent Demirel

Prof. Dr. Yusuf. Z. Menceloglu

Prof. Dr. Ugur Yahsi

Date: _____

To Esra Bakar, my lovely wife, my child, my family, my friends

ABSTRACT

Developing Various Design Strategies for Poly (Ethylene Oxide) (PEO) Based Dry Polymer Electrolytes (SPEs)

Recep Bakar

Doctor of Philosophy in Materials Science and Engineering

December 2022

Poly (ethylene oxide) (PEO) based electrolytes promise high ionic conductivity because of high solubility of various lithium salts and fast ion mobility coupled with segmental dynamics of the polymer. Due to its simple monomer structure with no bulky side groups, PEO crystallizes at room temperature, therefore impedes ion transportation. Furthermore, its low glass transition temperature (-55^{o}C) results in poor mechanical performance. Obtaining highly conductive solvent-free polymer electrolytes without much sacrificing mechanical stability near room temperature remains as a major challenge. In this work, we systematically investigate the role of polymer architecture on crystallization, segmental dynamics, and ionic conductivity in various PEO-based solid polymer electrolyte types, including homopolymers, polymer blends, and nanocomposites. While the homopolymer electrolytes allowed to understand the effect of branching and nanoscale dynamics on Li-ion transport at the fundamental level, the blends of PEO of non-linear architectures of PEO, such as stars, hyperbranched, and bottlebrush, with linear PMMA and their nanocomposites with silica (SiO_2) nanoparticles enabled us to decouple segmental dynamics from ionic conductivity. Our results showed a remarkable suppression of crystallization of PEO in the nonlinear blends. Furthermore, the ionic conductivity of the electrolytes which depends on the salt concentration and polymer architecture could be improved with increased mechanical performance by simply modifying the PEO architecture from linear to branched structures. Overall, our study provides a promising and compelling experimental evidence that macromolecular architecture could be a powerful new tool for tuning the ionic conductivity PEO-based electrolytes, opening a new research avenue in the field of polymer electrolytes for lithium-ion batteries.

ÖZETÇE

Poli (Etilen Oksit) (PEO) Bazlı Kuru Polimer Elektrolitler (SPE'ler) için Çeşitli Tasarım Stratejilerinin Geliştirilmesi

Recep Bakar

Malzeme Bilim ve Mühendisliği Doktora Tezi

Aralık 2022

Poli (etilen oksit) (PEO) bazlı elektrolitler, çeşitli lityum tuzlarının yüksek çözünürlüğü ve polimerin segmental dinamikleri ile birleştiğinde hızlı iyon hareketliliği nedeniyle yüksek iyonik iletkenlik vaat eder. Hacimli yan grupları olmayan basit monomer yapısı nedeniyle, PEO oda sıcaklığında kristalleşir, bu nedenle iyon taşınmasını engeller. Ayrıca düşük camsı geçiş sıcaklığı (-55^{o}C) düşük mekanik performansa neden olur. Oda sıcaklığına yakın mekanik stabiliteden fazla ödün vermeden yüksek düzeyde iletken solvent içermeyen polimer elektrolitler elde etmek büyük bir zorluk olmaya devam etmektedir. Bu çalışmada, homopolimerler, polimer karışımları ve nanokompozitler dahil olmak üzere çeşitli PEO bazlı katı polimer elektrolit tiplerinde polimer mimarisinin kristalleşme, segmental dinamikler ve iyonik iletkenlik üzerindeki rolünü sistematik olarak araştırıyoruz. Homopolimer elektrolitler, dallanma ve nano ölçekli dinamiklerin Li-iyon taşınımı üzerindeki etkisini temel düzeyde anlamaya izin verirken, PEO'nun yıldızlar, aşırı dallanmış ve şişe fırçası gibi doğrusal olmayan mimarilerinin PEO'sunun doğrusal PMMA ile karışımları ve bunların silika (SiO_2) nanopartikülleri içeren nanokompozitler, segmental dinamikleri iyonik iletkenlikten ayırmamızı sağladı. Sonuçlarımız, doğrusal olmayan karışımlarda PEO'nun kristalleşmesinin kayda değer bir şekilde bastırıldığını gösterdi. Ayrıca, tuz konsantrasyonuna ve polimer mimarisine bağlı olan elektrolitlerin iyonik iletkenliği, PEO mimarisinin doğrusaldan dallı yapılara basit bir şekilde değiştirilmesiyle artan mekanik performansla iyileştirilebilir. Genel olarak, çalışmamız, makromoleküler mimarinin, lityum-iyon piller için polimer elektrolitler alanında yeni bir araştırma yolu açarak, iyonik iletkenlik PEO bazlı elektrolitleri ayarlamak için güçlü ve yeni bir araç olabileceğine dair umut verici ve ikna edici bir deneysel kanıt sunmaktadır.

ACKNOWLEDGMENTS

First, my sincere gratitude goes to appreciation to my advisor, Assist. Prof. Dr. Erkan Senses, who encouraged, guided, and helped me during my PhD studies at Koç University. I also would like to express my warm appreciation to my committee members, Assist. Prof. Dr. Umut Aydemir and Prof. Dr. Yusuf. Z. Menceloglu for their great support, help, guidance, patience, and kindness during my study. I also thank Prof. Dr. Metin Muradoglu, Assist. Prof. Dr. Fevzi Cakmak Cebeci, Assist. Prof. Dr. Ugur Unal, Prof. Dr. Alper Uzun, Prof. Dr. Adem Levent Demirel, and Prof. Dr. Ugur Yahsi for being part of my committee members on my way towards my PhD degree. I also extend my thanks to all faculty and administrative staff, especially Turkan Eryigit, Ayse Kızıltas, Muzaffer Butun, Yılmaz Sevinc, Güleser Bolat, and Hasan Bolat in engineering and chemistry departments at Koç University.

Special thanks go to Prof. Dr. Ugur Yahsi, Prof. Dr. Cumali Tav, Assist. Prof. Dr. Umut Aydemir and Associate. Prof. Dr. Sedat Nizamoglu for giving us permission to use their laboratories namely Marmara Positron/Positronium Laboratory (MARPOS), Koç University Boron and Advanced Materials Application and Research Center (KUBAM) and Innovative Devices and interfaces Laboratory (IDEALAB) for their help with electrolyte sample preparation and electrochemical impedance measurements in this study. We also acknowledge Koç University Surface Science and Technology Center (KUYTAM) and Dr. Hadi Jahangiri for their assistance on the XRD measurements. Furthermore, we are thankful to Dr. Melek Sermin Ozer for her help and guidance on NMR analysis. We are grateful to The Center for Nanophase Materials Sciences (CNMS) at Oak Ridge National Laboratory (ORNL) for their support in this work.

I also would like to thank especially my friends, Saeid Darvishi and Emine Ayse Turhan for their great help and support in this research and acknowledge the support of my other friends from our Soft & Active Material Laboratory and Koç University. Most importantly, I would like to express my special thanks to my wife and my child, who has endured a lot of difficulties being next to me and patient with me. Mom, Dad, Sister and other family members, thanks for your support, guidance, and help. I love you all.

TABLE OF CONTENTS

LIST OF TABLES

LIST OF FIGURES

ABBREVIATIONS

ACN	Acetonitrile
BDS	Broadband Dielectric Spectroscopy
CE	Coulombic Efficiency
DMAc	Dimethyl Acetamide
DEC	Diethyl Carbonate
DLS	Dynamic Light Scattering
DMC	Dimethyl Carbonate
DSC	Differential Scanning Calorimetry
EC	Ethylene Carbonate
EMC	Ethyl Methyl Carbonate
EIS	Electrochemical Impedance Spectroscopy
EP	Electrode Polarization
EV	Electrical Vehicles
FC	Faraday's Constant
FTIR	Fourier Transform Infrared Spectroscopy
FWHM	Full Width at Half Maximum
GPE	Gel Polymer Electrolyte
HG	High Grafting
HN	Havriliak–Negami
IL	Ionic Liquid
$LiAsF_6$	Lithium Hexafluoroarsenate
$LiBF_4$	Lithium Tetrafluoroborate

$LiClO_4$	Lithium Perchlorate
LiFAP	Lithium Tris(pentafluoroethyl) Trifluorophosphate
LG	Low Grafting
LIB	Lithium-Ion Battery
$LiPF_6$	Lithium Hexafluorophosphate
LiTFSI	Lithium Bis(trifluoromethanesulfonyl)imide
LVR	Linear Viscoelastic Region
LM	Lodge-McLeish Model
MAH	Maleic Anhydride
MCR	Modular Compact Rheometer
MDSC	Temperature-Modulated Scanning Calorimetry
MMA	Methyl Methacrylate
NMR	Nuclear Magnetic Resonance
NP	Nanoparticles
PAN	Poly(acrylonitrile)
PALS	Positron Annihilation Lifetime Spectroscopy
PC	Propylene Carbonate
PEO	Poly(ethylene oxide)
PMMA	Poly(methyl methacrylate)
PNC	Polymer Nanocomposites
PPO	Propylene Oxide
PVC	Polyvinyl Chloride
P(VDF-HFP)	Poly-(vinylidene fluoride-hexafluoropropylene)

PVDF	Poly(vinylidene fluoride)
PTSA	pToluene Sulphonic Acid
SAOS	Small-Amplitude Oscillatory Shear
SAXS	Small-angle X-ray Scattering
SN	Succinonitrile
SPE	Solid Polymer Electrolytes
TGA	Thermal Gravimetric Analysis
VFT	Vogel–Fulcher–Tammann
WAXS	Wide-Angle X-ray Scattering
XRD	X-ray Diffraction

Chapter 1

INTRODUCTION

Today, the needs of our modern societies are heavily provided by the fossil fuels.[1] The global population is also estimated to reach around approximately 10 billion in midst of 2200s according to the recent report released by Department of Economic and Social Affairs of the United Nations in 2019.[2] Additionally, the energy outlook 2022 released by BP reveals that the world economy will be developed more than doubles by 2050.[1] As a result of the expectations regarding the world economy and population, the energy consumption and production from fossil fuels throughout the world will increase dramatically. This could even deepen one of the most challenging crisis we are facing today: global warming and climate change.[3] The essential reason, primarily because of burning hydrocarbons, is the increased greenhouse gas concentrations consisted of mainly CO_2 for which the total emissions recently reached out to a record high of 36.3 Gt in 2021.[3] Thus the world-wide efforts of the governments to solve this crises have increased significantly in various forms. Since the main contributors of the CO_2 emissions are predominantly composed of transport, electricity, and heat sectors given in Figure 1.1, application of alternative clean energy sources new wind and solar power facilities and electric vehicles have been prioritized and even subsidized for a wide-scale and successful transformation the globe into having low-carbon emission energy system in an effort to protecting both health and economic well-being of world.[1, 3]

Although the implementations of these different ways with advanced technologies will help decarbonatization of the world energy supply, it has certain shortcomings. Firstly, renewable energy is naturally irregular and unforeseen. Secondly, not only the supply of energy fluctuates but also the load required by the system could be varying in some installations such as in electric cars. Both reasons can cause instabilities within the systems between supply and load demands. Although the implementations of these different ways with advanced technologies will help decarbonatization of the world energy supply, it has certain shortcomings.

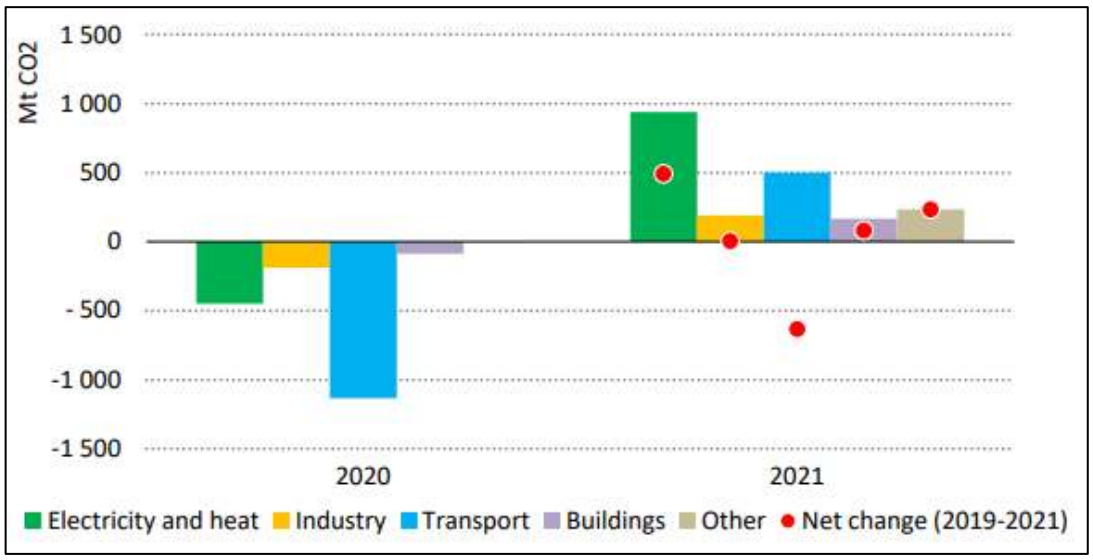

Figure 1.1: The sectorial contributions for CO_2 emissions between 2020-2021.[3]

Firstly, renewable energy is naturally irregular and unforeseen. Secondly, not only the supply of energy fluctuates but also the load required by the system could be varying in some installations such as in electric cars. Both reasons can cause instabilities within the systems between supply and load demands. To sustain the energy balance within the renewable energy system that could substitute the fossil fuel dependent chain of energy supply as much as possible, employing energy storage is indispensable, playing a vital role in integrating and stabilising alternative energy systems. Among all different energy storage techniques, rechargeable batteries were found to be the most convenient and could be easily used for large- and small-scale energy storage and conversion for both stationary and mobile installations because of several good characteristics including lightweight packed structure, more importantly high energy, power density, and discharge rate. When compared to other secondary battery systems, the usage of lithium-ion batteries in powering the consumer electronics and electric vehicles has been developing the fastest due to its various excellent properties such as higher energy density, longer cycle life, wide range of operating temperatures, lower self-discharge rate loss and toxicity.

One of the key elements of all commercial Li-ion batteries is composed a separator immersed with a liquid electrolyte allowing the ions to move back and forth, which is associated with very high ionic conductivities.

Nevertheless, they usually happen to be extremely volatile, flammable, and toxic, which may result in environmental and safety hazards such as fire, leakage, explosion, and short circuit, , limiting their usage in the commercial lithium-ion batteries.[4-7] To address these issues, solid polymer electrolytes (SPEs) have attracted much attention in recent years as the most promising candidates to substitute these liquid electrolytes owing to their very useful features such as higher flexibility, greater energy density and processability, good thermo-mechanical stability, nonflammability, and wide electrochemical stability, leading to more compacted and safer batteries. [4, 8-10] However, their commercial utilization is severely limited because of their extremely low ionic conductivity at room temperature ($<10^{-5}$ S/cm)[11] compared to the liquid electrolytes ($\sim10^{-2}$ S/cm)[11], being a major challenge.[12]

Several polymers, including poly(acrylonitrile), poly-(vinylidene fluoride) (PVDF), poly(methyl methacrylate) (PMMA) have been studied as SPEs [13]; the most commonly used one is poly(ethylene oxide) (PEO) due to its fast segmental dynamics[8], low glass transition temperature ($T_g \sim 220$ K[8]), electrochemical stability as well as the excellent ability for solving a wide range of lithium salts.[13-16] However, it has some drawbacks. Below its melting temperature ($T_m = 60$℃)[8, 17], it is highly a semi-crystalline polymer with low ionic conductivities ranging between $10^{-6} - 10^{-8}$ S/cm whereas above the melting temperature its ionic conduction rapidly increases, but this time it mechanically lacks because of melting crystals.[18] Therefore, the emphasis for developing better designs of the PEO-based SPEs essentially revolve around enhancing both the ionic conductivity and mechanical toughness at the same time.

To accomplish this in a PEO-based polymer electrolyte, polymer scientists have been working on various methods including blending polymers [8, 18], using different topologies [8], cross-linking [13], copolymerization [19, 20], addition of fillers [9, 21] and plasticizers. [21-23] In this context, this PhD thesis here systematically aims at exploring and investigating several new and innovative PEO-based solid polymer electrolytes for lithium-ion batteries focusing two different techniques including blending PEO with another polymer namely PMMA and addition of a passive inorganic filler such as silica nanoparticles (SiO_2) into PEO matrixes architectures along with using non-linear architectures of PEO such as stars, hyperbranched, and bottlebrush in preparing PEO-

based SPEs. We also investigated the dependence of the electrolyte properties including ionic conduction and mechanical strength on the salt concentration.

Finally, we synthesized new PEO-based grafted copolymer that will be used to be explored its potential as polymer electrolytes in further studies.

1.1 Objectives and Scope

The aim of this thesis study at the fundamental level is to specifically investigate polymer architecture effect on ion conduction mechanisms in solid polymer-based electrolytes suitable for rechargeable Li-ion batteries using different techniques blending, using addition of fillers, changing molecular weight of the host polymer and salt concentration. Poly (ethylene oxide) (PEO) is chosen as the host polymer for the polymer electrolyte preparation due to high solubility of lithium salts and fast ion mobility that is coupled with the segmental dynamics of the polymer. Due to its simple monomer structure with no bulky side groups, PEO crystallizes at room temperature, thus impedes ion motion. Furthermore, its low glass transition temperature (-55^{o}C) [8] results in poor mechanical performance. To overcome these challenges, The investigations will focus on four different aspects in the preparation and characterization of the Poly (ethylene oxide) (PEO) based electrolytes for improving electrolyte properties: (1) to develop a blend electrolyte by blending various topologies of soft (low Tg) PEO with a rigid PMMA (high Tg) polymer, (2) to form a polymer composite based electrolyte including different architectures of Poly (ethylene oxide) (PEO) as the polymer matrix and nanoscale silica as fillers, (3) to synthesize a PEO-grafted-PMMA copolymer and to prepare its corresponding electrolyte, and finally (4) to investigate the effect of polymer architecture, salt concentration and molecular weight of the PEO host polymer on the phase and conductivity behaviours to develop the performance characteristics in neat PEO-based electrolytes

1.2 Organization of Thesis

Chapter 2 introduces a literature review about the advantages and disadvantages of different methods used for the energy storage and conversion have been applied in power systems. Later, among these various methods, the chemical storage namely the batteries which is the most convenient and commonly used method for the energy storage and is more intensely discussed, including different types of primary and secondary batteries.

The fundamental materials and concepts in relation to the different battery systems are presented in terms of how a cell assembly for a battery works. Then, the lithium-ion batteries, the most promising one within the rechargeable batteries, is extensively investigated in the aspects of properties and recent status including anode and cathode materials, more importantly various electrolyte types such as liquid and solid based ones. Next, the advantages and disadvantages of the liquid electrolyte, the commercially used in the state of art of the lithium-ion batteries, are comprehensively presented and discussed. Finally, PEO-based solid polymer electrolytes are deeply examined from the standpoints of the background and mechanism of ion transportation and consistently analysed using various methods including blending polymers, addition of fillers, and applying various PEO topologies in terms of materials preparation, structural and dynamical characterization.

Chapter 3 includes the experimental details used in this study. The experimental apparatus and procedures are presented in detail, along with the facilities utilized in this research.

Chapter 4 shows the effects of chain architecture on miscibility, glass transition, segmental dynamics, and ionic conductivity for the PEO/PMMA doped with a fixed amount of LiTFSI in the blend electrolyte systems. Various well-defined PEO architectures, specifically linear, stars, hyperbranched, and bottlebrushes, and compositions were investigated.

Chapter 5 presents the application of a series of different topologies (linear, stars, and hyperbranched) for PEO polymer with varying molecular weight and salt concentration as model to further improve the performance of solid polymer electrolytes for Li-ion batteries.

Chapter 6 summarizes for the findings related to the performance of the newly designed new polymer nanocomposites (PNCs) based electrolytes composing of different PEO topologies (linear, stars, and hyperbranched), and silica nanoparticles with the addition of fixed amount LiTFSI.

Chapter 7 proposes the approaches of the newly synthesised PEO-grafted-PMMA copolymer with varying graft density and length for PEO onto PMMA backbone and presents the characterization results for this grafted copolymer in detail.

All our experimental results indicate that the macromolecular architecture can be an effective and promising tool for improving performance characteristics primarily ionic conductivity and mechanical strength in PEO-based polymer electrolytes, thus opening a new research avenue in the field of energy and environment concerning lithium-ion batteries and polymer electrolytes.

Eventually, Chapter 8 concludes a detailed overview, summary of the results, as well as suggestions for future works in this thesis.

Chapter 2 Literature Review

2.1 Energy Storage and Conversion in Batteries

In an effort to fighting against the climate change, the structure of the energy demand will be rapidly shaped with a transition towards increasing the share of the renewable energy sources including solar and wind, resulting a growing electrification of the world.[1] More specifically, the contribution of these replenishable natural sources in the global primary energy is expected to reach something between 35% and 65% by 2050. Combining this with the increasing attempts to decarbonize the transportation industry from internal combustion engine dominated domain to electrically operated vehicles will skyrocket the demand for the safer, more sustainable and reliable transition.[1] The large-scale integration of this transition in the energy supply will only be accomplished by the cutting-edge technological developments in the materials chemistry, a significant aspect of which essentially revolves around energy storage and conversion.[24, 25] To meet this huge demand for the change over from fossil fuel dependent power sources, the device which will play a key role in the energy storage and conversion must have the fundamental characteristics such as high energy, great power density, and possibility for large scale production and application.[24-26] Additionally, the charge and discharge of this device called as cycle life must be numerously performed at the desired rates for particular applications within an economically reasonable period of time from a commercial point of view. [24, 26] Furthermore, it should be cost effective, packed, lightweight in terms of manufacturing and easily employed for both immobile and mobile applications such as electric cars and consumer electronics.[26-28]

Several studies focused on developing different technologies for the energy storage and conversion have been applied in power systems.[24-26] One of the conventional methods is to use a mechanical device including pumped hydroelectric or compressed air, and flywheel. Although these well-established methods are safe, stable and could provide either high energy in the case of pumped hydroelectric and compressed air, or high power, in the case of flywheels, they have certain disadvantages limiting their commercial use for the energy storage and conversion at this very large scale. More specifically, pumped hydro storage and compressed air depend highly on the geographical locations to provide the essential water and compressed air reservoir storage areas and they are costly to operate.[24, 25] In addition to this, flywheels could provide and preserve power at a very

high rate, yet they must be stored within a vacuum and yield large standby losses, which makes them very expensive and unsustainable to maintain for long period of times.[24, 26] Most importantly, none of these traditional methods supply high energy and density at the same which have a vital importance in terms of energy storage and conversion towards electrification of the globe in great numbers, these devices are extremely limited by their size, structure, applicability to mobile applications. On the other hand, electrical devices such as capacitors and superconducting magnetic technologies could also be used for energy storage and conversion. Even though they could supply very high-power density, they significantly lack the ability to fulfil large-scale energy storage requirements and they are very expensive to implement.[24, 26]

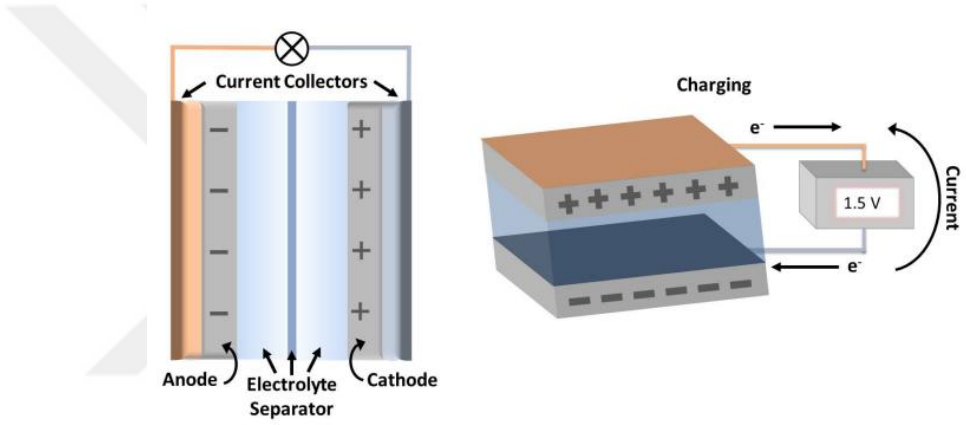

Figure 2.1: The general structure of a cell assembly for a battery.[26]

The most promising and widely used method for the energy storage and conversion is using the chemical storage namely the batteries. Because not only they provide high energy and power density with a variety of current and voltage ranges when utilized in series or in parallel, but also, they could be employed for both stationary and mobile applications due to their packed and lightweight structure.[4, 5] The structure of cell assembly for a battery is given in figure 2.1. Each battery is consisted of fundamental components including a positive (cathode) electrode, a negative (anode) electrode, an electrolyte, a separator, and current collectors.[26] The electrodes are key components directly controlling the electrochemical processes: the cathode is an electron acceptor such as lead oxide, manganese dioxide, or lithium cobalt oxide whereas the anode is an electron donor such as lead, zinc, or lithium and they should be particularly chosen with tunable properties based on operational conditions such as cost, temperature, mobility. In addition to this, the current collectors must be selected depending on working conditions

including temperature, type of the electrolyte (aqueous, nonaqueous, ionic liquids, solid, acids, bases), and etc and are generally made of extremely conductive materials (stainless steel, aluminium, and copper). They should also be readily malleable, cost-effective, packed, and form excellent contact with the electrodes as much as possible. Moreover, the electrolyte commonly made of a salt, acid, or base dissolved in an organic, aqueous, ionic liquid or polymer solvent plays a significant role by providing the ionic migration between the electrodes. The electrolytes, which are generally soaked within a porous medium consisting of typically polymers, should be thermally and chemically stable under the working conditions. This polymeric material soaked with the electrolyte is also known as the separator that should prevent the electrons move through but let ion movement back and forth during the processes of charging and discharging of the batteries.

Several parameters such as the equilibrium potential, specific capacity, and cycle rate have been primarily dictating performance characteristics of the batteries. In case of discharging the battery, a thermodynamically driven process, when these electrodes are attached by an external device, the electrons naturally flow out of the negative electrode to the positive electrode, which happens in the reverse direction in another process known as charging. In either of these operations, ions are transferred through the electrolyte separating the electrodes, preserving the charge balance. The driving force for these chemical processes are attributed to the difference in Gibbs free energy between the products and the reactants given as:

$$\Delta G^{o}_{rxn} = \sum \Delta G^{o}_{f}(products) - \sum \Delta G^{o}_{f}\ (reactants) \tag{2.1}$$

From this relationship, we could estimate the average voltage of the battery, also known as the equilibrium potential E^{o} for the reaction, using the calculated difference in Gibbs free energy of the reaction, the number of electrons (n) transported in the reaction and the Faraday's constant (FC) (96,485 C mol^{-1}), which is related by the following equation:

$$E^{o} = \frac{\Delta G^{o}_{rxn}}{nF} \tag{2.2}$$

Furthermore, the amount of energy that can be stored per unit mass of total electrode material which is usually known as the specific energy ($W_{battery}$) and often is given in terms of Wh kg^{-1} can be calculated as:

$$W_{battery} = E^o \times \frac{C_{cathode} \times C_{anode}}{C_{cathode} + C_{anode}} \quad (2.3)$$

Where $C_{cathode}$ and C_{anode} account for specific capacities of the cathode and anode materials, respectively, also known as the amount of charge in the respective electrode that can be stored per unit mass of material, and is commonly given in terms of mAh g^{-1}, could be calculated for the corresponding electrode using the relationship consisting of the number of electrons transferred in the reaction (n), the Faraday's constant (FC) (96,485 C mol^{-1}), and finally the molar mass of the electrode material (M g mol^{-1}) :

$$C_{electrode} = \frac{nF}{M} \times \frac{1000}{3600} \quad (2.4)$$

The Coulombic efficiency (CE), given as the ratio of the discharge to the charge capacity, also one of the important parameters that indicates the ability of the battery to reverse the lithiation/lithiation process which affects cycle life in the aspect of battery performance. CE value is usually less than 100% because of undesired reactions, such as a reaction happening with the electrolyte by forming an interfacial layer in the electrode. Additionally, the rate at which the battery is charged and discharged is another key factor in evaluating battery performance. In this context, the current required for a complete discharge or charge the battery in 1/n hours can be equal to Cn, where C stands for the cycle rate (C-rate) determined during different charge/discharge process depending on the power requirement for various applications. This cycle rate is also theoretical and highly based on the electrode material.

Although various scientific progress has been made in terms of both designs and chemistry in developing the batteries since the existence of the first battery invented by Alessandro Volta in two hundred years ago [29-31], they can be essentially classified into two types: primary and secondary. Primary batteries, also called 'disposable or non-rechargeable batteries', still depend on the concept of a voltaic cell in which electrochemical energy generated because of decaying electrode material and electrolyte.[30, 32] This decomposition is also not reversible, so when this process is over, the battery does not produce electricity and cannot be charged, thus it must be replaced by a new battery.[30, 33] These batteries have been the simplest and most suitable sources for portable electronic and electrical device applications like lights, cameras, watches, toys, radios etc, since they are typically light weight, small, and easily manufactured in different shapes. Having said that zinc anode-based primary batteries

were at the forefront of this type of cells up to 1970s, other types such as zinc–carbon, zinc / alkaline manganese dioxide, and metal–air-depolarized based primary batteries were developed, and they were finally replaced by the advancement of lithium based over traditional ones due to higher specific energy and longer shelf life.[30, 32, 34, 35] Although these primary batteries have been dictating the market share over secondary batteries for a small-scale usage within a specific range of applications, the change-over towards rechargeable batteries is inevitable due to fundamentally their environmentally unfriendly character (disposability) as well as some other performance related properties such as low discharge rate and temperature range, which could be obviously an obstacle for the above mentioned large-scale integration of this transition to be more reliable, robust, and sustainable in the energy supply of the globe.

A secondary battery, also known as a rechargeable battery, is the most actively studied cell systems because of a wide variety of reasons related to the chemistries, operating conditions, and applications.[26, 36, 37] As opposed to the primary batteries, they can be electrically recharged and discharged again for many times over a long period of time instead of discarding. Traditional secondary batteries are composed of four major categories including lead–acid batteries, nickel–cadmium (Ni–Cd) batteries, nickel–metal hydride (Ni–MH) batteries, and lithium–ion batteries. The energy densities of these rechargeable battery system are illustrated in figure 2.2. Among all the rechargeable batteries, the lead-acid battery systems, developed by Gaston Planté in late 1850's, are the most widely used and favoured ones. [24, 29, 35, 38] They depend on the usage of lead – lead Dioxide (Pb – PbO2) electrochemical couple with a sulfuric acid-based electrolyte. With a large voltage range and an electrical efficiency ranging approximately around 75%, they could reach up to a life span of 2000 cycles depending on the discharge rate, making them convenient to be used for a wide range of applications such as energy storage, communication systems and emergency lighting systems, etc.[24] Of these applications, the most commonly used application of the lead–acid batteries is for low cost, and easy maintenance.[24, 29, 39] Even though these advantages pave the way for the lead–acid batteries in comparison with the other secondary battery, they have significant certain drawbacks limiting their wider usage for the large-scale energy systems. They are environmentally unfriendly mainly because of the lead usage and more importantly their specific energy is extremely low revolving around (35 Wh kg^{-1}), and their cycle life is comparatively short and needs significant development. [24, 29] While

nickel-cadmium (Ni–Cd) batteries, which utilize nickel oxyhydroxide as the positive electrode and cadmium metal as negative electrode separated by an alkaline solution of potassium hydroxide, have a similar efficiency and are considerably developed in terms of cycle life approaching to 3000 cycles when compared to the lead–acid batteries, they are not the potential candidates for the large-scale energy storage and conversion because their low energy density along with progressively high self-discharge rate loses is not sufficient and they contain environmental and health concerns due to their toxicity.[24, 29, 38, 40] Furthermore, relatively recent type of secondary batteries in which the positive electrode is the nickel oxyhydroxide (NiOOH) whereas the negative electrode is a metal alloy, where hydrogen is stored reversibly is nickel – metal hydride based batteries. The applications of these (Ni–MH) battery systems which have greater energy density in comparison with the former counterparts are various and consist of portable electronics, hybrid electric vehicles, and satellites.[29, 36, 37] Nevertheless, their energy density can only reach as close as about approximately half (~60 Wh kg-1) of the energy density generated by the lithium-ion batteries (LIB) which usually use graphite as anode and a metal oxide, originally $LiCoO_2$, as cathode, with an electrolyte including $LiPF_6$ salt dissolved in typically organic solvent composed of ethylene carbonate and dimethyl carbonate-(EC-DMC) as shown in figure 2.2.[41-43] Combined with new improvements in the materials chemistry, the energy density of the state-of-art rechargeable lithium-ion battery could increase up to three times (~400 Wh kg-1) when compared to other rechargeable batteries. In addition to these, the lithium-ion batteries have significant other advantages such as slow self-discharge rate, longer cycle life, wide range of operating temperatures, lightweight, high efficiency, being environmentally more friendly since they contain no lead or cadmium. Therefore, the applications of rechargeable lithium-ion batteries in the last couple of decades has been quite phenomenal for different industries such as electric vehicles, consumer electronics, and energy storage systems with a market cap of couple of billion dollars.[27, 36, 37, 44, 45] Because of having a very mature technology, extensive research, and most importantly excellent properties, rechargeable lithium-ion batteries have been the best candidate for the large-scale transformation towards highly decarbonized and electrified global energy supply within the years to come and will be discussed with further details in the subsequent sections of this thesis.

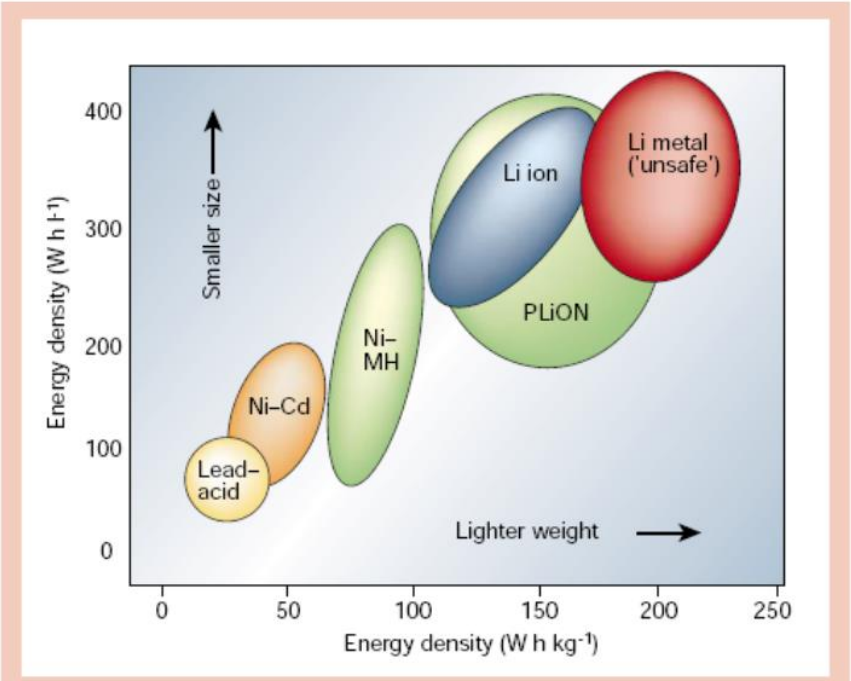

Figure 2.2: The schematic of the energy densities of various secondary (rechargeable) batteries.[46]

2.2 Fundamentals of the Lithium-ion batteries

The development of the first rechargeable lithium-ion batteries was started by Exxon corp. in 1970s using lithium metal and TiS_2 as electrodes and $LiPF_6$ in propylene carbonate as electrolyte. Following this, various studies have been done in 1980s in efforts to further increase battery performance of this early design by incorporation of the cathode and anode electrodes made up of other alternatives such as Li_xMO_2 (M: Co, Ni, Mn) and graphite, which did the groundwork for the first commercial lithium-ion battery manufactured by Sony and Asahi Kasei in 1991.[43] Since then, large-scale commercialization of secondary batteries using Li-ion chemistries has paved the way for advances in portable electronics and hybrid vehicles mainly owing to its excellent characteristics such as low density, relatively high reduction potential, long cycle life and extremely large energy density. [31, 41, 45] The conventional lithium-ion batteries compose of two electrodes namely, a lithium metal oxide-based cathode (positive) and a graphite-based anode (negative), a liquid electrolyte consisting of a lithium salt (e.g. LiPF6) and an organic solvent (e.g. ethylene carbonate and dimethyl carbonate-EC-DMC) which provides the medium for the ion transfer between the anode and the cathode,

and separator physically separating the anode and cathode to avoid a short circuit, which eliminates electron passage but facilitates ionic movement back and forth.[43, 46, 47] The fundamental parts and working principle for the commercial lithium-ion battery are shown in figure 2.3.[46]

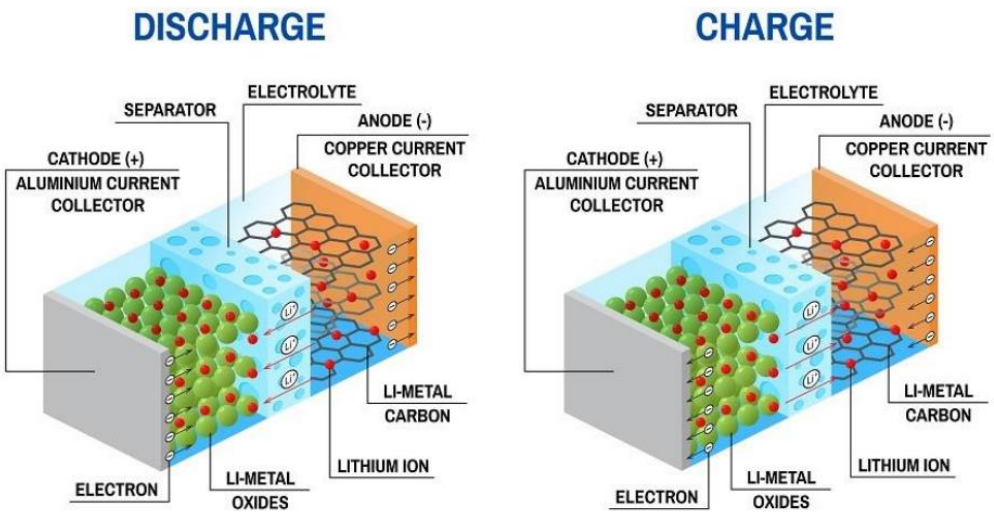

Figure 2.3: The fundamental parts and working principle during charging and discharging for the commercial lithium-ion battery.[44]

The operation of the traditional lithium-ion battery is based on electrochemical oxidation-reduction (redox) reaction. In the case of discharging, Li ions exit the anode and go into the cathode through the electrolyte and separator. The reverse reaction takes place during charging. In other words, the li-ions are removed reversibly from one side and intercalated into another side without causing structural damages in the host electrode to increase cycle life of the battery, known as intercalation mechanism. The chemical reactions including oxidation and reduction mechanisms happening in the case of charging within the electrodes can be seen below as:[43, 44, 47]

Anode (Reduction reaction): $C + yLi^+ + ye^- \rightarrow Li_yC$

Cathode (Oxidation reaction): $LiMO_2 \rightarrow Li_{1-x}MO_2 + xLi^+ + xe^-$

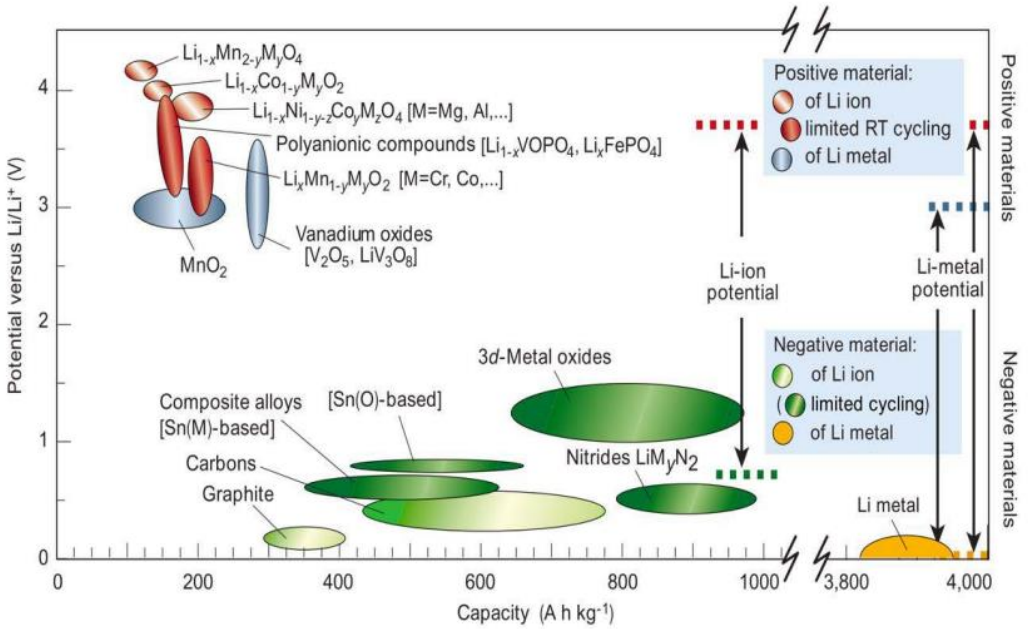

Figure 2.4: The detailed summary of the materials for the preparation of anode and cathode electrodes of the lithium-ion batteries.[43]

Designing of the lithium ion-battery in a suitable manner in terms of cathode, anode, and electrolyte has been a key player in optimizing the battery performance. Although several materials for both anode and cathode electrodes for the lithium-ion battery (LIB) have been studied, extensively summarized in figure 2.4, commercial LIBs generally comprise of graphite-based anode and a metal oxide-based cathode namely $LiCoO_2$, both of which has a layered structure, facilitation the lithium-ion intercalation.[43, 44, 46, 47] While graphite and its doped derivatives as anode material are accompanied with supplying perfect interfacial stability and low potential, $LiCoO_2$ and its based derivatives have been providing better thermal stability for the cathode electrode, eliminating safety concerns in relation to the overheating issues encountered in other layered oxide-based cathodes such as Li_xNiO_2.[46, 47] Since both cathode and anode electrodes play a very essential role in the evaluation of the performance characteristics of the lithium-ion battery, it is significant that the materials used for cathode and anode preparation must own certain properties to have high specific capacity, long cycle life, high energy density and these properties could be generally summarized as follows:[41, 46]

Anode electrode:

- Low potential for the continuous lithium intercalation and deintercalation in the anode with respect to lithium
- High storage of the lithium within the anode material
- Structural stability during charging/discharging, not being very reactive with the electrolyte
- Fairly good electrical and ionic conductivity
- Cost efficiency, environmental friendliness, and easily producible

Cathode electrode:

- High potential when compared to the Li/Li^+ reference electrode
- High capacity and ability of the electrochemical extraction of the lithium atoms from the cathode material
- High electronic conductivity and power density
- Structural stability during charging/discharging to avoid any damages
- Cost efficiency, environmental friendliness, and smooth manufacturing

2.3 Electrolytes for the Lithium-ion batteries

Although significant amount of research with regards to lithium-ion batteries have concentrated on developing better performing anode and cathode materials, it is also important to note the electrolytes are very vital for transporting positive lithium ions between electrodes, critically impacting the electrochemical performance of a battery in the aspects of power density, stability and safety. [8] Electrolytes are primarily divided in two types, depending on their states: (1) liquid, and (2) polymer electrolytes, which are subcategorized as aqueous, organic, and ionic in the case of liquid-based electrolytes while gel and solid electrolytes when polymers are employed. To have a good performing lithium-ion battery, all the electrolytes, regardless of the different types, must meet the following requirements: [8, 29, 41, 48, 49]

- Large electrochemical stability window
- Having thermal and chemical stability, ability to have good salt dissolution, as well as high boiling point for safety
- High ionic conductivity (σ), at least 10^{-3} S cm^{-1} at room temperature and low viscosity for the easier lithium-ion transportation
- Low electronic conductivity (~ < 10^{-10} S cm^{-1}) to prevent the formation of a short-circuit
- Being non-toxic and environmentally friendly

Currently, the commercial lithium-ion batteries mainly utilize a separator immersed in organic liquid electrolytes containing a dissolved salt and associated with certain advantages the most appreciated of which is the very high conductivity.[8, 49] However, however they have drawbacks and potential risks[13, 16, 50-52] such that they are usually highly volatile, flammable, toxic, and lithium dendrite formation at the interface between electrolyte and electrode due to high reactivity of the lithium metal, which may result in environmental and safety hazards such as fire, leakage, explosion, short circuit limiting its use commercially.[4-7, 31, 41, 42, 44, 45] Additionally, their working range with respect to temperature is limited and they are large and heavy in bulk size. On the contrary, polymer electrolytes towards which scientific community has been giving a lot of attention comprise simply of a lithium salt dissolved in a polymer matrix, providing some advantages over liquid electrolytes.

In this context, they could be very useful in offering increased mechanical strength and malleability. They could also be manufactured in different geometries, even in the form of packed and lightweight thin films, providing greater volumetric energy and power densities. Furthermore, when compared to liquid electrolytes, they lack leakage and are less reactive with the electrodes, which results in decreased dendritic growth. They can also often compensate the volume changes arising from the ion-electrode exchange processes. Despite they possess these significant advantages, their low ionic conductivity at room temperature (<10^{-5} S/cm)[11] compared to the liquid electrolytes (~10^{-2} S/cm)[11] remains as a major challenge for their large scale commercialization,[12] which is the main focus of this thesis. The figure 2.5 summarizes the characteristic properties between liquid and polymer electrolytes.

Property	Liquid electrolytes	Polymer electrolytes
Conductivity	High ionic conductivity	Low ionic conductivity
Safety	Leakage of liquid or gas formation	No leakage
Function	Ionic conductor with a porous separator (dead mass)	Ionic conductor and separator (active mass)
Design /Package	Protective case and packaging	Thin, flexible, and space-efficient designs with different configurations laminated packaging
Device performance	–	Increase in volumetric energy and power densities

Figure 2.5: The comparison of the properties for the different electrolytes used in the lithium-ion batteries.[49]

Since an electrolyte in the lithium-ion battery is made up of a salt and solvent, the chemical and physical interaction between the solvent and the salt(s) plays a key role in determining the battery performance. There are certain factors such as dissociation constant, ion mobility, solubility, thermal and chemical stability that need to be assessed for choosing the best option to prepare the electrolytes in the lithium-ion batteries.[41] The host solvent must own high salt solubility usually associated with a high dielectric constant and low viscosity to facilitate ionic movement and thus increasing ionic conductivity.

The salt should also have good chemical and large thermal stability over a wide range of temperature. The comparison below shows a detailed evaluation based on the mentioned-above factors among the most widely used various salts for both liquid and solid electrolytes salts including primarily lithium hexafluorophosphate ($LiPF_6$), lithium tris(pentafluoroethyl) trifluorophosphate (LiFAP), lithium tetrafluoroborate ($LiBF_4$), lithium hexafluoroarsenate ($LiAsF_6$), lithium perchlorate ($LiClO_4$), and lithium bis(trifluoromethanesulfonyl)imide (LiTFSI). LiTFSI also owns very high ionic conductivity in liquid solvents.[8, 42] Additionally, it has low lattice energy and bulky anions which could slow down the polymer crystallization when used with PEO-based solid polymer electrolyte which is the earliest and most studied SPE system.[8, 42] Because of these fundamental reasons, we chose as the LiTFSI salt candidate to be used in the solid polymer electrolytes investigated in this thesis. The subsequent sections will deal with liquid and polymer electrolytes in much more in detail.

- Dissociation constant: LiTFSI > $LiAsF_6$ > $LiPF_6$ > $LiClO_4$ > $LiBF_4$
- Solubility: LiTFSI > $LiPF_6$ > $LiAsF_6$ > $LiBF_4$
- Thermal stability: LiTFSI > $LiAsF_6$ > $LiBF_4$ > $LiPF_6$
- Chemically inertness: LiTFSI > $LiAsF_6$ > $LiBF_4$ > $LiPF_6$

2.3.1 Organic Liquid Based Electrolytes

When compared to other liquid electrolytes including aqueous and ionic liquids, organic liquid-based electrolytes have fundamental advantages such as increased energy density, wide electrochemical window for operating voltage reaching up to 2.5 V, and low viscosity favouring ion migration.[29, 49] Nevertheless, they have some drawbacks including lower ionic conduction, power output, as well as their highly volatile and flammable nature, causing environmental and safety risks.[29] Even though Acetonitrile (ACN) has been used as one of the first organic solvents for producing liquid electrolytes due to its excellent properties like low viscosity, good salt solubility, and high ionic conduction, it was later substituted, because of its extremely evaporable and poisonous features, by mostly alkyl carbonates including propylene carbonate (PC), ethylene carbonate (EC), ethyl methyl carbonate (EMC), diethyl carbonate (DEC), dimethyl carbonate (DMC).[41, 43, 49]

Furthermore, the most commonly used the state of art liquid electrolytes depend on binary/ ternary mixtures of these linear and cyclic carbonates, which is considered to be one of the most significant developments achieved when liquid electrolytes for Li-ion batteries are concerned. The essential reasons in using combinations of carbonates are relevant to their crucial distinctive characteristics. As it is known that low viscosity and high enough dielectric constant are desired for developing the performance characteristics of the electrolytes for easier ionic transportation and better salt dissolution respectively, therefore resulting in higher ionic conduction, the only way to accomplish these requirements appeared to be strongly related to using combinations of low viscosity of linear carbonates namely ethyl methyl carbonate (EMC), diethyl carbonate (DEC), as well as dimethyl carbonate (DMC) and cyclic carbonates associated with high dielectric constant such as propylene carbonate (PC) and ethylene carbonate (EC).[29, 41, 43] Other advantages of using mixtures of different solvents are mitigated exfoliation, toxicity and

the formation of gaseous compounds as well as increased ability to form a more stable solid electrolyte interphase with the electrodes. [29, 41, 53]

The figure 2.6 shows some of the properties of the most widely used organic solvents for the preparation of liquid electrolytes.

Solvent	*Melting Temperature* T_m *(°C)*	*Boiling Temperature* T_b *(°C)*	*Viscosity at 25 °C* η *(mPa s)*	*Dielectric constant* ε
Dimethyl carbonate (DMC)	4.6	91	0.59	3.1
Diethyl carbonate (DEC)	-74	126	0.75	2.8
Ethyl methyl carbonate (EMC)	-53	110	0.65	3.0
Ethylene carbonate (EC)	36	248	1.9 (40 °C)	90
Propylene carbonate (PC)	-49	242	2.5	66

Figure 2.6: The comparison of the properties of the most widely used organic solvents for the liquid electrolytes in the lithium-ion batteries.[29]

2.3.2 Aqueous Electrolytes

Since the water is extremely cheaper, more abundant, and easily accessible in comparison with the organic solvents, it has been considered the most convenient solvent and applied in the first electrolyte preparation for the batteries.[54] Although the water dissolves a variety of salts and yields the highest ionic conductivity among the liquid electrolytes, which is attributed to the very high dielectric constant (80)[29] and very low room temperature viscosity (0.89 mPa s)[29, 55, 56], it has certain shortcomings such as a very narrow maximum operating voltage limited by the electrolysis of the water (~1.2 V)[29, 55] and low thermal stability.[49] Therefore, scientists have been working on alternative solvents for the liquid electrolytes like ionic liquids (ILs) which is discussed in the following section.

2.3.3 Ionic Liquid Based Electrolytes

Ionic liquid (IL) based electrolytes have been studied as the substituting electrolytes when compared to more commonly known and conventional aqueous and organic electrolytes owing to their favouring properties including very wide potential window and

extremely high thermal stability.[29, 49] Furthermore, the ionic liquids, which are salts consisting of organic cations and organic and inorganic anions with a comparatively low melting point (< 100 °C)[49], could have structural changes and combinations, which make them suitable for better tunability in terms of properties for various battery applications. However, they have one major drawback that is they have very high viscosity widely ranging from 30 cP to 500 cP [49], which results in decreased ionic conductivities among liquid electrolytes. Thus, different types of methods such as mixing them with stable solvents within protic or aprotic ionic liquids have been investigated to enhance the ionic conductivity of these types of electrolytes.[49]

2.3.4 Polymer Based Electrolytes

Polymer based electrolytes is composed of ion conducting systems based on complexation between polymer matrix and salt by the dissolution of a salt in the polymer host.[8, 43, 57] Polymers have been proposed as suitable solvents for battery electrolytes thanks to their excellent mechanical properties, lack of solvent leakage, decreased dendritic growth, good interphase contact, as well as thermal and chemical stability.[8, 29, 37, 58] Other significant advantages of the polymer based electrolytes over liquid ones are light-weight packed structure, easy processability, good flexibility and elasticity, which is why polymer electrolytes could compensate better the volume change associated with charging and discharging processes.[8, 31, 45, 57] Additionally, the polymer host for a good performing polymer electrolyte should have the following fundamental characteristics.[31] First the polymer chain should be able to dissolve the lithium salts well and incorporate atoms capable of creating coordination bonds with the lithium cations, located within a suitable distance that allows relatively easy transfers of the ions to the next site.[8, 31, 43, 49] Secondly, as ionic conduction which is coupled with segmental dynamics of the chains occurs in the free volume of the amorphous phase, flexible polymers with low glass transition temperatures and low crystallinity are preferred.[8, 31, 49] Thirdly, the chemical and thermal stability as well as mechanical strength of the polymer host are also desired factors as they affect the overall performance of the polymer electrolyte. [8, 48, 49]

Since the earliest work conducted by Wright and Armand et al. on the polymer electrolytes dating back to 1970s[59-61], although several polymers have been considered in order to satisfy these criteria for the polymer electrolytes, polyethers (-

$(CH2)_mO-)n$ especially poly (ethylene oxide) (PEO) were the first ones that obtained great deal of attention from the scientific community mainly because of their superior ability of dissolving various salts through the interactions between the salt and ether oxygen atoms and providing enough cation coordination sides.[8, 29] The PEO, polyether with a very low glass transition temperature ranging about (~-55°C)[8] , with an appropriate lithium salt could reach very high ionic conductivities (~10^{-3} S/cm)[8] above its melting temperature (~60°C)[8]. Nevertheless, the major drawback of electrolytes based on PEO is the existence of the highly semi-crystalline phase below the melting temperature, which dramatically decreases the ionic conductivity (~10^{-5}-10^{-6} S/cm)[8]. Therefore, most of the studies have been focusing on completely inhibiting the crystallization of PEO using different techniques including blending polymers[8, 18], cross-linking[13], copolymerization[19, 20], addition of fillers[9, 21], plasticizers[5, 15, 16], and considering architectural variations[8]. Another example of the polymer host that has a very low and favourable glass transition temperature of about (~-60°C) is poly (propylene oxide) (PPO).

However, the ionic conductivity of the poly (propylene oxide) (PPO) based electrolytes is lower than PEO-based ones by far and not comparable, which could be attributed to the presence of higher distance and a smaller number of the cation coordination sites. Another polymer that could be considered is amorphous poly(methyl methacrylate) (PMMA). The carbonyl groups coordinating lithium via the oxygen atom are not located within the polymer backbone yet are connected to the main chain through side groups.[8, 49] The essential problems with PMMA are relatively very low and unsatisfied ionic conductivity (~10^{-5} S/cm at around 100°C)[8] accompanied with low segmental motions, as well as its rigidity and the brittleness associated with the high glass transition temperature (~120°C)[8]. Furthermore, another alternative polymer studied for polymer electrolytes with a reasonably low glass transition temperature (-40°C) is poly(vinylidene fluoride) (PVDF). Although the PVDF polymer matrix provides convenient mechanical properties, it is also highly semi-crystalline with a very high melting temperature (~170°C), resulting low fraction of the conductive amorphous phase, and thus limiting ionic conduction. Moreover, the efficient solution of the lithium salts could also be achieved by poly(acrylonitrile) (PAN) with the help of by nitrogen atoms from nitrile groups. The (PAN) polymer provides electrochemical stability, however its highly elevated glass transition (~125°C) and melting (~320°C) temperatures make it incomparable with other

polymers, lacking support for the ion transport by segmental motions and resulting poor ionic conductivity. In short, the investigation of PEO shows the advantages of poly (ethylene oxide) (PEO) are still unmatched by the polymers mentioned above. Therefore, we determined the focus of this thesis to be the formation a PEO based polymer electrolyte with increased ionic conductivity and mechanical strength to be the best promising potential for the next generation of solid polymer electrolytes.

To kind of summarize, regardless of the various types of the polymer electrolytes, they must meet the following criteria for solid-state flexible lithium batteries[29, 31, 41, 49, 57, 61]:

- High ionic conductivity
- Well chemical, thermal, and structural stability
- Strong mechanical strength with enough flexibility
- Availability and cost-effectiveness of the materials

There are mainly two different types of polymer electrolytes including gel and solid polymer electrolytes, each of will be discussed now with more detail.[48, 58]

2.3.4.1 Gel Polymer Electrolytes

The gel polymer electrolytes (GPEs), which were firstly employed for lithium-ion batteries, composed of a polymer and a liquid electrolyte, up to ~250 wt% and could be formed by placing this high amount of liquid electrolyte a lithium ion conducting organic solution in a polymer matrix (e.g. poly(ethylene oxide) (PEO), poly(vinylidene difluoride) (PVdF), polyvinyl chloride (PVC), poly(methyl methacrylate) (PMMA) and poly-(vinylidene fluoride-hexafluoropropylene) (P(VDF-HFP)) copolymer) through physical and chemical methods.[29, 62-64] They could have room temperature ionic conductivities on the order of 10^{-3} S/cm. [29, 63-65]

Even though gel polymer-based electrolytes are usually accompanied with high ionic conductivities (~10^{-3} S/cm) at room temperatures, as well as increased flexibility and safety in comparison with the liquid ones, however the problems associated with GPEs are similar to those encountered for liquid electrolytes, like compatibility, flammability, formation of interfacial layers, and mechanical strength, and are still need to be solved, which remains as challenging obstacles for their widely use in the transition of safer and more reliable electrolyte systems for the next generation of the lithium-ion batteries. [42,

63] Therefore, it is urgent to improve the electrochemical properties of solid polymer electrolytes which lack of overheating, electrolyte leakage and fire safety because of no incorporation of liquid part and provide necessary developments in the form of higher flexibility and easier manufacturing, which will be extensively reviewed from different aspects of it like advantages, shortcomings, and ion transport mechanism in the following parts of this thesis.

2.3.4.2 Solid polymer electrolytes

Solid polymer electrolytes (SPEs) which are commonly comprise of a polymer host and a salt have been widely investigated by many scientists owing to their excellent properties such as increased mechanical strength, ease of manufacturing, enhanced flexibility, improved ability of forming interfacial contact between electrode and electrolyte, large electro-chemical window, superior energy density, and nonflammability, which leads to more compacted and safer batteries.[8, 41, 49, 66] [61, 67-69] These advantages significantly paved the way for the worldwide interest of researchers towards developing SPEs with desired electrochemical properties to replace the liquid electrolytes since the first discussion and application that used a solid polymer electrolyte composed of PEO/alkali salt complex was explored at the of 1970s.[29, 31, 41, 69] Then, more efforts were made in the 1980s for understanding the ion transport mechanism as well improving the ionic conductivity within these PEO-based polymer electrolytes.[41, 70] These extensive and intense studied conducted in 1980s led to the production of the first lithium battery consisting of a PEO electrolyte in 1985, which is followed by the development of the first commercial and successful lithium-ion batteries by Yoshino and Sony Corporation in the 1991s.[41, 69] This started the use of lithium-ion batteries in the mass production of portable electronics. [8, 41, 69] At the same time, having a successful transformation towards clean energy sources including wind and solar power facilities as well as electric vehicles in an effort fighting with climate change and global warming increased dramatically the importance and wide application of the research for the usage of lithium-ion battery in these systems, which will intensify the need for these types of batteries. However, the state of art lithium-ion batteries continued to use liquid electrolytes associated with numerous significant drawbacks. They contain types of solvents that are toxic, flammable, and volatile, which could pose safety and environmental concerns such as explosions, fires, and short circuits. [8, 41, 45] They also

have problems like dendrite formation, exfoliation or degradation, leading further safety risks, and lack of performance. [41, 42, 45] Therefore, it is needed to have a more compact, safer, cost-efficient, lightweight, and packed structures with higher energy and power density in great numbers for the lithium-ion batteries[8, 49, 69], which could be provided by solid state- batteries composing of solid polymer electrolytes, cathode, anode, and insulated separator as shown by the figure 2.7 below.

2.3.4.2.1 Background

Among the polymers used for solvent-free polymer electrolytes, the most widely used polymer matrix is PEO composed of ethylene oxide repeating units (Figure 2.8), due to its various number of favourable properties.

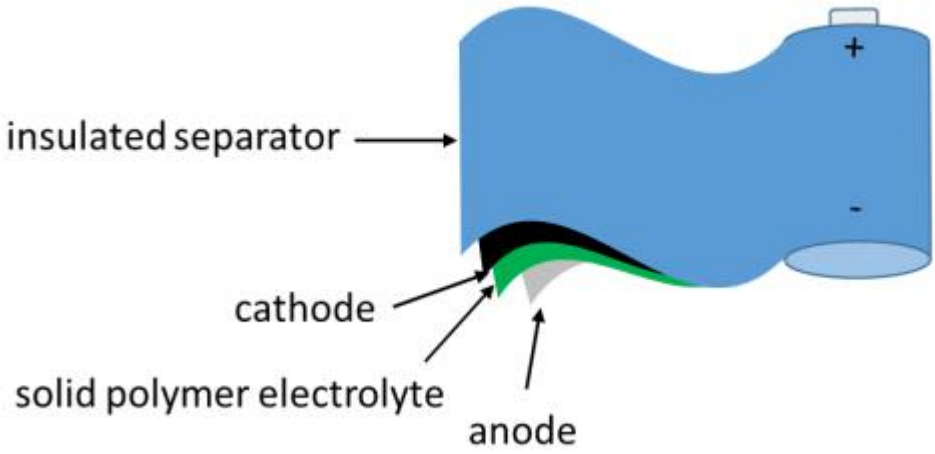

Figure 2.7: The representation for the parts of solid-state batteries.[69]

First, PEO has the ability to solve a variety of ionic conducting salts such as LiTFSI and $LiClO_4$ which are the most commonly used salts in PEO-based electrolytes.[8, 49, 66] The strong solvating ability of PEO could be attributed to the increased ionic dissociation provided by the C-O polar groups in the backbone.[8, 29, 49] Furthermore, other beneficial characteristics in relation to PEO are wide range of electrochemical and thermal stability, as well as exceptional compatibility with other organic or inorganic materials.[8, 49, 69] As the ionic transportation in SPEs primarily takes place through the free volume in the amorphous phase, where the movement of ions is coupled with the segmental motion of the polymer chain (Figure 2.8), more importantly, another advantage

of PEO is related to the its very fast segmental dynamics (low glass transition temperature ($T_g \sim 220$ K[8, 61]), which facilitates ion transport.

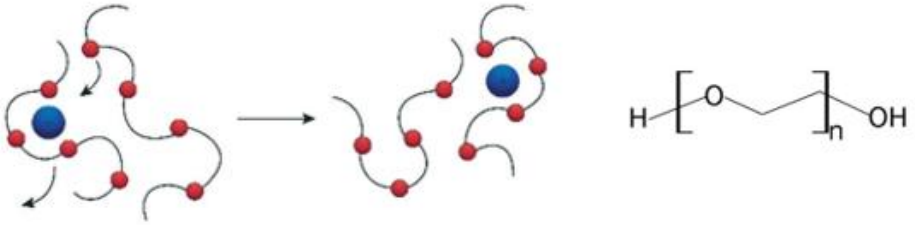

Figure 2.8: The chemical structure of PEO and schematic illustration of the Li ion (filled blue symbols) conduction through segmental dynamics of the cation coordinating PEO chains (Filled red symbols represent the oxygen atom).[8, 71]

However, the PEO based SPEs are usually semi-crystalline with the crystalline phase due to PEO chains having the tendency to ability of close packing of the polymer chains (chain folding). Because of this high degree of crystallinity impeding the ion transport (Figure 2.9), the room temperature ionic conductivities ($\sim 10^{-6} - 10^{-8}$ S/cm)[8] of neat PEO-based electrolytes are not certainly comparable as far as liquid electrolytes are concerned. The ionic conduction is extremely increased up to the values ranging around (10^{-3} S/cm)[8] above its melting temperature ($T_m = 60$°C)[8], but this results in a tremendous decrease in the mechanical strength, limiting its use in a solid-state electrolyte [18], both of which hampers its wide and practical uses in a solid-state battery. Therefore, the emphasis for developing better designs of the PEO-based SPEs essentially revolve around increasing both the ionic conductivity and mechanical toughness simultaneously.

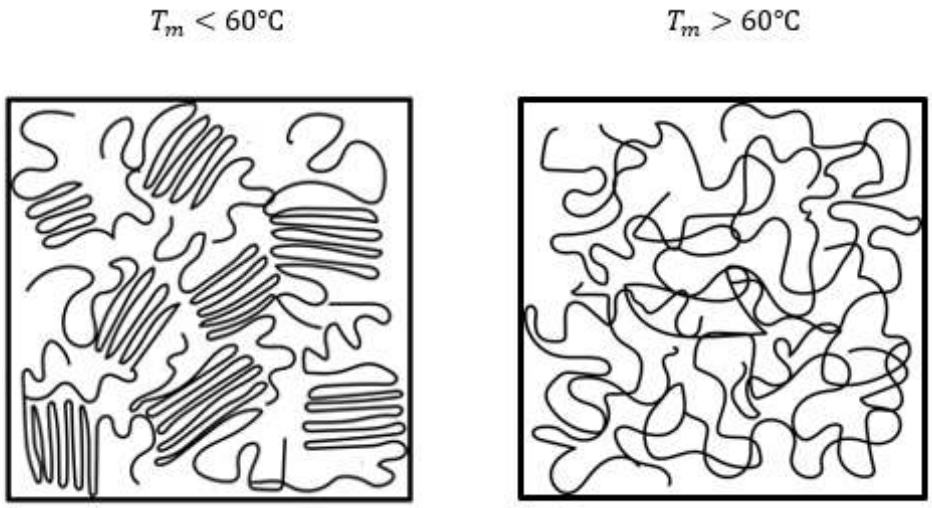

Figure 2.9: The semi-crystalline nature of PEO at temperatures below T_m and completely amorphous state above T_m in PEO-based electrolytes.

To accomplish this, numerous approaches have been deeply investigated, which have been successful to some extent in increasing mechanical strength without sacrificing the ionic conductivity. These methods commonly include addition of organic and inorganic fillers[9, 21], plasticizers[5, 15, 16], and cross-linkers[13] into PEO matrix. Additionally, the use of PEO with other polymers[8, 18] in blends and synthesizing new PEO-based copolymers[19, 20] have been extensively applied. Eventually, another effective method in improving the electrochemical characteristics of the PEO-based electrolytes is based on using architectural variations in PEO architecture with varying branching and salt content, which has been relatively new and less employed when compared to previously discussed former approaches,[8] thus being the fundamental focus of this thesis in developing PEO-based solid polymer electrolytes.

Before discussing the new approach based on topological variations of PEO proposed in this thesis, the ion transport mechanism in SPEs is examined in the following section.

2.3.4.2.2 Ion Transport Mechanism

The ionic conductivity (σ) in a polymer electrolyte which is one of the most significant parameters in evaluating the performance of an electrolyte is greatly affected by two fundamental factors including the segmental motion of the polymer chains and ion dissociation in the polymer host. [8, 29, 31, 45, 49, 58, 69]

It is generally expressed as:[29, 57, 69]

$$\sigma = \sum n_i q_i \mu_i \tag{2.5}$$

Where n_i is the number of charge carriers, q_i is their charge and μ_i is their mobility. Furthermore, the temperature plays a key role in affecting the ionic conduction by changing the charge mobility, known as ion mobility as well, which can also be expressed by the relationship as follows:[69]

$$\mu = \frac{Dq}{k_B T} \tag{2.6}$$

Based on the Eq. 2.5, it could be said that enhancing the conductivity could be achieved by increasing ion concentration and charge accompanied with fast mobility. However,

increasing the salt concentrations (amount dissolved salts) does not inevitably result in higher ionic conductivity, because increasing charge carries over certain concentration leads the formation of the formation of ion pairs and aggregates due to increased interaction between the ions.[8, 14, 29] More specifically, ion pairs do not contribute to the ionic conductivity, leaving less available free ions for the ion transport and ionic aggregates increases mainly the viscosity of electrolytes, decreasing the ionic mobility, thus ionic conductivity. [8, 14, 29, 72-74] Moreover, the ionic conduction generally decreases with increasing molecular weight (MW) of the polymer host used in the polymer electrolyte.[29] The figure 2.10 shows the dependence of the ionic conductivity on the salt concentration in solid polymer electrolytes.[29]

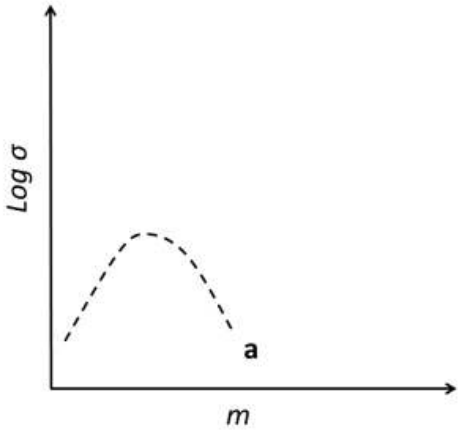

Figure 2.10: The dependence of the ionic conductivity with respect to salt concentration (m) in an SPE.[29]

Solid polymer electrolytes (SPEs) including lithium salts dissolved in dissolved in polymer matrices composed of atoms or functional groups such as only oxygen, nitrogen, and sulphur have an ability of forming coordination bonds with the lithium ions, which facilitates ion migration.[8, 69, 75] Especially, in the case of PEO-based solid polymer electrolyte containing the most stable lithium complexes among the atoms mentioned above, the Li ions transport is coupled with segmental dynamics of PEO chains through coordination bonds between PEO chain and the salt and are transferred through hopping provided by the segmental motion of the polymer chains between any two adjacent coordinating sites in the intra as well as inter chain movements as depicted in figure 2.11.

It is also very important to remind that that ion conduction is accepted to primarily occur in the free volume of the amorphous phase where ion transport is highly coupled with

segmental dynamics, [8, 15, 18, 76] Therefore, the ionic conductivity of solid polymer electrolytes based on polymer hosts with semi-crystalline nature, such as PEO-based electrolyte (Figure 2.9), has been also impacted by the presence of phase transformations depending on the temperature such as the formation of crystallization at temperatures below its melting temperature ($T_m = 60$℃)[8], which restricts the segmental motion of the chains and hinders the ionic conduction,[8, 29, 49] whereas At above the melting point, the polymer electrolyte is fully amorphous state in which the polymer chains are flexible and could facilitate the ion migration.[8, 49]

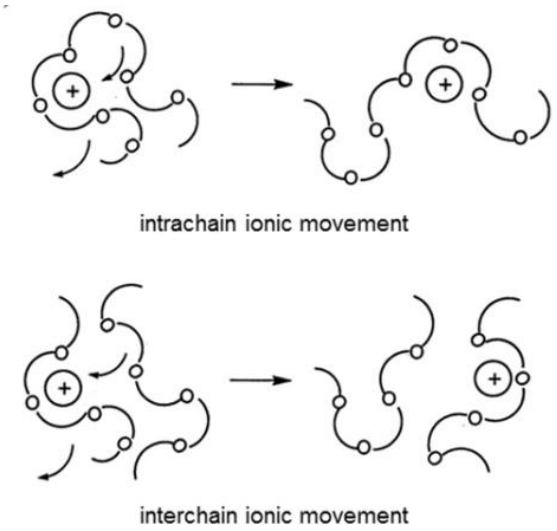

Figure 2.11: The schematic representation of inter and intrachain transportation for Li ions assisted by segmental motion in a PEO-based polymer electrolyte above the glass transition temperature of PEO.[49]

Although several methods such as Arrhenius and Vogel–Fulcher–Tammann models have been developed to capture the relationship between ionic conductivity as a function of temperature in polymer electrolytes,[8, 49, 69] the best model to describe this relationship is proposed by the Vogel–Fulcher–Tammann (VFT) equation given as:[8, 29, 45, 49, 69]

$$\sigma = \sigma_0 \, exp^{\left(\frac{B}{T-T_v}\right)} \tag{2.7}$$

where σ_0, B, and T_v are VFT constants for a given component in a particular electrolyte. They are attributed to the factors related to the ionic conductivity at the equilibrium glass transition temperature, the pseudo activation energy of conductivity which is estimated by the relationship of $E_a = R * B$ where R is the universal gas constant, and the ideal glass transition temperature at which the available free volume can be neglected,

respectively. Eventually, it can be summarized that Li ion transportation in a solid polymer electrolyte happens in the free volume of the amorphous phase of the polymer matrix through ion hopping between coordination sites, which is considerably linked with the polymer segmental dynamics.

Now, in the following part of this thesis, the new approach using the architectural variations of the PEO will be presented and discussed in detail about how to improve to increase ionic conductivity, mechanical strength, chemical and thermal stability in PEO-based solid polymer electrolytes.

2.3.4.2.3 A New Approach – Topological Variations in PEO-based Solid Polymer Electrolytes

As discussed above, the fundamental challenging drawback associated with PEO-based electrolytes is the high degree of crystallizations of PEO chains at room temperature, reducing chain dynamics and ionic conductivity significantly ($\sim 10^{-6} - 10^{-8}$ S/cm)[8] whereas when the temperature is increased above its melting temperature ($T_m = 60$℃)[8], the ion transport is considerably increased up to the values revolving around (10^{-3} S/cm)[8] due to melting crystals, but this comes with a disadvantage, a dramatic decrease in the mechanical strength, both of which limit its usage commercially in battery applications over a wide range working temperature.[18] Thus, Therefore, the studies proposed have been primarily focused on enhancing both the ionic conductivity and mechanical toughness simultaneously through various approaches and modifications in the PEO-based SPEs. These different methods and modifications of the PEO-based electrolytes could be classified in the following five major categories:

1. Blending PEO with another rigid polymer with high glass transition temperature where the fundamental goal is to develop the mechanical properties of the PEO without slowing down segmental dynamics of the PEO, mobile component, hence not decreasing the ionic conductivity.[8, 18]

2. Preparation of crosslinked polymer networks and synthesis of new and various PEO-based copolymers in order to reduce crystallization to enhance the ion transportation with sufficient mechanical strength.[19, 20]

3. The addition of inorganic and/or organic additives, with the objective of decreasing the crystallization ability of the PEO chains and increasing mechanical characteristics of the

electrolyte without compromising the ionic conductivity, usually called as polymer composite based electrolytes.[9, 21]

4. The incorporation of topological variations in the polymer architecture for suppressing PEO crystallization with the objective of increasing ionic migration through increased free volume provided by the architectural variations such as branching.[8, 18]

5. Use of modifications with various salt concentrations and chain lengths for the host polymer in PEO-based electrolyte to optimize the electrochemical properties.[8, 51]

Of these major categories, among the studies investigating blending linear PEO with another polymers,[7, 18, 77, 78] the most widely used is polymer poly(methyl methacrylate) (PMMA) associated with a high glass transition temperature (T_g). Addition of PMMA into PEO considerably developed the mechanical properties of PEO/PMMA blends, making the liquid-like behavior of PEO to a more solid-like behavior. [18, 79] Furthermore, because of a slight attractive interaction between PEO and PMMA (χ ranges between -0.005 to -0.001),[80] the blend could be thermodynamically miscible up to 370 K[81], which led into elimination of the PEO crystallization effectively in blends as shown in Figure 2.12. However, despite these advantages provided by PMMA, the incorporation of PMMA also resulted in a significant disadvantage that is tremendous slowdown of linear PEO segmental dynamics which could be attributed to the high interpenetrability of these linear polymers and the large difference between the T_g's of the homopolymers ($\Delta T_g \sim$200 K).[82-84] This decreases the ion transportation drastically since it fundamentally happens in the amorphous phase, and is coupled with the segmental dynamics,[8] therefore remains as a challenging problem for the aspect of blend based electrolyte performance.

Another promising method is to distribute inorganic nanoparticles (e.g., SiO_2) into the PEO polymer electrolyte to fundamentally impede the crystallization of the polymer chains and improve the mechanical properties of the polymer matrix.[6, 9, 21-23, 85-88] Other benefits of incorporation of the passive inorganic silica nanofillers into PEO could be facilitated ionic dissociation owing to the Lewis acid-base interaction between the surface polar groups of the inorganic silica nanofiller and the ionic species in the electrolyte and increased ionic transportation which could be due to the additional conducting sites composed of the interfacial region between the particles and the polymer matrix.[49, 89-91]

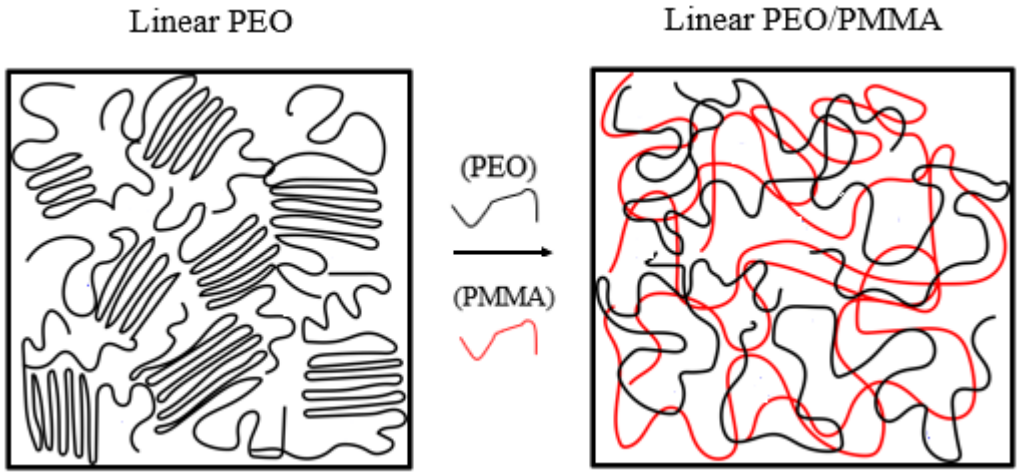

Figure 2.12: The schematic for semi-crystalline nature of pure PEO and complete elimination of the PEO crystallization with the incorporation of PMMA in linear PEO/PMMA blends.[8]

Although addition of silica particles into linear PEO was performed and has been successful in increasing mechanical strength of the polymer matrix and reducing of the crystallization effectively as shown in Figure 2.13, the ionic conductivity was lowered significantly as high as by an order of magnitude when compared to pure PEO based electrolytes. Therefore, these composites need to be investigated more with the aim of enhancing the ionic conduction.

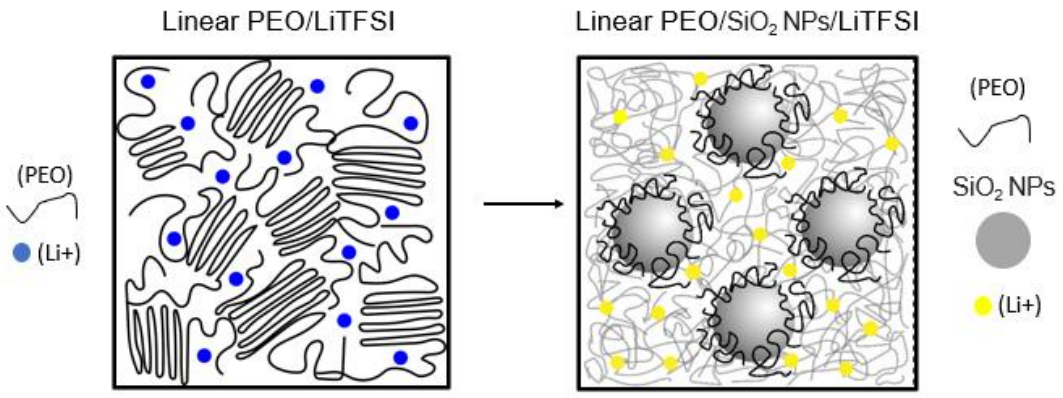

Figure 2.13: The schematic for semi-crystalline nature of pure PEO and the elimination of the PEO crystallization with the incorporation of Silica nanoparticles in linear PEO based composite electrolytes.

Although these previous studies provided significant amount of knowledge in comprehending linear PEO/PMMA blend based as well as linear PEO/Silica composite based solid polymer electrolytes including LiTFSI salt, however they did not incorporate the architectural variations of PEO in these SPEs further improve the electrolyte performance including ionic conductivity and mechanical strength which could be enhanced when non-linear PEO architectures, instead of widely used linear chains in both blend and composite electrolytes, are used, [12, 92-94] because, several previous studies investigating the dependence of crystallization and free volume on non-linear PEO architectures revealed branched PEOs had lesser degree of crystallinity, slower crystallization kinetics, enhanced free volume when compared to their linear counterparts.[16, 21, 51, 71, 92, 93, 95-98] In other words, these former findings suggest that using non-linear PEO architectures can increase the fraction of amorphous PEO phase with increased free volume, which could result in facilitated transportation of Li^+ ions with the tremendous potential to increase the ionic conductivity in these SPEs, leaving the critical fundamental questions in relation to the application of the architectural variations in these blend and composite electrolytes on the crystallization, the segmental dynamics, nanoparticle dispersion and correspondingly, the ionic conductivity and mechanical properties unanswered, thus needs further investigation.

Even though effect of the changes in PEO architecture in PEO/PMMA and PEO/silica based electrolytes containing LiTFSI salt, the architectural changes in neat PEO/LiTFSI based SPEs have been applied by various studies with the goal of improving Li^+ ion conductivity.[8, 13, 15, 16, 18, 99, 100] In almost all of these important studies, the enhancement in the ionic conductivity was fundamentally attributed to the increased amorphous fraction and free volume provided by the characteristics of non-linear topologies along with the salt concentration particularly optimized for each electrolyte system when used in preparing these SPEs. [8, 13, 92-94] As mentioned in Figure 2.8, the ionic conductivity in an SPE could be strongly dependent on the salt concentration. Increasing salt content, also known as salt molar ratio, generally results in enhancing the ionic conduction because of mainly increased salt dissolution and free ions, however further increase in the salt loading decreases the ion transportation which could be attributed the formation of ion pairs and aggregates due to increased interaction between the ions.[8, 14, 29]

The salt molar ratio that maximized the ionic conduction for linear PEO based electrolytes was [Li^+]/ [EO] ratio of 0.085[8], but this ratio could be architecture-dependent, which means it needs further investigation when non-linear PEO architectures are employed to enhance the performance of the homopolymer and blend-based SPEs. Additionally, since PEO is highly semi-crystalline, forming different variations of phases depending on composition, temperature, and the salt concentration when used in through different methods and modifications in polymer electrolytes, the interdependence of ionic conductivity and the phases and proportion of these phases present has also attracted a great amount of interest in PEO based electrolytes. [57, 101]

To observe these changes in the phases which could importantly affect electrolyte properties such as ionic conduction and mechanical strength, it is very crucial specifically to draw first a phase diagram for each PEO electrolyte system investigated that could clearly present which phases are present in the system based on composition, temperature, and salt concentration. Although several studies investigated the phase diagrams of PEO systems with most used salts for solid polymer electrolytes salts including primarily lithium hexafluorophosphate ($LiPF_6$), lithium triflate ($LiCF_3SO_3$), lithium tetrafluoroborate ($LiBF_4$), lithium hexafluoroarsenate ($LiAsF_6$), lithium perchlorate ($LiClO_4$), and lithium bis(trifluoromethanesulfonyl)imide (LiTFSI) and helped our understanding of these systems, [101-105] architectural variations have not been taken into account in forming these phase diagrams related to PEO/LiTFSI systems, which could also dramatically affect the degree crystallization, segmental dynamics, ion dissolution, ion pairing, thus impacting the phase diagrams and electrolyte characteristics essentially ionic conduction and mechanical strength.

With all being said, as could be seen in the discussions above, the previous studies have been leaving the critical fundamental questions about the effect of polymer architecture in these electrolytes on the crystallization, the segmental dynamics, optimized salt concentration, phase behavior, nanoparticle dispersion and correspondingly, the ionic conductivity and mechanical properties unanswered, hence the main objective of this thesis is to investigate these factors more extensively in a more systematic way in PEO/LiTFSI, PEO/PMMA/ LiTFSI blend, and PEO/Silica/LiTFSI composite based electrolytes.

Chapter 3 Experimental Apparatus and Characterizations Techniques

In this chapter, the physical and electrochemical characterization techniques for the samples as well as production of various polymer membranes and electrolytes are described in detail.

3.1 Characterizations techniques

3.1.1 X-ray Diffraction (XRD) measurement

The structural characterization of most materials including polymers is performed through the diffraction of X-rays associated with a wavelength comparable to interatomic distance in materials with crystals. The reflections of x-rays arising from the crystal planes with a spacing of d happen when the constructive interference of the reflections occur fulfilling the Bragg's law given as:[8, 45, 49]

$$2dsin\theta = n\lambda \tag{3.1}$$

where d accounts for the spacing of the atomic lattice crystal planes, θ stands for the angle between the X-ray beam and the planes, λ is the wavelength of the X-ray, and n is an integer.

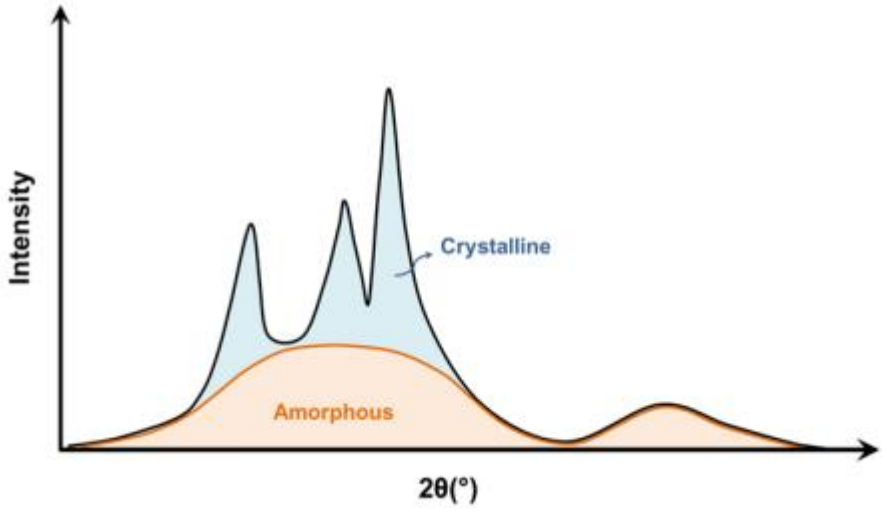

Figure 3.1: Representation of an XRD pattern for the semi-crystalline polymer with amorphous and the crystalline diffraction peaks.[49]

The XRD patterns of a semi-crystalline polymer are characterized by the broad amorphous peaks and the crystalline diffraction peaks satisfying the Bragg's law as shown in Figure 3.1. Knowledge of the Bragg peaks fulfilling the Bragg's law helps us

identify the type of the unit cell for the crystal structures and combining that with the information of the d spacing allows us to calculate the lattice parameters of the crystals. In this thesis, crystal structure and phase composition of the materials are characterized via X-ray diffraction (XRD) using D8 Advance (Bruker Co.) with Cu Kα X-ray source (1.54 Å) as can be seen in Figure 3.2.

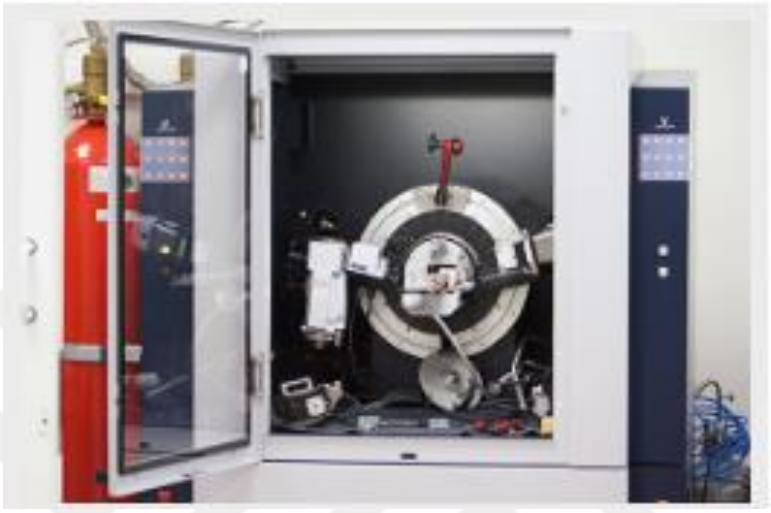

Figure 3.2: The Bruker D8 advance diffractometer XRD system.

3.1.2 Differential Scanning Calorimetry (DSC) and Temperature-Modulated Scanning Calorimetry (MDSC) measurements

Differential scanning calorimetry (DSC) is a conventional thermal analysis technique which has been based on linear temperature programme modulated by a small perturbation to understand the structure and morphology of polymeric materials including melting temperature, glass transition temperature, heat of fusion, latent heat of melting, specific heat or heat capacity, crystalline phase transition temperature etc.[8, 45, 49, 106] In a modulated differential scanning calorimetry (MDSC) which is developed extension of DSC, a sinusoidal modulation is preferred over the conventional linear heating or cooling ramp to yield increased sensitivity for detecting weak transitions and melts and also separates complex transitions into kinetic and thermodynamic components.[107, 108]

In both methods, the difference in the amount of heat required to increase the temperature of a sample and reference is measured as a function of temperature. The figure 3.3 shows phase transition processes during heating and cooling encountered in a typical DSC such

as glass transition temperature, melting crystals and crystallization with corresponding enthalpies.

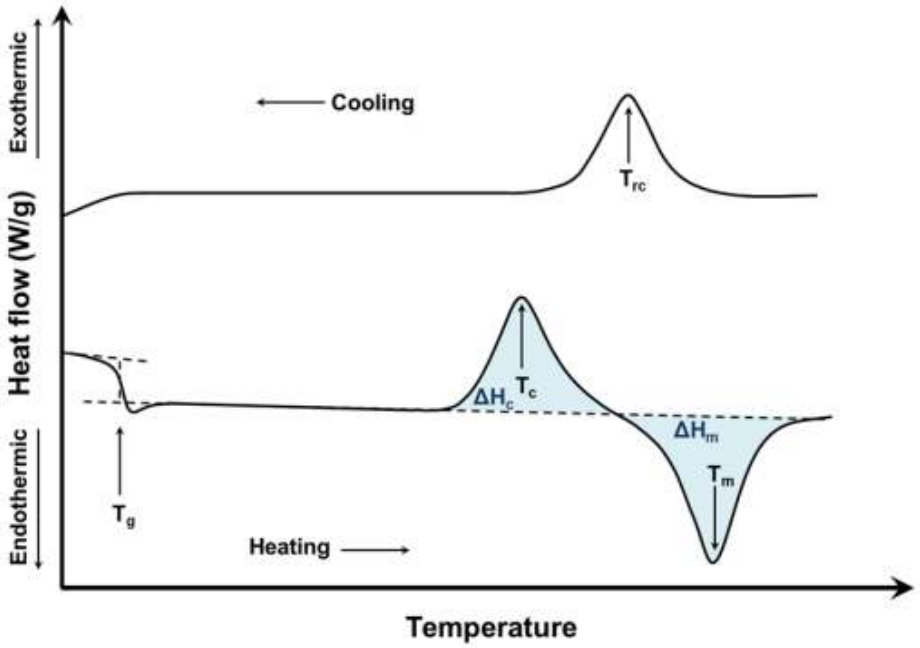

Figure 3.3: Schematic representation of A typical DSC thermogram including phase transition processes with corresponding enthalpies.[49]

The degree of crystallization (X_c) in percent for the polymeric material could also be estimated using the relationship:[8, 49]

$$X_c = \left(\frac{\Delta H_m}{\Delta H_c}\right) * 100 \tag{3.2}$$

where ΔH_m stands for the melting enthalpy of the sample estimated from DSC and ΔH_c is the melting enthalpy of completely crystalline of the material. All DSC experiments in this thesis are conducted with a TA Instruments DSC25 instrument equipped with a liquid nitrogen cooling system given in Figure 3.4 and an aluminium pan was used as the reference.

Figure 3.4: TA Instruments DSC25 instrument equipped with a liquid nitrogen cooling system.

3.1.3 Broadband Dielectric Spectroscopy (BDS) measurement

Broadband DS (BDS) which is a very powerful and excellent method to explore the collective relaxation phenomena and to study the electrical properties of the material of interest such as polymers, composites, and nanomaterials is depend on the interaction of an external field with the electric dipole moment of the sample sandwiched between gold-coated electrodes as shown in Figure 3.6 and represented by permittivity values of the sample.[48, 49, 109] In a BDS, the dielectric properties are measured over a wide range of frequencies ranging around 10^{-5}–10^{12} Hz under different temperatures, pressures, and environmental conditions, allowing one to monitor a large variety of mechanisms at various timescales, which makes it more advantageous in comparison with similar techniques used to study molecular dynamics.[109, 110] A typical illustration of the dielectric function with respect to wide range frequency of the electric field is given in Figure 3.5, which has certain characteristic domains such as electrode polarization (EP) at low frequencies usually due to ion accumulation at the electrode-electrolyte interface and relaxation arising from polymer segmental or secondary relaxations occurs at high frequencies.

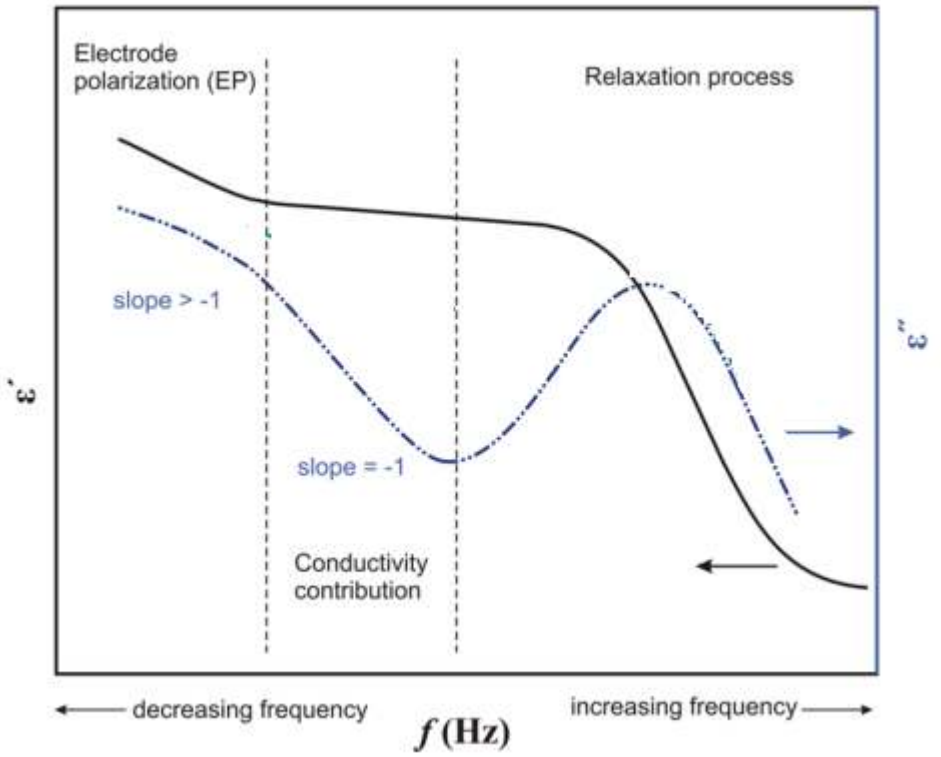

Figure 3.5: A typical illustration of the dielectric function with respect to wide range frequency obtained in a BDS experiment.[49]

The dielectric function is a complex number composing of dielectric permittivity (ε′) associated with the polarization of the polymer electrolyte under the electric field, and the dielectric loss (ε″) attributed to the fluctuations of molecular dipoles and the motion of charge carriers.[48, 49, 110] In this study, dielectric relaxation spectra are obtained in the frequency range of $10^{-2} - 10^{7}$ Hz and the temperature range of 30℃ to 90℃ using an Alpha A analyzer (Novocontrol Co.) shown in figure 3.6.

3.1.4 Electrochemical Impedance Spectroscopy (EIS) measurement

Electrochemical Impedance Spectroscopy (EIS) measurement is one of the fundamental methods to evaluate performance of electrolytes in which the magnitude and the phase relation of an AC current is monitored in response to an applied low-amplitude fluctuating voltage.[45, 49, 111] A sinusoidal voltage is employed to the sample and the resulting current oscillation recorded where the current signal has a phase separation when compared to the voltage as shown in figure 3.7.

Figure 3.6: The Alpha A analyzer (Novocontrol Co.) equipment for Broadband Dielectric Spectroscopy.

Based on this relationship, two parameters that are in requirement to have a relationship the voltage to current are defined, which are found by taking the ratio of the maximum voltage to the maximum current (V_{max}/I_{max}), known as opposition to the flow of charge and phase difference (θ) between the two waves, combination of which used to find the impedance, Z of the cell. Since both the magnitude and phase angle of the impedance are controlled by the employed frequency, electrochemical impedance spectroscopy measurement includes continuous observation over wide range of applied frequency.[29, 45]

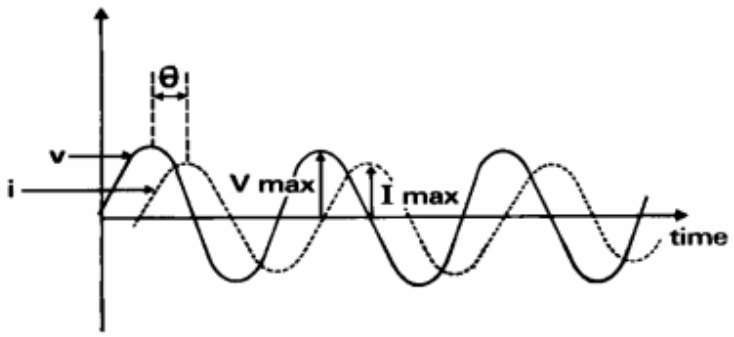

Figure 3.7: Phase separation indicating the relationship between alternating current and voltage signals with a phase difference (θ).[45, 49]

Additionally, the impedance which is a vector with magnitude and direction which is given in Figure 3.8 and also known as Nyquist plot when plotted over the frequency range can be defined using complex numbers as follows:

$$Z = Z_r + jZ_j \tag{3.3}$$

where Z_r and Z_j are defined to as the real and imaginary components, which could be attributed to the resistance defined with the Ohm´s law in DC regime and the reactive impedance depending on frequency.[29, 45]

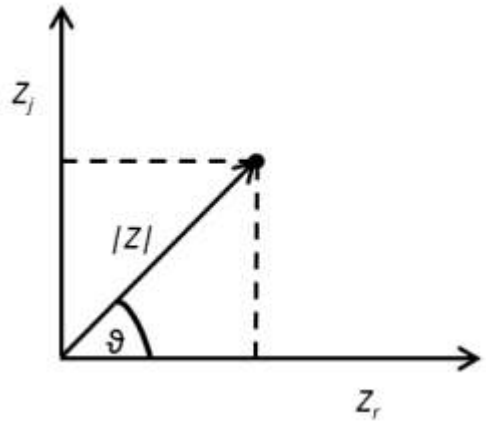

Figure 3.8: The impedance Z plot of a cell consisting of complex number where Z_r and Z_j are defined to as the real and imaginary components.[29]

In the case of a single resistor in which no phase separation would be available between the voltage and the current, there will be only real component in the complex impedance, resulting in its modulus simply being equal the resistance (R). Based on this resistance value, the ionic conductivity (σ, S/cm) of the electrolytes is estimated using the following relationship in which where d (cm) stands for the thickness of the electrolyte and A is defined as the area of the electrolyte membrane between the electrodes.:

$$\sigma = \frac{d}{R*A} \tag{3.4}$$

In this thesis, impedance characterization was carried out using an Autolab Potentiostat Galvanostat PGSTAT (Metrohm, Netherlands) in two-electrode configuration as displayed in Figure 3.9.

Figure 3.9: The Electrochemical Impedance Spectrometer.

3.1.5 Fourier Transform Spectroscopy (FT-IR) measurement

Fourier transform infrared spectroscopy (FTIR) in which the mathematical process (Fourier transform) to translate the raw data (interferogram) into the actual spectrum is applied, is a method to obtain the infrared spectrum of transmission or absorption of the sample. In infrared spectroscopy, some of the infrared radiation is absorbed by the sample and some of it is passed through.[112-114] The resulting spectrum represents the molecular absorption/transmission, forming a molecular fingerprint of the sample by identifying organic and inorganic compounds in the sample.[112-114] In a FTIR spectroscopy, data can be collected with high spectral resolution which is typically 4 cm^{-1} over a wide range, usually between 5000 and 400 cm^{-1} for mid-IR region wavelength.[112-114] In this study, Fourier transform infrared (FTIR) spectra of samples were recorded on a Thermo Scientific Nicolet iS10 FT-IR Spectrometer given in Figure 3.10.

Figure 3.10: The equipment for Thermo Scientific iS10 FT-IR.

3.1.6 Rheology measurement

One of the important aspects is related to the study of the flow behavior of the polymeric materials from the standpoint of polymer processing operations, which is also called as the science of flow or deformation of polymeric materials, namely polymer rheology.[115-117] In a rheology measurements, viscosity is often defined as the measure of the resistance of a material when under an applied stress.[115, 118]

When more complex materials such as polymer blends or polymer composites are being studied, rheology is used in order to properly study these complicated structures to optimize their properties at various conditions including changes in temperature, and polymer related factors such as molecular weight and architecture.[117] These materials are primarily defined by properties which are between purely elastic material and Newtonian fluids.[115, 117, 118] Anton-Paar's Modular Compact Rheometer 302 (MCR) shown as 3.11 is a rheometer composed of EC motor technique, low friction bearing, and an optimized normal force sensor for optimizing its performance. These line of MCR's could be fundamentally used to conduct different rheological tests, such as rotational, oscillatory, and a combination of both. The RheoCompass software is utilized for control of the system. The modularity of the system lets for the integration of a large range of temperature devices and application-specific accessories.

Figure 3.11: Modular Compact Rheometer (MCR 302).

3.1.7 Small-angle X-ray scattering (SAXS) Measurement

Small-angle X-ray scattering (SAXS) is a small-angle scattering technique which is sensitive to nanoscale differences in the electron density of a sample.[119, 120] When X-rays travel through the material with heating option at different levels, their elastic scattering at small angles is recorded.[119-121] This allows to determine the size, shape, and oligomeric state of the extensive range materials including for polymers, surfactants, colloids, proteins, porous media, nanoparticles, and nanocomposites on a size scale of one to several hundred nanometers.[120, 121]

In this work, SAXS measurements for the samples were performed using SAXSpoint 5.0 Anton Paar equipment shown in Figure 3.12.

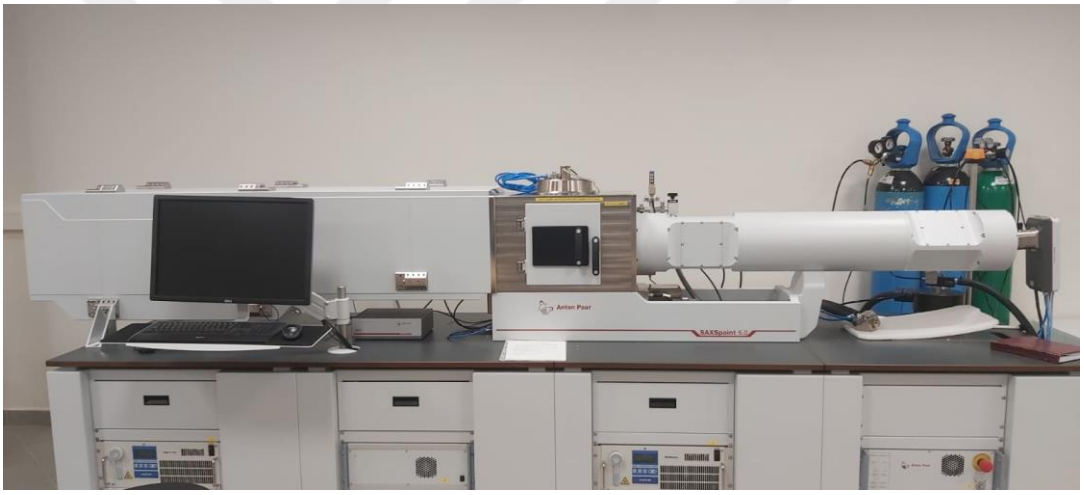

Figure 3.12: SAXSpoint 5.0 Anton Paar equipment.

3.1.8 Thermal Gravimetric Analysis (TGA)

The thermochemical stability of materials over an extensive range of temperature can be assessed by observing its gravimetric variation upon heating through a thermal gravimetric analysis (TGA) for which a typical schematic of a TGA equipment is illustrated in Figure 3.13.[29, 122, 123] The apparatus basically consists of a highly sensitive scale to measure weight changes, a programmable furnace to control the heat up rate of the sample, sample holder with a balance usually consisting of aluminium (for T < 600 °C), platinum or alumina for higher temperatures to place the sample as well as gas outlet/inlet parts to allow gas flow such as usually nitrogen (N_2) or Argon (Ar) through

the sample to remove volatile decomposition products.[29, 122, 123] In this study, the simultaneous thermal analyser NETZSCH STA 449 F3 Jupiter given in Figure 3.14 was used to carry out the thermal gravimetric analysis (TGA) of the samples.

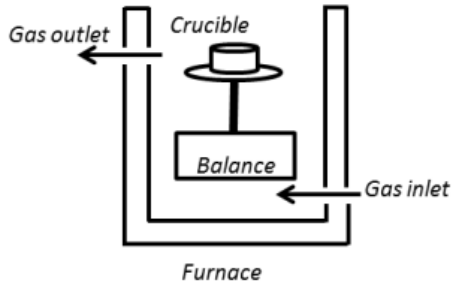

Figure 3.13: Typical illustration of a TGA equipment.[29]

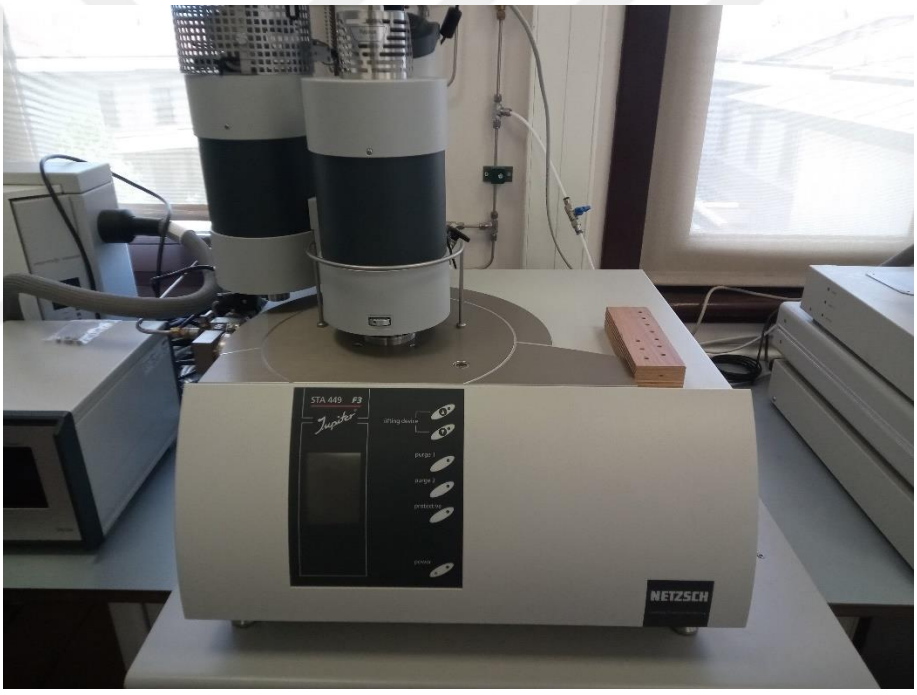

Figure 3.14: Equipment for Thermal Gravimetric Analysis (TGA).

3.1.9 Nuclear Magnetic Resonance (NMR) Measurement

Nuclear magnetic resonance (NMR) spectroscopy is an extremely developed characterization technique used to identify the molecular structure at the atomic level of a sample by analysing the chemical shift of the resonance frequencies of the nuclear spins in the test samples.[124, 125] Besides, it would be also possible to monitor the physicochemical properties including phase changes, conformational and configurational alterations, solubility, and diffusion potential in the material of interest. [124, 125]

Here, in this PhD thesis, we used Bruker 500 MHz NMR Nuclear Magnetic Resonance Spectrometer equipped with BBO double resonance solution state probe and BBO double resonance solid state probe to perform NMR Measurements. This device is also equipped with wide range sample temperature controller and sampleXpress autosampler for liquid state.

3.1.10 Dynamic Light Scattering (DLS)

Dynamic Light Scattering (DLS), based on the Brownian motion, is one of the non-invasive techniques commonly used to estimate the size distribution profile of macromolecules such as polymers in solution.[126-129] The Brownian motion causes collisions, which results in certain energy transfers related to the movements of the macromolecules.[130, 131] In this context, the higher the particle size is, the smaller the speed of the particles is. From these movements, hydrodynamic diameter upon on the size and shape of macromolecules could be predicted.[126, 129, 130] In this study, the MALVERN ZS – ZETASIZER shown in Figure 3.15 was utilized to calculate hydrodynamic particle size and distribution.

Figure 3.15: Equipment for measuring the hydrodynamic radius of polymers used in this work (DLS).

3.1.11 Positron Annihilation Lifetime Spectroscopy (PALS)

Positron annihilation lifetime spectroscopy (PALS) displayed in Figure 3.16 is a well-established and very sensitive non-destructive spectroscopy technique that allows studying a variety of phenomena and material properties on an atomic scale including free volume and its fraction.[132-135] The PALS spectra were divided using the computer program LT polymers into four lifetime components corresponding to annihilation of para-positronium (p-Ps), free positrons, and two ortho-positronium (o-Ps)

in the increasing order of their lifetime, respectively. τ_1 (the shortest-lived component with an intensity I_1) τ_2 (the intermediate-lived component with an intensity I_2) and τ_3 (the longest-lived component with an intensity I_3).[132-135] τ_1 and I_1 are associated with the annihilation of para- positronium (p-Ps), τ_2 and I_2 are allied with direct annihilation of positrons, and τ_3 with I_3 and τ_4 with I_4 are associated with pick off annihilation of ortho-positronium (o-Ps within the crystalline and amorphous regions of the polymers. In estimating the longest lifetime parameters, τ_1 and τ_2 were assumed as independent of free volume and used as fixed at 125 and ? ps, respectively. Ortho-positronium lifetime, τ_3 and τ_4 are known to be sensitive to calculate free volume and their corresponding hole sizes and I_3 and I_4 have straight correlation with the number of free holes in the materials. [132, 135, 136]

The relation between the radius of free volume hole (R) and pick-off annihilation lifetime is given by Tao-Eldrup Model, the radius was related with the lifetime τ by the equation below[133-135, 137];

$$\tau(ns)\frac{1}{2}\left(1-\frac{R}{R_0}+\frac{1}{2\pi}\sin\frac{2\pi R}{R_0}\right)^{-1} \tag{3.5}$$

Where $R_0 = R + \Delta R$ with $\Delta R = 0.1656$ nm as an adjustable parameter for a measure of electron layer inside the spherical potential well. By assuming spherical free volume, the size of free volume holes (V_f) is finally then calculated by using the following equation;

$$V_f = \frac{4}{3}\pi R^3 \tag{3.6}$$

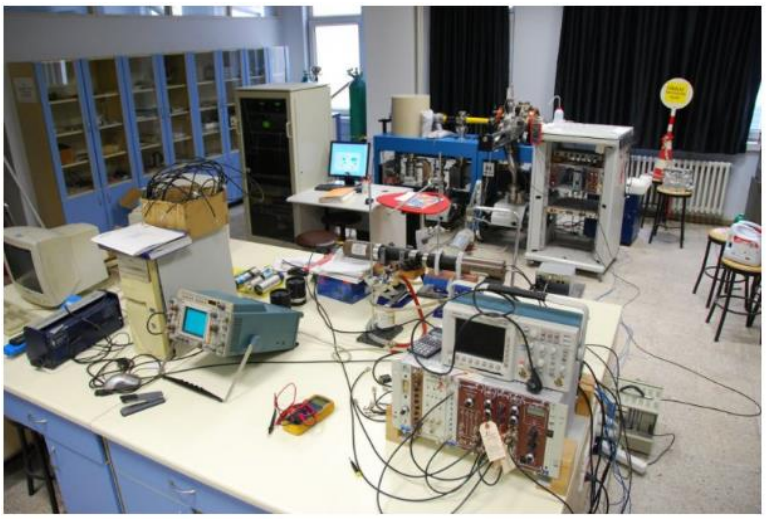

Figure 3.16: The Positron Annihilation Spectroscopy (PALS) for Free Volume Analysis.

3.2 Experimental apparatus

3.2.1 Glove box & MTI Split Cell holder for EIS Measurements

The each SPE disc was sandwiched between two stainless steel blocking electrodes under an argon atmosphere in a glove box given in Figure 3.17 (left figure) located at Koç University Boron and Advanced Materials Application and Research Center (KUBAM) and sealed in MTI Split Cell illustrated in Figure 3.17 (right figure) to carry out electrochemical properties of the samples.

Figure 3.17: (Left) Argon atmosphere controllable glove box used for assembling, (Right) MTI Split Cell on the right.

3.2.2 Special Mould for Sample Preparation of the polymeric membranes

This special mould shown in Figure 3.18 was used to fabricate the PEO membranes with different sizes in diameters under vacuum which later was used for the relative experiments and doped with LiTFSI salt for the electrochemical characterization.

Figure 3.18: Illustration of the Special Mould used for Sample Preparation of the polymeric membranes.

INTRODUCTION

Polymers and their blends have been widely applied in various industries from aerospace and electric vehicles to consumer electronics and energy storage devices.[52, 138-142] For most of these applications, lithium-ion batteries play a significant role, in which electrolytes are very critical for transporting positive lithium ions between electrodes.[143] Liquid electrolytes that are currently in use are often flammable, volatile, toxic, and more prone to short circuit and leakage, leading to environmental and safety concerns.[53, 144, 145] To overcome these disadvantages, solid polymer electrolytes (SPEs) have emerged as alternative systems for the fabrication of sustainable lithium-ion batteries.[53, 144, 145] While SPEs provide decent mechanical stability,[11, 18] deformability[146] and biocompatibility,[147] their low ionic conductivity at room temperature ($<10^{-5}$ S/cm)[11] compared to the liquid electrolytes ($\sim10^{-2}$ S/cm)[11] remains as a major challenge for their commercial use.[12]

Linear poly(ethylene oxide) (PEO) has gained significant attention as SPE[12, 17, 18, 76] due to its excellent characteristics including fast segmental dynamics as well as the ability of form complexes with a wide range of different lithium salts. It is generally believed that ion conduction occurs in the amorphous phase where ion transport is coupled with segmental dynamics.[7, 12, 18, 51, 71, 76-78, 148] At room temperature, however, PEO is a semi-crystalline polymer with an ionic conductivity ranging between $10^{-6} - 10^{-8}$ S/cm,[17] in which crystalline regions impede ion transport (see Figure 1a for scheme). The ionic conductivity increases up to 10^{-3} S/cm above its melting temperature ($T_m = 60$°C),[17] yet with severe reduction in mechanical strength, which limits its application in a solid-state battery. To overcome these drawbacks in relation to crystallization and mechanical stability, one method is to blend PEO with another polymer that can provide mechanical rigidity and eliminate crystallinity.[7, 18, 77, 78] In this sense, a high glass transition temperature (T_g) polymer poly(methyl methacrylate) (PMMA) is commonly used (Figure 1b). Incorporation of PMMA into PEO significantly increased the mechanical properties, such as storage modulus, of PEO/PMMA blends, making the liquid-like behavior of PEO to a more solid-like behavior. [18, 79]

The elimination of crystallinity requires thermodynamic miscibility of the polymers. Due to a slight attractive interaction between PEO and PMMA (χ ranges between -0.005 to -0.001),[80] the system is shown to be miscible up to 370 K.[81]

Moreover, studies showed that crystallization of linear PEO in the blends is observed at concentrations exceeding 30% PEO.[149, 150] Also, the large difference between the T_g's of the homopolymers (ΔT_g ~180 K) causes significant slowdown of linear PEO segmental dynamics with the addition of PMMA.[82-84]As the lithium-ion transport occurs primarily in the amorphous phase, and is coupled with the segmental dynamics, increasing the amount of PEO without forming crystalline regions at higher concentrations and accelerating the segmental dynamics in the amorphous phase in the blend could further enhance the electrolyte performance. In this study, we show that both miscibility and dynamics of PEO in the blends with PMMA could be significantly enhanced when 'non-linear' PEO architectures, instead of commonly used linear chains, are employed.

Several studies on the 'neat' PEO showed the effect of polymer architecture on crystallization.[12, 92-94] Zardalidis and co-workers[93] investigated the dependence of crystallization on molecular weight and architectures including linear and ring topologies and revealed that PEO with ring architecture exhibited lower crystallinity and apparent melting temperature compared to the linear analogue due to its more strained structure. In another work, Chen et al.[151] compared the degree of crystallization in linear and star PEO architectures (3-arms and 4-arms) and reported the crystallinity of star polymers was approximately 20% lower. Similarly, Coppola and co-workers studied crystallization of poly(ethylene oxide) star polymers of varying arm number and size and unveiled a slower crystallization kinetics of the stars compared to their linear analogues due to the high degree of branching with slowed diffusivity.[92]

Moreover, studies conducted by Yao et al.[94] and Lee et al.[16] showed that the crystallization of hyperbranched Poly(ethylene oxide) effectively decreased when compared to linear one because of the increased number of branching. These previous findings suggest that using non-linear PEO architectures can increase the fraction of amorphous PEO phase in which the ions are transported within SPEs, therefore, the PEO/PMMA blends have a significant potential to enhance the ionic conductivity when the nonlinear PEO architectures are used is the SPEs.

Also, the effect of free volume, which results from the free spaces between monomers along the (same or different) polymer chains,[21] on ionic conductivity was investigated by various studies in PEO-based SPEs.[21, 51, 71, 95] The increase in free volume in the polymer matrix resulted in assisted ion migration, enhancing the ionic

conductivity in these SPEs. Recent studies confirmed that the hampered crystallization of PEO due to the addition of nano-fillers or other polymers could increase the free volume.[80, 152] Furthermore, it is known that increasing number of branches in the non-linear topologies resulted in a decrease in crystallization, increasing free volume.[97, 98] The ion-migration within SPEs, known as hopping mechanism, is well established, in which the available free volume helps lithium ions to transport through hopping provided by the polymer segmental motions.[21, 51, 71, 95] In this manner, Utpalla et al.[21] investigated the role of free volume and segmental dynamics on the ion conductivity of PEO based SPEs and found the increase in free volume with the addition of inorganic nano-fillers enhances the free volume fraction and decreases the crystallinity of pure PEO by increasing free available spaces between polymer chains, thus promotes the ionic conductivity. Similarly, Michael et al.[153] reported that the polymer chains leaning to coil up around nano-fillers added into PEO pawed the way for the transportation of Li^+ ions by providing the additional free volume as a result of decreasing crystallization. It is known that increasing number of branches in the non-linear topologies can result in an increase in free volume[97, 98] due to enhanced number of chain ends compared to the linear chains.

Here, we take the advantage of enhanced free volume due to increased number of free end-groups in non-linear PEOs and suppressed crystallization arising from branching as well as PMMA addition to facilitate transportation of Li^+ ions in PEO/PMMA blend electrolytes.

Very recently, the ionic conductivity in PEO/PMMA based solid polymer electrolytes (SPEs)[18] was investigated with star PMMA and linear PEO. Glynos and his co-workers revealed that the star PMMA in blends with linear PEO led to extremely fewer contacts between PEO and PMMA segments in comparison to the linear PMMA/PEO blends, giving rise to faster PEO segmental dynamics, thus resulting high ionic conductivity.[18] However, the key fundamental questions about the role of polymer architecture on the polymer-polymer miscibility, the component segmental dynamics and correspondingly the ionic conductivity remain unanswered. In this work, we used various PEO topologies as shown in Figure 4.1 including linear, 4-arms, 8-arms, hyperbranched (6^{th} generation, 6G) and bottlebrush, and dispersed in linear PMMA matrices to make SPEs and investigated the role of polymer compactness, branching and

interpenetration on phase behaviour, local dynamics, and ionic conductivity in polymer blend electrolytes.

4.2 Experimental methodology

In this part, materials used in this study are explained and defined, respectively.

4.2.1 Materials

The PMMA homopolymer (MW~120kDa), linear PEO, hyperbranched (6^{th} generation) PEO, and Lithium bis(trifluoromethane)sulfonamide, LiTFSI salt were purchased from Sigma-Aldrich. 4-arms and 8-arms star PEO were supplied by Creative PEGWorks. The bottlebrush PEO was synthesized in Center for Nanophase Materials Science (CNMS) of Oak Ridge National Laboratory. All polymers were used as received without modification. Chemical structure of the PEOs is provided by figure 4.2. Table 4.1 displays their functionality, molar masses, and dispersities.

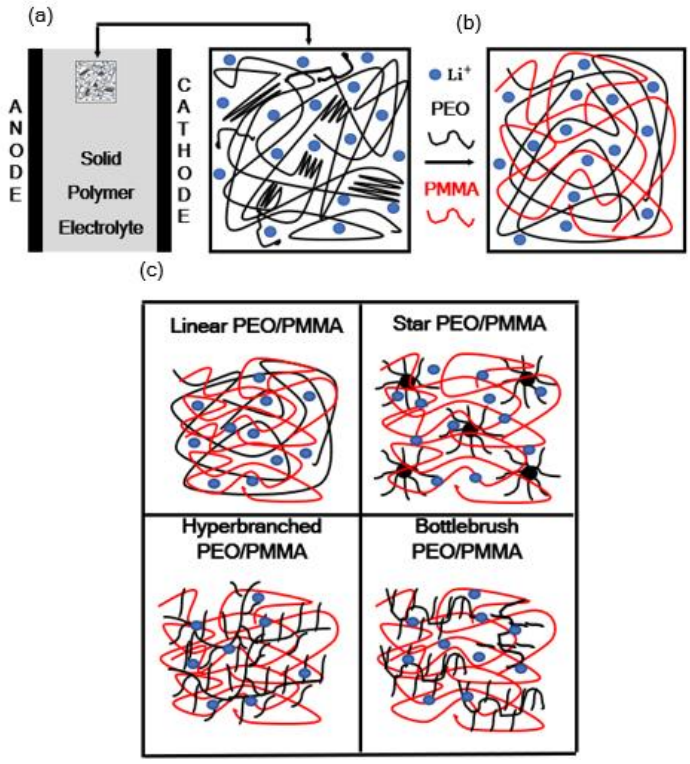

Figure 4.1: (a) Schematic depicting Li^+ ions in a semi-crystallized PEO electrolyte. (b) Sketch of an amorphous blend of Linear PEO/PMMA doped with Li^+ ions. (c) Schematic representation of linear and various non-linear topologies of PEO in blends.

Table 4.1: Molecular characteristics of the PEO samples used in this study.

PEO architecture	Sample ID	Functionality (f)	MW [kg/mol]	M_{arm} [kg/mol]	Dispersity ($Đ$)
Linear	L20	2	20	10	1.10
4-arms star	4F20	4	20	5	1.03
8-arms star	8F20	8	20	2.5	1.10
Hyperbranched	HB6G	6^{th} generation	35	NA	<1.5
Bottlebrush	BB	80	32	0.35	<1.4

4.2.2 Preparation of Salt-Free Blend Samples

Blends of various compositions of (PEO/PMMA) with topologies of linear (MW~20 kDa), 4-arms star (MW~20 kDa), 8-arms star (MW~20 kDa), HB6G (MW~35 kDa), bottle brush (MW~32 kDa) PEO as well as pure PEO and PMMA were prepared by the solution casting technique. Polymers at desired ratios were first dissolved in chloroform at 30 mg/ml. Then, the solutions were stirred with a magnetic stirrer at room temperature for 6 hours. The solutions were then cast onto either glass petri dishes, and evaporated slowly for overnight at room temperature. Then, the dry films were transferred into a vacuum oven and annealed for 48 hours at 150℃ to remove residual solvent. Finally, dielectric samples were prepared by hot pressing in a vacuum environment to form discs of 20 mm diameter and 200μ thickness.

4.2.3 Preparation of Polymer Electrolytes

The desired amount of the lithium bis(trifluoromethane)sulfonamide, LiTFSI, was dissolved in acetonitrile, stirred for 48 hours. Then the disc samples were doped with (Li/EO=0.085) LiTFSI by solution uptake. The electrolytes were first dried at room temperature for overnight in glovebox filled with Argon and annealed at 120℃ in vacuum oven for 48 hours to ensure complete removal of the solvent.

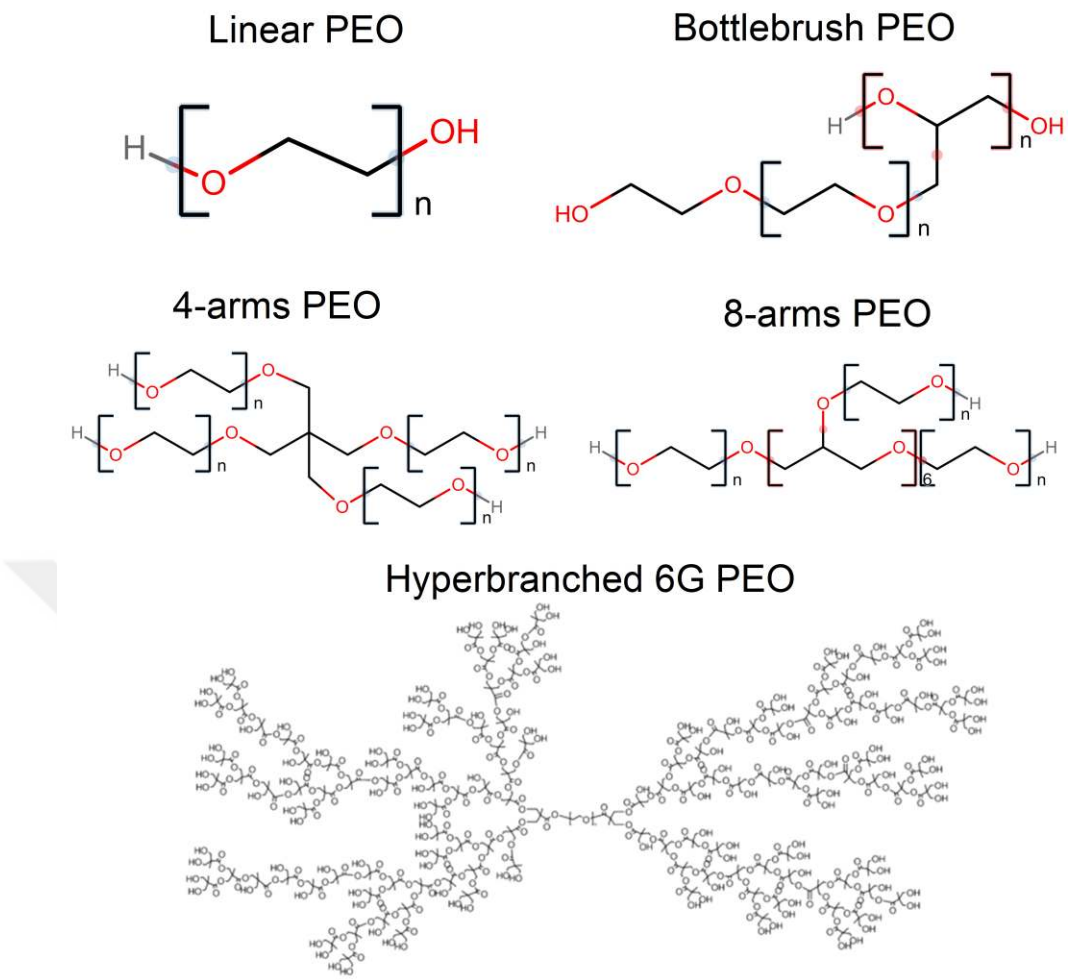

Figure 4.2: Chemical structure of the PEO polymers. The structure for the hyperbranched PEO was taken from the manufacturer (Sigma-Aldrich)'s page.

4.2.4 Characterization

X-ray Diffraction (XRD): The XRD patterns of the pure PMMA, PEO and PEO/PMMA blends were recorded using the Bruker D2 Phaser – X-ray diffractometer with Cu K (α) source. The diffraction data were obtained at room temperature with the Bragg's angles (2θ) varying from 10 to 50 degrees.

Modulated differential Scanning Calorimetry (MDSC): The temperature modulated differential scanning calorimetry (MDSC) samples were prepared by putting ~8-10 mg of material in aluminium pans provided by TA Instruments. MDSC experiments of the pure PMMA, PEO and PEO/PMMA blends were carried out with a TA Instruments DSC25 instrument equipped with a liquid nitrogen cooling system. An aluminium pan

was used as the reference. To get rid of the temperature history completely, all the samples were heated to 180 ℃ and waited there for 5 minutes. Samples were then quickly cooled down to -85℃ at the rate of 20 ℃/min. DSC scans were then collected during heating of the sample in modulated temperature mode at the ramp rate of 1 ℃/min with a modulation amplitude ± 0.5℃ and period of 60 s.

Broadband Dielectric Spectroscopy (BDS): Dielectric relaxation spectra are obtained in the frequency range of $10^{-2} - 10^{7}$ Hz and the temperature range of 30℃ to 90℃ using an Alpha A analyzer (Novocontrol Co.). BDS measurements for linear and non-linear PEO/PMMA blends were performed with a temperature increase of 10℃ and 30℃, respectively. At each temperature increase, the experiments were started once the temperature stability was reached within 0.05 K interval. After the experiments at high temperatures were over, we let the sample cool to temperatures lower than 50℃, and only then the new sample was placed into the sample holder for the next measurements.

Electrochemical Impedance Spectroscopy (EIS): Impedance characterization was carried out using an Autolab Potentiostat Galvanostat PGSTAT (Metrohm, Netherlands) in two-electrode configuration for all PEO/PMMA blend electrolytes. This arrangement was used to investigate electrode properties in solid-state systems.

The measurement frequency was varied between 1 Hz to 1 MHz. Each SPE blend disc was sandwiched between two stainless steel blocking electrodes under argon environment in a glove box located at Koç University Boron and Advanced Materials Application and Research Center (KUBAM) and sealed in MTI Split Cell to measure the complex impedance spectra. After waiting for the temperature stabilization of 0.1℃, the experiments were also carried out at various temperatures including 30, 60, and 90℃, respectively. The data was analysed to characterize real and imaginary impedances using the NOVA software.

4.3 Results and Discussion

In this section, we analysed the results and proposed a discussion in relation to the findings.

4.3.1 Effect of PEO Architecture on the Crystallization in PEO/PMMA Blends

The polymer characteristics are displayed in Table 4.1. The total molar masses of linear and star polymers are 20 kDa, and the molar masses of the hyperbranched and bottlebrush PEO are about 35 kDa due to excessive branching, yet the backbone molar masses are close to 20 kDa. We first investigate the crystallization of neat PEO homopolymers and their blends with PMMA using XRD at room temperature. Figure 4.3 displays the PEO wt% concentration dependent intensity profiles at the room temperature for blends with L20, 8F20 and BB PEO architectures and without salt (see the additional experimental detailed results for 4F20 and HB6G in Figure S1 in the SI). The peaks observed for the neat PEO samples at 2θ=19° (120-plane) and 23° (032-plane) confirmed the semi-crystalline nature of PEO[17, 18, 154] and are the characteristic peaks of monoclinic lattice as the primary crystal structure.[93] Furthermore, regardless of the structural changes in PEO topologies, the positions of these peaks did not change, implying the primary monoclinic crystal structure as well as relative d-spacing of the predominant (120) and (032) planes are retained. Additionally, we found the degree of neat PEO crystallinity for different architectures severely decreased with the number of branching.

The representative melting enthalpies and crystallinity ratios for various PEO architectures with different weight fraction of PEO blended with PMMA are indicated by Table 4.3.

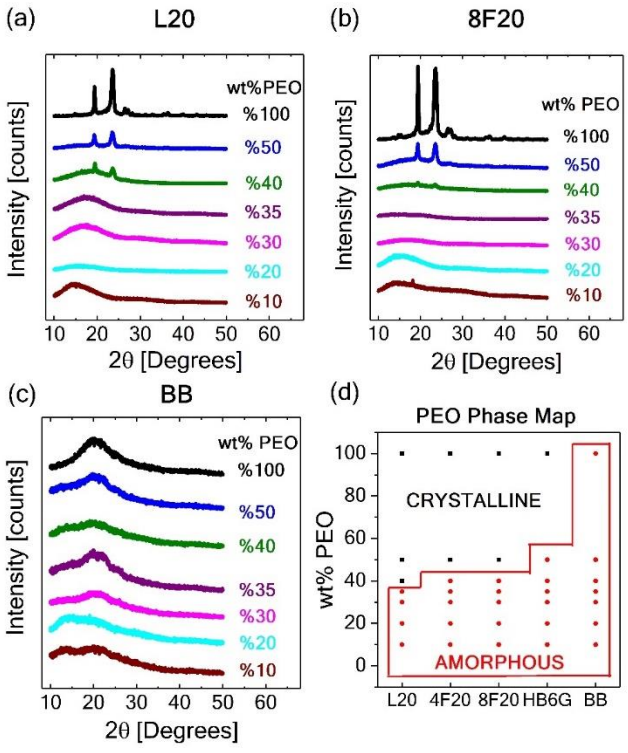

Figure 4.3: (a-c) XRD results for PEO/PMMA blends in different PEO wt% concentrations and with various PEO topologies: (a) linear, (b) 8-arms star, and (c) bottle brush. (d) Crystallization phase map for various PEO architectures in blends with PMMA with respect to extensive PEO weight faction.

The addition of PMMA resulted in suppression of semi-crystalline nature of PEOs drastically, as also shown in previous studies in linear PEO/PMMA blends.[150, 155-157] However, we show here that the degree of suppression changes differently based on the PEO architecture. The linear PEO blended with PMMA crystallizes over 35wt% PEO in the blends whereas in the case of non-linear architectures, the amorphous blends containing higher amount of PEO (up to 100%) can be formed. Specifically, in the case of 4-arms and 8-arms stars, the amorphous blends are obtained at 40% PEO concentrations, whereas this number can even reach up to 50% for the hyperbranched PEO. In the most extreme case, bottlebrush PEO (BB) was amorphous in its neat form and in blends with PMMA at all compositions, due to its densely grafted short side chains impeding formation of close-packed structure. Figure 3d displays the resulting phase diagram. The degree of crystallinity estimated using MDSC are displayed in Table S1. All these results indicate that the crystallization in PEO/PMMA blends can be eliminated more effectively using PEO chains with high degree of branching. To the best of our knowledge, such a architecture dependent crystallization in miscible blends is investigated for the first time in this work. As the ion transport is mediated by the amorphous phase of SPEs, this approach is of practical importance.

We chose 20% PEO concentration, where all blends are in the amorphous phase, to investigate the role of polymer architecture on dynamics, including glass transition, and segmental motion.

4.3.2 Effect of PEO Architecture on the Glass Transition

We first investigate the effect of PEO architecture on the glass transition in PEO/PMMA blends using modulated differential scanning calorimetry (MDSC). Figure 4.4a shows the specific heat capacities (Cp's) of neat PMMA and the blends with 20% PEO having different architectures. We found glass transition temperatures of neat PMMA and PEO with various architectures around 394 K and 220 K, respectively, in agreement with the previous reports (Additional Modulated differential scanning calorimetry (MDSC) results section for the details of T_g values for different PEO

topologies are summarized by Table 4.4).[7, 51, 77, 82, 158] Since PMMA is the majority component, the heat flow in the blends is overwhelmed by PMMA signal. It is seen that the PMMA glass transition temperature in the blends shifts to lower values due to enhanced mobility provided by low-T_g PEO segments. Even from the raw Cp data, it is evident that the transition is strongly architecture dependent.

Apart from the experimental techniques, several mathematical methods have been developed for estimating the glass transition temperature of mixtures from knowledge of the properties of the pure components. One of the most widely used equations for predicting glass transition temperatures of amorphous mixtures is the Fox equation given by the Eq.4.1:

$$\frac{1}{T_g(\phi)} = \frac{\phi}{T_g^a} + \frac{1-\phi}{T_g^b} \tag{4.1}$$

where $T_g(\phi)$ and T_g^a as well as T_g^b are the glass transition temperature of the mixture and of the components, respectively, and ϕ is the weight fraction of component a. This model estimates one T_g, around 340 K for all blend systems, accounts for the glass transition temperature of the mixture using T_g values of the neat components and their weight fraction in a binary polymer blend. However, we observed two glass transition temperatures (T_g's): one located at lower temperatures corresponding to the glass transition of the faster component, PEO, in the system and another one positioned at higher temperatures attributed to the slower component, PMMA. Although these polymers are miscible at macroscopic level, they are not homogenous at monomer level due to chain connectivity. Thus this forms a local heterogeneity, leading to concentration fluctuations in which some local regions spontaneously rich in one of the components in a binary polymer blend.[83] This results in an average composition of the local environment around any chosen segment in comparison with the bulk composition is enriched in the same species, called as effective concentration.[83] This results in two composition-dependent T_g's (namely 'effective' T_g's) in binary blends (see Modulated differential scanning calorimetry (MDSC) results section in the Supporting Information for the details of the Lodge-McLeish model).[83] To highlight the effective T_g's in the blends, the temperature derivative of the heat capacities are used (see Figure 4. 4b). We fit a Gaussian $\propto \exp[-(T-T_g)^2/\left(2(\Delta T_g)^2\right)$ to find T_g and the entire peak widths at

half-maximum height (ΔT_g) values more precisely.[159] The resulting effective T_g's are given in Table 4.2 and displayed in Figure 4.4c.

Table 4.2: T_g and the transition width (ΔT_g) for all polymer blends, and its electrolytes containing 20wt% PEO with various PEO architectures.

Sample	BLEND				BLEND ELECTROLYTE	
	PEO		PMMA		PEO	PMMA
	Tg,eff, K	ΔTg, K	Tg,eff, K	ΔTg, K	Tg,eff, K	Tg,eff, K
L20	248.03	38.09	333.15	29.07	259.69	342.12
4F20	244.15	45.23	338.73	59.8	248.72	347.68
8F20	240.62	30.56	330	22.29	245.75	344.38
HB6G	260	32.48	360.5	36.51	266.15	371.57
BB	218.65	20	387.93	8.94	221.7	388.5

In addition, in comparison of T_{g-eff} values of PMMA in the blends with the T_g of neat PMMA, we found T_{g-eff} values were greatly shifted to the lower values due to increased mobility provided by low-T_g PEO segments. We also observed this transition was highly dependent on the PEO architecture. It was seen the highest decrease in T_{g-eff} values of PMMA happened to be in blends with L20. The moderate increase in the number of branching in PEO architecture such as 4-arms and 8-arms stars slightly changed the degree of this decrease in T_{g-eff} values. As the degree of branching increased further for HB6G when compared to linear and star PEO topologies, the change in Tg-eff of PMMA in the blend became less intense because of lower interpenetration. Nevertheless, in BB PEO/PMMA blend-the most extreme case in terms of degree of branching, Tg-eff of PMMA showed the least deviation from Tg of its neat form due to densely attached very short side chains to the bottlebrush backbone. Higher architectural constraints result severe reduction in the monomer level mixing between PEO and PMMA chains. These findings are highly in accordance with our hypothesis that less interaction and interpenetration between PEO and PMMA was present in the case of non-linear PEO/PMMA blends.

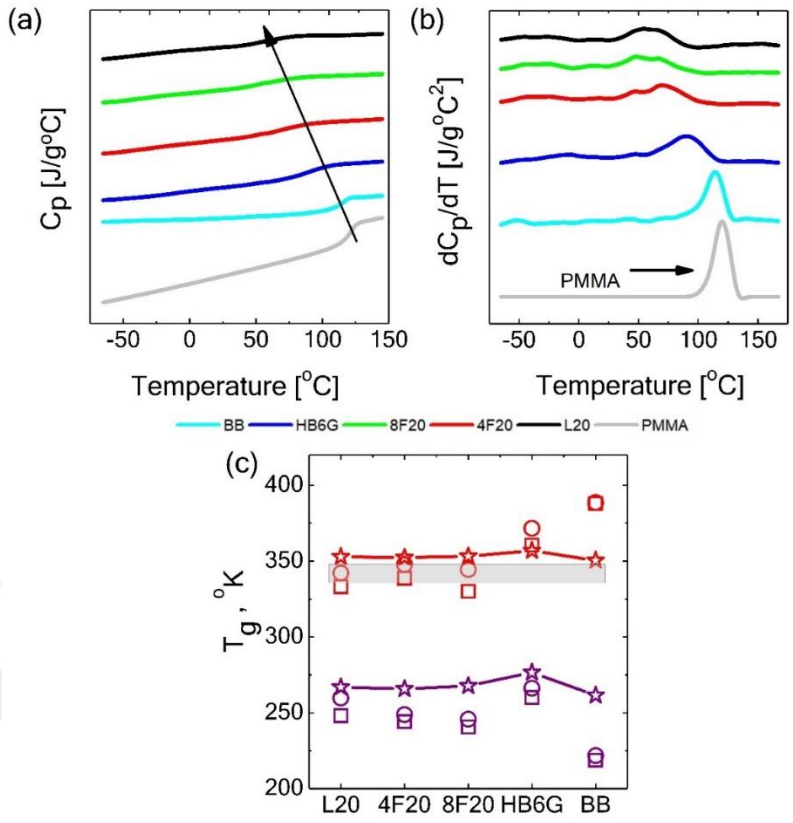

Figure 4.4: The dependence of the reversible heat flow (a) and its derivative (b) with respect to temperature for PEO with various topologies including linear, 4-arms, 8-arms, hyperbranched and bottle brush in blends with PMMA as well as neat PMMA. (c) The comparison of the experimental effective glass transition ($T_{g\text{-}eff}$) values for PEO and PMMA with the estimations obtained from DSC (Red and purple for filled squares and circles account for experimentally obtained values for $T_{g\text{-}eff}$ of PMMA and PEO for blends and its electrolytes, respectively), Lodge-McLeish model (Red and purple stars with lines account for LM model estimated values for $T_{g\text{-}eff}$ of PMMA and PEO for blends, respectively) and Fox model (Shaded region represent Fox model estimates for the blend T_g values).

We would like to emphasize that the Lodge-McLeish model has been tested by many studies with no emphasis on topological changes for these PEO/PMMA.[84, 159-164] Recently, Lodge et al.[84, 160] investigated the miscible blend system consisting of poly(ethylene oxide) (PEO) and poly(methyl methacrylate) (PMMA) over the entire composition range using differential scanning calorimetry (DSC) to further comprehend the existence of two glass transition phenomenon. In their work, two distinct glass transition temperatures were clearly found in the mid-composition range.[84, 160] In a

different work, Colmenero and co-workes[159] examined the same polymer blend system through Modulated differential scanning calorimetry (MDSC) which depends on the changes in the heat capacity (C_p) of polymer samples and the presence of two glass transition temperatures within a certain composition for the PEO/PMMA blend was validated. Other significant studies applying the Lodge and McLeish model to PEO/PMMA blends have also confirmed the presence of two effective glass transition temperatures for the PMMA in PEO/PMMA blends.[162, 163, 165] Our results are also consistent with these previous findings in terms of the existence of two effective glass transition temperatures. However, our experimentally obtained results through MDSC quantitatively differed. In this context, the Figure 4.4c shows the comparisons between experimentally obtained T_{g-eff} values for PEO and PMMA and the estimations obtained using the prevalent mathematical models including Lodge and McLeish (self-concentration model) and Fox model. Regardless of the different topological changes in PEO topologies, both Lodge-McLeish and Fox Models were overestimating T_{g-eff} values for PEO, however they were generally better at predicting T_{g-eff} values for PMMA in all blends investigated. It appears that the theoretical self-concentration formulations which have been commonly used for linear polymer blends need to be modified when estimating the effective T_g's in blends with non-linear topologies. Nevertheless, the research of this paper is not essentially interested in investigating the Lodge-McLeish model for non-linear polymer blends, which will be the subject of another work.

We finally analysed the PEO/PMMA/LiTFSI based polymer electrolytes for the same PEO topologies including linear, 4-arms, 8-arms, hyperbranched and bottle brush. The reversible heat flow (a) and its derivative with respect to temperature (b) for PEO/PMMA/LTFSI based polymer electrolytes with regards to various PEO topologies including linear, 4-arms, 8-arms, hyperbranched and bottle brush in blends are given in Figure 4.12. Based on the derivative of the reversible heat flow with respect to temperature, estimated T_g effective values for PEO and PMMA using the derivative of the reversible heat flow with respect to temperature are shown in Table 4.2. We observed the architectural dependent transitions in the T_{g-eff} values of PMMA for all blends containing lithium salt (given in dots symbols in Figure 4.4c), thus the changes in the segmental dynamics associated with different polymer architectures and observed in salt-

free samples in dielectric spectroscopy (discussed below) are effective also in the blend electrolytes.

4.3.3 Effect of PEO Architecture on the Segmental Dynamics and Ionic Conductivity

We next investigated the relaxation behaviour of the blends using broadband dielectric spectroscopy (BDS). Our aim here is to understand how different polymer topologies influence the segmental dynamics; thus, we use the salt-free blends at 20% PEO concentrations. Figure 4.5a and 4.5b display some representative dielectric spectra along with fits for neat PMMA and its 20wt% PEO blends at two different distinctive temperatures, specifically 328 K (lower than $T_{g,\,eff,\,PMMA}$) and 348 K (higher than $T_{g,\,eff,\,PMMA}$ for blends with linear and star PEOs). The dielectric loss spectra of PMMA and its 20wt% PEO blends (Figure 4.5a) at 328 K showed two processes, β-relaxation, and DC conductivity. However, at 348 K (Figure 4.5b) the α-relaxation of PMMA is also observed for L20, 4F20 and 8F20. Therefore, at 328 K, one Havriliak–Negami (HN) function was sufficient to define the PMMA dynamics for its neat form and respective blends with different PEOs whereas at 348 K, two Havriliak-Negami (HN) functions could define the relaxation involving β and α processes. In the frequency domain, the HN function is given as:[166]

$$\varepsilon^* = \varepsilon_\infty + \frac{\Delta\varepsilon}{\left[1+\left(\frac{i\omega}{\omega_0}\right)^a\right]^b} \tag{4.2}$$

where $\omega = 2\pi f$ is the angular frequency, and $\omega_0 = 2\pi f_0$ is a characteristic angular frequency related with the dielectric loss peak frequency (f_{max}). The relaxation strength $\Delta\varepsilon$ accounts for the difference between the real permittivity for low-frequency limiting value and that for high-frequency limiting value ε_∞. The HN fitting parameter a is related to the broadness of the relaxation spectrum, while the parameter b describes its asymmetry, (0 < a, b< 1).

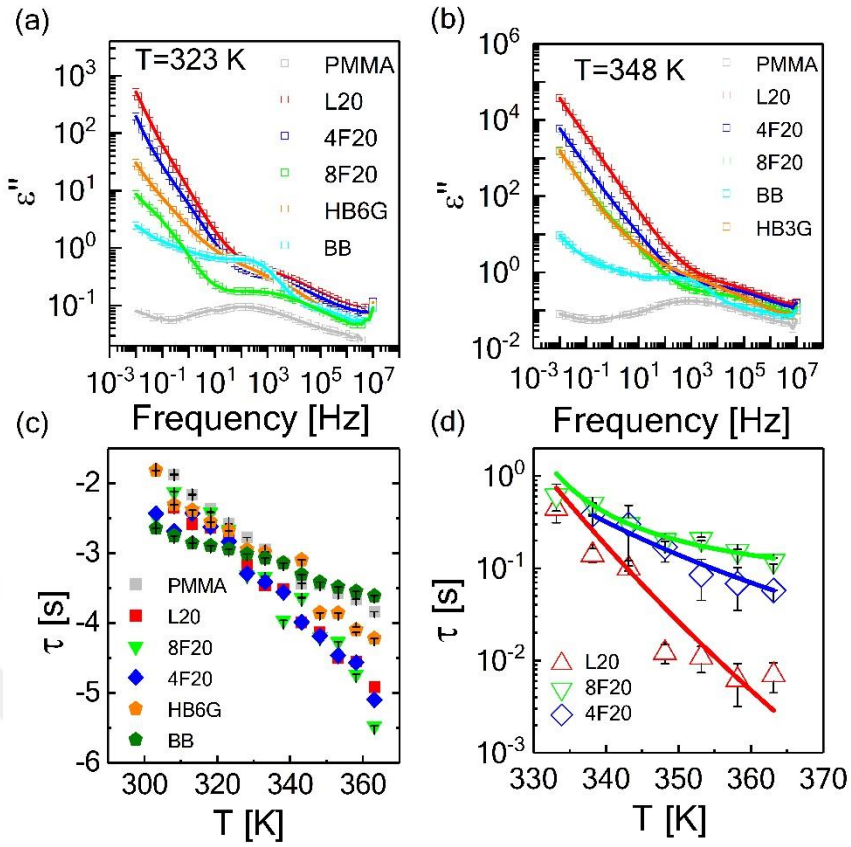

Figure 4.5: The frequency dependence of the dielectric relaxation data at 323 K (a) and 348 K (b) along with HN fits in linear and non-linear PEO/PMMA blends. The temperature dependence of β relaxation (c) for neat PMMA, linear, 4-arms, 8-arms, hyperbranched, and bottle brush PEO architectures , and α relaxation dynamics (d) for PMMA in blends with various PEO architectures including only linear, 4-arms, and 8-arms.

We found shape parameters for high and low frequency domains at 323 and 348 K is dependent on PEO architecture. The fitted shape parameters for the different PEO architectures are shown in Figure 4.6. It is well established that the α-relaxation peak shape is correlated with segmental motions and essentially influenced by heterogeneity[167]. It is seen that values for a parameter in the low frequency domain at 348 K increase with the increasing number of branching while b remains almost unchanged.

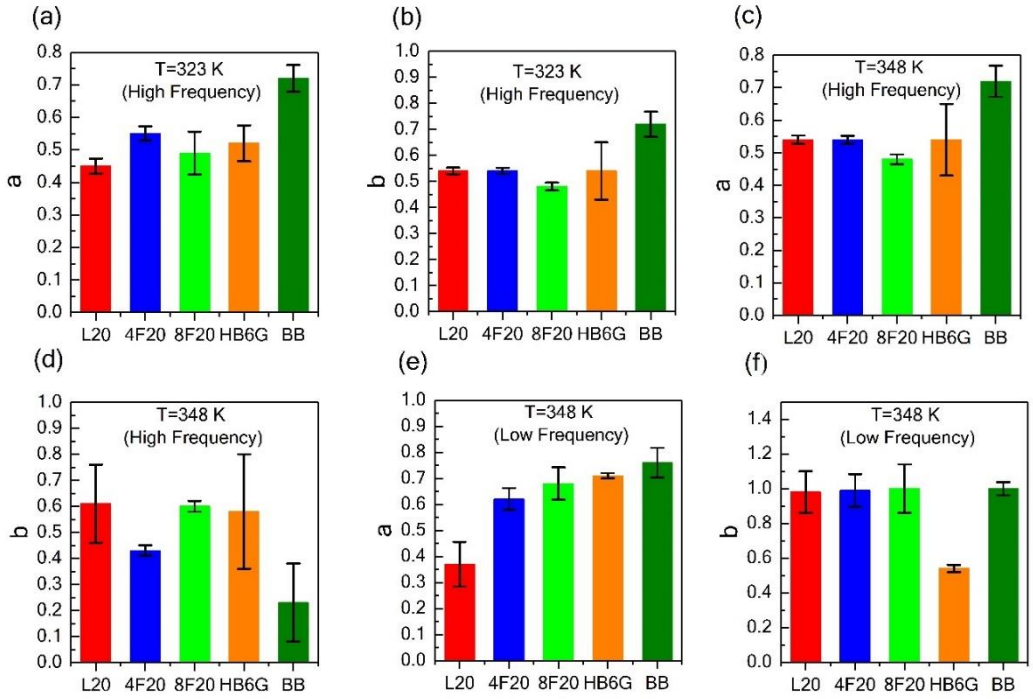

Figure 4.6: High and low frequency domain fitting shape parameters (a), (c), and (e) accounting for the broadness of the relaxation spectrums and (b), (d), and (f) accounting for its asymmetries, for PEO/PMMA blends containing 20wt% PEO from Havriliak-Negami (HN) function for various PEO architectures. Data are collected for the temperatures of 323 and 348 K. Comparison of the shape parameters a and b for Havriliak-Negami (HN) function fitted for relaxation data from different PEO architectures. (a) and (b) compare the parameters obtained at high frequency and 323 K; (c) and (d) compare the parameters obtained at high frequency and 348 K; (d) and (e) compare the parameters obtained at low frequency and 348 K.

These results suggest that the PMMA α-relaxation spectra of the linear PEO/PMMA blend is broader than the non-linear ones. Furthermore, the values for the low frequency domain at 348 K are hardly affected by PEO architecture whereas b values decrease in the case of non-linear blends, indicating that β relaxation spectra being more asymmetric as degree of branching become higher. Also, a parameter for 323 K increase with decreasing b values as more compact PEO was employed. Smaller a and higher b values indicate the spectra for the β relaxation becomes narrower and less symmetric when non-linear PEO/PMMA blends are employed, suggesting more heterogeneous dynamics. Figure 4.5c and 4.5d show the relaxation times as a function of temperature for β and α processes of PMMA in its neat form and its 20%wt PEO blends ,respectively. For all

samples within the temperature of investigation, we observed the β relaxation process following the Arrhenius behaviour expressed as:[149, 166, 168-170]

$$\tau_\beta = \tau_0 exp^{\left(\frac{E_\beta}{RT}\right)} \tag{4.3}$$

where τ_0 is the reference time, E_β is the active energy of relaxation, and R is the gas constant number ($8.314\frac{J}{mol\,K}$). Based on these Arrhenius fits, the activation energy (E_β) and τ_0 for pure PMMA were calculated as 7.55 kJ/mol and $1.86 * 10^{-15}$ s, which is in very good agreement with the reported results.[166, 168-170] All the results regarding the activation energy (E_β) and reference time (τ_o) for L20, 4F20, 8F20, HB6G, and BB PEO architectures in the blends are plotted in Figure 4.7.

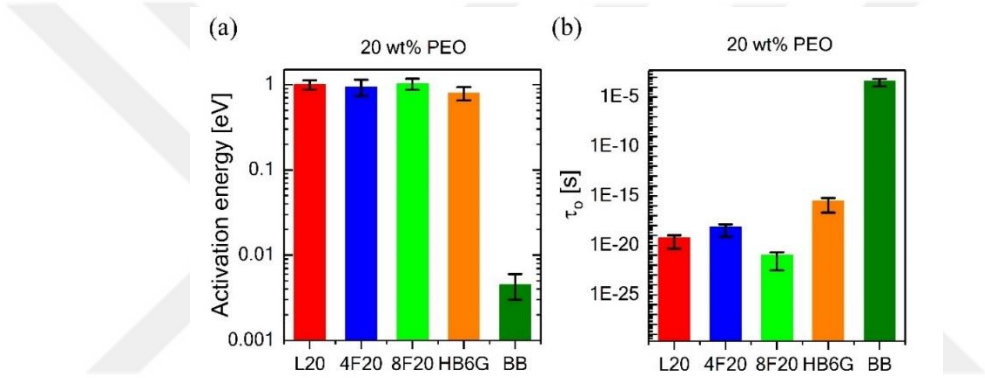

Figure 4.7: Arrhenius fit parameters of activation energy (E_β) (a) and τ_0 (b) for the β relaxation in PEO/PMMA blends containing 20wt% PEO.

Furthermore, it was seen that α relaxation for PMMA dynamics in all blends with PEO decreased with temperature following a Vogel-Fulcher- Tamman (VFT) type of behaviour given by:[165]

$$\tau_\alpha = \tau_\infty exp^{\left(\frac{B}{T-T_v}\right)} \tag{4.4}$$

where τ_∞, B, and T_v are VFT constants for a given component in a particular blend. They account for the factors related to the extrapolated relaxation time at infinite temperatures, the pseudo activation energy of conductivity which is calculated by the relationship of $E_\sigma = R * B$ where R is the universal gas constant, and the ideal glass transition temperature, respectively.[171] VFT parameters for 20wt% blends of L20, 4F20, and 8F20 are given in Figure 4.8.

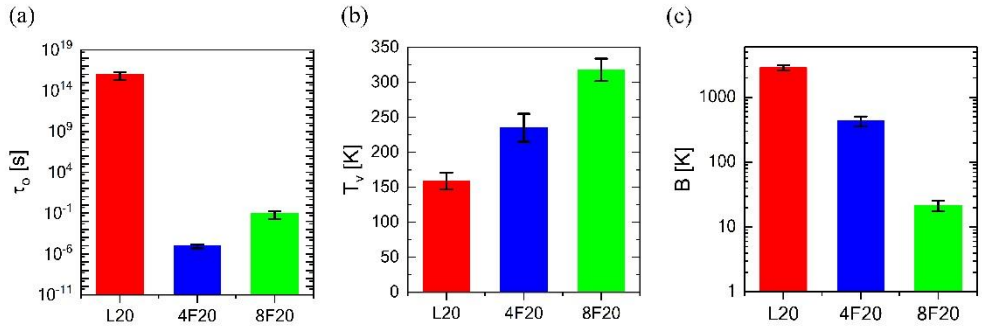

Figure 4.8: VFT fitting parameters related to (a) the extrapolated relaxation times (τ_o) at infinite temperatures, (b) the ideal glass transition temperatures (T_v), (c) the pseudo-activation energies (B) for the PEO/PMMA blends containing 20wt% PEO.

We specifically observed PMMA segmental dynamics in blends with L20 to be faster due to enhanced mobility provided by low T_g-PEO, resulting declines in its relaxation times. More strikingly, compared to the linear blend, it was found that the α relaxation of PMMA is slower in the case of non-linear PEO architectures, including 4-arms and 8- arms stars, (see Figure 4.5d). As the compactness increases with branching, the interpenetrability of PMMA and PEO decreases with increasing number of arms; thus, PMMA in the presence of 8 arms-star PEO exhibit slower segmental dynamics.

Using the argument, the influence of PMMA on the slowing down of PEO segmental motion is also less in the case of non-linear topologies. Therefore, the PEO segmental dynamics is expected to be faster in the non-linear PEO/PMMA blends when compared to the linear counterpart.

However, segmental dynamics alone may not account for the ionic conductivity in solid polymer electrolytes (SPEs).[172] There are other factors affecting the ionic conductivity such as ion-coordination, free volume, segmental motion, and ion connectivity. We conducted BDS experiment on the PEO/PMMA blend containing 20wt% linear PEO and LiTFSI ([Li/EO] =0.085 MR) to understand the effects of lithium addition on polarity, ion-coordination (solvation), and connectivity at 353 K, which can be seen in Figure 4.14. As it is apparent in the dielectric loss spectra of the salt containing sample, incorporation of lithium salt increased the dielectric loss, suggesting the dissociation of the salt in the blends. In this case, the conductivity part dominates the studied frequency domain, and no specific relaxation peak is apparent, making it impossible to explore the segmental dynamic of the sample. Hence, we used BDS results of the salt free blend to discuss about the segmental dynamics.

These changes in the dielectric loss and the relaxation peak showed that ion-coordination (solvation) is present and higher conductivities could be achieved in the blends containing salt in comparison with salt-free samples, which agrees with previous findings.[172-174] The enhancement in the ionic conductivity could be also attributed to increased ion connectivity.[172] The vibrational dynamics of the polymer backbone and side chains along could be escalated with increased free volume at elevated temperatures.[172] The increase in the vibrational amplitude can make ion coordination sites closer together and allow the ions to hop from their site to the adjacent site with less energy.[172] To test this hypothesis, we prepared PEO/PMMA blend electrolytes containing 50 wt.% PEO and LiTFSI at $[Li^+]/[EO] = 0.085$ ratio.

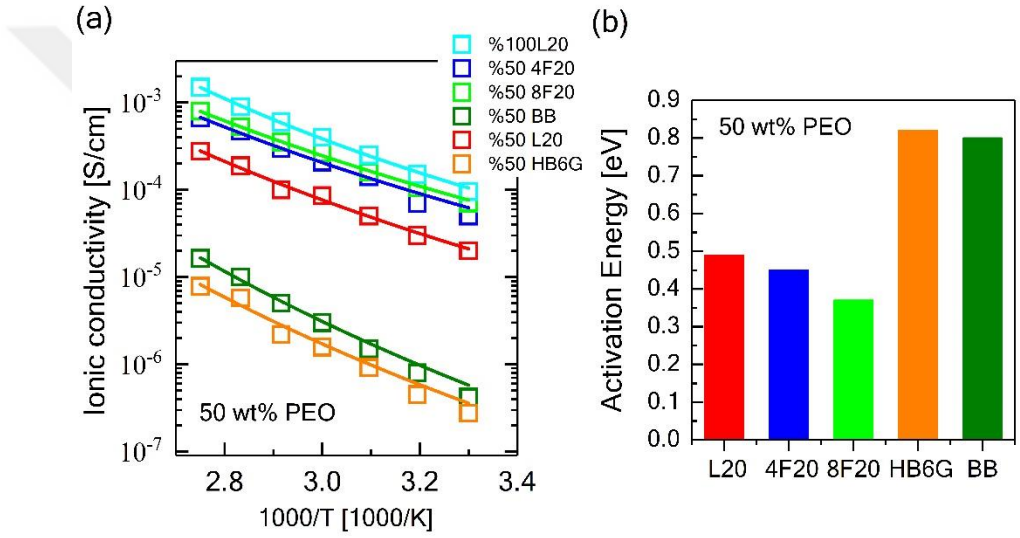

Figure 4.9: (a) The ionic conductivity measurements with corresponding VFT fit lines for the solid polymer blend electrolytes prepared using neat PEO and 50wt% PEO in blends with PMMA at various temperatures between 30°C and 90°C with a temperature increase of 10°C for different PEO architectures (b) Estimated pseudo-activation energies for the blend electrolyte containing %50 wt PEO with various PEO architectures.

Figure 4.9a illustrates the ionic conductivities of the electrolytes at different temperatures between 30°C and 90°C with $\Delta T = 10°C$ obtained from electrochemical impedance spectroscopy (the Nyquist plots for the calculation details of the ionic conductivity are shown in Figure 4.13).We have also prepared an electrolyte with the linear PEO only to compare with the blends. The neat PEO/LiTFSI resulted in an ionic conductivity ~ 10^{-3} S/cm at 60°C, which is in agreement with previously reported results.[9, 12, 18, 21, 76] In the case of the blend electrolytes, the ionic conductivity for

blend with the linear PEO decreased about an order of magnitude, as expected due to its slower segment dynamics in presence of PMMA.[18] More importantly, we found that the temperature dependence of ionic conductivity for the PEO/PMMA blend electrolytes using different PEO topologies well fit the VFT model well over the temperature range studied, suggesting that Li ion transfer is mainly correlated to the segmental dynamics.

VFT fitting parameters for the ionic conductivity measurements with respect to temperature for the blend electrolytes are shown by the Figure 4.10.

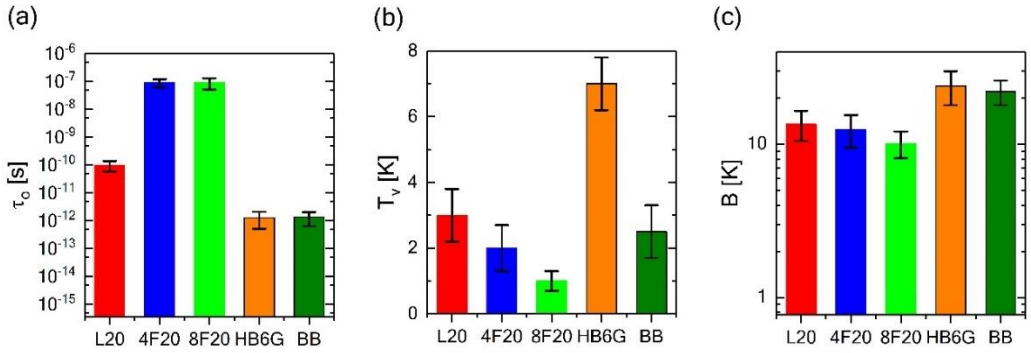

Figure 4.10: VFT fitting parameters related to (a) the extrapolated relaxation times (τ_o) at infinite temperatures, (b) the ideal glass transition temperatures (T_v), (c) the pseudo-activation energies (B) for the PEO/PMMA blend electrolytes containing 50wt% PEO.

Additionally, the ionic conductivity in the blends is strongly architecture dependent .The electrolytes with 4-arms and 8-arms stars significantly enhanced the conductivity, specifically 2.5x for 4-arms (2.1 10^{-4} S/cm) and 3x for 8-arms (2.6 10^{-4} S/cm) at 60°C, mainly due to faster PEO segmental dynamics compared to the linear one as predicted from BDS measurements. However, blends electrolytes with the bottlebrush and hyperbranched PEO resulted in dramatic decrease in conductivity (25x for BB (5.4 10^{-6} S/cm) and for 55x HB6G (1.5 10^{-5} S/cm) compared to L20 (8.6 10^{-5} S/cm) at 60°C). This is likely due to high fraction of hydroxyl-terminated end groups which interact with the salt ions by forming a transient cross-linking and limit its mobility as well as lithium migration. Previous experimental studies unravel that the unfavourable effect of OH terminated hydrogen bonds on the ionic conductivity of the PEO/LiTFSI complexes intensify for lower molar mass PEOs due to the increase in the number of end groups[51, 175, 176]. Since the total mass of the PEOs are the same, further increase in the number of branching in PEO architectures may dramatically reduce the positive effects provided by faster PEO segmental dynamics, increasing free volume and lowered degree of

crystallization provided by non-linear PEO topologies in the blends, and can even decrease the lithium mobility as seen here for the extreme cases of hyperbranched and bottlebrush PEO.

The activation energies obtained from the VFT plots in Figure 4.9 suggests that the lithium-ion transportation in the SPEs is highly affected by the segmental dynamics[177], regardless of the PEO architecture. However, the estimated activation energies are strongly architecture dependent. These activation energies for the blend electrolytes are illustrated in Figure 4.9b for the various PEO topologies. The blend electrolyte with linear PEO has activation energy 0.49 eV (comparable to the previously reported values ~0.5 eV[178]) whereas it decreases to 0.44 and 0.37 for 4-arms and 8-arms star PEO which display higher ionic conductivity, supporting the notion that the lower activation energy means the rapid ionic conduction due to the increase in PEO segmental mobility. On the other hand, the activation energies estimated for the electrolytes with hyperbranched, and bottlebrush PEO increase to ≈ 0.82 eV, supporting the argument that increased hydroxyl-Li^+ interaction in these highly branched structures impede the ion mobility.

Finally, we would like to note that we used the same $[Li^+]/[EO]$ ratio of 0.085 for all blend electrolytes as the conductivity peaks at this ratio for PEO (See Figure 5.3 in Chapter 5). However, this might also be architecture dependent and the phase behaviour or PEO-LiTFSI need to be further investigates with non-linear polymer architectures to further improve the performance of the homopolymer and blend based SPEs. This is currently under investigation and will be discussed in another article.

4.4 Conclusions

In conclusion, we studied the effects of chain architecture on miscibility, glass transition, segmental dynamics, and ionic conductivity for the poly(ethylene oxide)-poly(methyl methacrylate) doped with lithium bis(trifluoromethane-sulfonyl)-imide (LiTFSI) blend systems. Various well-defined PEO architectures, specifically linear, stars, hyper-branched and bottlebrushes, and compositions were investigated. Our XRD results reveal that room temperature miscibility of these polymers can be significantly extended by using non-linear architectures of PEO relative to the linear blend which crystallizes above 35% of PEO concentration. In the amorphous PEO/PMMA blends including 20%PEO, temperature modulated DSC results suggest tunability of the effective glass transition temperatures of both PEO and PMMA components with

polymer architecture. Additionally, our broadband dielectric spectroscopy measurements show strong dependence of PMMA segmental dynamics on the PEO topologies. Increasing number of branches in the PEO helps to maintain its fast segmental dynamics even in the blends with glassy PMMA due to less interaction sites and interpenetration of PMMA into compact and nonlinear PEO. This manifests as 2.5- and 3-fold higher ionic conductivity (with respect to the linear PEO at the same molar mass) in blends with 4-arms and 8-arms stars, respectively. Interestingly, the electrolytes with hyperbranched and bottlebrush PEO displayed more than an order of magnitude decrease in conductivity, possibly due to lithium complexation with the hydroxyl terminated end groups and/or chain connectivity. For all different PEO topologies, the temperature dependence of ionic conductivity for the PEO/PMMA blend electrolytes using different PEO topologies well fit the Vogel-Fulcher-Tammann (VFT) model well over the temperature range studied, suggesting that Li ion transfer is mainly correlated to the segmental dynamics. The activation energy values decrease with increasing ionic conductivity and vice-versa. Overall, our results show that the macromolecular architecture can be an effective tool for improving ionic conductivity in polymer blend based solid electrolytes.

4.5 Supporting Information

X-ray diffraction Analysis (XRD):

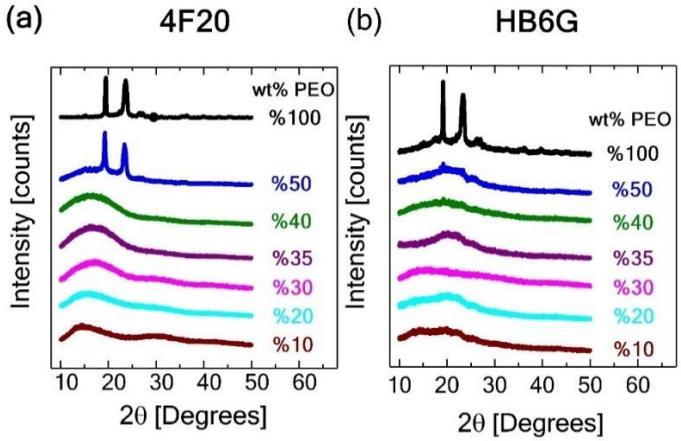

Figure 4.11: XRD results for PEO/PMMA blends in different PEO wt% concentrations and with various PEO topologies (a) 4-arms, (b) HB6G.

Modulated differential scanning calorimetry (MDSC)

Table 4.3: Glass transition temperatures with entire peak widths at half-maximum height (ΔT_g) for neat PEO with various architectures in the blends with PMMA.

Sample	Neat PEO	
	Tg,eff, K	**ΔTg, K**
L20	221.76	10.62
4F20	220.49	9.49
8F20	222.69	10.56
HB6G	232.84	13.41
BB	215.68	9.99

Calculation of the crystallization (%) in the PEO/PMMA blends

To estimate the degree of neat PEO crystallinity for different polymer structures along with the effect of number of arms and arm molecular weight on the crystallization, we used the following equation $X_c = \left(\frac{\Delta H_m}{\Delta H_c * f_{PEO}}\right) * 100$, where f_{PEO} is the weight fraction of PEO in the polymer blend, ΔH_m is the melting enthalpy of the sample, and ΔH_c is the melting enthalpy of completely crystalline PEO, which is 196.4 J/g.[157]

Table 4.4: Melting enthalpies and degree of crystallizations of various PEO architectures over different weight fraction of PEO in blends with PMMA.

Sample	wt% of PEO	Melting enthalpy	Crystallinity
		ΔH_m, J/g	X_c, %
L20	**100.00**	143.74	73.19
	75.00	88.00	44.91
	50.00	55.48	28.25
	40.00	17.67	9.00
	35.00	4.45	2.26
4F20	**100.00**	125.00	63.65
	75.00	46.26	23.55
	50.00	10.90	5.55
8F20	**100.00**	120.00	61.10
	75.00	76.00	38.10
	50.00	40.00	20.24
	40.00	0.96	0.49
HB6G	**100.00**	61.13	31.12
	75.00	37.04	18.86
	50.00	14.73	7.50
	40.00	7.11	3.62
	35.00	2.02	1.03

Lodge-McLeish Self-concentration Model

T_g for each component in the blend could be also estimated via the effective volume fraction of each component, ϕ_{eff}, determined by the Eq. 4.5,[179]

$$\phi_{eff} = \phi_s + (1 + \phi_s)\phi \tag{4.5}$$

where ϕ_s is the self-concentration (volume fraction) of the polymer due to chain connectivity effects and ϕ is the bulk blend composition. Self-concentration, ϕ_s, is also based on the appropriate volume surrounding the polymer segment under consideration. Even though it is usually to be on the order of the Kuhn length cubed (l_k^3), it can be changed by a multiplicative constant of order unity, as the choice of $V = l_k^3$ is arbitrary.[162] Then the self-concentration, ϕ_s, is estimated using the Eq. 4.6,[179]

$$\phi_s = \frac{C_\infty M_0}{k\rho N_{av} V} \tag{4.6}$$

where C_∞ is the characteristic ratio, M_0 is the repeat unit molar mass, N_{av} is the Avogadro number, ρ is the density of the polymer and k is the number of backbone bonds per repeat unit. The model associates the average local concentration of each component with a local glass temperature given by the Eq. 4.7,[179]

$$T_{g,eff} = T_g(\phi)|_{\phi=\phi_{eff}} \tag{4.7}$$

In other words, the effective glass temperature, $T_{g,eff}$, is calculated from the macroscopic $T_g(\phi)$, however, evaluated at ϕ_{eff}. For the macroscopic composition dependence of the glass transition temperature, the well-known Fox equation was used but with the effective concentration, ϕ_{eff}, for each component.

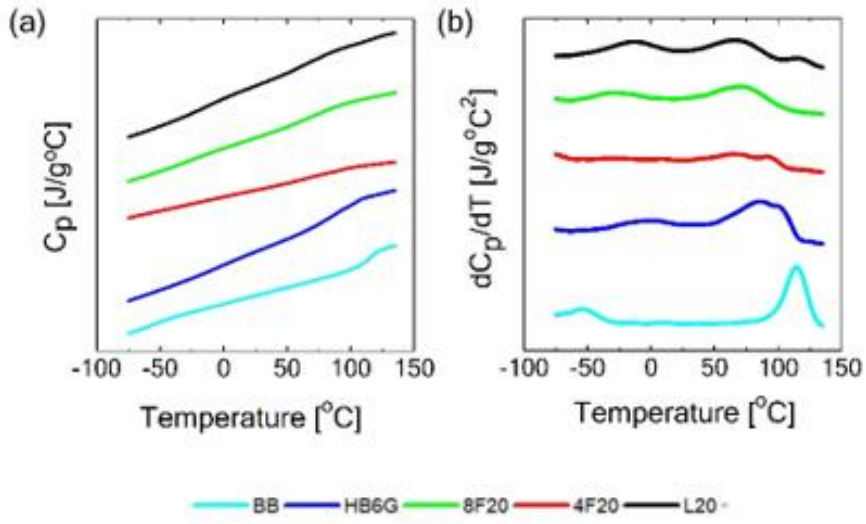

Figure 4.12: The dependence of the reversible heat flow (a) and its derivative with respect to temperature (b) for PEO/PMMA/LiTFSI based polymer electrolytes with regards to various PEO topologies including linear, 4-arms, 8-arms, hyperbranched and bottle brush.

Electrochemical Impedance Spectroscopy (EIS):

The ionic conductivity (σ) of the PEO/PMMA blend electrolytes was calculated using the equation 4.8[180]:

$$\sigma = \frac{l}{R_b A} \tag{4.8}$$

where l is the polymer electrolyte thickness, A accounts for the area of the SPE and R_b is the bulk resistance. The bulk resistance was obtained from the complex impedance plot shown by Figure 4.13 below.

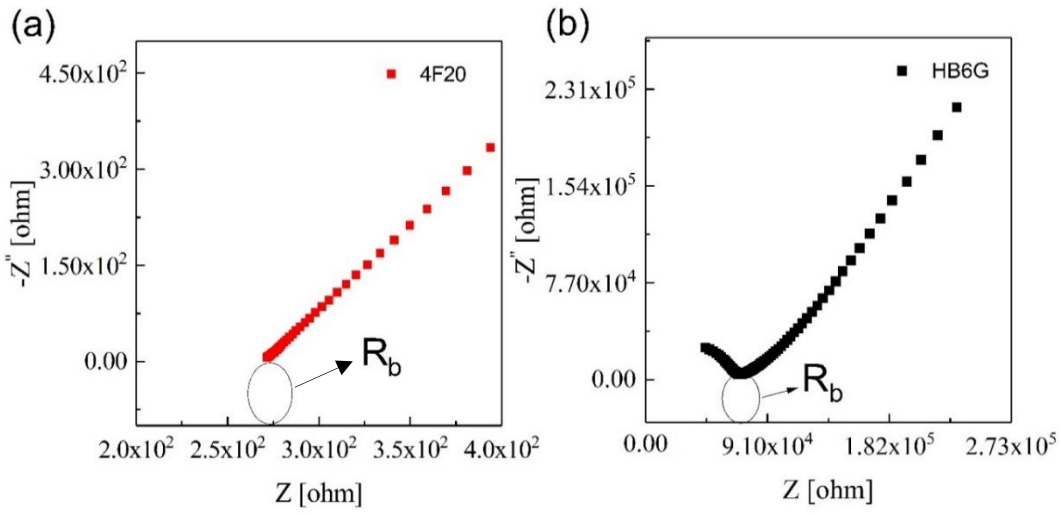

Figure 4. 13: Example of Nyquist plots at 60ºC used in the ionic conductivity calculations for the PEO blend electrolytes containing %50 4F20 (a) and HB6G PEO (b).

Broadband Dielectric Spectroscopy (BDS):

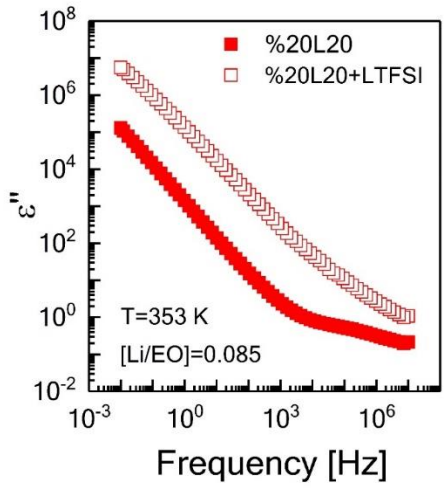

Figure 4.14: The frequency dependence of the dielectric loss (ε") data at 353 K for 20wt% linear PEO/PMMA blend with (open) and without (filled) salt.

INTRODUCTION

Lithium-ion rechargeable batteries have been extensively used in various applications including electric vehicles, electronics, and energy storage systems.[16, 27, 28, 50, 154] Currently, these batteries utilize liquid electrolytes associated with disadvantages and potential risks, that could lead explosions, leakages, fires, and short-circuits.[13, 16, 50-52] To overcome these problems, polymer electrolytes (PEs) have been widely investigated as replacement of liquid electrolytes in lithium-ion batteries.[13-16] Despite they offer significant advantages such as high flexibility, decent mechanical stability, facile processability, large electro-chemical window, and superior energy density,[13, 15, 52, 154, 181] their low ionic conductivity at room temperature ($<10^{-5}$ S/cm)[8, 11] still remains as a major challenge for large scale commercialization.

Various polymers, including poly(acrylonitrile), poly-(vinylidene fluoride) (PVDF), poly(methyl methacrylate) have been studied as SPEs[13] ; the most preferred one is still poly(ethylene oxide) (PEO) due to its fast segmental dynamics in amorphous state[8], low glass transition temperature ($T_g \sim 220$ K[8]), good electrochemical stability as well as its ability to dissolve different types of lithium salts.[13-16] Below its melting temperature ($T_m = 60℃$, in the neat form)[8, 17], it has extremely low ionic conductivities ranging between $10^{-6} - 10^{-8}$ S/cm whereas above the melting temperature the ionic conductivity rapidly increases while losing its mechanical strength upon melting of the crystals which otherwise reinforce the material.[18] Ion conduction primarily occurs in the amorphous phase where ion motion is coupled with segmental dynamics of the polymer. [8, 15, 18, 76]

Therefore, the main objective of the previous studies on PEO-based SPEs was to suppress the crystallization of PEO without much sacrificing the mechanical strength.

Since ion migration primarily occurs in the free volume of the amorphous phase, it could be facilitated by the increased free volume accompanied with lower bulk viscosity in the polymer matrix if possible, [8, 15, 18, 76, 182-185] therefore several methods such as employing architectural changes and various chain lengths in PEO-based SPEs have been applied by different studies with the objective of developing high Li^+ ion conductivity.[8, 13, 15, 16, 18, 99, 100] This could be attributed mainly to the fact that free volume within the amorphous fraction could be increased through less degree of crystallization and chain size, as reported in other previous studies.[8, 13, 51] Furthermore, increasing branching would lower friction by diffusing polymer chains with smaller molecular weight, resulting low viscosities due to the lack of entanglements in the polymer architecture when non-linear topologies are used in preparing these SPEs. [8, 13, 51, 92-94] For example, Butzelaar et al.[15] and Lee et al.[19] developed the PEO-based electrolytes using star PEO topologies with a constant number of arms at the constant LiTFSI salt concentration and found significantly enhanced room temperature ionic conductivity attributed to extremely suppressed crystallization by the non-linear architecture. In a similar study conducted by Marzantowicz and co-workers[100] using a star-branched poly (ethylene oxide) with nearly 20 arms over a limited range of LiTFSI salt concentration reported ionic conductivity values comparable to linear PEO based electrolytes, which reached its maximum at the molar ratio of [EO/Li=10] and declined with further lithium addition because of possible ion clustering formation, suggesting highly dependent ionic conductivity with the salt concentration. Furthermore, Lee et al.[16] and Chen et al.[13] employed hyperbranched Poly (ethylene oxide) with a fixed LiTFSI salt loading and reported enhanced Li-ion conductivity with sufficient mechanical stability mainly because of efficiently suppressed crystallization, faster segmental motion, and decreasing viscosity owing to nanoconfinement effects and end group modification, respectively. In

another work studying PEO/LiTFSI system with a fixed salt concentration, Thelakkat et al.[186] studied highly branched copolymers having PEO side chains and rigid polymer forming the backbone by correlating the ionic conductivity with changing polymer stiffness and found that higher ionic conductivity was achieved with decreasing chain stiffness. In another study investigating the effects of chain length and viscosity on the ionic conductivity in linear PEO/LiTFSI complexes, Devaux and his-coworkers[51] reported decreasing the chain length reduced the viscosity with the incremental contribution of the end groups in increasing free volume, which eventually resulted higher ionic transportation. These previous findings absolutely play a significant role in our understanding on the importance of variations in both architecture and chain lengths when designing PEO/LiTFSI based polymer electrolytes, however, they are very insufficient in providing the dependence of the ionic migration in these electrolytes on a wider salt concentration, more extensive chain length, polymer compactness, and functionality when non-linear architectures are employed. Furthermore, none of them quantitatively investigated the change of free volume and its corresponding effect on the ionic conductivity with respect to polymer architecture in these PEO based electrolytes.

As discussed above, since the ionic conductivity in these electrolytes using linear PEO architectures could be affected by the salt concentration and chain lengths due to suppressed crystallization (increased free volume in the amorphous phase), lower viscosity, as well as ion accumulation and clustering, the ion transportation could also be influenced by those factors in non-linear PEO/LiTFSI-based electrolytes. Since the influence of the PEO architecture with varying functionality, chain length, and salt concentration on a wider range is still not extensively and systematically known in literature and not well understood in terms of correlating the ionic conduction with free

volume and viscosity together, further fundamental work is required in this regard, which could improve the electrolyte performance.

The interdependence of ionic conductivity and the phases and proportion of these phases present has also obtained a vast amount of attention in polymer electrolytes. In the case of PEO that is highly semi-crystalline, the distinctive variations of the phases could occur.[57, 101] To monitor these variations in the phases which could affect electrolyte properties especially ionic conduction and mechanical strength, it is very important particularly to establish first a phase diagram for each PEO electrolyte system investigated There have been numerous studies investigating the phase diagrams of PEO systems with most widely used various salts for both liquid and solid electrolytes salts including primarily lithium hexafluorophosphate ($LiPF_6$), lithium triflate ($LiCF_3SO_3$), lithium tetrafluoroborate ($LiBF_4$), lithium hexafluoroarsenate ($LiAsF_6$), lithium perchlorate ($LiClO_4$), and lithium bis(trifluoromethanesulfonyl)imide (LiTFSI).[101-105]

The earliest study in relation to PEO phase diagram carried by Berthier et al.[102] in 1980s belongs to PEO/ $LiCF_3SO_3$ system showed the presence and dependence of both amorphous and crystalline phases composed of two different crystalline phases using DSC and X-ray diffraction techniques. In a similar work done by Gorecki et al.[103] reaffirmed the existence of two specific crystalline complexes with varying conductivities for the PEO/$LiClO_4$ based electrolyte. Additionally, other studies done in late 1980s concentrating on the phase and conductivity diagrams of the PEO based electrolytes consisting of $LiBF_4$ and $LiAsF_6$ salt systems reported multiple-intermediate phase formations with different stoichiometries depending on the salt, which impacted the ionic conduction and activation energies of the systems.[104, 105] Furthermore, the first study done by Lascaud and co-workes[101] dating back to mid-1990s explored the dependence

of phase and conductivity behaviors over a varying range of lithium salt concentration in linear PEO/LiTFSI network based electrolyte. They found PEO/LiTFSI system showed a phase diagram composed of various crystalline regions because of the changes in the ion-polymer interaction with the salt concentration, resulting in very high ionic conductivity at moderate concentrations, but it decreased significantly at other concentrations due to infiltration threshold.[101] Even though all these important works focusing on establishing phase diagrams have helped us understand the PEO-based systems composed of various salts, no architectural variations have been considered for these neat PEO based electrolytes including the most commonly used PEO/salt complex (PEO/LiTFSI)[8], which could also affect the degree crystallization, ion dissolution, ion pairing, thus impacting the phase diagrams and electrolyte characteristics.

Also, very recently, in our study,[8] we investigated the effect of different PEO topologies (linear, stars, hyperbranched, and bottle brush) more systematically in PEO-based electrolytes with a constant and most widely used lithium salt in SPEs, LiTFSI [Li/EO] =0.085 molar ratio on the ionic conductivity and found higher ionic conductivities for the electrolytes including non-linear PEO architectures with moderate branching when compared to their linear counterpart mainly because of increased amorphous PEO fraction and faster PEO segmental dynamics. We not only think that the molar ratio where the maximum conductivity observed could be architecture dependent, but also electrochemical properties could be correlated and increased with the changes in free volume and bulk viscosity with non-linear PEO architectures. Therefore, the phase and conductivity diagrams of PEO along with free volume characteristics and rheological properties over a wide LiTFSI salt concentration needs to be investigated systematically in detail when architectural variations in the PEO architecture are concerned to further improve the electrolyte performance. We utilized various PEO topologies with hydroxyl

end groups including linear, stars (4-arms, 8-arms), and hyperbranched PEOs shown in Figure 1. Our results show that phase diagrams were completely distinctive depending on non-linear PEO architectures when compared to linear PEO, forming completely amorphous mixtures at lower salt loadings with increasing branching. Additionally, conductivity behavior was similar for all PEO topologies, resulting in ionic conductivities maximizing at the salt concentration of [Li/EO = 0.085] followed by a dramatic decrease because of ion pairing and clustering effects.

However, the ionic conductivity for the PEO architectures increased with increasing degree of branching such that the electrolyte with hyperbranched PEOs yielded as much as nearly 3x higher ionic conductivity at 60°C.

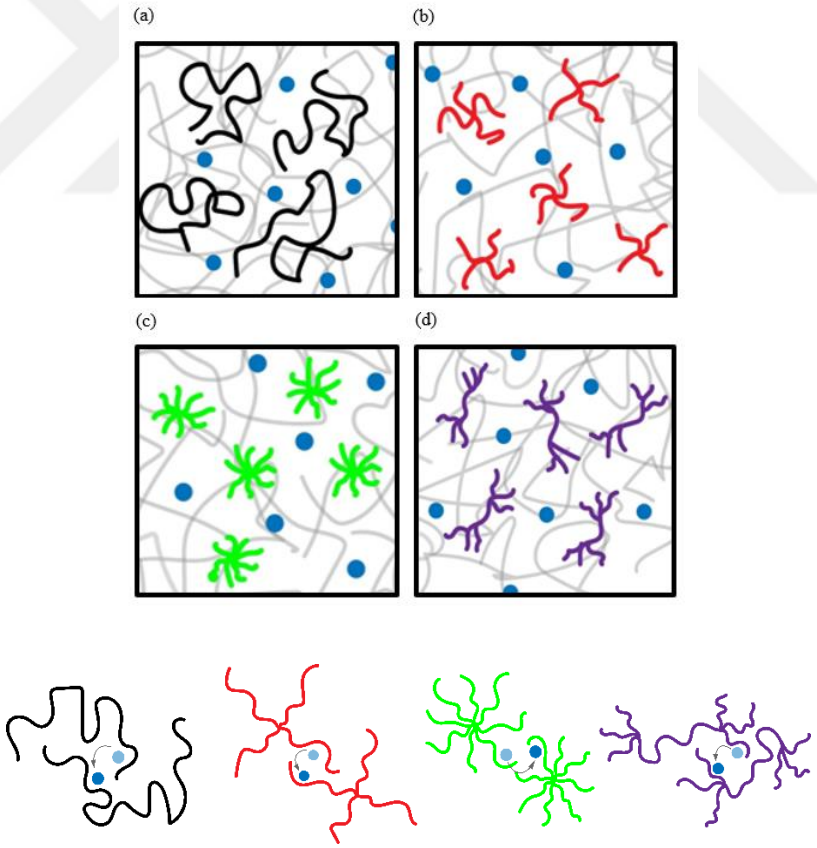

Figure 5.1. Schematic representation of the PEO-based solid polymer electrolytes with the architectural variations (a) linear, (b) 4-arms star, (c) 8-arms star, (d) hyperbranched

used in this study (Blue filled circle represents the Li^+ ion). Schematics in the below show the interchain ion hopping between the studied polymer architectures.

5.2 Experimental methodology

In this part, materials used in this study are explained and defined, respectively.

5.2.1 Materials

Linear PEO, hyperbranched (3^{rd} and 6^{th} generation) PEO, and Lithium bis(trifluoromethane)sulfonamide, LiTFSI salt were purchased from Sigma-Aldrich. 4-arms and 8-arms star PEOs were supplied by Creative PEGWorks. All polymers were used as received without modification. The polymer characteristics are displayed in Table 1. The chemical structure of the PEOs with hydroxyl end groups is provided in Figure 5.8.

5.2.2 Preparation of salt-free samples & electrolytes

Salt-free samples for neat PEOs with linear (M_w~20 kDa), 4-arms star (M_w~5, 10, 20 kDa), 8-arms star (M_w~10, 20, 40 kDa), HBG3 (M_w~20 kDa), and HBG6 (M_w~35 kDa) topologies, were prepared by the solution casting technique. Polymers were first dissolved in acetonitrile (ACN) at 30 mg/ml. Then, the solutions were stirred with a magnetic stirrer at room temperature for 6 hours. Later, the desired amount of the lithium bis(trifluoromethane)sulfonamide, LiTFSI, was dissolved in acetonitrile in glovebox filled with Argon and the salt solution was stirred with a magnetic stirrer at room temperature for 6 hours. Next, the desired amount of salt solution was added into the polymer solutions to have$[Li^+]/[EO]$ ratios ranging between 0 and 0.2 molar in the glove box, and they were continuously stirred for 48 hours.

The electrolyte solutions were then cast onto glass petri dishes and evaporated slowly at room temperature overnight in a glovebox filled with Argon and annealed at 100℃ in a vacuum oven for 48 hours to ensure complete removal of the solvent.

Table 5.1. The molecular characteristics including functionality, dispersity, total, and arm molecular weight of the PEO samples used in this study.

PEO architecture	**Short name**	**Functionality /Arm number (f)**	**Total molecular weight (Mn) [kg/mol]**	**Arm molecular weight [kg/mol]**	**Dispersity (*Đ*)**
Linear	L20	2	20	10	1.10
4-arms star	4F5	4	5	1.25	1.03
4-arms star	4F10	4	10	2.5	1.03
4-arms star	4F20	4	20	5	1.03
8-arms star	8F10	8	10	1.25	1.10
8-arms star	8F20	8	20	2.5	1.10
8-arms star	8F40	8	40	5	1.10
Hyperbranched	HBG3	3rd generation	20	NA	<1.5
Hyperbranched	HBG6	6th generation	35	NA	<1.5

5.2.3 Characterization

X-ray Diffraction (XRD): The XRD patterns of the pure PEO and the electrolytes were recorded using the Bruker D8 Phaser – X-ray diffractometer with Cu K (α) source. The samples were placed on the surface of a glass plate which is heated to 90°C by a

thermoelectric peltier heater and waited until temperature stabilization was reached on the surface. Then, the diffraction data were obtained at this temperature with the Bragg's angles (2θ) varying from 5 to 60 degrees at a rate of 0.1 degrees.

Differential Scanning Calorimetry (DSC): The differential scanning calorimetry (DSC) samples were prepared by putting ~8-10 mg of material in aluminum pans provided by TA Instruments. DSC experiments of the neat PEOs and their electrolytes were carried out with a TA Instruments DSC25 instrument equipped with the refrigerated cooling system. An aluminum pan was used as a reference. To eliminate the temperature history completely, all the samples were heated to 120 ℃ and waited for 5 minutes. Samples were then quickly cooled down to -85℃ at the rate of 20 ℃/min. DSC scans were then collected with the rate of 10 ℃/min during the heating process to 120 ℃. Eventually, the step of the heat capacity in DSC measurements was used to estimate the glass transition temperatures for the samples.

Fourier Transform Spectroscopy (FT-IR): FTIR characterization was performed on the pure PEOs and the electrolytes using the Thermo Scientific iS10 FT-IR spectrometer in the wave number of 4000 to 600 cm^{-1} with 64 scans for each spectrum.

Dynamic Light Scattering: The DLS experiments have been performed on a Zetasizer NanoZS (Malvern Instrument) operating in backscattering mode at an angle of 173° and at a temperature of 25°C using a dilute PEO/solvent (Acetonitrile) solution containing PEO concentration of 1 mg/ml.

Rheology: Rheological measurements in the melt state were performed using an Anton Paar's (MCR 302) rheometer, equipped with a cone geometry (diameter 25 mm, and 1 degree angle), and at a constant temperature of 75 °C. The viscosity of the samples investigated in a shear rate table mode (0.1 to 1000 rad/s).

Electrochemical Impedance Spectroscopy (EIS): Impedance characterization was carried out using an Autolab Potentiostat Galvanostat PGSTAT (Metrohm, Netherlands) in two-electrode configuration for PEO-based electrolytes. This arrangement was used to investigate electrode properties in liquid-state systems. The measurement frequency varied between 1 Hz to 1 MHz. Each SPE blend disc was sandwiched between two stainless steel blocking electrodes under an argon atmosphere in a glove box located at Koç University Boron and Advanced Materials Application and Research Center (KUBAM) and sealed in MTI Split Cell to measure the complex impedance spectra. After waiting for the temperature stabilization with a margin of 0.1℃ at the experimental temperature of interest, the experiments were also carried out at various temperatures between 30℃ and 90℃. The data were analyzed to characterize real and imaginary impedances using the NOVA software to form Nyquist plots used for estimating resistance of the samples and the ionic conductivity.

Positron annihilation lifetime spectroscopy (PALS): The purpose of PALS measurement is to determine free volume behavior of PEOs with varying topologies (Linear, 4-arms, 8-arms, and HBG3) for temperature range from 30 to 90℃. To accomplish this, we employed a fast-fast coincidence system measuring the time interval between the prompt γ-ray of 1274 keV as the start signal and the annihilation γ-ray of 511 keV as the stop signal. About 30 μCi of ^{22}NaCl source on a thin aluminum foil (5 μm thick) was inserted between two pieces of film samples with a thickness of 2 mm or more. For each γ-ray detection, a plastic scintillator (BC422, Saint-Gobain Crystals, Hiram, OH, USA) was connected to photomultiplier tubes (PMT R2059, Hamamatsu Photonics Deutschland GmbH, Herrsching, Germany) mounted on a PMT Base (265A, Ortec AMETEK GmbH, Meerbusch, Germany) operating at negative 2100 volts. Two constant fractional differential discriminators (CFDD 583B, Ortec AMETEK GmbH, Meerbusch, Germany)

for the window settings of 1274 keV and 511 keV and for timing signals were used. These were connected to a time-to-amplitude converter (TAC 266, Ortec AMETEK GmbH, Meerbusch, Germany) to convert pulses of different heights into a time-to-pulse-height signal. The converted signals were fed to a multi-channel analyzer (MCA ASPEC-927, Ortec AMETEK GmbH, Meerbusch, Germany). The spectroscopic data obtained from MCA were analyzed using the LT polymer to obtain the lifetimes and intensities, providing facts on the free volume. The resolution of the system was about 350 ps using a Si crystal as a reference and the source contribution was about 10.5%, with lifetime contributions of 0.2 ns and 0.4 ns and respective intensities of 80% and 20%.

5.3 Results and Discussion

In this section, we analysed the results and proposed a discussion in relation to the findings.

5.3.1 The effect of PEO architecture, Molecular weight, Functionality and Lithium concentration on the crystallization, melting and glass transition temperatures in neat PEO-based Electrolytes

The effect of PEO topologies and lithium concentration on the crystallization, melting and glass transition temperatures of PEO/LiTFSI electrolytes was investigated using differential scanning calorimetry (DSC). Figure 5.2 shows the constructed phase diagrams with the specific variations of the phases as a function of melting temperature depending on the salt concentration ranging from 0 to 0.2 [Li/EO] molar ratio for linear, 4-arms and 8-arms stars, and hyperbranched PEO with varying molecular weights. This phase diagram contains two distinctive PEO phases ,namely completely liquid phase shown by $PEO_{(l)}$ in no crystalline PEO presents and the combination of both crystalline $PEO_{(s)}$ and liquid phase $PEO_{(l)}$ in which crystalline and amorphous PEO domains coexist. In addition, estimated glass transition temperatures (T_gs) which change based on salt loadings are shown. The open symbols represent the glass transition temperatures

whereas filled symbols are used to show the melting points (T_ms). The glass transition and melting temperatures of the neat (salt-free) PEOs for various architectures ranged around -55ºC and 60ºC, respectively. (The representative DSC thermographs for the melting and glass transition behavior is given in Figure 5.9. See DSC results section in the Supporting Information for the details of DSC thermographs obtained for all PEO topologies).

There was no significant change in T_g between different architectures for the neat PEO, in agreement with the previous reports. [187-189] T_m, however, were more architecture-dependent such that the non-linear chain topologies display usually lower melting temperatures (with shift in T_m as high as 20 K). It was also clear that T_m values of PEOs with varying architectures estimated from DSC thermographs well agreed with free volume measurements probed the PALS which indicated a sharp increase in the free volume at melting temperatures for all architectures due to the melting crystals in the PEO matrix (Figure 5.12). Also, T_m decreases with decreasing arm molecular weight of star PEOs for the same functionality. This is likely due to slower crystallization kinetics with decreasing arm length, resulting in thinning of the crystalline lamellae.[92, 190, 191] It is also seen in Figure 5.9 that melting enthalpies for the neat non-linear topologies were lower, suggesting less crystallization with higher degree of branching when compared to the linear one. It is seen that **t**he degree of crystallinity for the salt-free neat PEO with non-linear architectures is considerably lower when compared to the linear PEO due to the restricted mobility of the densely packed monomers near the branch points.[92, 94, 190, 192] This is clearly seen for linear, 4-arms star, 8-arms star and hyperbranched at the same total molar mass of 20 kDa, where X_c is monotonically decreased from 74.9 % for linear to 31.5% for hyperbranched PEO (HBG6).

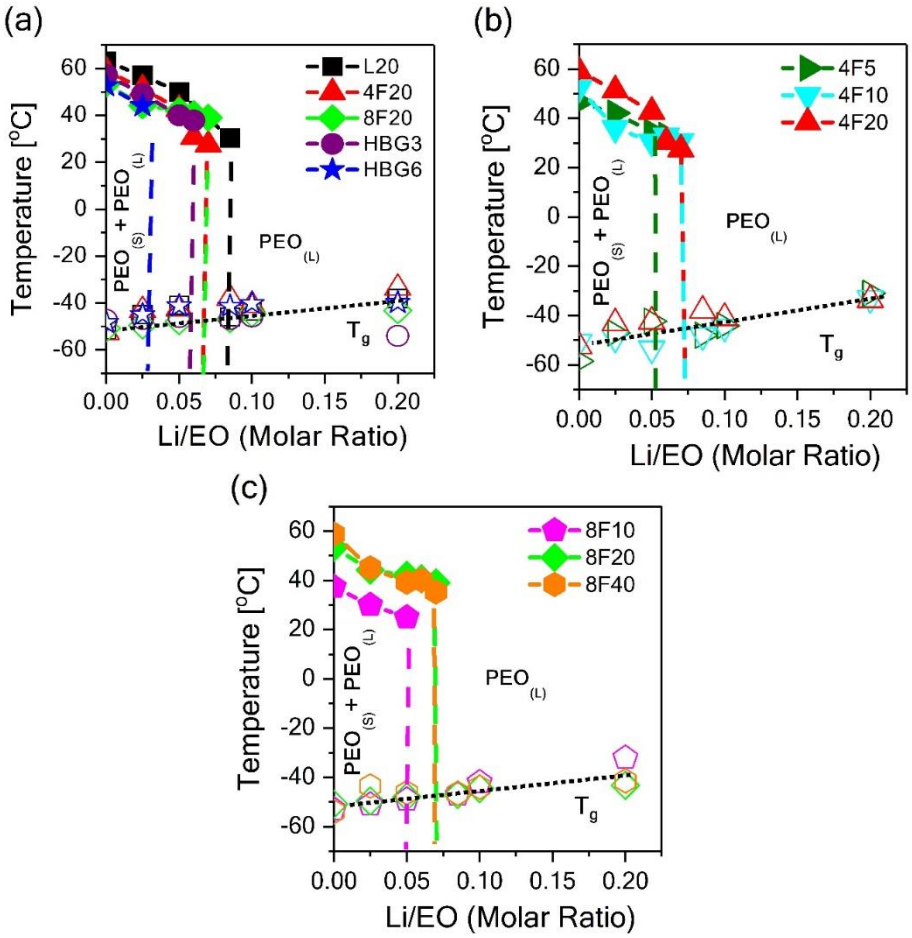

Figure 5.2. Phase diagrams of the PEO-LiTFSI systems with respect to different PEO architectures including linear, stars, and hyperbranched topologies with (a) the same molecular weight (MW~ 20 kDa), (b) and (c) with varying molecular weights (MW~ 5, 10, 20 kDa) for 4-arms and (MW~ 10, 20, 40 kDa) 8-arms star topologies over a wide range of salt concentration ([Li/EO] ranging from 0 to 0.2). The diagram was derived from a calorimetric analysis of the DSC data. The filled and unfilled squares represent melting and glass transition temperatures, respectively.

Addition of salt gradually results in elevations of the T_g values whereas it declined melting temperatures (T_m) in all electrolytes fundamentally because of ion dipole interactions between EO and salt ions, which impedes the mobility of polymer segments.[100, 101, 193-195] Previous phase diagrams were constructed based on linear

PEO architecture; [101] we include various other PEO topologies more systematically to explore the topological influences on the phase behavior. As can be seen in Figure 2, incorporation of the lithium salt into the PEO matrix considerably affected the phase diagram regardless of the topological changes. The decreasing effect of the lithium salt addition on the melting temperatures (T_m) was much more dependent on the PEO architecture employed as opposed to the effect on T_g. More specifically, increasing the branching at the same total molar mass of 20 kDa lowered T_m more..[38] Similarly, the addition of the LiTFSI salt into PEO matrixes severely decreased the crystallization with decreasing melting enthalpies for all topologies, but the extent of the relative decrease was architecture dependent such that the higher the degree of branching with shorter arm lengths (same total molar mass of 20 kDa) became much lower.[8, 92, 190, 191] Furthermore, we observed the system for all non-linear topologies consisted of an amorphous phase in equilibrium with the crystalline PEO for lower salt concentrations (Li/EO<0.05) and gradually became amorphous with additional salt depending distinctively on the architecture as seen in Figure 5.2. To be more specific, highly branched PEO systems namely HBG6 and HBG3 happened to be amorphous with less salt addition ((Li/EO>0.05) for HB6G and (Li/EO>0.06) for HBG3) whereas the amount of salt needed PEO salt complexes without any crystalline region for moderate number of branched PEOs (4-arms and 8-arms) increased up to the molar ratio of (Li/EO>0.07). On the other hand, the linear PEO/LiTFSI blend electrolyte retained the semi-crystalline nature of PEO up to the molar ratio of Li/EO=0.085 over which all mixtures were free of any crystalline phase. The ability of dissolving the lithium salt in non-linear architectures with higher degree of branching is enhanced.[100, 196] Therefore, branched PEOs with increasing number of arms could form completely amorphous PEO/LiTFSI salt complexes with less amount of salt loadings. This could be important to enhance ionic

conductivity in these systems, because of using lower salt concentration when compared to linear PEO, we could eliminate not only crystallization in non-linear topologies but also increase T_g and the bulk viscosity less as well as decrease the possibility of the formation of ion clusters, which eventually help us optimize salt concentration and facilitate the ion transportation. Overall, all these results indicate the addition of LiTFSI salt into PEO matrix could significantly affect the phase diagram depending on architecture which supports our hypothesis that constructing a phase diagram with a wide range of salt loadings for the specific polymer/salt system could affect the polymer electrolyte properties, thus is very important to be done before designing any SPEs.

5.3.2 The effect of PEO architecture, Molecular weight, Functionality and Lithium concentration on the Ionic Conductivity

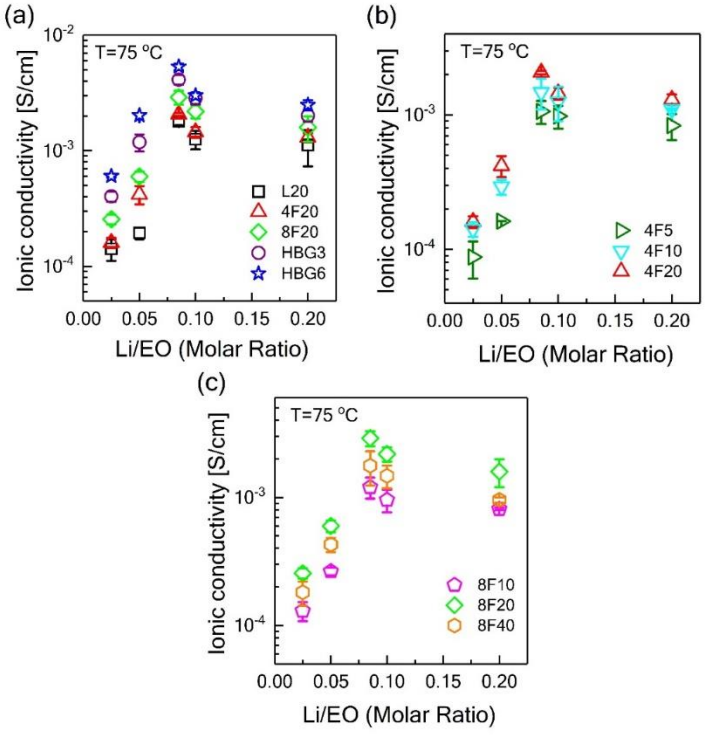

Figure 5.3. Ionic conductivity of PEO-based electrolytes at 75°C with various architectures including linear, stars, and hyperbranched topologies with (a) the same molecular weight (MW~ 20 kDa), (b) and (c) with varying molecular weights (MW~ 5,

10, 20 kDa) for 4-arms and (MW~ 10, 20, 40 kDa) 8-arms star topologies over a wide range of salt concentration ([Li/EO] ranging from 0 to 0.2).

The salt concentration-dependent Li-ion conductivities with varying topologies for PEO-based electrolytes are shown in Figure 5.3. Irrespective of the polymer architecture, the addition of LiTFSI up to a certain molar ratio into the polymer matrix increases the ionic conductivity of the electrolytes. In this sense, [Li/EO = 0.085] gives the highest conductivity for all architectures. Moreover, further increasing the salt concentration ([Li/EO>0.085]) drastically reduces the ionic conductivity due to an extremely bulk viscosity arising from ion pairing, and aggregation effects observed from XRD and FTIR. Figure 5.3a compares the conductivity data for the same total molecular weight. The PEO electrolytes yielded higher ionic conductivity with the increasing branching. More specifically, PEOs with the most extreme branched cases namely HBG3 and HBG6 architectures resulted as much as 3 times higher ionic conductivity ($3.9\ 10^{-4}$ S/cm) whereas non-linear architectures with moderate number of arms namely (4-arms and 8-arms star) resulted in as much as nearly 2x higher ionic conductivity ($2.3\ 10^{-4}$ S/cm) when compared to the linear analogue ($1.2\ 10^{-4}$ S/cm). The reason for this can be explained by two essential properties of the hyperbranched PEOs which facilitated the ionic conduction: higher branching of the PEOs results in much lower bulk viscosity (see Figure 5.6) and significantly increased free volume in the architecture, facilitating ion transport (Figure 5.7) while its loose structure provides higher solubility of the salt and enhance the ion diffusion in the polymer matrix[197, 198] (See Table 5.4 for the polymer compactness). Depending on their architecture, polymer chains with the same monomer chemistry and same molecular weight can have both loose and compact forms. Uniformly distributed monomers in linear polymers are reported to possess a random coil structure.

In hyperbranched polymers, the distribution of the monomers is toward the end of the chains, making them adapt to an even looser structure when compared to linear chains. However, in symmetric star polymers, by increasing the number of arms (functionality) and decreasing the arm length the density of the chain increases at the center of the star and creates a compact and impenetrable core region, while dangling free ends occupies more space. The closely packed region prevents the interpenetration of chains and makes the star polymers adapt colloidal form at the core. The dominance of this core region can be tuned simply by changing the arm length and functionality. The extent of the hard sphere like center relative to the radius of gyration (R_g) of the star polymer is a measure of chain '*compactness*'.[199] $\frac{R_c}{R_g} \approx \frac{l_p}{0.365\sqrt{M_{arm}}}\sqrt{\frac{f^2}{3f-2}}$, is used to estimate the compactness in the chains, where l_p is the persistence length (0.41 nm for PEO[200]). Table 5.4 displays the compactness of the polymers used in this study. We found that the polymers with the higher degree of branching and looser topology show the highest conductivity. In other words, decreasing compactness of the non-linear PEOs for all architectures at the same molecular weight (20kDa) facilitated the lithium-ion migration by enabling faster ion diffusion[197, 198]. (See DLS results section in the Supporting Information for the details of polymer compactness obtained for various PEO topologies). We also investigated the effect of arm molecular weight in 4-arms and 8-arms star structures. Figures 5.3b and 5.3c display the changes in the ionic conductivities with respect to different salt concentration in 4-arms and 8-arms star PEOs with varying arm lengths.

Based on the data in Figure 5.3b, increasing the arm molecular weight slightly enhanced the ionic conduction in 4-arm star PEO-based electrolytes. The reason why the ionic conduction was lower for the 4-arms PEO with shorter arm lengths could be related to

the transient crosslinking effect arising from the strong interactions between terminal OH and either anion and cation, slowing down the ion transport[51]. The number of chains in neat 4F5 and 4F10 PEO-based electrolytes is four and two times higher than the number of chains in neat 4F20-based electrolytes, respectively. This means that higher number of OH terminated end groups in these samples causes higher transient crosslinking between 4-arm star chains (4F5 and 4F10) and ions which ultimately reduces the ion conductivity in the samples. Additionally, we had the same observation for the 8-arms star PEOs-based electrolytes (8F10 and 8F20), however the ionic conductivity of the 8F40 was lower than the 8F20, which may be due to higher bulk viscosity when compared to other 8-arms star PEO architectures (see Figure 5.6c).

5.3.3 The effect of PEO architecture, Molecular weight, Functionality and Lithium concentration on the Ion Pairing and Clustering

Since salt ions tends to aggregate, leading to decreased Li^+ conductivity[201] when the salt concentration increases above the critical point as shown by the salt concentration-dependent Li-ion conductivities in Figure 5.4, we performed Fourier transform infrared (FT-IR) (see Fourier transform infrared Spectroscopy (FT-IR) and high-temperature x-ray diffraction measurements for neat PEOs and its electrolytes with the various molar ratios ([Li/EO]) including 0, 0.085, 0.1, and 0.2 to evaluate ion pairing and aggregate formation of the ions.

Figure 5.10 shows the full FTIR spectra of neat PEOs and PEO−LiTFSI salt complexes with varying salt concentration and topologies. The characteristic peaks monitored for pure PEO at 1467, 1341, 1240, 1097, 958, and 841 cm^{-1} could be attributed to CH_2 scissoring, asymmetric CH_2 wagging, asymmetric CH_2 twisting, C−O−C stretching, gauche C−C conformation, and CH_2 rocking, respectively.[202, 203] The broad peak from 2750 to 3000 cm^{-1} corresponds to asymmetric CH_2 stretching.[137, 203]

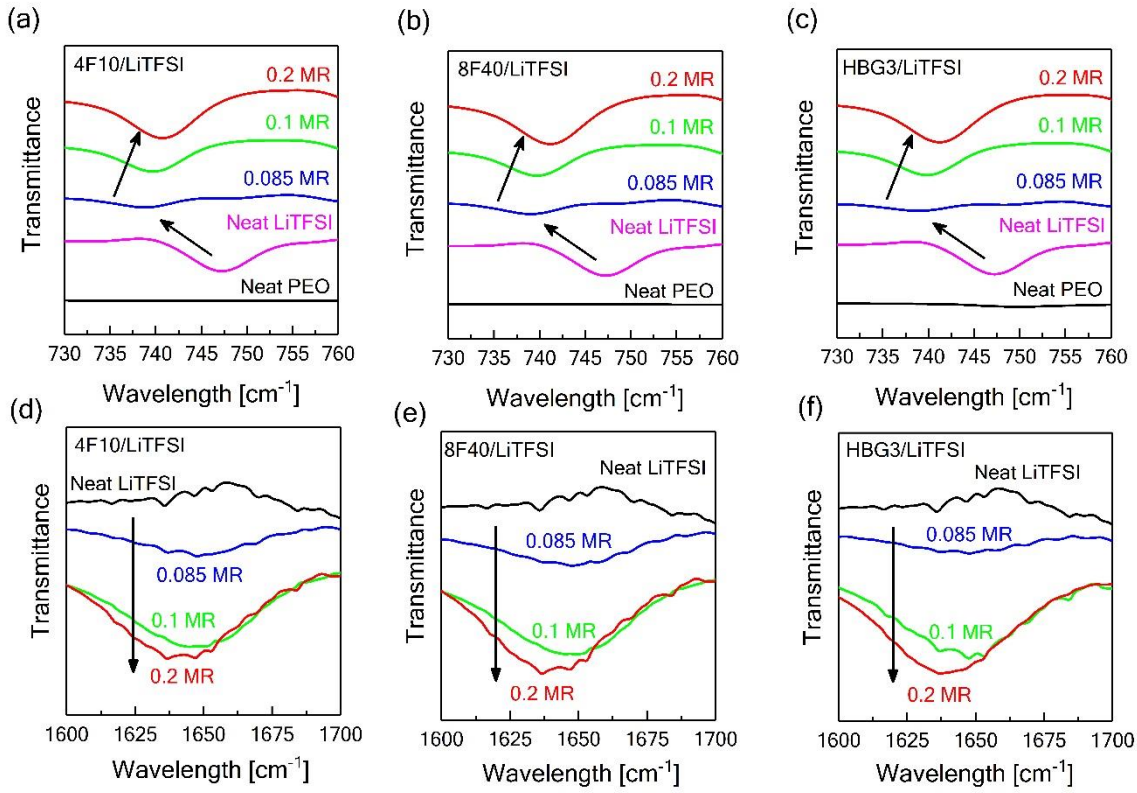

Figure 5.4. FT-IR measurements on the neat LiTFSI, PEOs and its electrolytes containing high lithium amounts [Li/EO>0.085] and polymer architectures of 4F10 (a and d), 8F40 (b and e), and HB3G (c and f). Data are vertically shifted for the clear observation of the changes.

These characteristic peaks are also seen in the case of electrolyte samples with significant changes in peak positions and intensities with increasing salt concentration for those two fundamental peaks positioned at 746 cm^{-1} and 1634 cm^{-1}, because these peaks have been the commonly used representative vibrational modes attributed to ion pair formation and aggregation, respectively,[201, 202, 204-208] which indicates ion pairing and clustering effects. For the neat LiTFSI salt, the peak located at 746 cm^{-1} accounts for CF_3 bending coupled with the S− N stretching vibration of the TFSI anions.[201, 207, 208] After the dissolution of the salt in different PEO matrixes ([Li/EO]=0.085), this peak shifted to the lower value of 738 cm^{-1} (see the left arrow in Figure 5.4a, 5.4b, and 5.4c), which is

associated with the coordination of Li^+ with PEO and, forming free TFSI− anions, in agreement with the previous reports.[201, 202, 204] When the molar ratio ([Li/EO]) increased to 0.1 and 0.2, respectively, the peak was broader and shifted to higher wavenumbers, from 738 cm^{-1} to 743 cm^{-1} (see the right arrow in Figure 5.4a, 5.4b, and 5.4c), showing enhancement in the coordination of Li^+ with $TFSI^-$ anions, forming ion-pairs, causing the electrolytes with lower ionic conductivity due to less free $TFSI^-$ ions. Additionally, since the position of peak at 1467 cm^{-1} remained unchanged among all FT-IR spectra for PEOs, it was used as a reference point in comparisons for the intensity ratios regarding the transmittance of the peak positioned at 1634 cm^{-1} corresponding to LiTFSI aggregation, it was found this peak reduced more with increasing salt content and there was a slightly higher decrease with extreme degree of branching such as hyperbranched polymer architecture (see the downward arrow in Figure 5.4d, 5.4e, and 5.4f), confirming the formation of LiTFSI aggregates which could be attributed to higher ion dissociation with increased branching.[205, 209, 210]

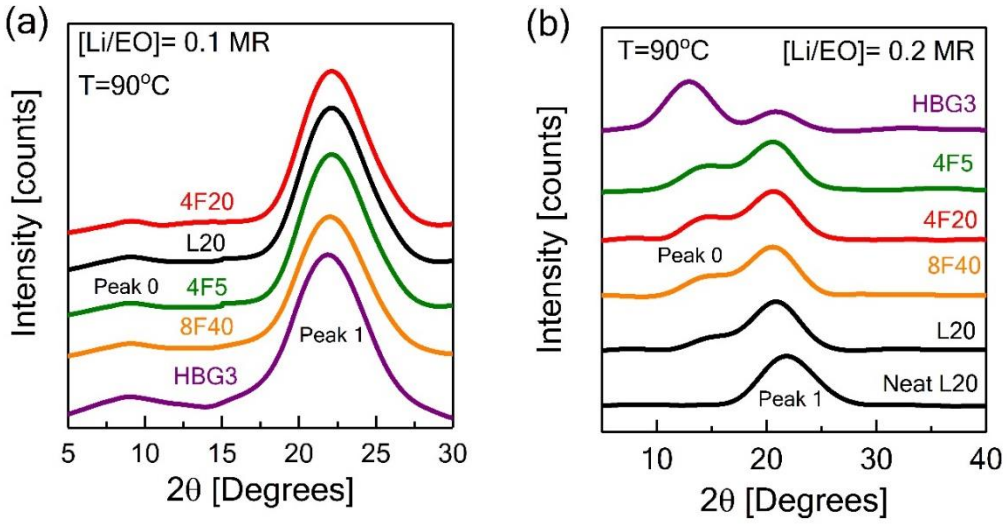

Figure 5.5. High temperature X-ray Diffraction (XRD) measurements on the neat PEO and its electrolytes with different architectures containing L20, 4F5, 4F20, 8F40, and HB3G, and high lithium concentrations (a) [Li/EO=0.1] and (b) [Li/EO=0.2] at 90°C.

Figure 5.5 shows the intensity profiles as a function of topological variations for the neat linear PEO and different salt concentrations performed at 90°C in PEO/LiTFSI complexes. In the case of salt-free sample for linear PEO (L20), the intensity profile only reveals one peak at the 2Θ of 22 degrees, attributed to the amorphous halo of the PEO chains marked as "Peak 1" in Figure 5.5.[14] With increasing salt concentration with the molar ratios ([Li/EO]) of 0.1 and 0.2 for all different architectures of PEO, another peak marked as "Peak 0" appears at lower 2Θ angle around 9°C which becomes more intense at the highest salt content ([Li/EO=0.2]) at approximately around 15°C, which is associated with the LiTFSI ion cluster formations,[14] in agreement with the previous results[14] and supporting our FT-IR results.

Furthermore, we would also like to state that the intensity of the ionic clusters is controlled by the polymer architecture with extremely high salt concentration (([Li/EO=0.2])) as seen in Figure 5.5b. More specifically, we observed that the intensity of Peak 0 increased gradually with increasing degree of branching and maximized significantly for the hyperbranched case. The representative calculations for the 2Θ angles, scattering vector, and the distance between clusters with the corresponding polymer architecture is given in Table 5.3. Peak 0 generally moves to smaller Q-values with increasing branching, indicating that the length scales associated with the correlations between clusters slightly increase with degree of branching.

5.3.4 The effect of PEO architecture, Molecular weight, Functionality and Lithium concentration on the Bulk Viscosity

In the next step, we investigated the impacts of the salt addition on the bulk viscosity of the electrolytes. We observed a Newtonian behavior (see Figure 5.11 in SI) in the viscosity measurements of the electrolytes at 75°C (above the melting temperature of the samples) which is due to the relatively low MW of the polymers. The conductivity of the

polymer electrolyte can be explained in terms of the trade-off between increasing number of charge carriers and ion migration and increased viscosity due to ion pairing and clustering effects. Figure 5.6a, shows the viscosity of the PEO/LiTFSI samples with four different architectures (Linear, 4-arms star, 8-arms star, and hyperbranched) with the same total MW (20 kDa).

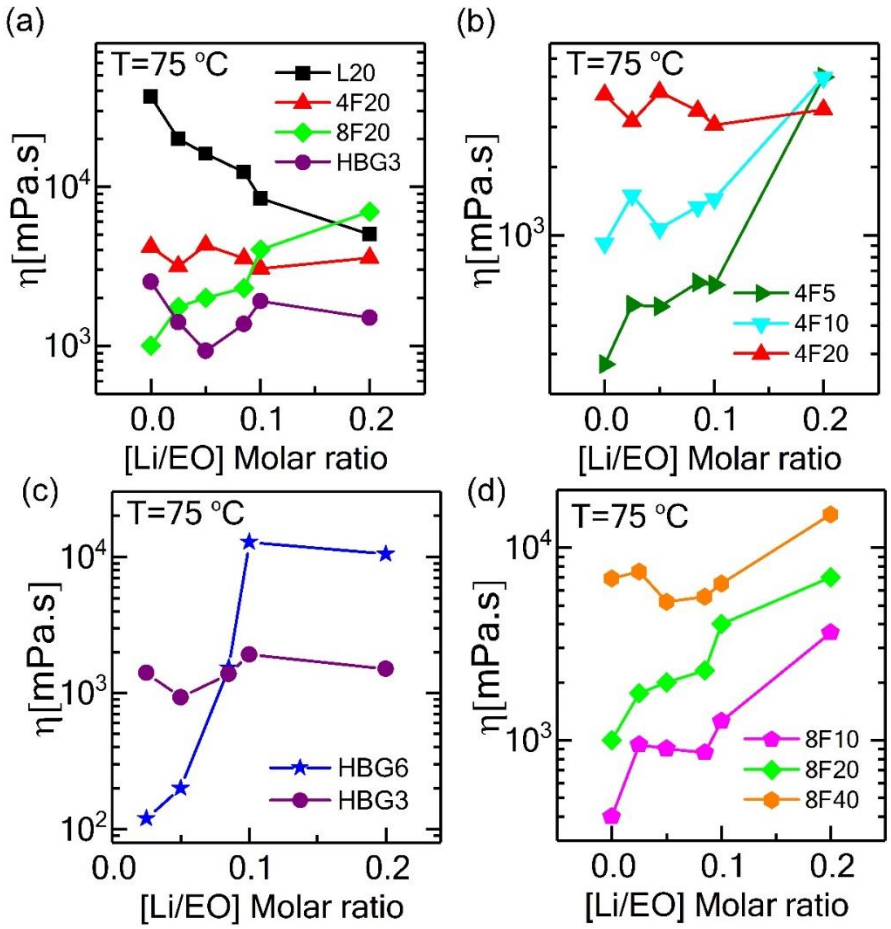

Figure 5.6. Viscosity of the PEO-based electrolytes at 75°C with various architectures including linear, stars, and hyperbranched topologies with (a) the same molecular weight (MW~ 20 kDa), (c) hyperbranched architectures (b) and (d) with varying molecular weights (MW~ 5, 10, 20 kDa) for 4-arms and (MW~ 10, 20, 40 kDa) 8-arms star topologies over a wide range of salt concentration ([Li/EO] ranging from 0 to 0.2).

The effect of salt addition on the viscosity of the samples has two sides. On one hand, ions would act as a solvent in the polymer matrix and will reduce the melting temperature (see Figure 5.2) and bulk viscosity of the samples. The higher entanglement of the linear polymer leads to the higher viscosity of this sample, which is in line with lower ionic conductivity of this polymer compared to the nonlinear chains (see Figure 5.3a). By increasing the salt content, viscosity of the linear polymer decreases, as the ions act like a solvent for the linear chains and melting temperature decreases. For hyperbranched samples (Figure 5.6c), viscosity decreases in low salt concentrations ([EO/Li] < 0.05). However, for [EO/Li] > 0.05 ratios viscosity increases due to ion clustering and pairing effects. The viscosity of the electrolytes with 4-arms star does not vary to much due to the balance between reduction in melting temperature and chain-ion interactions. However, as the functionality increases in 8-arms star chins, the transient crosslinking between the end groups of the star arms increases, which leads to increase in bulk viscosity of these samples. Figure 5.6b, 5.6d, shows the viscosity of the samples with 4-arms and 8-arms star polymers. As it was expected, viscosity increases monotonically by increasing the arm molecular weight. At high salt loading, ion clustering and ion chain interactions further slows the bulk dynamic and viscosity increase. Since ion transfer in the polymer electrolytes is directly affected by the bulk mobility of the samples, the viscosity results are in line with the conductivity data (Figure 5.3).

It means that ions can move more freely in polymer electrolyte samples with lower bulk viscosity and yield higher ionic conductivity.

5.4 Discussions

Since addition of salt concentration with the molar ratio of [Li/EO]= 0.085 yielded the highest ionic transportation for all PEO architectures at 75^0C (Figure 5.3), the ionic conductivity of all PEO based electrolytes containing constant salt loading ([Li/EO]=

0.085) as a function of temperature between 30 and 90°C with ΔT = 15°C was investigated. The temperature-dependent Li-ion conductivities shown with excellent Arrhenius fits as seen in Figure 5.7a suggest that the ion transport is mainly controlled and facilitated by the bulk viscosity (Figure 5.7c) and increased free volume (Figure 5.7d) in non-linear topologies with higher degree of branching, rather than ion-hopping in these polymer electrolytes [71] (See the Positron annihilation lifetime spectroscopy section in the supporting information for the details of free volume measurements). Furthermore, the free volume measurements for linear PEO were found to be comparable to the previously reported values.[21, 137, 211, 212]

Varying the polymer architecture with increased branching resulted in higher ionic conductivity values for the electrolytes with non-linear polymer chains when compared to the linear one with the molecular weights of 20 kDa and 1.5 kDa. (See Figure 5.13 in the Supporting Information)

The changes in the ionic conductivity of the non-linear PEO architectures which are one of vital electrolyte properties to develop for better polymer electrolytes (SPEs) could be explained by two fundamental reasons such as lower viscosity (Figure 5.7c) and substantially increased free volume (Figure 5.7d) in highly branched PEO architectures probed by PALS. More specifically, the ionic conductivity of the PEO-based electrolytes with extreme branching such as hyperbranched architectures has shown as much as 3-fold increase, which may be attributed to its loose structure leading to lower bulk viscosity as much as more than one order of magnitude and increased free volume by 20% in comparison with the linear counterpart. On the other hand, this increase in the ion transportation of the PEO electrolytes with other non-linear topologies (8 arms and 4 arms) was as much as nearly 2-fold mainly due to higher viscosity and less increased free volume (as much as 10% when compared to linear) in the case of star architectures. These

conclusions indicate the ion transport is primarily controlled by the bulk viscosity and facilitated by the free volume in the polymer matrix.

Furthermore, the estimated activation energies obtained from the Arrhenius fits displayed in Figure 5.7b are architecture dependent and in well agreement with the conductivity data.; lower activation barrier results in higher ionic conductivity.[8] In other words, the relationship between the bulk viscosity and the ionic movement is also observed from the activation energies.

The Arrhenius model is given by [8],

$$\sigma_{\alpha} = \sigma_0 \exp E/RT \quad (1)$$

where σ_0 is the reference conductivity, E is the active energy, and R is the gas constant number (8.314 $J{\cdot}K^{-1}{\cdot}mol^{-1}$). Fitting the conductivity data to the Arrhenius model gives the estimated pseudo-activation energies as shown in Figure 7b. The electrolyte with the linear PEO has an activation energy ranging around ≈ 0.27 eV for the salt molar ratio of [Li/EO] = 0.085, which results in the lowest ionic conductivity among the PEO investigated architectures. On the other hand, activation energy decreased to 0.23 and 0.22 in the case of star architectures and further lowered to 0.20 and 0.19 eV for HBG3 and HBG6, respectively which results the highest ionic conductivity among the PEO investigated architectures. (All these activation energies are comparable to the previously reported values[8, 213]). Eventually, our study quantitively shows for the first time, to the best of our knowledge, the relationship between ion conduction and other two significant and dominant factors including free volume and bulk viscosity in neat PEO based electrolytes with non-linear topologies.

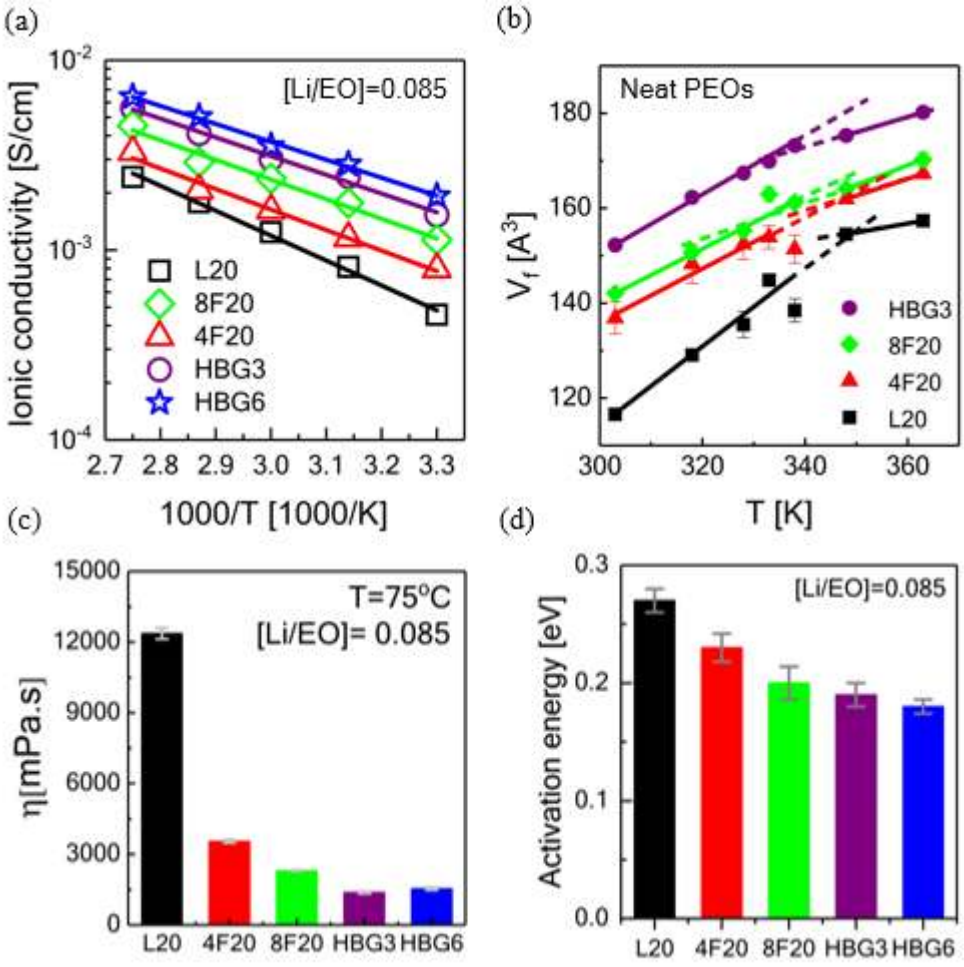

Figure 5.7. Ionic conductivity measurements of PEO-based electrolytes as a function of temperature with various architectures including linear, stars, and hyperbranched topologies with (a) the same molecular weight (MW~ 20 kDa) over a salt concentration ([Li/EO] ranging from 0.085 to 0.1) (b) Estimated pseudo-activation energies for the electrolytes with different topologies (c) Zero-shear viscosity measurements of PEO/LiTFSI salt complexes with [Li/EO]= 0.085 at 75°C (d) Temperature dependent-free volume measurements of neat PEOs with different topologies probed by PALS.

5.5 Conclusions

The series of different topologies (linear, stars, and hyperbranched) for PEO polymer with varying concentration have been thoroughly investigated as model polymer electrolytes for Li-ion batteries. To the best of our knowledge, this is the first work up to date that

correlates phase diagram, free volume, and bulk viscosity with the ionic conduction in PEO/LiTFSI electrolytes with branched architectures. The constructed phase diagrams which distinctively depends on the employed PEO architecture and salt concentration showed effectively decreasing degree of crystallization with increasing branching and salt addition owing to the restricted mobility of the polymer chains. The completely amorphous electrolytes were accomplished using lesser salt concentration with the higher degree of branching, especially, significantly lower in the case of hyperbranched PEO architectures. Furthermore, the salt concentration-dependent Li-ion conductivities for different PEO topologies unveiled the ionic conduction for all architectures maximized with the molar ratio of [Li/EO = 0.085] above which it decreased drastically due to the formations of ionic clustering and pairing. More specifically, the PEO electrolytes including highly (hyperbranched) and moderately branched architectures (4-arms and 8-arms) with the molar ratio of [Li/EO = 0.085] resulted in nearly three and two-fold higher ionic conductivity at 60^{o}C, respectively, when compared to the linear analogue, mainly due to lower bulk viscosity with significantly increased higher free volume in non-linear topologies. In addition to this, regardless of the PEO architectures, the temperature dependence of ionic conductivity in neat PEO/LiTFSI electrolytes with a fixed salt content ([Li/EO = 0.085]) was well defined using the Arrhenius mechanism, suggesting

that ion transport is fundamentally through ion hopping and essentially affected by bulk viscosity and free volume. The estimated activation energy values decrease with the increasing ionic conductivity. The activation energies for ion hopping also agrees well with the conductivity data, lowering activation barrier results in higher ionic conductivity for highly branched PEO architectures. Overall, our results show that the ionic conductivity in PEO-based electrolytes could be significantly enhanced employing non-linear topologies with the optimized salt content.

5.6 Supporting Information

EXPERIMENTAL METHODOLOGY

Materials

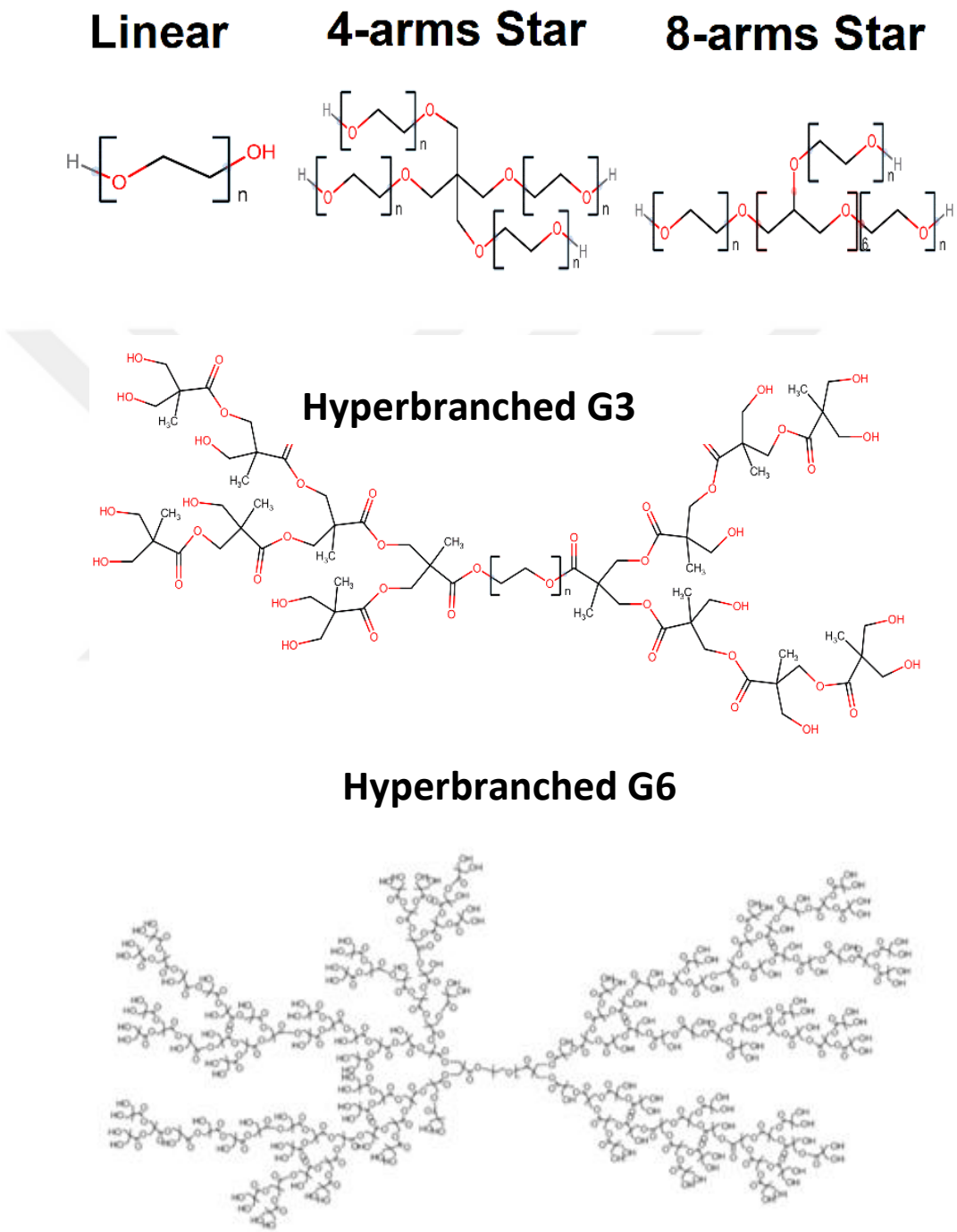

Figure 5.8: Chemical structure of the PEO polymers. The structure for the hyperbranched PEO (G6) was taken from the manufacturer (Sigma-Aldrich)'s page.

RESULTS AND DISCUSSION

Differential Scanning Calorimetry (DSC):

To estimate the degree of crystallinity for neat PEOs with the different number of arms and arm molecular weights, we used the following equation $X_c = \left(\frac{\Delta H_m}{\Delta H_c}\right) * 100$, where ΔH_m is the melting enthalpy of the sample estimated from DSC (see the experimental results in Table 5.2 in the Supporting Information), and ΔH_c is the melting enthalpy of completely crystalline PEO, which is 196.4 J/g.[8]

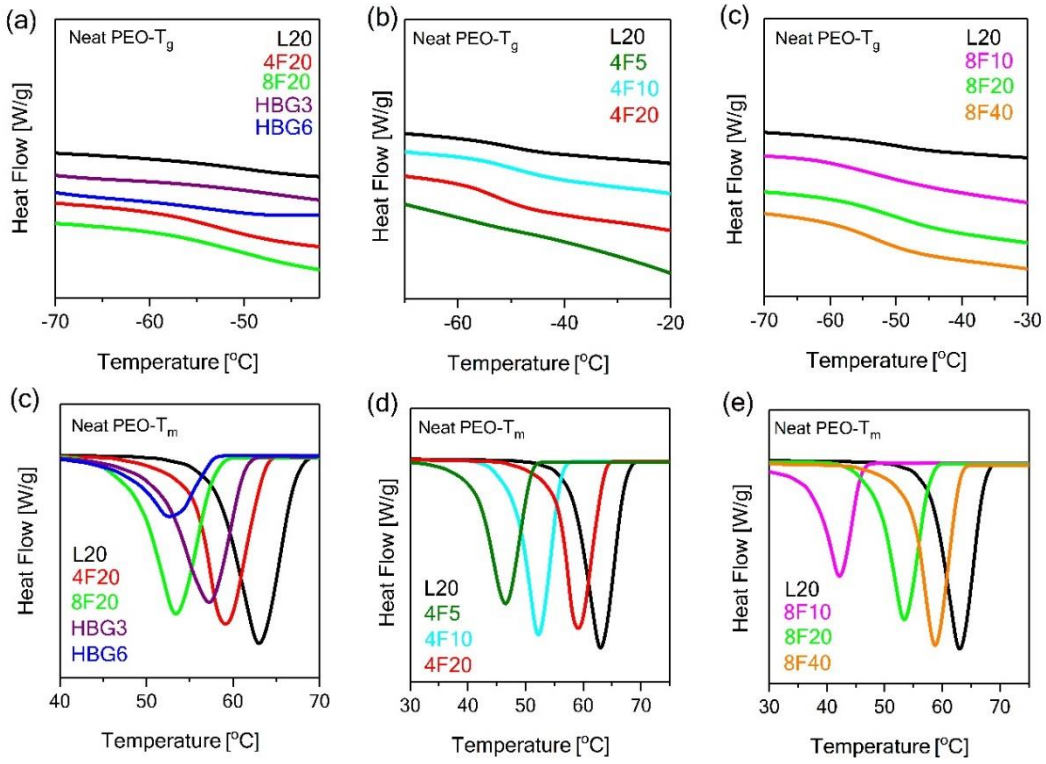

Figure 5.9: DSC thermographs with emphasis on glass transition (a,b,c) and melting (d,e,f) temperatures for the neat PEOs with various architectures.

Table 5.2: Glass transition and melting temperatures with the estimated enthalpies and degree of crystallizations of various PEO architectures over different salt fraction.

Estimated Parameters	PEO topologies with varying molecular weights									
	Li/EO	**L20**	**4F5**	**4F10**	**4F20**	**8F10**	**8F20**	**8F40**	**HBG3**	**HBG6**
T (Melting Temp),C	0	63.0	46.5	52.2	59.1	42.2	53.4	58.8	57.3	52.7
	0.025	56.9	42.1	45.0	51.4	26.0	44.2	52.6	49.1	44.1
	0.05	50.0	34.4	30.5	42.7	18.0	33.0	39.3	20.0	-
	0.085	30.27	-	-	-	-	-	-	-	-
Tg (Glass Transition),C	0	-51.6	-58.5	-50.7	-52.5	-53.0	-50.8	-53.9	-47.2	-48.4
	0.025	-45.0	-47.0	-49.0	-43.2	-46.0	-49.6	-43.4	-46.8	-45.0
	0.05	-41.0	-42.3	-53.4	-42.4	-43.0	-47.8	-46.2	-46.0	-41.2
	0.085	-46.0	-48.0	-48.0	-41.0	-45.0	-47.0	-46.4	-46.6	-41.4
	0.1	-43.0	-44.1	-44.5	-40.9	-42.0	-44.5	-44.0	-45.8	-40.3
	0.2	-38.0	-31.0	-33.0	-33.6	-32.0	-43.2	-41.4	-54.0	-39.8
Melting Enthalphy, J/g	0	146.8	117.5	122.5	120.0	79.383	126.13	135.3	122.5	61.7
	0.025	86.0	68.0	70.0	74.2	60	103.58	74.7	58.7	2.4
	0.05	35.4	33.0	42.4	48.5	30	46	35.6	30.5	-
	0.085	7.51	-	-	-	-	-	-	-	-
The degree of crystallazation, %	0	74.9	60.0	62.5	61.2	40.5	64.4	69.0	62.5	31.5
	0.025	43.9	34.7	35.7	37.8	30.6	52.8	38.1	29.9	1.2
	0.05	18.1	16.8	21.6	24.7	15.3	23.5	18.2	15.6	
	0.085	3.8		-	-	-	-	-	-	-

Fourier transform infrared Spectroscopy (FT-IR):

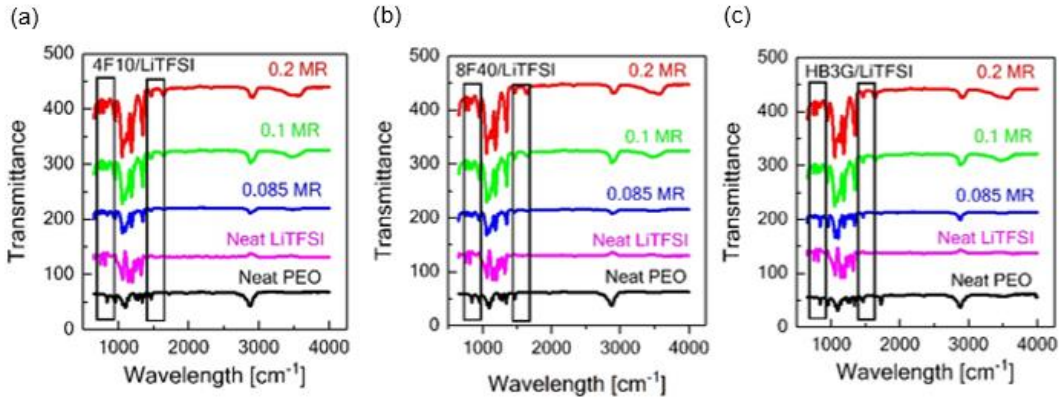

Figure 5.10. Full spectra of the FT-IR measurements on the neat LiTFSI, PEOs and its electrolytes containing different lithium amounts [Li/EO>0.085] and polymer architectures of 4F10 (a), 8F40 (b), HB3G (c), respectively.

X-ray Diffraction (XRD):

Table 5.3: The representative calculations for the 2Θ angles, scattering vector, and the distance between clusters with the corresponding polymer architectures.

Salt Molar Ratio	PEO Architecture	2Θ [◦]	Q=4πSinΘ/λ [1/nm]	d=2π/Q [nm]
[EO/Li]=0.2	**HB3G**	11.5	8.1	0.78
	8F40	12.5	9.6	0.65
	4F20	12.25	8.7	0.72
	4F5	12	8.5	0.74
	L20	14	9.9	0.63

Rheology Measurements:

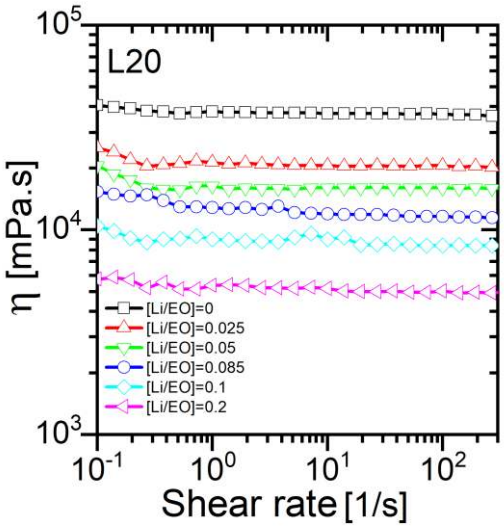

Figure 5. 11: Viscosity of L20 electrolytes with respect to lithium content (0 < [Li/EO] < 0.2) show Newtonian flow behavior at 75°C.

Dynamic Light Scattering (DLS):

Table 5.4. The change of compactness with respect to different polymer architectures.

PEO	M_{total} (kDa)	M_{arm} (kDa)	PID	R_g (nm)	R_h (nm)	R_{core}/R_g
8F10	10	1.25	1.02	2.02	1.43	0.27
4F5	5	1.25	1.03	1.93	1.70	0.21
8F20	20	2.5	1.10	2.90	2.28	0.13
4F10	10	2.5	1.03	2.72	2.04	0.11
8F40	40	5	1.09	4.04	3.07	0.07
4F20	20	5	1.03	3.85	2.41	0.05
L20	20	10	1.5	5.2	3.22	≈ 0
HBG3	20	-	<1.5	-	2.94	≈ 0

Positron annihilation lifetime spectroscopy (PALS): Positron annihilation lifetime spectroscopy (PALS) is a well-established and very sensitive non-destructive spectroscopy technique that allows studying a variety of phenomena and material properties on an atomic scale including free volume and its fraction.[132-135] The PALS spectra were divided using the computer program LT polymers into four lifetime components corresponding to annihilation of para-positronium (p-Ps), free positrons, and two ortho-positronium (o-Ps) in the increasing order of their lifetime, respectively: τ_1 (the shortest-lived component with an intensity I_1), τ_2 (the intermediate-lived component with an intensity I_2) and τ_3 (the longest-lived component with an intensity I_3). [132-135] τ_1 and I_1 are associated with the annihilation of para- positronium (p-Ps), τ_2 and I_2 are allied with direct annihilation of positrons, and τ_3 with I_3 and τ_4 with I_4 are associated with pick off annihilation of ortho-positronium (o-Ps within the crystalline and amorphous regions of the polymers. In estimating the longest lifetime parameters, τ_1 and τ_2 were assumed as independent of free volume and the former was assumed not to chance in vacuum and matter so we have taken as 125 ns fixed. O-Ps lifetimes, τ_3 and τ_4, are sensitive to the free

volume hole size and I_3 and I_4 have straight correlation with the number of free holes in the materials. [132, 135, 136]

The relation between o-Ps lifetime and radius of free volume hole (R) is given by Tao-Eldrup model with the assumption of spherical holes as follows:[133-135, 137]

$$\tau(ns) = \frac{1}{2}\left(1 - \frac{R}{R_0} + \frac{1}{2\pi}\sin\frac{2\pi R}{R_0}\right)^{-1} \quad (1)$$

where $R_0 = R + \Delta R$ with $\Delta R = 0.1656$ nm as an empirical parameter for a measure of electron layer inside the spherical potential well. The size of free volume holes (V_f) is finally then calculated by using the following equation.

$$V_f = \frac{4}{3}\pi R^3 \quad (2)$$

The obtained results from PALS measurements for the free volume estimations with intensities I_3 and I_4 as a function of temperature and polymer architecture corresponding to crystalline and amorphous regions in the polymer along with heat flow thermographs of neat PEOs with architectural changes were given by Fig 5.12.

It is evident that there were two different clear trends for the free volume above and below a certain temperature which turns out to be melting temperature for all architectures and this temperature agrees well with the estimations from the differential scanning calorimetry experiments. This changing trend could be well related to the melting crystals in the PEO matrix, creating additional free volume significantly. This is also supported by the decreasing intensity of I_3 accompanied by the increasing intensity for I_4 *(Figures 5.12a and 5.12b).*

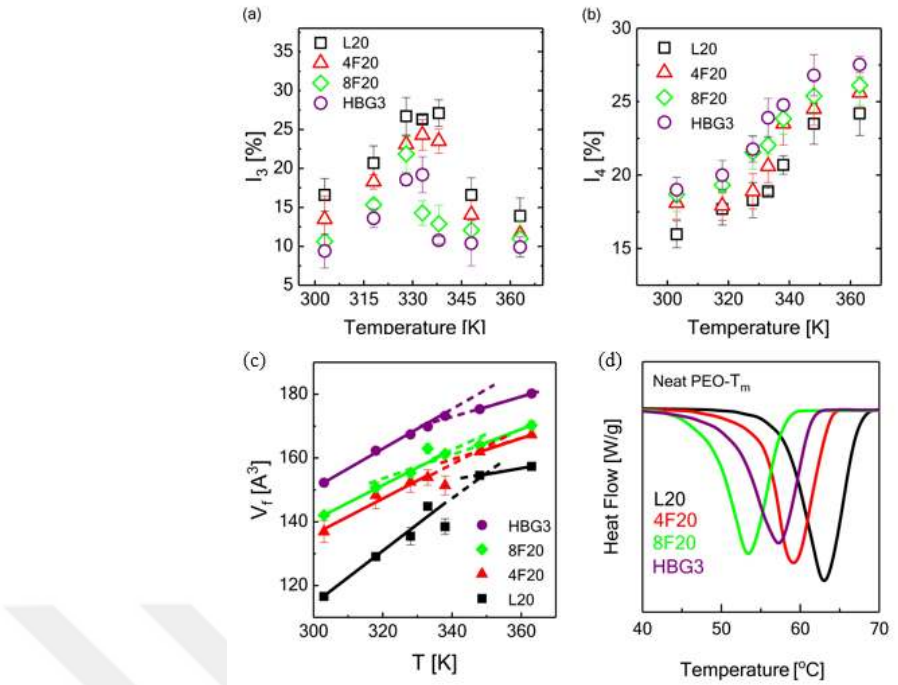

Figure 5.12. The intensities (a) *I3* and (b) *I4* as a function of temperature and polymer architecture corresponding to crystalline and amorphous regions in the polymer, respectively (c), Free volume measurements as a function of temperature, (d) Heat flow thermographs of neat PEOs with architectural changes.

Electrochemical Impedance Spectroscopy (EIS):

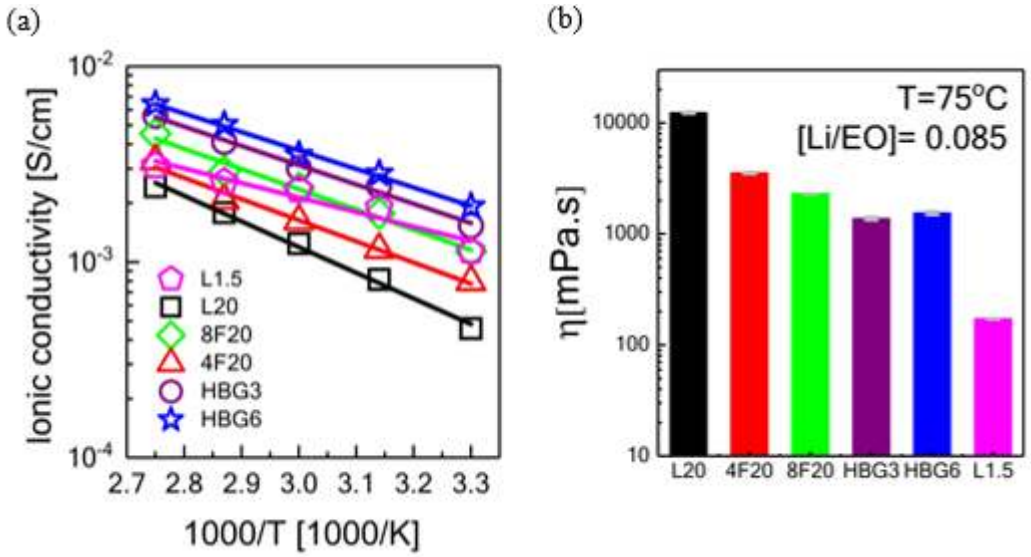

Figure 5.13. Ionic conductivity measurements of PEO-based electrolytes as a function of temperature with various architectures including linear, stars, and hyperbranched

topologies with (a) the molecular weights of 20 kDa and 1.5kDa over a salt concentration ([Li/EO] ranging from 0.085 to 0.1) (b) Zero-shear viscosity measurements of PEO/LiTFSI salt complexes with [Li/EO]= 0.085 at 75ºC.

INTRODUCTION

The development of better, safer, and sustainable power sources has been one of the most important technological challenges because of ever-growing increase in requirement for packed, lightweight, and mobile consumer electronics and energy storage devices.[1-3] To satisfy the demand, chemical evergy storage in batteries appears to be the most promising and widely used method when compared to conventional technologies such as pumped hydroelectric or compressed air, and flywheel.[24-26] Batteries, with their high energy density with a variety of current and voltage ranges, can be utilized for both stationary and mobile applications due to their packed and lightweight structure.[4, 5] Despite environmental and sustainability risks related to toxic and rare cathode materials (lithium, cobalt, or nickel), volatility of the organic solvent-based electrolytes, and greater CO_2 emissions due to heavier specific weights of the liquid electrolytes than water-based electrolytes [214, 215] when compared to zinc–carbon and zinc/alkaline manganese dioxide based primary batteries, [30, 32, 34, 35] lithium-ion batteries (LIBs) have increasingly attracted more attention due to their low maintenance, high energy density, prolonged cycling stability, longer shelf life, electrochemical potential, and its recyclability. [4, 8, 23, 214, 216]

The commercial LIBs mostly use liquid electrolytes with high ionic conductivities[216], however they are often highly volatile, flammable, and toxic, which may result in environmental and safety hazards such as fire, leakage, explosion, short circuit, and lithium dendrite formation, which endangers battery safety and human and environmental health. [4-6, 216] To overcome these disadvantages, solid polymer electrolytes (SPEs), have gained significant attention [4, 5, 9, 216].

SPEs, in general, provide many advantages over liquid electrolytes, including higher flexibility, greater energy density and processability, good thermo-mechanical stability,

nonflammability, and wide electrochemical stability, leading to more compact and safer batteries. [4, 8-10, 214, 217] However, their commercial use is limited due to their low ionic conductivity, *e.g*. room temperature ionic conductivities of SPEs are (10^{-5} S/cm) at least 2–3 orders of magnitude lower than common liquid electrolytes (~10^{-2} S/cm)[8].

Among the water-soluble polymers including polyacrylamides, polyacrylic acid, and polyvinyl alcohol, poly(ethylene oxide) (PEO) based SPEs have been a common choice due to various reasons. PEO has very low glass transition temperature (T_g ~ 220 K) when compared to other water-soluble polymers such as polyacrylamides (T_g ~ 450 K), [218] polyacrylic acid (T_g ~ 390 K),[219] and polyvinyl alcohol (T_g ~ 350 K),[220] which allows fast segmental relaxation (and hence ion transport) [8], easy processability at room temperature [146, 147, 221]. Also, as opposed to polyacrylamides PEO is a biodegradable polymer-an important feature for battery implants and wearable electronics [147, 221, 222], and provides higher thermal decomposition temperature compared to polyacrylic acid, and polyvinyl alcohol. [219, 222-224] From the practical point of view, PEO can solve a variety of different salts through the complexation between ether-oxygen and the lithium ions, [8, 13, 15] and its electrolytes properties in the neat form have been well studied, thus, allowing for a meaningful evaloation of conductivity performance of the electrolytes.

As ion transport primarily occurs in the amorphous phase [8, 51, 71, 153], inherently high degree of crystallinity of PEO impedes ionic mobility at room temperature, resulting in low conductivities (~ 10^{-6} – 10^{-8} S/cm) [8].

Above its melting temperature (T_m = 333 K), the conductivity of the molten PEO electrolyte is increased up to the values ranging around (10^{-3} S/cm), yet, the decrease in the mechanical stability limits its use as a solid-state electrolyte.[18] Enhancing ionic conductivity of PEO electrolytes without much sacrificing, or even improving, the

mechanical strength remains as a major challenge. In this regard, incorpration of nanoparticles into the electrolytes to form composite elecrolytes is a promising approach. [21, 86, 153] For example, Utpalla *et al*.[21] studied the addition of silica nanoparticles into PEO and reported that enhanced free volume using inorganic nano-fillers improved the ionic conductivity in PEO/Silica based copolymer electrolytes. Similarly, Michael et al.[153] revealed incorporation of nano-fillers into PEO matrix increased free volume by decreasing crystallization, hence facilitated ion migration. Schaefer and co-workers [86] the incorporated the SiO_2 nanoparticles (NPs) grafted by the PEO in the composite electrolyte, which resulted in drastically higher mechanical modulus along with high conductivity because of SiO_2 core fractions and increasing free volume, respectively. All these studies on nanocomposite electrolytes aimed for enhancing ion mobility by impeding crystallization by adding NPs into linear polymer matrices; however, in most of the cases, the NP dispersion in salt containing matrices remained poor and was not controlled.

Different from the previous approaches, this study focuses on the polymer component by systematically increasing the degree of branching of the polymer chains and explore the possibility of using composites electrolytes with nonlinear matrices and well dispersed silica nanoparticles to achieve simultaneous improvement in the ionic conductivity and mechanical moduli of SPEs. This is rationalized by the fact that the free volume is enhanced by branching in the nonlinear topologies due to excessive number of chain ends compared to the linear chains [97, 98]. Fro examples, Chremos and co-workers [98] studied star polymers of different number of arms and arm molar mass, and reported that increasing the arm number promoted the free volume and mobility compared the linear chains. Moreover, a variety of studies on the ‘neat’ PEO architectures including linear, stars, and hyperbranched also investigated the effect of polymer architecture on

crystallization.[8, 16, 92-94] In this sense, Zardalidis *et al*.[93] studied the dependence of crystallization on topological changes using linear and ring PEO architectures and reported that the ring PEO possessed lower degree of crystallinity compared to the linear analogue due to its more restrained structure. In a similar work, Chen *et al*.[225] investigated crystallization behavior in linear and star PEO topologies (3-arms and 4-arms) and found the crystallinity of star polymers was significantly reduced. Similarly, the study conducted by Coppola and co-workers [92] using different PEO topologies (linear and stars) uncovered crystallization kinetics of the star topologies was slower than their linear analogues mainly because of high degree of branching with slowed diffusivity in stars. Furthermore, in different works, Yao *et al*.[94] and Lee *et al*.[16] unveiled that the crystallization of hyperbranched Poly(ethylene oxide) was effectively hindered compared to crystallization of the linear architecture. Very recently, a previous work of the authors [8] on the PEO/PMMA-based electrolytes using various architectures (linear, stars, hyperbranched, and bottle brush) showed that the degree of neat PEO crystallinity for different architectures severely decreased with the increasing number of branching. These previous works show that the degree of PEO crystallization could be decreased more effectively when non-linear PEO architectures are applied, resulting in an increase in the amorphous fraction of the PEO, thus the electrolytes prepared using branched PEO topologies could have higher ionic conduction.

In this study, the advantages provided by the enhanced free volume due to the increased number of end groups and suppressed crystallization arising from branching in the nonlinear PEO architectures are combined with the mechanical reinforcement due to the nanoparticles to obtain a synergystic effect on improved ionic conductivity and mechanical moduli. PEO with linear, 4-arms, 8-arms, and hyperbranched (3rd generation, 3G) architectures were employed to explore the role of polymer compactness on

nanoparticle dispersion, ionic conductivity, and rheological behavior in polymer nano-composite based electrolytes, which was as schematically shown in Figure 6.1.

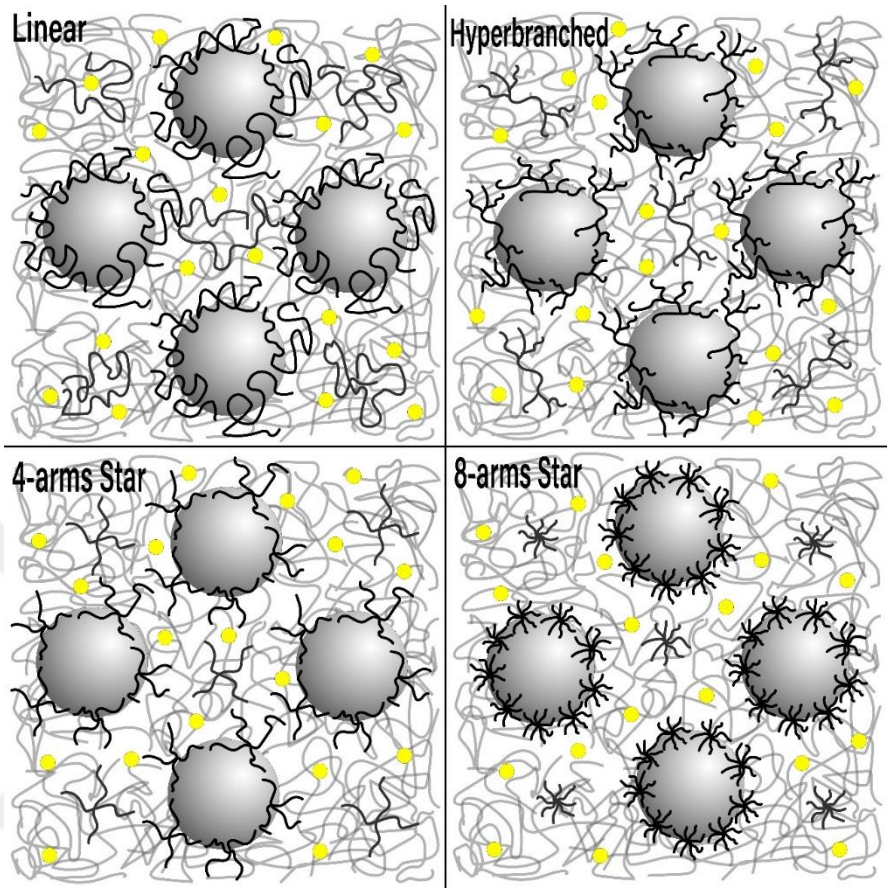

Figure 6.1. Schematic representation of the PNC based solid polymer electrolytes composing of PEO and Silica nanoparticles (big grey circles) with the architectural variations including linear, 4-arms star, 8-arms star, hyperbranched (3rd generation) used in this study (Yellow filled circle represents the Li^+ ion).

6.2 Experimental methodology

In this part, materials used in this study are explained and defined, respectively.

6.2.1 Materials

Linear PEO, hyperbranched (3rd generation) PEO, and Lithium bis(trifluoromethane)sulfonamide, LiTFSI salt were purchased from Sigma-Aldrich. 4-arms star and 8-arms star PEO were supplied by Creative PEGWorks. All polymers were used as received without modification. Chemical structures of the polymers are provided

in Figure 6.6. Table 6.1 displays their functionality, molar masses, and dispersities. The methyl ethyl ketone (MEK)-based colloidal spherical silica (diameter of 50 nm) solution was supplied by Nissan Chemical America Incorporation (USA).

Table 6.1. Molecular characteristics including functionality, dispersity, total, and arm molecular weight of the PEO samples used in this study.

PEO architecture	**Sample ID**	**Functionality (f)**	**MW [kg/mol]**	**M_{arm} [kg/mol]**	**Dispersity (~~*Đ*~~)**
Linear	L20	2	20	10	1.10
4-arms star	4F20	4	20	5	1.03
8-arms star	8F20	8	20	2.5	1.10
Hyperbranched	HB3G	3rd generation	20	NA	<1.5

6.2.2 Preparation of salt-free samples & electrolytes

First PEO polymers with linear (MW~20 kDa), 4-arms star (MW~20 kDa), 8-arms star (MW~20 kDa), and HB3G (MW~20 kDa) architectures were dissolved in acetonitrile at 30 mg/ml concentration. Then, the solutions were stirred with a magnetic stirrer at room temperature for 6 hours. Then, the desired amount (to get the final 30 vol% NP concentration) of the colloidal silica solution was added into the polymer solutions, which was followed by another 6- hour continuous stirring with a magnetic stirrer at room temperature.

Next, a proper amount of lithium bis(trifluoromethane)sulfonamide, LiTFSI, was dissolved in acetonitrile in glovebox filled with Argon and the salt solution was stirred with a magnetic stirrer at room temperature for 6 hours. Later, to prepare the PNC based electrolytes, the desired amount of salt solution was added into the PEO/silica solution in

the glovebox filled with Argon and then was stirred with a magnetic stirrer at room temperature for another 6 hours. Then, the solutions were then cast onto glass petri dishes and dried for ≈12 h at room temperature for overnight in glovebox filled with Argon. Finally, the dried films were annealed at 90 ^{o}C in vacuum oven for 48 hours to remove the residual solvents.

6.2.3 Characterization

X-ray diffraction (XRD): The XRD patterns of the pure PEOs and the electrolytes were recorded using the Bruker D8 Phaser – X-ray diffractometer with Cu Kα source at room temperature with the Bragg's angles (2θ) varying from 5 to 60 degrees.

Differential scanning calorimetry (DSC): The differential scanning calorimetry (DSC) samples were prepared by putting ~8-10 mg of material in aluminum pans provided by TA Instruments. DSC experiments of the neat PEOs and its electrolytes were carried out with a TA Instruments DSC25 instrument equipped with a refrigerated cooling system. An aluminum pan was used as a reference. To get rid of the temperature history completely, all the samples were heated to 120℃ and waited there for 5 minutes. Samples were then quickly cooled down to -85℃ at the rate of 20℃ /min. DSC scans were then collected during the heating process to 120℃ at the rate of 10℃ /min.

Electrochemical impedance spectroscopy (EIS): Impedance characterization was carried out using an Autolab Potentiostat Galvanostat PGSTAT (Metrohm, Netherlands) in two-electrode configuration for PEO based electrolytes. This arrangement was used to investigate electrode properties in solid-state systems. The measurement frequency was varied between 1 Hz to 1 MHz. Each SPE blend disc was sandwiched between two stainless steel blocking electrodes under argon environment in a glove box located at Koç University Boron and Advanced Materials Application and Research Center (KUBAM) and sealed in MTI Split Cell to measure the complex impedance spectra. After waiting

for the temperature stabilization of 0.1°C, the experiments were also carried out at various temperatures. The data was analyzed to characterize real and imaginary impedances using the NOVA software.

SAXS measurements: The small-angle X-ray scattering (SAXS) data on molten nanocomposites were collected using Anton Paar's SAXS Point 5.0 at Koç University. The samples were sealed between Kapton films and equilibrated at 80°C (well above their melting temperatures) for 15 min before the measurements. The static SAXS profiles were used to evaluate the state of nanoparticle dispersion in the nanocomposites. Frames were collected for 5-minute period over a total duration of 15 minutes per sample. The transmission data was obtained for each sample and the Kapton background for proper reduction and subtraction. Data reduction was performed using the SAXS/WAXS analysis program of SAXSPoint 5.0.

Rheology measurements: All rheological measurements in the melt state are performed using an Anton Paar MCR 302 rheometer equipped with a parallel geometry with diameter of 25 mm. For small-amplitude oscillatory shear (SAOS) measurements at 80°C, first amplitude sweep test performed from 0.01 to 10% strain to find the linear viscoelastic region (LVR). Then, the frequency sweep measurements were performed between 0.01 to 100 rad/s at LVR.

6.3 Results and Discussion

In this section, we analysed the results and proposed a discussion in relation to the findings.

6.3.1 The effect of Polymer architecture and Silica nanoparticle addition on the dispersion of the particles in PEO/Silica composite polymer electrolytes

NP agglomeration could lead non-homogenous dispersion of the particles and adversely affect the characteristics of the composite electrolytes such as crystallization, ionic

conductivity, [21, 87, 88, 226, 227] The dispersion of silica nanoparticles in the PEO matrix was investigated by performing SAXS measurements in the molten state of the composite electrolytes. The intensity profiles as a function of scattering vector, $Q = 4\pi \sin\theta/\lambda$, (where 2θ is the angle between the incident and the scattered beam and λ is the wavelength of the x-rays) are shown in Figure 6.2 for all samples. At low Q, the intensity from all samples reaches Q-independent plateau, confirming the absence of large-scale agglomerates, hence individual NP dispersion in all samples. In addition, for the samples with linear, 8-arms star, and hyperbranched architectures, we observe the structure factor peaks at $Q \approx 0.1$ nm^{-1} corresponding to the average Bragg spacing of $2\pi/Q \approx 63$ nm. This value is consistent with the theoretical prediction for the center-to-center interparticle distance ($h = d\,[2/(\pi\phi)]^{1/3} \approx 64$ nm) of spherical NPs of diameter $d = 50$ nm and 30 vol. % loading. This further supports the individual NP dispersion in each matrix. The peak intensity in nanocomposite samples with 4-arms matrix is not as sharp as in other samples possibly due to more uneven spacing between the dispersed NPs although the particles disperse individually (as evidence from the lack of low-Q upturn in intensity). Overall, the NPs remain well-dispersed in all electrolyte samples; thus, the observed differences in the rheological behavior and ionic conduction of the composite electrolytes are not caused by the NP structuring, rather the difference in the architecture of the matrix polymers.

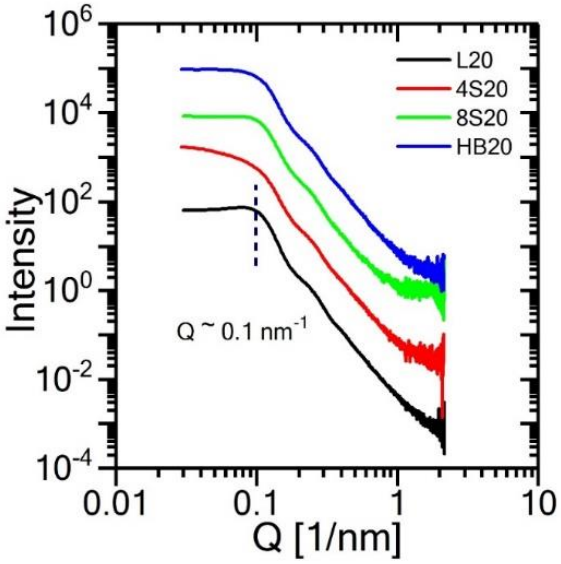

Figure 6.2. SAXS intensity profiles for the PEO-based PNCs electrolytes containing 30 vol% Silica nanoparticles and LiTFSI (Li/EO=0.085 MR) with various PEO topologies. Profiles are shifted vertically for clarity.

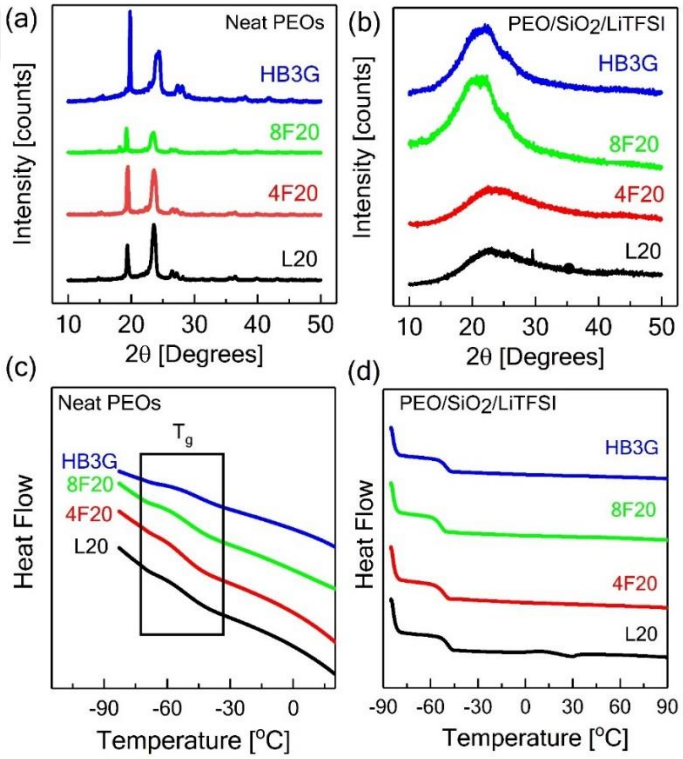

Figure 6.3. XRD and DSC results for neat PEOs (a), (c) and its respective PNCs based electrolytes (b), (d), respectively, containing 30 vol% Silica nanoparticles and LiTFSI (Li/EO=0.085 MR) with various PEO topologies.

Next, the crystallization of the neat PEO homopolymers and polymer nanocomposite electrolytes involving 30 vol.% silica nanoparticles and LiTFSI ([Li/EO=0.085]) were examined.

Figures 6.3a and 6.3b show the room temperature X-ray diffraction (XRD) spectra for the neat PEOs with various topologies without salt and their corresponding PNC electrolytes. The intensity profiles of the pure PEOs with different architectures (Figure 3a) displayed primary peaks positioned at the same Bragg's angles such as 2θ=19° (120-plane) and 2θ=23° (032-plane) due to the strong tendency of PEOs to crystallize at room temperature. However, crystal structure and interplanar distance remain identical for different PEO architectures.[8, 17, 18, 92, 93] Additionally, the degree of neat PEO crystallinity (% $X_c = \Delta H_m/\Delta H_c \times 100$) for different polymer topologies was estimated from the DSC thermograms given in Figure 6.7 by taking the ratio of the melting enthalpy (ΔH_m) of the sample to the enthalpy of melting of completely crystalline PEO (ΔH_c) which is taken as 196.4 J/g. [8] (see Figure 6.7 in the Supporting Information for the DSC thermographs for neat PEOs with different architectures). In this context, when compared to linear counterpart, the melting enthalpies for the branched topologies considerably reduced, suggesting effective suppression of the PEO crystallization in these architectures because of the restricted mobility of the polymer chains to form crystal structures mainly due to the topological constraints introduced by the branching.[92, 190, 192] This reduction appears to be slightly dependent on the polymer architecture such that higher fraction of amorphous phase was formed with increased number of arms in these non-linear architectures. This could be understood by the fact that lowering arm length arising from the increasing branching decreased the ability of the arms along with the slower crystallization kinetics in these non-linear architectures in order to reorient for the

formation of their own crystals.[8, 92, 228] Nevertheless, a significant level of crystal phase remains in all neat PEO architectures, which is not desirable for ionic conductivity. As seen in Figure 6.3b, the incorporation of 30 vol% SiO_2 nanoparticles and LiTFSI salt with a molar ratio (Li/EO=0.085) resulted in a dramatic decrease in the peak intensity for L20/SiO_2/LiTFSI composite electrolyte whereas it completely prevented crystalline domains in the case of non-linear PNCs-based electrolytes. The representative melting enthalpies and crystallinity ratios for neat PEOs with the architectural variations and it corresponding composite electrolytes are indicated by Table 6.2. Furthermore, the apparent melting temperature (T_m) values estimated from DSC results for neat PEOs with various PEO topologies in Figure 6.7 were also architecture-dependent such that the non-linear architectures had usually lower melting temperatures as the branching increased, which agrees with the previous findings.[8, 17, 225] The lower melting temperature of the branched architectures could be attributed to the thinning of the crystalline lamellae with slower crystallization rate as well as the increased ability for the salt dissolution arising from the stronger interaction between polymer chains and the lithium salt due to increased branching in these non-linear topologies. [8, 17, 225] Overall, regardless of the topological variations, all these results suggest that the crystallinity of PEO can be remarkably inhibited in PEO-based electrolytes using well-dispersed SiO_2 nanoparticles.

6.3.2 The effect of Polymer architecture and Silica nanoparticle addition on the crystallization and glass transition temperature in PEO/Silica composite polymer electrolytes

The effect of silica nanoparticles and salt on the glass transition temperature of the electrolytes was negligibly small. The figures 6.3c and 6.3d shows the DSC thermograms in which the glass transition and melting process of both amorphous and crystalline phase is clearly noticed. As summarized in Table 6.1, the glass transition temperature of neat PEOs (T_g~-55 ^oC) (Figure 6.3c) showed no significance change with varying PEO

architecture, implying preserved plasticity at room temperature. With the loadings of SiO_2 NPs and LiTFSI salt (Figure 6.3d), we observed no significant variation in the glass transition temperature (T_g) for the composite polymer electrolytes.

Table 6. 2. Glass transition and melting temperatures with the estimated enthalpies and degree of crystallizations of various PEO architectures with 30 vol% Silica nanoparticles and constant lithium concentration (Li/EO=0.085 MR).

Estimated Parameters	**PEO/Silica Nanoparticles/LiTFSI System**				
	Li/EO	**L20**	**4F20**	**8F20**	**HB3G**
T (Melting Temperature), °C	0	57.8	55.3	48.4	51.2
	0.085	29	-	-	-
T_g (Glass Transition), °C	0	-51.1	-52.5	-51.0	-48.0
	0.085	-49.7	-51.7	-53.0	-51.0
Melting Enthalpy, J/g	0	145.8	125.8	125.0	124.9
	0.085	1.1	-	-	-
The Degree of Crystallization, %	0	74.2	64.1	63.6	63.0
	0.085	0.6	-	-	-

6.3.3 The effect of Polymer architecture and Silica nanoparticle addition on the ion conduction in PEO/Silica composite polymer electrolytes

Oscillatory shear rheology measurements on these composite polymer electrolytes helped to understand the relationships between their microscopic dynamics and the bulk transport properties. Linear viscoelastic moduli in small amplitude oscillatory shear regime for the composite electrolytes and neat linear polymer at 80°C is presented in Figure 6.4a.

Adding NPs to the polymer matrix significantly reinforces the PNC electrolytes and causes an increase in both storage (G') and loss (G") moduli. For all nanocomposite samples, G' exceeds G", while making their frequency-dependence weaker, which is a characteristic of a gel-like solid behavior.[229, 230] The nanocomposite electrolyte with linear PEO shows the highest viscoelastic moduli compared to the branched architectures due to its flexible and entangling nature. 4-arms PEO matrix does not significantly change the moduli (although slightly lower values are noted), whereas the nanocomposite electrolytes with highly branched structures have significantly lower moduli. For example, the electrolyte with 8-arms star matrix has storage modulus that is two orders of magnitude lower compared to the nanocomposite sample with linear PEO.

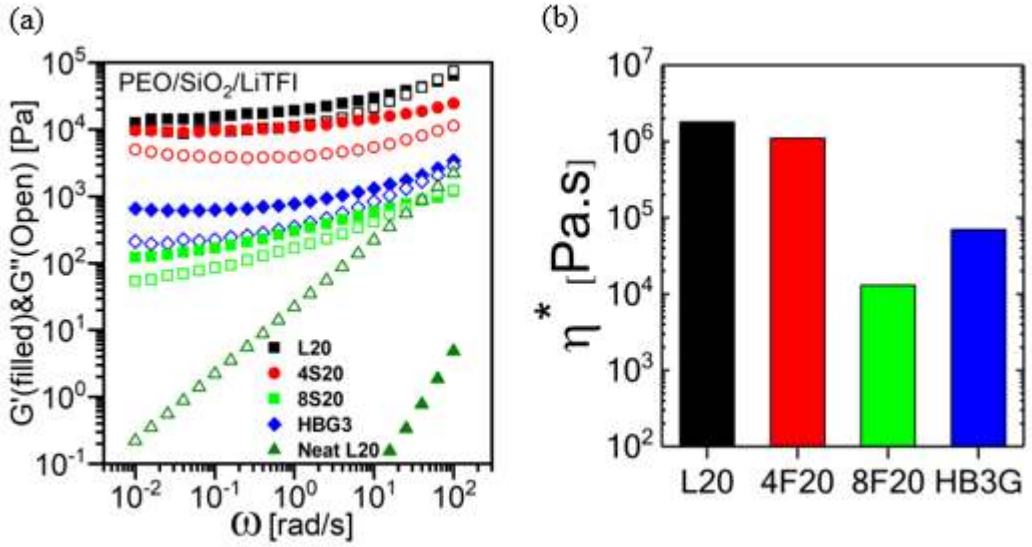

Figure 6.4. (a) Storage (G') and loss (G") moduli obtained from oscillatory shear measurements at 80°C for the neat linear PEO and PEO-based composite electrolytes containing 30 vol % silica nanoparticles, and LiTFSI with MR = 0.085. (b) complex viscosity of the nanocomposite electrolytes.

Figure 6.4b shows also the complex viscosity of the nanocomposite electrolytes. Overall, decreasing the arm length of the polymer chains, lowers the interpenetrability of the chains which leads to lower entanglement and higher mobility. Among the PNC

electrolytes with non-linear matrices, 8-arms star has the most compact form with shortest arm length leading to lower interchain interactions in the matrix, hence induces the lowest viscoelastic moduli and viscosity. We emphasize that the sample is still highly reinforced and solid like as seen from more than three orders of magnitude shift in the low-frequency moduli compared to the neat PEO matrix. The nanocomposite electrolytes with branched architectures are therefore both solid-like and easier to process, which is desired for flexible batteries.

6.3.4 The effect of Polymer architecture and Silica nanoparticle addition on the storage and loss modules in PEO/Silica composite polymer electrolytes

To understand how the bulk rheological behavior reflects on the ionic conductivity, the electrochemical impedance spectroscopy (EIS) (an example of the Nyquist plots for the calculation details of the ionic conductivity are shown in Figure 6.8) experiments were performed. Figure 6.5 shows the ionic conductivities of the electrolytes at different temperatures between 30 and 90°C with ΔT = 15°C. Of all the electrolytes, the ones prepared with non-linear topologies resulted in higher ionic conduction, which could be attributed to lower viscosity (Figure 6.4b) as well as higher free volume with the increased branching. More specifically, the enhancements in the ionic conductivity were approximately as high as 40% for 8-arm star, 28% for 4-arms star, and %16 for hyperbranched case in comparison with the composite with the linear matrix.

Furthermore, the temperature dependence of ionic conductivity follows the Arrhenius behavior over the temperature range studied, indicating the ion transport is primarily controlled by the bulk diffusion in the viscous matrix, rather than ion-hopping.[71] This is primarily due to the fact that the time-scale of the segmental dynamics (which facilitates ion hopping between different coordination sites along the polymer backbone and between different chains) is too short as the samples are well-above their T_g. The

correlation between the bulk viscosity and the ion diffusion is also seen from the activation energies for the conduction. The Arrhenius fitting parameters for the ionic conductivity measurements with respect to temperature for the electrolytes are shown in Table 6.3. The Arrhenius model is given by [8],

$$\sigma_{\alpha} = \sigma_0 \exp E/RT \quad (1)$$

where σ_0 is the reference conductivity, E is the active energy, and R is the gas constant number (8.314 $J \cdot K^{-1} \cdot mol^{-1}$). Fitting the conductivity data to the Arrhenius model gives the estimated the pseudo-activation energies as shown in Figure 6.5b. The activation energies for ion hopping agrees well with the conductivity data; lower activation barrier results in higher ionic conductivity.[8] The electrolyte with the linear PEO has an activation energy of 0.4 eV for the salt molar ratio of [Li/EO] = 0.085, which results the lowest ionic conductivity among the PEO investigated architectures. On the other hand, activation energy decreased to 0.33, 0.32 and 0.29 eV for HB3G, 4-arms, and 8-arms star PEOs respectively which display higher ionic conductivity. This study shows, for the first time, that the activation energy for the conductivity in nanocomposite electrolytes is highly dependent on the architecture of the polymer used.

Increasing branching enhances the polymer mobility in the nanocomposite electrolytes without sacrificing their solid-like nature, and thus allows to obtain higher ionic conductivity compared to the conventional nanocomposite electrolytes made of linear polymer chains.

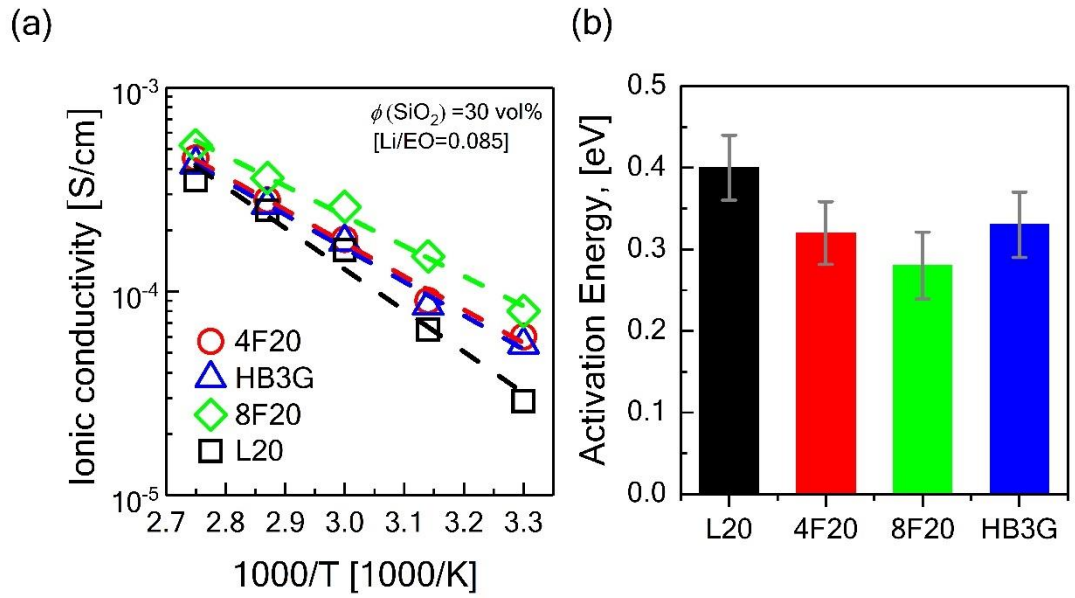

Figure 6.5. (a) Ionic conductivity measurements with corresponding Arrhenius fit lines as a function of varying temperatures between 30 and 90 °C with a temperature increase of 15°C for different PEO architectures (b) estimated pseudo-activation energies for the PNCs- based electrolytes with various PEO architectures for the solid composite polymer electrolytes prepared using PEO, 30 vol% Silica nanoparticles, and LiTFSI (0.085 MR).

6.4 Conclusions

In conclusion, new polymer nanocomposites (PNCs) based electrolytes composing of a biocompatible and biodegradable polymer, PEO, with varying topologies (linear, stars, and hyperbranched), and silica nanoparticles with the addition of fixed amount LiTFSI were designed. It is clearly seen that PEO crystallization of the branched topologies with higher degree of branching was considerably reduced in comparison with the linear one, which facilitated the ionic conduction. Furthermore, the glass transition temperature (T_g~-55°C) of nanocomposites showed no significant change with varying PEO architecture, suggesting preservation of the flexible nature at room temperature for non-linear PEOs when compared to linear PEO. Furthermore, compared to the reported PEO based polymer electrolytes in the literature, the addition of nanoparticles reinforced the

electrolytes with more elasticity and on the other hand the idea of using non-linear polymer chains as a host in the composite electrolytes significantly enhances the ion mobility in the matrix, when compared to the linear counterpart. In short, newly developed PEO-nanocomposite based electrolytes provide significant advantages such as being more environmentally friendly, sustainable, and easily malleable. Consequently, obtained results for the composite electrolytes with branched PEOs show a new compelling direction for the applications especially including battery implants and wearable electronic which require flexibility, biocompatibility, and biodegradability.

6.5 Supporting Information

EXPERIMENTAL METHODOLOGY

Materials

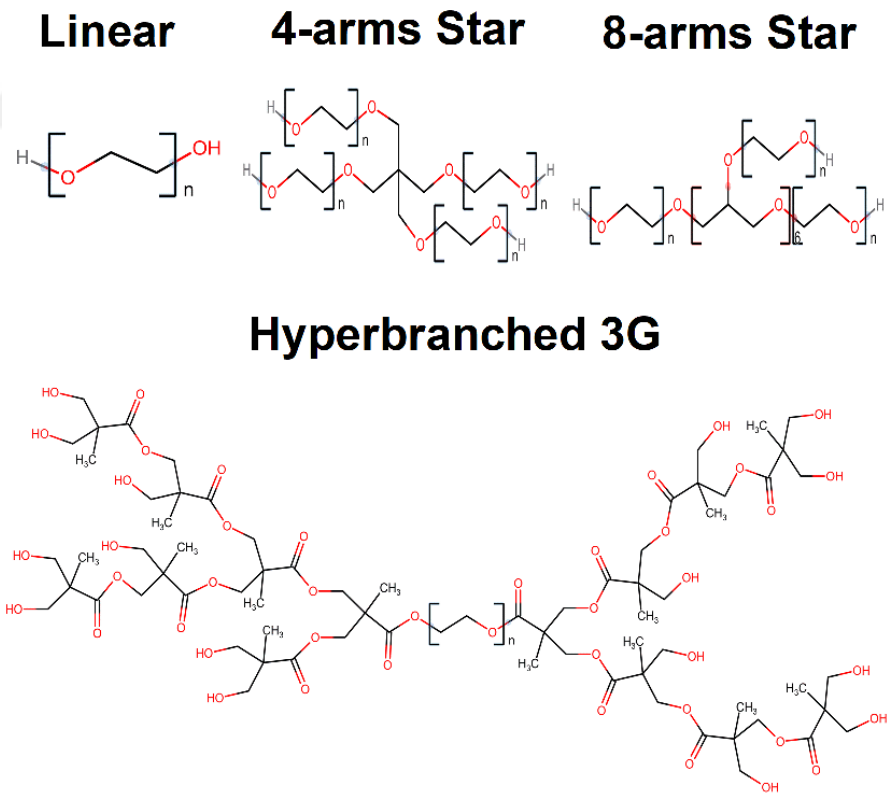

Figure 6.6: Chemical structure of the PEO polymers.

RESULTS AND DISCUSSION

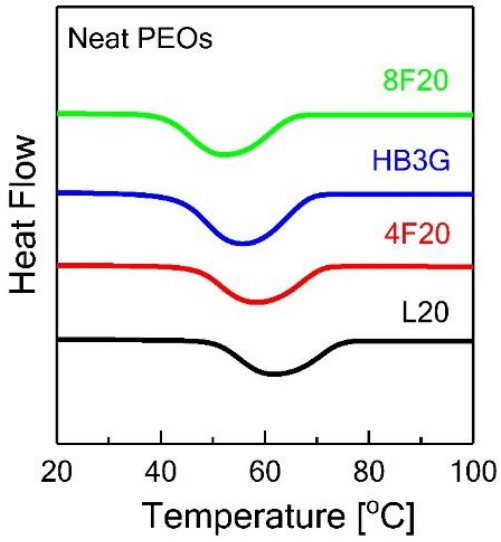

Figure 6.7: DSC results for neat PEOs with various PEO topologies.

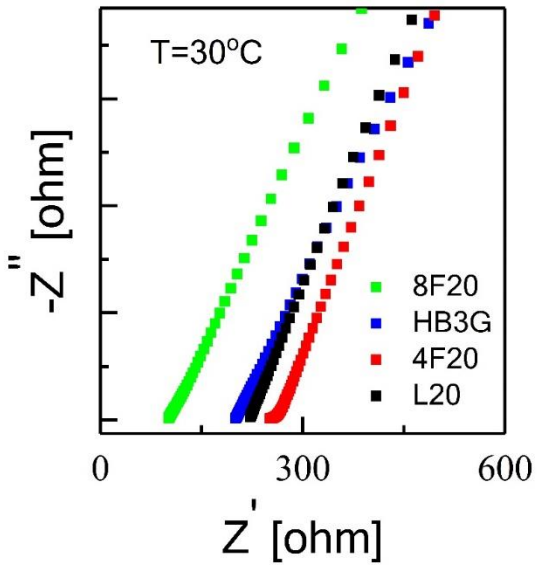

Figure 6.8: Example of Nyquist plots at 30°C used in the ionic conductivity calculations for the PEO-based electrolytes with various topologies.

Table 6.3: Arrhenius fitting parameters for different PEO topologies used in PNCs-based electrolytes.

Sample	PEO/Silica Composite	
	Activation Energy E, eV	ln τ_0, s
L20	0.40	2.17
4F20	0.32	1.14
8F20	0.33	0.79
HB3G	0.29	1.15

INTRODUTION

Ever-growing demand arising from the significantly increasing production of portable consumer electronic devices such as laptops and smartphones, and electric vehicles which have been subsidized in an effort of combatting the climate change, have led to everlasting investigation of reliable, sustainable, cost-effective, and easily processed energy storage systems. [20, 231-246] Among different energy storage systems, rechargeable lithium-ion batteries have gathered a lot of attention for large and small-scale energy storage and conversion technologies for both stationary and mobile installations because of excellent characteristics including high ionic conductivity, great energy density, long cycle life, wide range of operating temperatures, low self-discharge rate loss and toxicity.[8, 27, 36, 37, 44, 45] But in these commercial systems which are currently based on organic liquid electrolytes, environment and safety with sustainability is the ever-increasing trouble-making issue due to their undesired characteristics such as being extremely volatile, flammable, and toxic, which could cause fire, leakage, explosion, and short circuit, limiting their usage in the commercial lithium-ion batteries.[4-7] To overcome these safety and environmental concerns in a more sustainable manner, substituting these liquid electrolytes with solid polymer electrolytes (SPEs) has been commonly considered favourable, because solid polymer electrolytes (SPEs) in comparison with the traditional liquid electrolytes have proposed many benefits such as easy manufacturing, flexibility, mechanical strength, light-weight packed structure, environmentally friendly, nonflammability, good thermochemical stability, and safer batteries. [4, 8-10].

Since 1970s [59-61], the incorporation of linear poly oxyethylene oxide (PEO) within polymer electrolytes have been extensively studied and have proposed full of promise to be employed in lithium-ion batteries due to their very low glass transition temperature revolving around (~-55°C) [8], extremely fast segmental dynamics [8], excellent ability

to form complexes with alkali metal salts favouring Li-ion complexation [245, 247], outstanding electrochemical stability [8, 242], easy and cost effective processability [242, 244], but their practical applications are very limited by extremely low ionic conductivity ranging between $10^{-6} - 10^{-8}$ S/cm at room temperature [8] stemming from its high degree of crystallinity and poor mechanical performance at elevated temperatures attributed to the melting crystals.[8, 245]

Therefore, it is of primary importance to develop a PEO-based SPE with a simultaneous enhancement of ionic conductivity and mechanical strength. Since lithium-ion transportation happens primarily in the free volume of the amorphous phase in PEO-based SPEs, [8, 242-246] various techniques including blending polymers [8, 18], using branched architectures [8], cross-linking [13], copolymers [19, 20], addition of fillers [9, 21] and plasticizers [10, 11, 45, 248] have been employed to increase amorphous free volume and mechanical strength without sacrificing ionic diffusion in SPEs.

The PEO based copolymer (CP) electrolytes is one of the extensively studied method with significant developments in enhancing their electrolyte performance and our understanding essentially about their chemistry, structure, electrochemical properties, and charge transport mechanism., because they could be synthesized with tailorable properties that could result in increasing flexibility, ion conduction, and mechanical strength. [20, 99, 238, 239, 242, 243, 245, 246, 249, 250]. Among various PEO based copolymers (CP), the amphiphilic copolymers consisting of hydrophilic PEO chains with two other most commonly used hydrophobic polymers such as polystyrene (PS) and poly(methyl methacrylate) (PMMA) have been of great interest, [20, 69, 234-238, 241, 242, 246, 250-254] mainly due to the fact that the conducting routes for the ions are supplied by the PEO whereas a nonconducting polymer PS or PMMA yields the desired mechanical properties in these systems. Balsara et al.[20, 236] studied a series of polystyrene-

poly(ethylene oxide) (SEO) block copolymers in the aspects of the electrical and mechanical properties and reported that improved ionic conductivity due to the presence of mobile PEO segments with extremely enhanced storage shear modulus which was fundamentally controlled by the number of PS blocks. Similarly, studies investigated by Bouchet and his-coworkers[238] for block copolymer electrolytes (BCE) consisting of triblock PS−PEO−PS segments proposed that ionic conduction is not only affected by the volume fraction of conducting PEO phase but also is a function of the conducting pathways defined by the tortuosity parameters of the PEO network. Additionally, Butzelaar et al.[242] synthesized another styrene-based poly(ethylene oxide) (PEO) side-chain block copolymer electrolyte with an optimization on the PEO chain length and grafting density and showed reasonably well electrolyte properties such as enhanced ionic conduction and mechanical stability with developments in the thermal and electrochemical stability.

Although there are several works investigating synthesis and characterization of PEO/PMMA based copolymers[253, 255-259], showing that PMMA is not only rigid but also is miscible with PEO at the macromolecular level as opposed to number of PS/PEO based polymer electrolyte studies[260], the ones that look into their potential properties to be used as PEO/PMMA based electrolytes are very limited. In this context, only the studies conducted by Kofinas and his-coworkers[241, 252] investigated the electrochemical properties of a polymer electrolyte composed of a diblock polymer (PEO-b-(PMMA-ran-PMAALi)) including randomly poly(ethylene oxide) (PEO), poly(methyl methacrylate) (PMMA), and lithium salt of acrylic acid blocks reported high ionic conductivity attributed to micro phase separation. Subsequently, they achieved a wide range electrochemical stability window and perfect interface features with the lithium metal electrode.[241, 252] More recently, Wang et al.[258, 259] synthesized a

branched copolymer based electrolyte consisting of poly(methyl methacrylate)-block-poly(poly(ethylene glycol) methyl ether methacrylate and the electrolyte showed ionic conductivities on the order of 10^{-4} S/cm at elevated temperatures with good interfacial compatibility, wide electrochemical potential, and cycle life in a battery cell mainly because of fast segments of PPEGMA and oxidative decomposition of ethylene oxide units in the high potential regions, respectively.

Very recently, we investigated the effects of chain architecture on miscibility, glass transition, segmental dynamics, and ionic conductivity in non-linear (branched) poly(ethylene oxide) (PEO) based SPEs including poly(methyl methacrylate) (PMMA) along with systematically increased number branching in the PEO architecture. [8] In this study, we found that the increasing number of branches in PEO helps to retain its fast segmental dynamics even in the blends with glassy PMMA mainly due to faster PEO segmental dynamics arising from less interaction sites and interpenetration of PMMA into compact and nonlinear PEO, which resulted in as much as 3-fold higher ionic conductivity. The fundamental reason for the lower ionic conduction in linear PEO/PMMA miscible blend was related to the significant slowing down of the PEO segmental motion with the addition of PMMA into linear PEO. To overcome this challenge, it is evidently of great importance to design a novel architecture for PEO/PMMA grafted copolymer where PEO segmental dynamics has not been affected as much as in linear PEO/PMMA blends. Therefore, herein, in this study, we propose a different synthetic approach toward grafted PEO/PMMA copolymers that not only overcomes the high degree of crystallinity of PEO with insufficient mechanical stability, but also could help PEO maintain inherently fast segmental dynamics to yield high ionic conductivities. In this approach, PMMA was chosen as the nonconducting block being in the backbone to provide the mechanical strength due to its very high T_g of around 120

°C[8] whereas PEO with different molecular weights and grafting density was preferred in the sidechain to facilitate the ionic transportation in the electrolyte because of its very low T_g of around -55 °C [8] with fast segment mobility. In this work, we showed successfully synthesized PEO-grafted-PMMA copolymers composing of linear PEO (1.5 kDa and 20 kDa) and PMMA (120 kDa) using various characterization techniques including X-ray diffraction (XRD), modulated differential scanning calorimetry (MDSC), Fourier transform infrared spectroscopy (FTIR), thermal gravimetric analysis (TGA), nuclear magnetic resonance (NMR) spectroscopy, and rheology measurements. Then, we incorporated the lithium bis(trifluoromethane-sulfonyl)-imide (LiTFSI) into these novel PEO-grafted-PMMA copolymers and found substantial amount of enhancement in the ionic transportation with tunable mechanical modulus for them, essentially owing to lower degree of crystallization and effective glass transition temperature for PEO (faster PEO segmental dynamics) when compared to their linear PEO/PMMA analogue.

7.2. EXPERIMENTAL METHADOLOGY

7.2.1. Materials

Poly(ethylene glycol)s (PEGs) with the molecular weights of 1500 g mol^{-1} (PEG1500) and 20,000 $gmol^{-1}$ (PEG2000), Maleic anhydride (MAH), Methyl methacrylate (MMA), pToluene sulphonic acid (PTSA), Benzoyl peroxide (BzO)2, Dimethyl acetamide (DMAc) and the other chemical reagents, purchased from Sigma-Aldrich Inc., were all technical grade and used for the synthesis of PEG-g-PMMA copolymers without further purification.

7.2.2. Synthesis of PEG-g- PMMA copolymers

Prior to grafting reactions, poly(ethylene glycol) (PEG) two particular molecular weights (PEG1500 and PEG20000) with high grafting densities (HG) were submitted to transesterification reaction with maleic anhydride (MAH) to obtain more reactive macromonomers of PEG-MA.[261, 262] The steps of transesterification reaction between PEG and MAH are shown in Fig. 7.1.

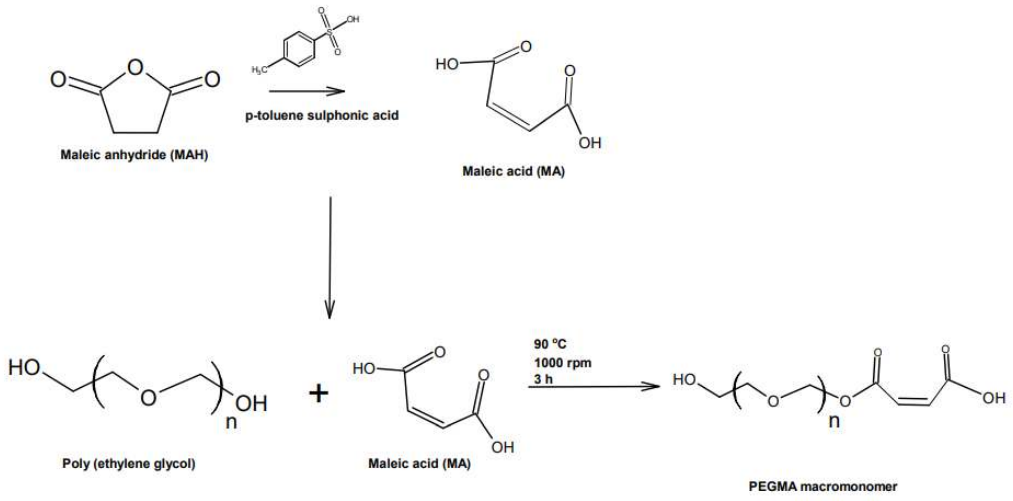

Fig. 7.1: The transesterification reaction between a PEG oligomer and MAH to synthesize PEG-MA macromonomer.

In a three-necked round-bottomed flask equipped with a magnetic stir bar, stoichiometric amounts of PEG and MAH were mixed and heated to 60 °C under a slightly positive nitrogen atmosphere while stirring at 1000 rpm for 30 min. Then PTSA, which was 1% by mole of MAH, was added into the reaction mixture as a catalyst. The flask temperature was then raised to 80°C and refluxed for 3 h at 1000 rpm. After cooling to room temperature, the reaction mixture was precipitated in hexane (100 mL) and filtered. The filter cake of PEG-MA macromonomer was washed in excess hexane for purification, and then dried overnight in a petri dish. After preparation of PEG-MA macromonomers,

the syntheses of PEG-g-PMMA copolymers by free radical polymerization were performed.[263] The known amount of PEG-MA was dissolved in 25 mL dimethyl acetamide (DMAc) in a three-necked round-bottomed flask in an oil bath at 70 °C. The equivalent amount of methyl methacrylate (MMA) monomer was then slowly injected into the flask under nitrogen atmosphere while stirring at 500 rpm for 30 min. Under given conditions, the initiator benzoyl peroxide (BzO)2, which was 1% by mass of MMA, was added slowly to the reaction mixture. The copolymerization reaction between PEG-MA ester and MMA was carried out at temperature of 70 °C for 24 h under inert nitrogen atmosphere while stirring the system at 500 rpm. Grafting of PEG-MA with MMA by a free radical polymerization is as given in Fig. 7.2. The PEG-g-PMMA copolymers were obtained as yellowish white precipitate at the bottom of the reaction vessel. After cooling to room temperature, each product mixture was 3–4 times reprecipitated in 3 volume ethanol-1 volume hexane mixture to remove unreacted residues. The PEG-g-PMMA copolymer was then dried in vacuum at room temperature and stored in a closed glass bottle.

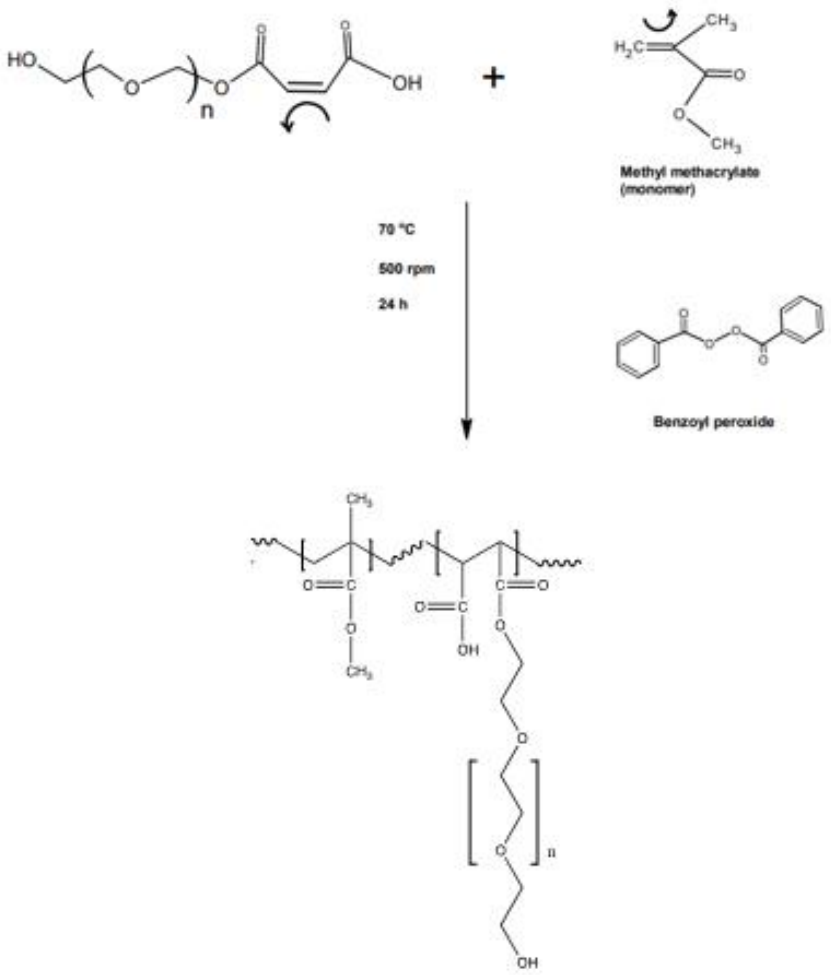

Fig. 7.2: Grafting of PEG-MA with MMA by a free radical polymerization to form PEG-grafted-PMMA.

7.2.3. Preparation of salt-free samples and their corresponding electrolyte systems

Salt-free samples for neat PEG-g-PMMA copolymer were prepared by the solution casting technique. Polymers were first dissolved in acetonitrile (ACN) at 30 mg/ml. Then, the solutions were stirred with a magnetic stirrer at room temperature for 6 hours. Later, the electrolyte solutions were then cast onto glass petri dishes and evaporated slowly at room temperature overnight in a glovebox filled with Argon and annealed at 100℃ in a vacuum oven for 48 hours to ensure complete removal of the solvent.

Then, the desired amount of the lithium bis(trifluoromethane)sulfonamide, LiTFSI, was dissolved in acetonitrile, stirred for 48 hours. Then the disc samples were doped with (Li/EO=0.085) LiTFSI by solution uptake. The electrolytes were first dried at room temperature for overnight in glovebox filled with Argon and annealed at 120℃ in vacuum oven for 48 hours to ensure complete removal of the solvent.

7.3. Characterization

X-ray Diffraction (XRD): The XRD patterns of the pure PEOs and the electrolytes were recorded using the Bruker D8 Phaser – X-ray diffractometer with Cu K (α) source. Then, the diffraction data were obtained at this temperature with the Bragg's angles (2θ) varying from 5 to 60 degrees.

Differential Scanning Calorimetry (DSC): Modulated Differential Scanning Calorimetry. The temperature modulated differential scanning calorimetry (MDSC) samples were prepared by putting ~8−10 mg of materials in aluminium pans provided by TA Instruments. MDSC experiments of the pure PMMA, PEO, and PEO/PMMA blends were carried out with a TA Instruments DSC25 instrument equipped with a liquid nitrogen cooling system. An aluminium pan was used as the reference. To get rid of the temperature history completely, all the samples were heated to 180 °C and allowed to remain there for 5 min. Samples were then quickly cooled down to −85 °C at the rate of 20 °C/min. DSC scans were then collected while heating the sample in modulated temperature mode at the ramp rate of 1 °C/min with a modulation amplitude of ±0.5 °C and period of 60 s.

Thermal Gravimetric Analysis (TGA): Thermal gravimetric analysis (TGA) of the samples was performed from 25 to 600 °C at 10 °C min^{-1} under an argon atmosphere

flow of 50 mL/min purged by the simultaneous thermal analyser NETZSCH STA 449 F3 Jupiter TG/DTA instrument. In the measurements, platinum pans were used.

Fourier Transform Spectroscopy (FT-IR): FTIR characterization was performed on the pure PEOs and the electrolytes using the Thermo Scientific iS10 FT-IR spectrometer in the wave number of 4000 to 600 cm^{-1} with 64 scans for each spectrum.

Rheology: All rheological measurements in the melt state are performed using an Anton Paar MCR 302 rheometer equipped with a parallel geometry with diameter of 25 mm. For small-amplitude oscillatory shear (SAOS) measurements at constant $T\text{-}T_{geff\text{-}PMMA}$ which was 40°C, first amplitude sweep test performed from 0.01 to 10 % strain to find the linear viscoelastic region (LVR). Then, the frequency sweep measurements were performed between 0.01 to 100 rad/s at LVR.

Nuclear Magnetic Resonance (NMR) Measurement: ^{1}H and ^{13}C Nuclear Magnetic Resonance (NMR) spectra of all the PEG-g-PMMA specimens were processed on Varian by operating at 500 MHz in deuterated chloroform ($CDCl_3$). NMR spectra were analysed with Bruker TopSpin 4.1.0 program. Also, chemical shifts (δ) were shown with ppm in deuterated chloroform ($CDCl_3$).

7.4. RESULTS and DISCUSSION

We first investigate the crystallization of PEO-grafted-PMMA samples using XRD at room temperature. Figure 7.3 displays the intensity profiles at the room temperature for neat PEOs and PEO-grafted-PMMA with two different molecular weights of PEO (1.5kDa and 20kDa) with high grafting densities (HG). In the case of synthesized PMMA having PEO side chains with the molecular weight of 20Kda, when compared to the degree of crystallization for neat linear PEO of molecular weights of 1.5kDa and 20kDa [8], even though the degree of crystallinity of PEO (see Table 7.1) severely hampered due

to the restriction of the branched side chains provided by the grafting on to PMMA backbone, the semi-crystalline regions with the same crystal structure (monoclinic lattice) still preserved which is attributed to the peaks observed at 2θ=19° (120-plane) and 23° (032-plane).[8, 17, 18, 93, 154] On the other hand, the crystalline domains for PEO-grafted-PMMA composing of high and low grafted PEO side chains with low molecular weight (1.5Kda) were completely suppressed because of highly grafted short side chains with limitations on the chains mobility, impeding formation of close-packed structure.[8, 92, 93]

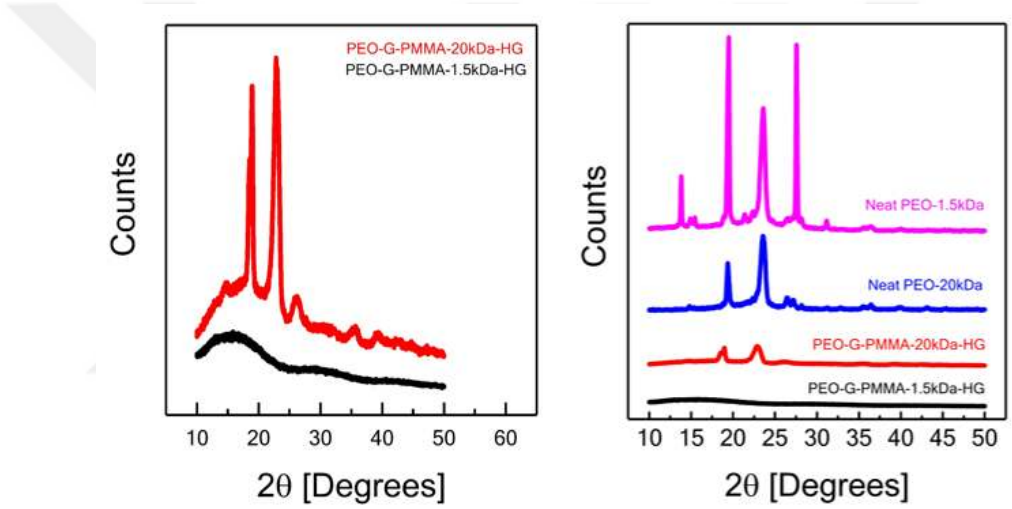

Figure 7.3: The intensity profiles of XRD at the room temperature for neat PEOs and PEO-grafted-PMMA with two different molecular weights of PEO1.5kDa (black) and PEO20kDa (red) with high grafting densities (HG).

Figure 7.4 illustrates the full FTIR spectra of the PEG-grafted-PMMA copolymers with different PEO molecular weights and grafting densities. All distinctive bands of PEG, MA and PMMA chains were captured in the expected regions of the FTIR spectra of the synthesized copolymers with some slight shifts, suggesting successful grafting of PEG-MA macromonomers and MMA chains. The characteristic peaks around 1700-1750 cm^{-1} (Figure 7.4b) and 2900-3000 cm^{-1} (Figure 7.4a) in the FTIR spectrum of all PEG-

grafted-PMMA copolymers, which were assigned to the C=O stretching and CH_3 stretching groups, respectively, confirming the formation of PMMA chains in the structure of the copolymers. [157, 264, 265]

Furthermore, The broad band at 3400–3500 cm^{-1} (Figure 7.4a) and the medium band at 1600–1650 cm^{-1} (Figure 7.4b) were attributed to the stretching and bending vibrations of -OH groups of PEG, correspondingly; while the bands, related with stretching vibrations of ether groups ($-H_2C-O-CH_2-$) of PEGs and carboxyl group (O-C=O) of MA, appeared as strong and medium bands positioned at 1281 cm^{-1}, 1243 cm^{-1} and 1150–1100 cm^{-1} (Figure 7.4c).[157, 262, 264, 266] All these bands were characteristic bands for the existence of PEG-MA chains in the structure of synthesized copolymers. Meanwhile, as can be seen in Figures 7.4a and 7.4d, he strong bands at around 2950 cm^{-1}, 2850 cm^{-1}, 950 cm^{-1}, 850 cm^{-1}, and 750 cm^{-1} were the signs of the stretching, rocking, and wagging vibrations of $-CH_3$, $-CH_2$, C-C groups of PEG and PMMA chains.[157, 262, 266, 267]

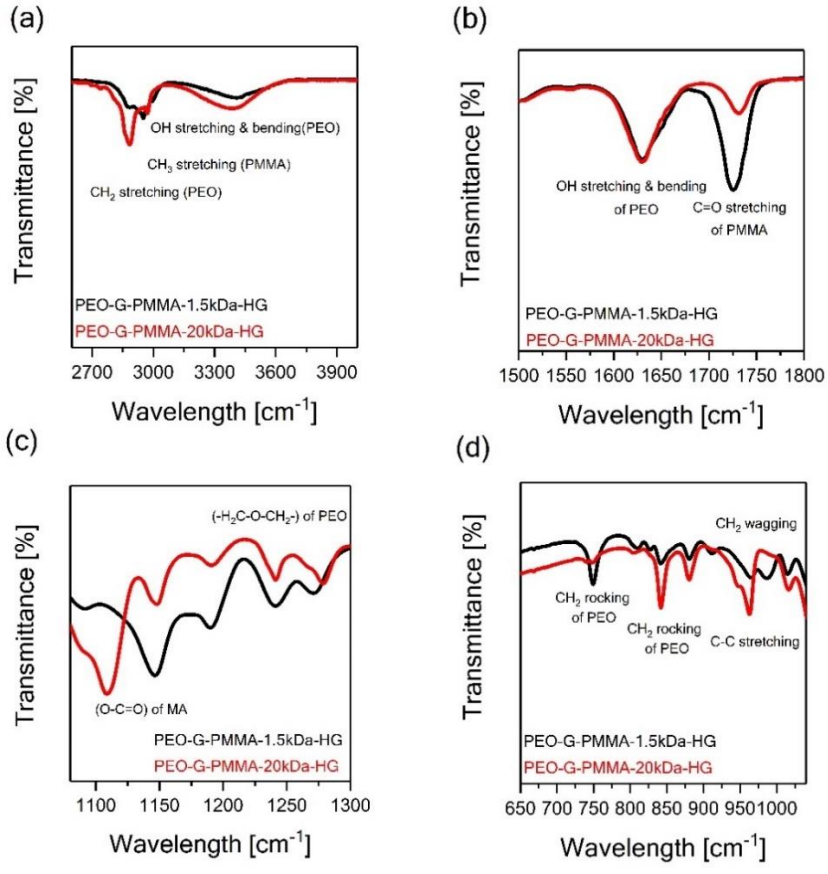

Figure 7.4: FTIR transmission spectra of PEG1.5kDa-grafted-PMMA-HG (Black), and PEO20kDa-grafted-PMMA-HG (red) copolymers.

The TGA thermograms of neat PEO (20kDa) (red), PEG1.5kDa-grafted-PMMA (Black), PEG20kDa-grafted-PMMA (Green) are shown in Figure 7.5. Based on the figure 7.5, there was not any presence of weight loss between 25 and 200°C, which proved that the solvent containing the mixture of ethanol and hexane was removed thoroughly in vacuum drying oven.

According to the mass loss curves, the decomposition for the samples consisted of two steps starting at 200 °C and ending at 400 °C, which are associated with the monomer evolution and combined degradation of PEO and PMMA, whose decomposition temperature are 400°C and 380°C, respectively.[262, 268-271] Additionally, experimental findings showed that PMMA addition into PEO resulted in slight decrease in the onset temperature T_{onset} at which thermal decomposition of the copolymers started because of lower degradation temperature of PMMA, suggesting successfully synthesized PEO-grafted-PMMA polymers.

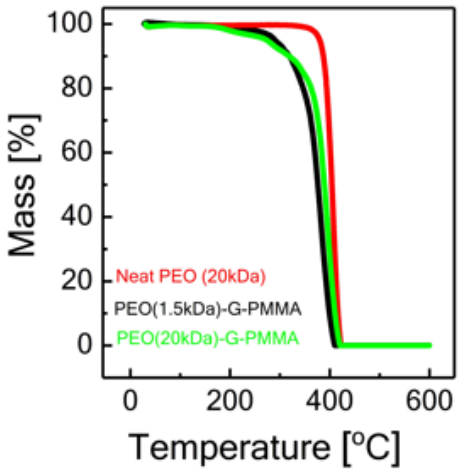

Figure 7.5: The TGA thermograms of neat PEO (20kDa) (red), PEG1.5kDa-grafted-PMMA (Black), PEG20kDa-grafted-PMMA (Green).

Then we examined the synthesized PEO-grafted-PMMA polymers using temperature modulated differential scanning calorimetry (MDSC). Figure 7.6 shows the heat flows and specific heat capacities (Cp's) with corresponding derivatives with respect to temperature of PEO-grafted-PMMA with different molecular weights of PEO1.5kDa da and PEO20Kda having different grafting densities. Based on the raw Cp data, it is evident that the PEO crystallization is dramatically decreased in comparison with the linear PEO, supporting the XRD findings.

Furthermore, we observed two glass transition temperatures (T_g's): one located at lower temperatures corresponding to the glass transition of the faster component, PEO, in the system and another one positioned at higher temperatures attributed to the slower component, PMMA. To highlight the effective T_g's in the blends, the temperature derivative of the heat capacities is used given in Figure 7.6e. We fit a Gaussian $\propto \exp[-(T-T_g)^2/\left(2(\Delta T_g)^2\right)$ to find T_g and the entire peak widths at half-maximum height (ΔT_g) values more precisely.[8, 159]

We found, in comparison of T_{g-eff} values of PMMA in the blends with the T_g of neat PMMA which is 120°C [8], we found T_{g-eff} values for PMMA were greatly shifted to the lower values with PEO grafting due to the mobility provided by low-T_g PEO segments while T_{g-eff} values for PEO chains were slightly shifted to higher values due to PMMA backbone, which implies that it could be possible to still maintain fast PEO segment mobility that could be fast enough to result high ionic conductivities, therefore these copolymers should be investigated for electrochemical measurements.

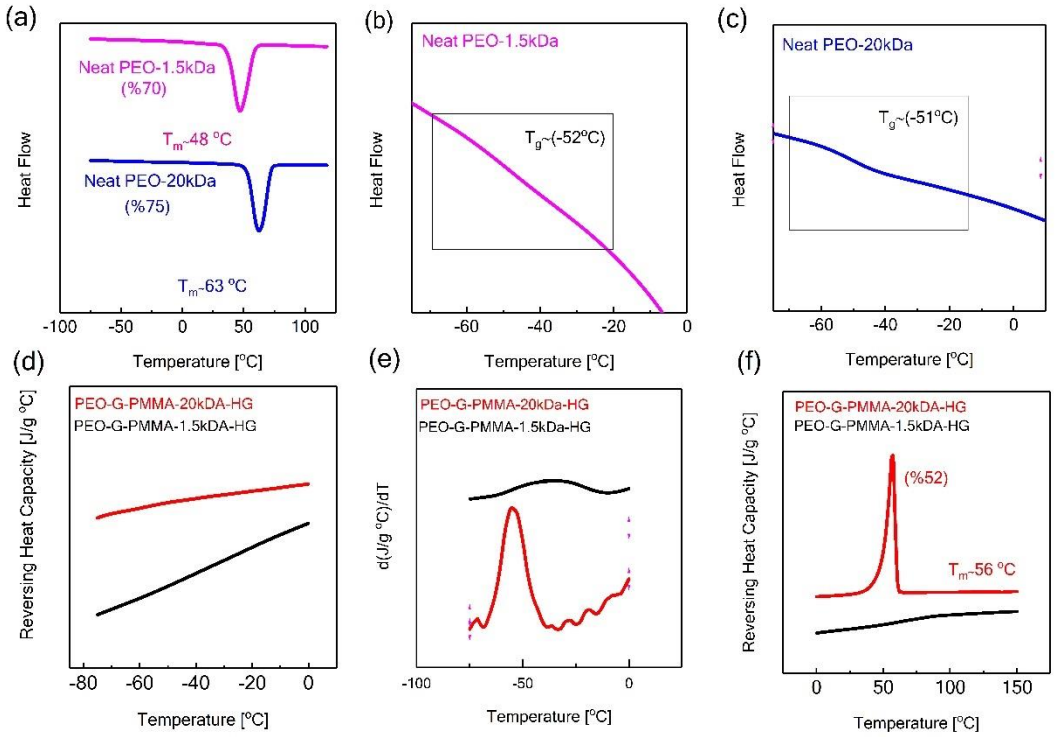

Figure 7.6: (a, b, c) DSC Thermographs with indications of melting and glass transition temperatures for neat PEOs with molecular weights of 1.5 kDa and 20 kDa. The dependence of the reversible heat capacity (d, f) and its derivative (e) with respect to temperature for PEO-grafted-PMMA with molecular weights of PEO1.5kDa-HG (black) and PEO20kDa-HG (red).

These results are suggesting successful grafting of PEG-MA macromonomers and MMA chains. The resulting effective T_g's with melting enthalpy and temperatures for neat PEOs and copolymers are given in Table 7.1.

Table 7.1: Effective Glass transition temperatures with melting enthalpy and temperatures for PEO and PMMA chains estimated from MDSC results for neat PEOs, PMMA, and PEO-grafted-PMMA copolymers consisting of PEO with two different molecular weights (1.5 kDa and 20 kDa).

Sample	PEO	PMMA	Melting Enthalphy, J/g	Melting Temperature, ◦C
	Tg,eff,◦C			
PEO1.5kDa-Grafted-PMMA	-35	60	NA	NA
PEO20kDa-Grafted-PMMA	-54	110	101.92	56
Neat PEO 1.5kDA	-52	NA	137.2	48
Neat PEO 20kDA	-51	NA	147	63
Neat PMMA 120kDA	NA	120	NA	NA

Next, we investigated based on the effective glass transition temperatures for PMMA the melt rheology behaviours including storage (G') and loss modulus (G'') within the linear viscoelastic region for PEG1.5kDa-grafted-PMMA-HG and PEO20kDa-grafted-PMMA-HG copolymers as a function of frequency and temperature at the same $T-T_{geff\text{-}PMMA}$ temperature, which is displayed in Figure 7.7. The storage and loss modulus of all investigated PEO-grafted-PMMA copolymers were found to be larger than those of neat PEOs while they were smaller than those of neat PMMA at all temperatures of interest.[230, 268, 272] More specifically, PEO-grafted-PMMA copolymer with a shorter side PEO chain had closer storage and loss modulus to those of neat PMMA at all temperatures and frequencies, meaning higher than those of both neat PEO and PEO-grafted-PMMA composing of 20kDa PEO polymer. In other words, PEG1.5kDa-grafted-PMMA had more solid-like rheological behavior than PEO20kDa-grafted-PMMA, which could be attributed to the fact that shorter PEO chains could cause restricted PEO chain motions, decreasing chain mobility.[230, 268, 272] Therefore, the rheological results confirm the achievement of a substantial reinforcements enhancement in mechanical properties of PEO/PMMA with varying modules including PEO-grafted-PMMA copolymer and blends compared to the neat PEO systems while increased flexibility was introduced by the addition of successfully grafted PEO side chains as far as neat PMMA was concerned.

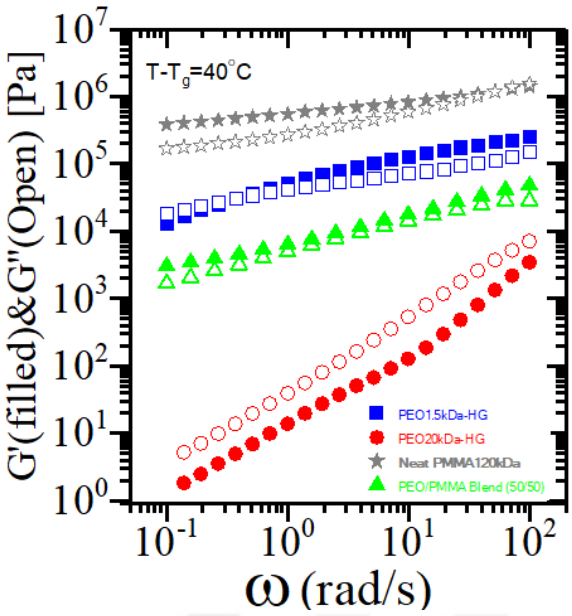

Figure 7.7: Storage (G') and loss (G") moduli obtained from oscillatory shear measurements within linear viscoelastic region as a function of frequency at the constant T-$T_{geff\text{-}PMMA}$ temperature for neat PMMA, PEO/PMMA Blend (%50/50), PEO1.5 kDa, and PEO20kDA with high grafting densities for PEO-grafted-PMMA copolymers.

Later, to characterise the chemical composition of the PEO/PMMA copolymers, nuclear magnetic resonance (^{1}H and ^{13}C NMR) spectra were performed using Bruker DMX500 NMR spectrometer (Bruker Optics, Germany) with CDCl3 as a solvent.

^{1}H NMR and ^{13}C NMR spectra of PEG1.5kDa-grafted-PMMA and PEO20kDa-grafted-PMMA copolymers with their peak assignments are shown respectively in Fig. 7.8 and Fig. 7.9. They all exhibited characteristic signals of PEG-MA and PMMA segments. The H signals at about 0.614-1 ppm (labelled as d,e) and 1.6- 2.1 ppm (labelled as f, g) belonged to the alkyl protons of the PMMA backbone.[255, 256, 273] The shifting 2.8-3 ppm belongs to the PEG-MA.[255, 256, 273] Additionally, broad signals at 3.3-3.6 ppm corresponds to the (H_2C –O-CH_2) groups of PEG units (labelled a and b).[255, 262] The peak at about 7.2 ppm referred to the solvent CDCI3. Eventually, based on the ^{1}H NMR data, the weight fraction of the ethylene oxide units was estimated to be 0.5 (%50) and

0.01 (%10) for PEO20kDa-grafted-PMMA and PEG1.5kDa-grafted-PMMA, respectively. (See Supporting Information for the details of the calculation)

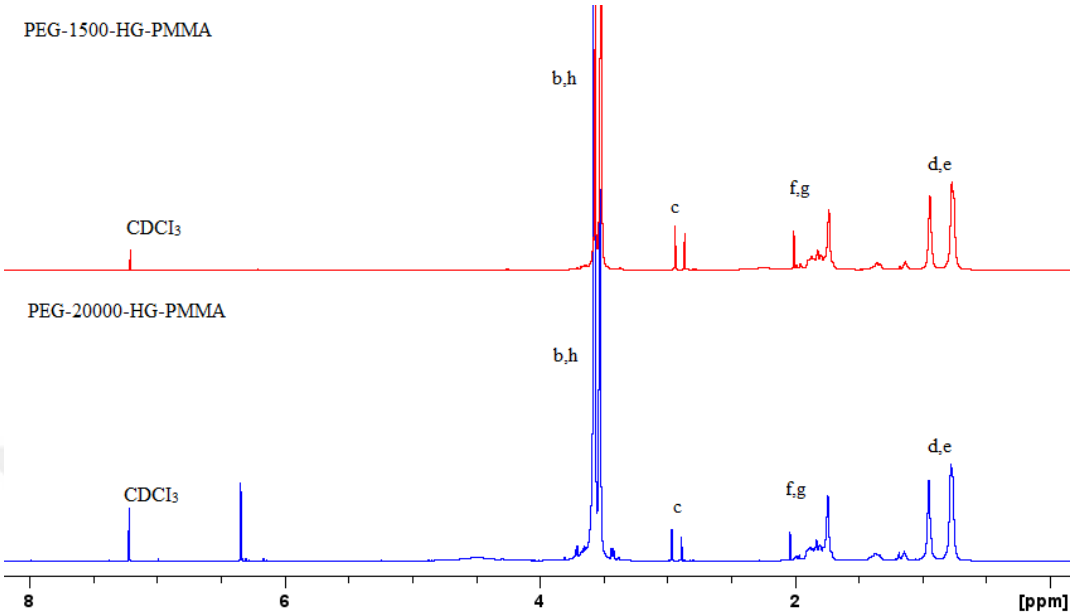

Figure 7.8: ^{1}H NMR spectra of PEG1.5kDa-grafted-PMMA (red) and PEO20kDa-grafted-PMMA (blue) copolymers.

Furthermore, the ^{13}C NMR spectra of all the synthesized copolymers displayed the main resonances of both PMMA as well as those of the ether and carboxyl units of PEG-MA oligomers. The signals labelled at 60–61 ppm characterized the terminal CH_2 unit next to the OH units at the end of PEG chains. [262] The C signals labelled at 70–73 ppm referred to the (H_2C –O-CH_2) units of PEG chains.[262] Moreover, the resonances labelled in the Fig. 7.9 due to the methyl groups (15-20 ppm) and carbonyl groups (170-180 ppm) in the PMMA.[274, 275] ^{1}H NMR and ^{13}C NMR results, which are in good agreement with FTIR results, approve successful grafting of PEG-MA oligomers onto PMMA backbone for all of the PEG-g-PMMA copolymers.

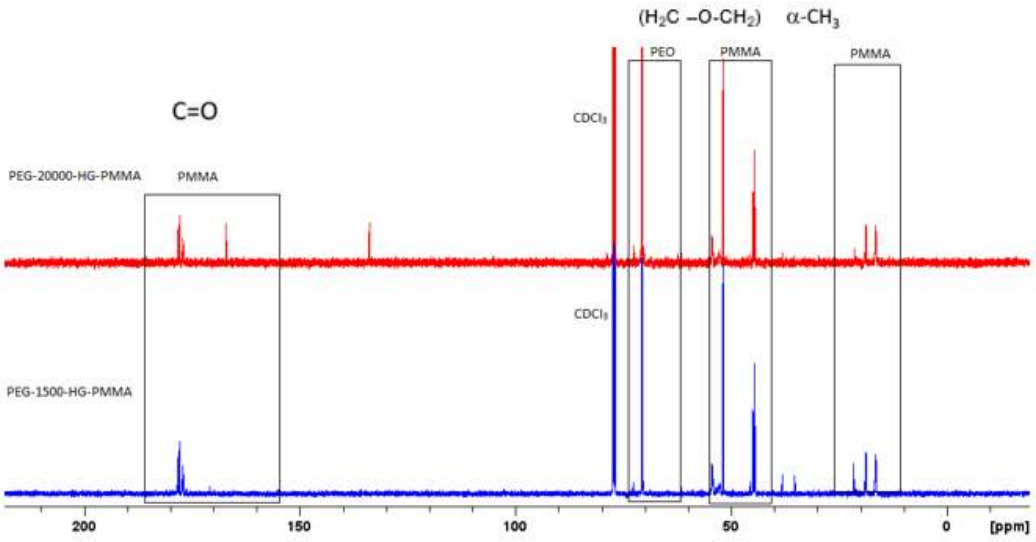

Figure 7.9: ^{13}C NMR spectra of PEG1.5kDa-grafted-PMMA (blue) and PEO20kDa-grafted-PMMA (red) copolymers.

7.5. CONCLUSION

In this work, we have successfully-accomplished the synthesis of series of PEO-grafted-PMMA copolymers composing of linear PEO (1.5 kDa and 20kDa) and PMMA (120 kDa) via two step free radical copolymerization. The results showed that the semi-crystalline nature for PEO, which had similar monoclinic crystal structure when compared to neat linear PEO, was dramatically decreased due to the reduced mobility of PEO chains with longer chain length whereas it was eliminated by densely grafted very short PEO chains associated with the low molecular weight. Additionally, all characteristically distinctive peaks of PEG, MA and PMMA chains were observed in the expected regions of the FTIR spectra of the synthesized copolymers. We also found effective glass transition temperature values for PMMA were significantly shifted to the lower values with PEO side chains due to the mobility provided by low-T_g PEO segments while T_{g-eff} values for PEO chains were slightly increased due to branching when compared to T_g of neat linear PEO, suggesting copolymers could possibly have fast

enough PEO segmental motion to facilitate ion transportation. In addition to these, TGA analysis proved the complete removal of the solvent in the copolymers evaporated in vacuum drying oven. The addition of the PMMA as a backbone in the copolymer structure significantly increased storage and loss modulus in comparison with those of neat PEO systems. NMR results also support the notion of successful grafting of PEG-MA monomers onto PMMA backbone for all PEO-grafted-PMMA copolymers.

All these finding provided by various characterization methods used in this study show that chemically and thermally stable PEO-grafted-PMMA copolymers were successfully manufactured and these copolymers which were associated with favourable characteristics could be promising to be applied as polymer electrolytes for energy storage applications especially including lithium-ion batteries. Therefore, further research will be conducted using other extensive characterization techniques for other important properties such as ionic conduction from the standpoint of battery applications.

7.6. SUPPORTING INFORMATION

To estimate the weight fraction of the ethylene oxide units in the synthesized grafted copolymers, we used the nuclear magnetic resonance (^{1}H) spectra's for PEO20kDa-grafted-PMMA and PEG1.5kDa-grafted-PMMA, respectively, shown in Figures S1 and S2 with the corresponding calculated areas for the peaks associated with the given structure by taking c as a reference resonance. Based on the ^{1}H NMR data for both samples, the weight fraction of the ethylene oxide units was estimated as follows:

Having known that the polymerization ended with methyl groups on both sides (which accounts for 6 protons indicated in d resonance), we were able to find the values of y for both samples in the following way. The areas under the resonance d were 66 and 36 for

PEO20kDa-grafted-PMMA and PEG1.5kDa-grafted-PMMA, respectively. Then, values of m*y could be found as follows:

$3y + 6 \cong 66 \rightarrow m * y \cong 20$ (PEG20kDa-grafted-PMMA)

$3y + 6 \cong 36 \rightarrow m * y \cong 10$ (PEG1.5kDa-grafted-PMMA)

Knowing the areas of the resonances as 24 and 163 (PEG20kDa-grafted-PMMA) and 24 and 8 for the corresponding peaks of e and b displayed with the estimated structures of the synthesized grafted copolymers the figures 7.S1 and 7.S2, we estimated the weight fraction of the ethylene oxide units as follows:

$$\frac{w_{EO}}{w_{Total\,Weight}} = \frac{(44*163)}{(100*24)+(44*163)+(206*20)+30} \cong 0.5 \cong 50\% \text{ (PEG20kDa-grafted-PMMA)}$$

$$\frac{w_{EO}}{w_{Total\,Weight}} = \frac{(44*8)}{(100*24)+(44*8)+(206*10)+30} \cong 0.01 \cong 10\% \text{ (PEG1.5kDa-grafted-PMMA)}$$

Where 44 g/mol, 100 g/mol, 206 g/mol, and 30 g/mol account for the ethylene oxide unit, the repeating in PMMA, the rest of the molecules in the structure, and end groups, respectively.

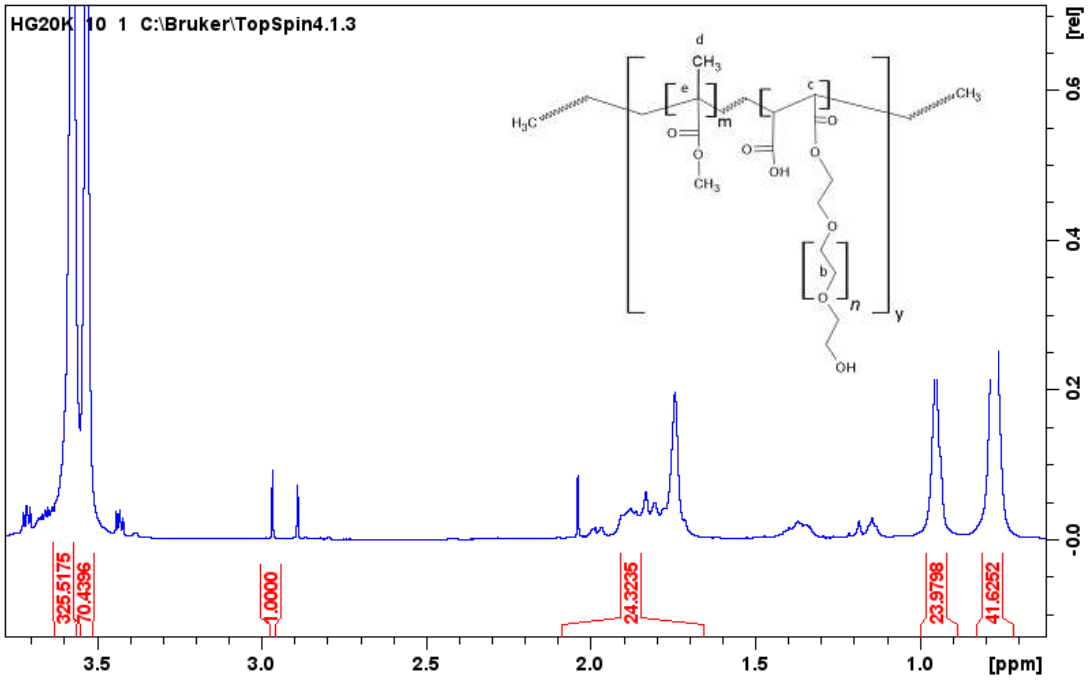

Figure 7.10: ^{1}H NMR spectra of PEO20kDa-grafted-PMMA copolymers with fundamental resonances with corresponding calculated areas.

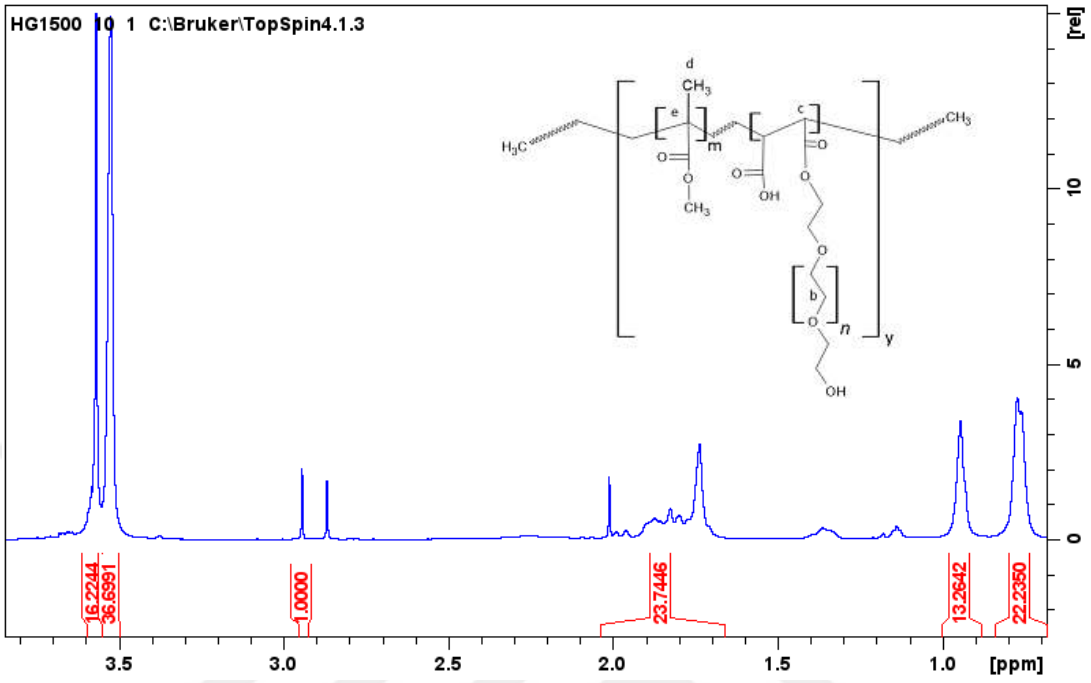

Figure 7.11: ^{1}H NMR spectra of PEO20kDa-grafted-PMMA copolymers with fundamental resonances with corresponding calculated areas.

CONCLUSIONS AND SUGGESTIONS FOR FUTURE WORK

8.1 Summary

Poly (ethylene oxide) (PEO) based electrolytes promise high ionic conductivity because of excellent solubility of various lithium salts and fast ion mobility coupled with the segmental dynamics of the polymer. Due to its simple monomer structure with no bulky side groups, PEO crystallizes at room temperature, therefore impedes ion transportation. Furthermore, its low glass transition temperature (-60^{o}C) results in poor mechanical performance. To circumvent these challenges, in this work, we systematically aim at exploring and investigating for the first time the role of polymer architecture on crystallization, segmental dynamics and ionic conductivity using a number of new and innovative PEO-based solid polymer electrolytes for lithium-ion batteries focusing two different primary techniques including blending PEO with another polymer namely PMMA and addition of a passive inorganic filler such as silica nanoparticles (SiO_2) into PEO matrixes architectures along with using non-linear architectures of PEO such as stars, hyperbranched, and bottlebrush in preparing PEO-based SPEs. Our results showed a remarkable suppression of crystallization of PEO in the nonlinear blends. Furthermore, the ionic conductivity of the electrolytes which depends on the salt concentration and polymer architecture could be improved with increased mechanical performance by simply modifying the PEO architecture from linear to branched structures. We also synthesized and characterized new PEO-based grafted copolymer. The results in relation to these newly synthesized copolymers are compelling in terms of desired properties such as fast PEO segmental dynamics with increased mechanical strength , thus they could be used to be explored its potential as polymer electrolytes in further studies. Our study provides a promising and compelling experimental evidence that macromolecular architecture could be a powerful new tool for tuning the ionic conductivity PEO-based

electrolytes, opening a new research avenue in the field of energy and environment concerning lithium-ion batteries and polymer electrolytes.

Eventually, we would like to propose the following steps to be performed as a continuation of this work in the future:

- Salt concentration dependence for the optimization of the ionic and mechanical properties for the salt systems PEO/PMMA,/LiTFSI, PEO/Silica/LiTFSI, and PEG-grafted-PMMA copolymers should be explored
- Functionalization of the end-groups such as using methyl group (CH_3) for the PEO with varying architectures and their corresponding salt complexes in PEO based blend and composite electrolytes should also be examined for the electrochemical properties
- The new electrolytes found with higher ionic conductivity and mechanical performance which composed of systems of PEO/PMMA,/LiTFSI, PEO/LiTFSI, and PEO/Silica/LiTFSI should be tested for galvanostatic charge-discharge cycling, rate capability and cyclic voltammetry (CV) using half battery cells
- Additionally, these electrolytes should be investigated for the formation of interfacial layer between electrolyte and electrode using various electrodes

BIBLIOGRAPHY

[1] BP, "Energy Outlook 2022," 2022.

[2] D. o. E. a. S. A. United Nations, Population Division, "World Population Prospects 2019: Highlights (ST/ESA/SER.A/423)," New York, 2019.

[3] IEA, "Global Energy Review: CO2 Emissions in 2021," Paris, 2022.

[4] G. Xi, M. Xiao, S. Wang, D. Han, Y. Li, and Y. Meng, "Polymer-Based Solid Electrolytes: Material Selection, Design, and Application," *Advanced Functional Materials,* https://doi.org/10.1002/adfm.202007598 vol. 31, no. 9, p. 2007598, 2021/02/01 2021, doi: https://doi.org/10.1002/adfm.202007598.

[5] P. Fan *et al.*, "High Performance Composite Polymer Electrolytes for Lithium-Ion Batteries," *Advanced Functional Materials,* https://doi.org/10.1002/adfm.202101380 vol. 31, no. 23, p. 2101380, 2021/06/01 2021, doi: https://doi.org/10.1002/adfm.202101380.

[6] D. Lin *et al.*, "A Silica-Aerogel-Reinforced Composite Polymer Electrolyte with High Ionic Conductivity and High Modulus," *Advanced Materials,* https://doi.org/10.1002/adma.201802661 vol. 30, no. 32, p. 1802661, 2018/08/01 2018, doi: https://doi.org/10.1002/adma.201802661.

[7] J. Feng, L. Wang, Y. Chen, P. Wang, H. Zhang, and X. He, "PEO based polymer-ceramic hybrid solid electrolytes: a review," *Nano Convergence,* vol. 8, no. 1, p. 2, 2021/01/10 2021, doi: 10.1186/s40580-020-00252-5.

[8] R. Bakar *et al.*, "Effect of Polymer Topology on Microstructure, Segmental Dynamics, and Ionic Conductivity in PEO/PMMA-Based Solid Polymer Electrolytes," *ACS Applied Polymer Materials,* vol. 4, no. 1, pp. 179-190, 2022/01/14 2022, doi: https://doi.org/10.1021/acsapm.1c01178.

[9] D. Lin *et al.*, "High Ionic Conductivity of Composite Solid Polymer Electrolyte via In Situ Synthesis of Monodispersed SiO2 Nanospheres in Poly(ethylene oxide)," *Nano Letters,* vol. 16, no. 1, pp. 459-465, 2016/01/13 2016, doi: 10.1021/acs.nanolett.5b04117.

[10] X. Wang, H. Hua, X. Xie, P. Zhang, and J. Zhao, "Hydroxyl on the filler surface promotes Li+ conduction in PEO all-solid-state electrolyte," *Solid State Ionics,* vol. 372, p. 115768, 2021/12/01/ 2021, doi: https://doi.org/10.1016/j.ssi.2021.115768.

[11] R. Chen, W. Qu, X. Guo, L. Li, and F. Wu, "The pursuit of solid-state electrolytes for lithium batteries: from comprehensive insight to emerging horizons," *Materials Horizons,* 10.1039/C6MH00218H vol. 3, no. 6, pp. 487-516, 2016, doi: 10.1039/C6MH00218H.

[12] N. A. Stolwijk, M. Wiencierz, C. Heddier, and J. Kösters, "What Can We Learn from Ionic Conductivity Measurements in Polymer Electrolytes? A Case Study on Poly(ethylene oxide) (PEO)–NaI and PEO–LiTFSI," *The Journal of Physical Chemistry B,* vol. 116, no. 10, pp. 3065-3074, 2012/03/15 2012, doi: 10.1021/jp2111956.

[13] P. Chen *et al.*, "Confining Hyperbranched Star Poly(ethylene oxide)-Based Polymer into a 3D Interpenetrating Network for a High-Performance All-Solid-State Polymer Electrolyte," *ACS Applied Materials & Interfaces,* vol. 11, no. 46, pp. 43146-43155, 2019/11/20 2019, doi: 10.1021/acsami.9b14346.

[14] W. S. Loo, C. Fang, N. P. Balsara, and R. Wang, "Uncovering Local Correlations in Polymer Electrolytes by X-ray Scattering and Molecular Dynamics Simulations," *Macromolecules,* vol. 54, no. 14, pp. 6639-6648, 2021/07/27 2021, doi: 10.1021/acs.macromol.1c00995.

[15] A. J. Butzelaar, M. Gauthier-Jaques, K. L. Liu, G. Brunklaus, M. Winter, and P. Theato, "The power of architecture – cage-shaped PEO and its application as a polymer electrolyte," *Polymer Chemistry,* 10.1039/D1PY00490E vol. 12, no. 30, pp. 4326-4331, 2021, doi: 10.1039/D1PY00490E.

[16] S.-I. Lee *et al.*, "Correlations between Ion Conductivity and Polymer Dynamics in Hyperbranched Poly(ethylene oxide) Electrolytes for Lithium-Ion Batteries," *Chemistry of Materials,* vol. 23, no. 11, pp. 2685-2688, 2011/06/14 2011, doi: 10.1021/cm103696g.

[17] E. Glynos, C. Pantazidis, and G. Sakellariou, "Designing All-Polymer Nanostructured Solid Electrolytes: Advances and Prospects," *ACS Omega,* vol. 5, no. 6, pp. 2531-2540, Feb 18 2020, doi: 10.1021/acsomega.9b04098.

[18] E. Glynos *et al.*, "Leveraging Molecular Architecture To Design New, All-Polymer Solid Electrolytes with Simultaneous Enhancement in Modulus and Ionic Conductivity," *Macromolecules,* vol. 51, no. 7, pp. 2542-2550, 2018, doi: 10.1021/acs.macromol.7b02394.

[19] D. Lee, H. Y. Jung, and M. J. Park, "Solid-State Polymer Electrolytes Based on AB3-Type Miktoarm Star Copolymers," *ACS Macro Letters,* vol. 7, no. 8, pp. 1046-1050, 2018/08/21 2018, doi: 10.1021/acsmacrolett.8b00474.

[20] M. Singh *et al.*, "Effect of Molecular Weight on the Mechanical and Electrical Properties of Block Copolymer Electrolytes," *Macromolecules,* vol. 40, no. 13, pp. 4578-4585, 2007/06/01 2007, doi: 10.1021/ma0629541.

[21] P. Utpalla *et al.*, "Role of free volumes and segmental dynamics on ion conductivity of PEO/LiTFSI solid polymer electrolytes filled with SiO2 nanoparticles: a positron annihilation and broadband dielectric spectroscopy study," *Physical Chemistry Chemical Physics,* 10.1039/D1CP00194A vol. 23, no. 14, pp. 8585-8597, 2021, doi: 10.1039/D1CP00194A.

[22] C.-W. Nan, L. Fan, Y. Lin, and Q. Cai, "Enhanced Ionic Conductivity of Polymer Electrolytes Containing Nanocomposite ${\mathrm{S}\mathrm{i}\mathrm{O}}_{2}$ Particles," *Physical Review Letters,* vol. 91, no. 26, p. 266104, 12/31/ 2003, doi: 10.1103/PhysRevLett.91.266104.

[23] W. Lyu, G. He, and T. Liu, "PEO-LITFSI-SiO2-SN System Promotes the Application of Polymer Electrolytes in All-Solid-State Lithium-ion Batteries," *ChemistryOpen,* https://doi.org/10.1002/open.202000107 vol. 9, no. 6, pp. 713-718, 2020/06/01 2020, doi: https://doi.org/10.1002/open.202000107.

[24] G. Coppez, S. Chowdhury, and S. P. Chowdhury, "The importance of energy storage in Renewable Power Generation: A review," in *45th International Universities Power Engineering Conference UPEC2010*, 31 Aug.-3 Sept. 2010 2010, pp. 1-5.

[25] S. Ould Amrouche, D. Rekioua, T. Rekioua, and S. Bacha, "Overview of energy storage in renewable energy systems," *International Journal of Hydrogen Energy,* vol. 41, no. 45, pp. 20914-20927, 2016/12/07/ 2016, doi: https://doi.org/10.1016/j.ijhydene.2016.06.243.

[26] J. Kelly, "Thermally Responsive Polymer Electrolytes for Inherently Safe Electrochemical Energy Storage," 2014.

[27] M. Marinaro *et al.*, "Bringing forward the development of battery cells for automotive applications: Perspective of R&D activities in China, Japan, the EU and the USA," *Journal of Power Sources,* vol. 459, p. 228073, 2020/05/31/ 2020, doi: https://doi.org/10.1016/j.jpowsour.2020.228073.

[28] M. M. Thackeray, C. Wolverton, and E. D. Isaacs, "Electrical energy storage for transportation—approaching the limits of, and going beyond, lithium-ion batteries," *Energy & Environmental Science,* 10.1039/C2EE21892E vol. 5, no. 7, pp. 7854-7863, 2012, doi: 10.1039/C2EE21892E.

[29] A. BOSCHIN, "Sodium Batteries: From Liquid to Polymer Electrolytes ", 2016.

[30] B. B. Owens, P. Reale, and B. Scrosati, "PRIMARY BATTERIES | Overview," in *Encyclopedia of Electrochemical Power Sources*, J. Garche Ed. Amsterdam: Elsevier, 2009, pp. 22-27.

[31] Z. SHUO, "POLY (ETHYLENE OXIDE)-BASED COMPOSITE POLYMER ELECTROLYTES FOR THE SECONDARY LITHIUM BATTERIES ", 2004.

[32] G. Tuna and V. C. Gungor, "2 - Energy harvesting and battery technologies for powering wireless sensor networks," in *Industrial Wireless Sensor Networks*, R. Budampati and S. Kolavennu Eds.: Woodhead Publishing, 2016, pp. 25-38.

[33] S. S. Hosseiny and M. Wessling, "13 - Ion exchange membranes for vanadium redox flow batteries," in *Advanced Membrane Science and Technology for Sustainable Energy and Environmental Applications*, A. Basile and S. P. Nunes Eds.: Woodhead Publishing, 2011, pp. 413-434.

[34] B. Viswanathan, "Chapter 12 - Batteries," in *Energy Sources*, B. Viswanathan Ed. Amsterdam: Elsevier, 2017, pp. 263-313.

[35] H. Schmidbaur and J. L. Cihonski, "Noble Metals (Chemistry)," in *Encyclopedia of Physical Science and Technology (Third Edition)*, R. A. Meyers Ed. New York: Academic Press, 2003, pp. 463-492.

[36] G. Pistoia, "APPLICATIONS – PORTABLE | Portable Devices: Batteries," in *Encyclopedia of Electrochemical Power Sources*, J. Garche Ed. Amsterdam: Elsevier, 2009, pp. 29-38.

[37] F. Sun, "Development of Novel Solid-State Electrolytes for Sodium Ion Batteries," 2019.

[38] K. C. Divya and J. Østergaard, "Battery energy storage technology for power systems—An overview," *Electric Power Systems Research,* vol. 79, no. 4, pp. 511-520, 2009/04/01/ 2009, doi: https://doi.org/10.1016/j.epsr.2008.09.017.

[39] K. Kordesch and W. Taucher-Mautner, "HISTORY | Primary Batteries," in *Encyclopedia of Electrochemical Power Sources*, J. Garche Ed. Amsterdam: Elsevier, 2009, pp. 555-564.

[40] J. Paska, P. Biczel, and M. Kłos, "Technical and economic aspects of electricity storage systems co-operating with renewable energy sources," *2009 10th International Conference on Electrical Power Quality and Utilisation,* pp. 1-6, 2009.

[41] Y. Subası, "Development of High Purity Lithium Bis(oxalate)borate, LiB(C2O4)2 (LiBOB) and Its Effect on the Stability of Standard and New Generation Electrode Materials," 2022.

[42] Q. Chen, "Printing 3D lithium-ion microbattery using stereolithography," 2016.

[43] M. R. Oduncu, "DEVELOPMENT OF A NOVEL POLYMER-GARNET SOLID STATE COMPOSITE ELECTROLYTE INCORPORATING LI-LA-ZR-BI-O AND POLYETHYLENE OXIDE," Master of Science, 2016.

[44] P. Zheng, "The Design and Optimization of a Lithium-ion Battery Direct Recycling Process," 2019.

[45] S. J. Lilley, "ENHANCING THE CONDUCTIVITY OF CRYSTALLINE POLYMER ELECTROLYTES," 2007.

[46] Y. Yao, "A study of electro materials for lithium-ion batteries," 2008.

[47] Z. W. SEH, "HIGH-ENERGY LITHIUM–SULFUR BATTERIES: FROM THEORETICAL UNDERSTANDING TO MATERIALS DESIGN," 2015.

[48] R. Giri, "“SYNTHESIS AND CHARACTERIZATION OF PMMA BASED POLYMER GEL ELECTROLYTE”," 2005.

[49] S. Ketabi, "Polymer–Ionic liquid Electrolytes for Electrochemical Capacitors," 2015.

[50] D. Zhou, D. Shanmukaraj, A. Tkacheva, M. Armand, and G. X. Wang, "Polymer Electrolytes for Lithium-Based Batteries: Advances and Prospects," (in English), *Chem,* vol. 5, no. 9, pp. 2326-2352, Sep 12 2019, doi: 10.1016/j.chempr.2019.05.009.

[51] D. Devaux, R. Bouchet, D. Glé, and R. Denoyel, "Mechanism of ion transport in PEO/LiTFSI complexes: Effect of temperature, molecular weight and end groups," *Solid State Ionics,* vol. 227, pp. 119-127, 2012/10/29/ 2012, doi: https://doi.org/10.1016/j.ssi.2012.09.020.

[52] J. Wang, S. Li, Q. Zhao, C. Song, and Z. Xue, "Structure Code for Advanced Polymer Electrolyte in Lithium-Ion Batteries," *Advanced Functional Materials,* vol. 31, no. 12, p. 2008208, 2021, doi: https://doi.org/10.1002/adfm.202008208.

[53] M. Armand *et al.*, "Lithium-ion batteries – Current state of the art and anticipated developments," *Journal of Power Sources,* vol. 479, p. 228708, 2020/12/15/ 2020, doi: https://doi.org/10.1016/j.jpowsour.2020.228708.

[54] B. Scrosati, "History of lithium batteries," *Journal of Solid State Electrochemistry,* vol. 15, no. 7, pp. 1623-1630, 2011/07/01 2011, doi: 10.1007/s10008-011-1386-8.

[55] M. J. N. Pourbaix, "Atlas of Electrochemical Equilibria in Aqueous Solutions," 1974.

[56] L. Korson, W. Drost-Hansen, and F. J. Millero, "Viscosity of water at various temperatures," *The Journal of Physical Chemistry,* vol. 73, pp. 34-39, 1969.

[57] M. A. Mehta, "MULTIVALENT IONS IN POLYMER ELECTROLYTES," 1993.

[58] C. Chanthad, "SYNTHESIS AND CHARACTERIZATIONS OF NOVEL POLYMER ELECTROLYTES," 2013.

[59] D. E. Fenton, J. M. Parker, and P. V. Wright, "Complexes of alkali metal ions with poly(ethylene oxide)," *Polymer,* vol. 14, p. 589, 1973.

[60] T. Himba, "Structural aspects of poly(ethylene oxide) salt complexes," *Solid State Ionics,* vol. 9-10, pp. 1101-1105, 1983/12/01/ 1983, doi: https://doi.org/10.1016/0167-2738(83)90137-6.

[61] R. C. Agrawal and G. P. Pandey, "Solid polymer electrolytes: materials designing and all-solid-state battery applications: an overview," *Journal of Physics D: Applied Physics,* vol. 41, no. 22, p. 223001, 2008/10/29 2008, doi: 10.1088/0022-3727/41/22/223001.

[62] W. Li, Y. Pang, J. Liu, G. Liu, Y. Wang, and Y. Xia, "A PEO-based gel polymer electrolyte for lithium ion batteries," *RSC Advances,* 10.1039/C7RA02603J vol. 7, no. 38, pp. 23494-23501, 2017, doi: 10.1039/C7RA02603J.

[63] A. Manuel Stephan, "Review on gel polymer electrolytes for lithium batteries," *European Polymer Journal,* vol. 42, no. 1, pp. 21-42, 2006/01/01/ 2006, doi: https://doi.org/10.1016/j.eurpolymj.2005.09.017.

[64] H. Gao, W. Zhou, K. Park, and J. B. Goodenough, "A Sodium-Ion Battery with a Low-Cost Cross-Linked Gel-Polymer Electrolyte," *Advanced Energy Materials,* https://doi.org/10.1002/aenm.201600467 vol. 6, no. 18, p. 1600467, 2016/09/01 2016, doi: https://doi.org/10.1002/aenm.201600467.

[65] T. E. Sutto, "Hydrophobic and Hydrophilic Interactions of Ionic Liquids and Polymers in Solid Polymer Gel Electrolytes," *Journal of The Electrochemical Society,* vol. 154, no. 10, p. P101, 2007, doi: 10.1149/1.2767414.

[66] N. K. Karan, D. K. Pradhan, R. Thomas, B. Natesan, and R. S. Katiyar, "Solid polymer electrolytes based on polyethylene oxide and lithium trifluoro- methane sulfonate (PEO–LiCF3SO3): Ionic conductivity and dielectric relaxation," *Solid State Ionics,* vol. 179, no. 19, pp. 689-696, 2008/08/01/ 2008, doi: https://doi.org/10.1016/j.ssi.2008.04.034.

[67] K. Lian and C. M. Li, "Solid polymer electrochemical capacitors using heteropoly acid electrolytes," *Electrochemistry Communications,* vol. 11, no. 1, pp. 22-24, 2009/01/01/ 2009, doi: https://doi.org/10.1016/j.elecom.2008.10.016.

[68] G. G. Cameron, "Solid polymer electrolytes: Fundamentals and technological Applications. Fiona M. Gray. VCH Publishers Inc., New York 1991. pp. x + 245, price £44.00. ISBN 0–89573–772–8," *Polymer International,* https://doi.org/10.1002/pi.4990320421 vol. 32, no. 4, pp. 436-436, 1993/01/01 1993, doi: https://doi.org/10.1002/pi.4990320421.

[69] X. Zhang, J.-C. Daigle, and K. Zaghib, "Comprehensive Review of Polymer Architecture for All-Solid-State Lithium Rechargeable Batteries," *Materials,* vol. 13, no. 11, 2020, doi: 10.3390/ma13112488.

[70] Y. Chatani and S. Okamura, "Crystal structure of poly(ethylene oxide)—sodium iodide complex," *Polymer,* vol. 28, no. 11, pp. 1815-1820, 1987/10/01/ 1987, doi: https://doi.org/10.1016/0032-3861(87)90283-7.

[71] D. Bresser, S. Lyonnard, C. Iojoiu, L. Picard, and S. Passerini, "Decoupling segmental relaxation and ionic conductivity for lithium-ion polymer electrolytes," *Molecular Systems Design & Engineering,* vol. 4, no. 4, pp. 779-792, 2019, doi: https://doi.org/10.1039/C9ME00038K.

[72] N. A. Stolwijk, M. Wiencierz, and S. Obeidi, "Mass and charge transport in the PEO–NaI polymer electrolyte system: effects of temperature and salt concentration," *Faraday Discussions,* 10.1039/B602143N vol. 134, no. 0, pp. 157-169, 2007, doi: 10.1039/B602143N.

[73] M. J. Hudson and C. A. C. Sequeira, "Electrochemical Impedance Spectroscopy Measurements on Lithium Salt Containing Interpenetrating Polymer Networks," *Journal of The Electrochemical Society,* vol. 142, no. 12, pp. 4013-4017, 1995/12/01 1995, doi: 10.1149/1.2048455.

[74] N. A. Stolwijk, M. Wiencierz, and S. Obeidi, "Self-diffusion versus ion conduction in polymer electrolytes: On the occurrence of pairs, triplets, and higher-order clusters," *Electrochimica Acta,* vol. 53, pp. 1575-1583, 2007.

[75] U. Olsher, R. M. Izatt, J. S. Bradshaw, and N. K. Dalley, "Coordination chemistry of lithium ion: a crystal and molecular structure review," *Chemical Reviews,* vol. 91, no. 2, pp. 137-164, 1991/03/01 1991, doi: 10.1021/cr00002a003.

[76] K. I. S. Mongcopa *et al.*, "Relationship between Segmental Dynamics Measured by Quasi-Elastic Neutron Scattering and Conductivity in Polymer Electrolytes," *ACS Macro Letters,* vol. 7, no. 4, pp. 504-508, 2018/04/17 2018, doi: 10.1021/acsmacrolett.8b00159.

[77] D. A. Jokhakar *et al.*, "All-solid-state Li-metal batteries: role of blending PTFE with PEO and LiTFSI salt as a composite electrolyte with enhanced thermal stability," *Sustainable Energy & Fuels,* 10.1039/D0SE00013B vol. 4, no. 5, pp. 2229-2235, 2020, doi: 10.1039/D0SE00013B.

[78] Y. Zhao, Y. Bai, W. Li, M. An, Y. Bai, and G. Chen, "Design Strategies for Polymer Electrolytes with Ether and Carbonate Groups for Solid-State Lithium Metal Batteries," *Chemistry of Materials,* vol. 32, no. 16, pp. 6811-6830, 2020/08/25 2020, doi: 10.1021/acs.chemmater.9b04521.

[79] N. F. A. Zainal, S. A. Lai, and C. H. Chan, "Melt Rheological Behavior and Morphology of Poly(ethylene oxide)/Natural Rubber-graft-Poly(methyl methacrylate) Blends," *Polymers,* vol. 12, no. 3, p. 724, 2020. [Online]. Available: https://www.mdpi.com/2073-4360/12/3/724.

[80] H. Ito, T. P. Russell, and G. D. Wignall, "Interactions in mixtures of poly(ethylene oxide) and poly(methyl methacrylate)," *Macromolecules,* vol. 20, no. 9, pp. 2213-2220, 1987/09/01 1987, doi: 10.1021/ma00175a028.

[81] S. Cimmino, E. Martuscelli, and C. Silvestre, "Miscibility prediction based on the corresponding states theory: poly(ethylene oxide)/atactic poly(methyl methacrylate) system," *Polymer,* vol. 30, no. 3, pp. 393-398, 1989/03/01/ 1989, doi: https://doi.org/10.1016/0032-3861(89)90003-7.

[82] E. Senses, M. Tyagi, M. Pasco, and A. Faraone, "Dynamics of Architecturally Engineered All-Polymer Nanocomposites," *ACS Nano,* vol. 12, no. 11, pp. 10807-10816, Nov 27 2018, doi: 10.1021/acsnano.8b02514.

[83] T. P. Lodge and T. C. B. McLeish, "Self-Concentrations and Effective Glass Transition Temperatures in Polymer Blends," *Macromolecules,* vol. 33, no. 14, pp. 5278-5284, 2000/07/01 2000, doi: 10.1021/ma9921706.

[84] T. P. Lodge, E. R. Wood, and J. C. Haley, "Two calorimetric glass transitions do not necessarily indicate immiscibility: The case of PEO/PMMA," *Journal of Polymer Science Part B: Polymer Physics,* vol. 44, no. 4, pp. 756-763, 2006, doi: 10.1002/polb.20735.

[85] Z. Jia, W. Yuan, H. Zhao, H. Hu, and G. L. Baker, "Composite electrolytes comprised of poly(ethylene oxide) and silica nanoparticles with grafted poly(ethylene oxide)-

containing polymers," *RSC Advances,* 10.1039/C4RA07262F vol. 4, no. 77, pp. 41087-41098, 2014, doi: 10.1039/C4RA07262F.

[86] J. L. Schaefer, S. S. Moganty, D. A. Yanga, and L. A. Archer, "Nanoporous hybrid electrolytes," *Journal of Materials Chemistry,* 10.1039/C0JM04171H vol. 21, no. 27, pp. 10094-10101, 2011, doi: 10.1039/C0JM04171H.

[87] Y. Shui, Y. Su, X. Kuang, W. Zhao, Y. Cai, and D. Wang, "Facile and controllable synthesis of hybrid silica nanoparticles densely grafted with poly(ethylene glycol)," *Polymer International,* https://doi.org/10.1002/pi.5391 vol. 66, no. 10, pp. 1395-1401, 2017/10/01 2017, doi: https://doi.org/10.1002/pi.5391.

[88] S. Choudhury, S. Stalin, Y. Deng, and L. A. Archer, "Soft Colloidal Glasses as Solid-State Electrolytes," *Chemistry of Materials,* vol. 30, no. 17, pp. 5996-6004, 2018/09/11 2018, doi: https://doi.org/10.1021/acs.chemmater.8b02227.

[89] B. Scrosati, F. Croce, and L. Persi, "Impedance Spectroscopy Study of PEO-Based Nanocomposite Polymer Electrolytes," *Journal of The Electrochemical Society,* vol. 147, no. 5, p. 1718, 2000, doi: 10.1149/1.1393423.

[90] P. Mustarelli, E. Quartarone, C. Tomasi, and A. Magistris, "New materials for polymer electrolytes," *Solid State Ionics,* vol. 135, no. 1, pp. 81-86, 2000/11/01/ 2000, doi: https://doi.org/10.1016/S0167-2738(00)00335-0.

[91] B. Singh and S. S. Sekhon, "Polymer Electrolytes Based on Room Temperature Ionic Liquid: 2,3-Dimethyl-1-octylimidazolium Triflate," *The Journal of Physical Chemistry B,* vol. 109, no. 34, pp. 16539-16543, 2005/09/01 2005, doi: 10.1021/jp051673c.

[92] S. Coppola, N. Grizzuti, G. Floudas, and D. Vlassopoulos, "Viscoelasticity and crystallization of poly(ethylene oxide) star polymers of varying arm number and size," *Journal of Rheology,* vol. 51, no. 5, pp. 1007-1025, 2007, doi: 10.1122/1.2751076.

[93] G. Zardalidis, J. Mars, J. Allgaier, M. Mezger, D. Richter, and G. Floudas, "Influence of chain topology on polymer crystallization: poly(ethylene oxide) (PEO) rings vs. linear

chains," *Soft Matter,* vol. 12, no. 39, pp. 8124-8134, Oct 4 2016, doi: https://doi.org/10.1039/C6SM01622G.

[94] Y. Yao *et al.*, "Capillary Imbibition, Crystallization, and Local Dynamics of Hyperbranched Poly(ethylene oxide) Confined to Nanoporous Alumina," *Macromolecules,* vol. 50, no. 21, pp. 8755-8764, 2017/11/14 2017, doi: 10.1021/acs.macromol.7b01843.

[95] M. SHOJAATALHOSSEINI, "Conductivity and Relaxation in Polymer Based Solid Electrolyte," Master Department of Physics, Chalmers University of Technology, 2016.

[96] S.-W. L. Er-Qiang Chen, Anqiu Zhang, Bon-Suk Moon, Ian Mann, Frank W. Harris, and Stephen Z. D. Cheng, "Isothermal Thickening and Thinning Processes in Low-Molecular-Weight Poly(ethylene oxide) Fractions Crystallized from the Melt. 8. Molecular Shape Dependence," 1999.

[97] A. Chremos and J. F. Douglas, "Communication: When does a branched polymer become a particle?," *The Journal of Chemical Physics,* vol. 143, no. 11, p. 111104, 2015/09/21 2015, doi: 10.1063/1.4931483.

[98] A. Chremos, E. Glynos, and P. F. Green, "Structure and dynamical intra-molecular heterogeneity of star polymer melts above glass transition temperature," *The Journal of chemical physics,* vol. 142, no. 4, p. 044901, 2015, doi: https://doi.org/10.1063/1.4906085.

[99] S. Ren, T. Zheng, Q. Zhou, L. Zhang, and H. Li, "Preparation and ionic conductivity of composite polymer electrolytes based on hyperbranched star polymer," *Ionics,* vol. 20, no. 9, pp. 1225-1234, 2014/09/01 2014, doi: 10.1007/s11581-013-1061-4.

[100] M. Marzantowicz, J. R. Dygas, F. Krok, Z. Florjańczyk, E. Zygadło-Monikowska, and G. Lapienis, "Ionic conductivity of electrolytes based on star-branched poly(ethylene oxide) with high concentration of lithium salts," *Solid State Ionics,* vol. 192, no. 1, pp. 137-142, 2011/06/16/ 2011, doi: https://doi.org/10.1016/j.ssi.2010.06.032.

[101] S. Lascaud, M. Perrier, A. Vallee, S. Besner, J. Prud'homme, and M. Armand, "Phase Diagrams and Conductivity Behavior of Poly(ethylene oxide)-Molten Salt Rubbery Electrolytes," *Macromolecules,* vol. 27, no. 25, pp. 7469-7477, 1994/12/01 1994, doi: 10.1021/ma00103a034.

[102] C. Berthier, W. Gorecki, M. Minier, M. B. Armand, J. M. Chabagno, and P. Rigaud, "Microscopic investigation of ionic conductivity in alkali metal salts-poly(ethylene oxide) adducts," *Solid State Ionics,* vol. 11, no. 1, pp. 91-95, 1983/09/01/ 1983, doi: https://doi.org/10.1016/0167-2738(83)90068-1.

[103] W. Gorecki *et al.*, "NMR, DSC, and conductivity study of a poly(ethylene oxide) complex electrolyte : PEO(LiClO4)x," *Solid State Ionics,* vol. 18-19, pp. 295-299, 1986/01/01/ 1986, doi: https://doi.org/10.1016/0167-2738(86)90130-X.

[104] C. D. Robitaille and D. Fauteux, "Phase Diagrams and Conductivity Characterization of Some PEO - LiX Electrolytes," *Journal of The Electrochemical Society,* vol. 133, no. 2, pp. 315-325, 1986/02/01 1986, doi: 10.1149/1.2108569.

[105] S. M. Zahurak, M. L. Kaplan, E. A. Rietman, D. W. Murphy, and R. J. Cava, "Phase relationships and conductivity of the polymer electrolytes poly(ethylene oxide)/lithium tetrafluoroborate and poly(ethylene oxide)/lithium trifluoromethanesulfonate," *Macromolecules,* vol. 21, no. 3, pp. 654-660, 1988/03/01 1988, doi: 10.1021/ma00181a020.

[106] K. K. Mahato, K. Dutta, and B. C. Ray, "6 - Emerging advancement of fiber-reinforced polymer composites in structural applications," in *New Materials in Civil Engineering*, P. Samui, D. Kim, N. R. Iyer, and S. Chaudhary Eds.: Butterworth-Heinemann, 2020, pp. 221-271.

[107] W. Brostow, S. H. Goodman, and J. Wahrmund, "8 - Epoxies," in *Handbook of Thermoset Plastics (Third Edition)*, H. Dodiuk and S. H. Goodman Eds. Boston: William Andrew Publishing, 2014, pp. 191-252.

[108] J. K. Fink, "Chapter 3 - Epoxy Resins," in *Reactive Polymers Fundamentals and Applications (Second Edition)*, J. K. Fink Ed. Oxford: William Andrew Publishing, 2013, pp. 95-153.

[109] S. Emmert *et al.*, "Electrode polarization effects in broadband dielectric spectroscopy," *The European Physical Journal B,* vol. 83, pp. 157-165, 2011.

[110] K. Deshmukh *et al.*, "Chapter 10 - Dielectric Spectroscopy," in *Spectroscopic Methods for Nanomaterials Characterization*, S. Thomas, R. Thomas, A. K. Zachariah, and R. K. Mishra Eds.: Elsevier, 2017, pp. 237-299.

[111] "Allen J. Bard and Larry R. Faulkner, Electrochemical Methods: Fundamentals and Applications, New York: Wiley, 2001, 2nd ed," *Russian Journal of Electrochemistry,* vol. 38, no. 12, pp. 1364-1365, 2002/12/01 2002, doi: 10.1023/A:1021637209564.

[112] P. Mohamed Shameer and P. Mohamed Nishath, "Chapter 8 - Exploration and enhancement on fuel stability of biodiesel: A step forward in the track of global commercialization," in *Advanced Biofuels*, A. K. Azad and M. Rasul Eds.: Woodhead Publishing, 2019, pp. 181-213.

[113] R. Sindhu, P. Binod, and A. Pandey, "Chapter 17 - Microbial Poly-3-Hydroxybutyrate and Related Copolymers," in *Industrial Biorefineries & White Biotechnology*, A. Pandey, R. Höfer, M. Taherzadeh, K. M. Nampoothiri, and C. Larroche Eds. Amsterdam: Elsevier, 2015, pp. 575-605.

[114] D. Titus, E. James Jebaseelan Samuel, and S. M. Roopan, "Chapter 12 - Nanoparticle characterization techniques," in *Green Synthesis, Characterization and Applications of Nanoparticles*, A. K. Shukla and S. Iravani Eds.: Elsevier, 2019, pp. 303-319.

[115] G. Ianniruberto, "Introduction on Polymer Rheology," in *Reference Module in Chemistry, Molecular Sciences and Chemical Engineering*: Elsevier, 2015.

[116] H. F. Giles, J. R. Wagner, and E. M. Mount, "3 - Single Screw Extruder: Equipment," in *Extrusion*, H. F. Giles, J. R. Wagner, and E. M. Mount Eds. Norwich, NY: William Andrew Publishing, 2005, pp. 13-34.

[117] V. G. Kulichikhin, V. S. Volkov, and N. A. Platé, "15 - Rheological Behaviour of Liquid Crystalline Polymers," in *Comprehensive Polymer Science and Supplements*, G. Allen and J. C. Bevington Eds. Amsterdam: Pergamon, 1989, pp. 385-406.

[118] B. A. Morris, "5 - Rheology of Polymer Melts," in *The Science and Technology of Flexible Packaging*, B. A. Morris Ed. Oxford: William Andrew Publishing, 2017, pp. 121-147.

[119] V. N. Uversky and A. K. Dunker, "3.9 Intrinsically Disordered Proteins," in *Comprehensive Biophysics*, E. H. Egelman Ed. Amsterdam: Elsevier, 2012, pp. 170-211.

[120] A. K. Singh, "Chapter 4 - Experimental Methodologies for the Characterization of Nanoparticles," in *Engineered Nanoparticles*, A. K. Singh Ed. Boston: Academic Press, 2016, pp. 125-170.

[121] H. Fatafta, S. Samantray, A. Sayyed-Ahmad, O. Coskuner-Weber, and B. Strodel, "Chapter Five - Molecular simulations of IDPs: From ensemble generation to IDP interactions leading to disorder-to-order transitions," in *Progress in Molecular Biology and Translational Science*, vol. 183, V. N. Uversky Ed.: Academic Press, 2021, pp. 135-185.

[122] T. Y. Inan, "2 - Thermoplastic-based nanoblends: Preparation and characterizations," in *Recent Developments in Polymer Macro, Micro and Nano Blends*, P. M. Visakh, G. Markovic, and D. Pasquini Eds.: Woodhead Publishing, 2017, pp. 17-56.

[123] S. Ebnesajjad, "4 - Surface and Material Characterization Techniques," in *Handbook of Adhesives and Surface Preparation*, S. Ebnesajjad Ed. Oxford: William Andrew Publishing, 2011, pp. 31-48.

[124] R. K. Mishra, J. Cherusseri, A. Bishnoi, and S. Thomas, "Chapter 13 - Nuclear Magnetic Resonance Spectroscopy," in *Spectroscopic Methods for Nanomaterials*

Characterization, S. Thomas, R. Thomas, A. K. Zachariah, and R. K. Mishra Eds.: Elsevier, 2017, pp. 369-415.

[125] M. K. Singh and A. Singh, "Chapter 14 - Nuclear magnetic resonance spectroscopy," in *Characterization of Polymers and Fibres*, M. K. Singh and A. Singh Eds.: Woodhead Publishing, 2022, pp. 321-339.

[126] N. Raval, R. Maheshwari, D. Kalyane, S. R. Youngren-Ortiz, M. B. Chougule, and R. K. Tekade, "Chapter 10 - Importance of Physicochemical Characterization of Nanoparticles in Pharmaceutical Product Development," in *Basic Fundamentals of Drug Delivery*, R. K. Tekade Ed.: Academic Press, 2019, pp. 369-400.

[127] A. V. Malm and J. C. W. Corbett, "Improved Dynamic Light Scattering using an adaptive and statistically driven time resolved treatment of correlation data," *Scientific Reports,* vol. 9, no. 1, p. 13519, 2019/09/18 2019, doi: 10.1038/s41598-019-50077-4.

[128] S. Falke and C. Betzel, "Dynamic Light Scattering (DLS)," in *Radiation in Bioanalysis: Spectroscopic Techniques and Theoretical Methods*, A. S. Pereira, P. Tavares, and P. Limão-Vieira Eds. Cham: Springer International Publishing, 2019, pp. 173-193.

[129] H. Jans, X. Liu, L. Austin, G. Maes, and Q. Huo, "Dynamic Light Scattering as a Powerful Tool for Gold Nanoparticle Bioconjugation and Biomolecular Binding Studies," *Analytical Chemistry,* vol. 81, no. 22, pp. 9425-9432, 2009/11/15 2009, doi: 10.1021/ac901822w.

[130] J. Stetefeld, S. A. McKenna, and T. R. Patel, "Dynamic light scattering: a practical guide and applications in biomedical sciences," (in eng), *Biophys Rev,* vol. 8, no. 4, pp. 409-427, Dec 2016, doi: 10.1007/s12551-016-0218-6.

[131] R. Ragheb and U. Nobbmann, "Multiple scattering effects on intercept, size, polydispersity index, and intensity for parallel (VV) and perpendicular (VH) polarization detection in photon correlation spectroscopy," *Scientific Reports,* vol. 10, no. 1, p. 21768, 2020/12/10 2020, doi: 10.1038/s41598-020-78872-4.

[132] U. Soykan, B. Ozturk Sen, S. Cetin, U. Yahsi, and C. Tav, "A detailed survey for determination of the grafted semifluorinated acrylic compound effect on thermal, microstructural, free volume, mechanical and morphological features of HDPE," *Journal of Fluorine Chemistry,* vol. 233, p. 109511, 2020/05/01/ 2020, doi: https://doi.org/10.1016/j.jfluchem.2020.109511.

[133] J.-W. Rhim, S. Kuzeci, S. Roy, N. Akti, C. Tav, and U. Yahsi, "Effect of Free Volume on Curcumin Release from Various Polymer-Based Composite Films Analyzed Using Positron Annihilation Lifetime Spectroscopy," *Materials,* vol. 14, no. 19, p. 5679, 2021. [Online]. Available: https://www.mdpi.com/1996-1944/14/19/5679.

[134] S. J. Tao, "Positronium Annihilation in Molecular Substances," *The Journal of Chemical Physics,* vol. 56, no. 11, pp. 5499-5510, 1972/06/01 1972, doi: 10.1063/1.1677067.

[135] M. Eldrup, D. Lightbody, and J. N. Sherwood, "The temperature dependence of positron lifetimes in solid pivalic acid," *Chemical Physics,* vol. 63, no. 1, pp. 51-58, 1981/12/01/ 1981, doi: https://doi.org/10.1016/0301-0104(81)80307-2.

[136] U. Yahsi *et al.*, "Ionic conductivity of PVdF-co-HFP/LiClO4 in terms of free volume defects probed by positron annihilation lifetime spectroscopy," *Radiation Effects and Defects in Solids,* vol. 174, no. 3-4, pp. 214-228, 2019/04/03 2019, doi: 10.1080/10420150.2018.1552959.

[137] P. Utpalla, S. K. Sharma, K. Sudarshan, S. K. Deshpande, M. Sahu, and P. K. Pujari, "Investigating the Correlation of Segmental Dynamics, Free Volume Characteristics, and Ionic Conductivity in Poly(ethylene oxide)-Based Electrolyte: A Broadband Dielectric and Positron Annihilation Spectroscopy Study," *The Journal of Physical Chemistry C,* vol. 124, no. 8, pp. 4489-4501, 2020/02/27 2020, doi: 10.1021/acs.jpcc.9b11722.

[138] A. K. M. A. Habib, M. K. Hasan, M. Mahmud, S. M. A. Motakabber, M. I. Ibrahimya, and S. Islam, "A review: Energy storage system and balancing circuits for electric vehicle

application," *IET Power Electronics,* vol. 14, no. 1, pp. 1-13, 2021, doi: https://doi.org/10.1049/pel2.12013.

[139] C. SubramanianDr., "An appraisal on intelligent and smart systems," *AIP Conference Proceedings,* vol. 2316, no. 1, p. 020003, 2021, doi: 10.1063/5.0037534.

[140] R. D. Rodriguez *et al.*, "Ultra-Robust Flexible Electronics by Laser-Driven Polymer-Nanomaterials Integration," *Advanced Functional Materials,* vol. 31, no. 17, p. 2008818, 2021, doi: https://doi.org/10.1002/adfm.202008818.

[141] Y. Xia, Y. He, F. Zhang, Y. Liu, and J. Leng, "A Review of Shape Memory Polymers and Composites: Mechanisms, Materials, and Applications," *Advanced Materials,* vol. 33, no. 6, p. 2000713, 2021, doi: https://doi.org/10.1002/adma.202000713.

[142] M. Rinaldi, F. Cecchini, L. Pigliaru, T. Ghidini, F. Lumaca, and F. Nanni, "Additive Manufacturing of Polyether Ether Ketone (PEEK) for Space Applications: A Nanosat Polymeric Structure," *Polymers,* vol. 13, no. 1, p. 11, 2021. [Online]. Available: https://www.mdpi.com/2073-4360/13/1/11.

[143] J. L. Schaefer, Y. Lu, S. S. Moganty, P. Agarwal, N. Jayaprakash, and L. A. Archer, "Electrolytes for high-energy lithium batteries," *Applied Nanoscience,* vol. 2, no. 2, pp. 91-109, 2012/06/01 2012, doi: 10.1007/s13204-011-0044-x.

[144] Y. Choo, D. M. Halat, I. Villaluenga, K. Timachova, and N. P. Balsara, "Diffusion and migration in polymer electrolytes," *Progress in Polymer Science,* vol. 103, p. 101220, 2020/04/01/ 2020, doi: https://doi.org/10.1016/j.progpolymsci.2020.101220.

[145] D. Zhou, D. Shanmukaraj, A. Tkacheva, M. Armand, and G. Wang, "Polymer Electrolytes for Lithium-Based Batteries: Advances and Prospects," *Chem,* vol. 5, no. 9, pp. 2326-2352, 2019/09/12/ 2019, doi: https://doi.org/10.1016/j.chempr.2019.05.009.

[146] S.-H. Kim *et al.*, "A shape-deformable and thermally stable solid-state electrolyte based on a plastic crystal composite polymer electrolyte for flexible/safer lithium-ion

batteries," *Journal of Materials Chemistry A,* 10.1039/C4TA00494A vol. 2, no. 28, pp. 10854-10861, 2014, doi: https://doi.org/10.1039/C4TA00494A.

[147] Y. Lin, Y. Cheng, J. Li, J. D. Miller, J. Liu, and X. Wang, "Biocompatible and biodegradable solid polymer electrolytes for high voltage and high temperature lithium batteries," *RSC Advances,* 10.1039/C7RA01601H vol. 7, no. 40, pp. 24856-24863, 2017, doi: 10.1039/C7RA01601H.

[148] D. T. H. Jr. and N. P. Balsara, "Polymer Electrolytes," *Annual Review of Materials Research,* vol. 43, no. 1, pp. 503-525, 2013, doi: 10.1146/annurev-matsci-071312-121705.

[149] X. Jin, S. Zhang, and J. Runt, "Broadband Dielectric Investigation of Amorphous Poly(methyl methacrylate)/Poly(ethylene oxide) Blends," *Macromolecules,* vol. 37, no. 21, pp. 8110-8115, 2004/10/01 2004, doi: 10.1021/ma049281b.

[150] M. Dionísio, A. C. Fernandes, J. F. Mano, N. T. Correia, and R. C. Sousa, "Relaxation Studies in PEO/PMMA Blends," *Macromolecules,* vol. 33, no. 3, pp. 1002-1011, 2000/02/01 2000, doi: 10.1021/ma9913818.

[151] E.-Q. Chen *et al.*, "Isothermal Thickening and Thinning Processes in Low-Molecular-Weight Poly(ethylene oxide) Fractions Crystallized from the Melt. 8. Molecular Shape Dependence. Volume 32, Number 15, July 27, 1999, pp 4784−4793," *Macromolecules,* vol. 32, no. 15, pp. 5174-5174, 1999/07/27 1999, doi: 10.1021/ma9824046.

[152] G. Homann, L. Stolz, J. Nair, I. C. Laskovic, M. Winter, and J. Kasnatscheew, "Poly(Ethylene Oxide)-based Electrolyte for Solid-State-Lithium-Batteries with High Voltage Positive Electrodes: Evaluating the Role of Electrolyte Oxidation in Rapid Cell Failure," *Scientific Reports,* vol. 10, no. 1, p. 4390, 2020/03/09 2020, doi: 10.1038/s41598-020-61373-9.

[153] M. S. Michael, M. M. E. Jacob, S. R. S. Prabaharan, and S. Radhakrishna, "Enhanced lithium ion transport in PEO-based solid polymer electrolytes employing a novel class of

plasticizers," *Solid State Ionics,* vol. 98, no. 3, pp. 167-174, 1997/06/02/ 1997, doi: https://doi.org/10.1016/S0167-2738(97)00117-3.

[154] Z. Xue, D. He, and X. Xie, "Poly(ethylene oxide)-based electrolytes for lithium-ion batteries," *Journal of Materials Chemistry A,* 10.1039/C5TA03471J vol. 3, no. 38, pp. 19218-19253, 2015, doi: 10.1039/C5TA03471J.

[155] G. C. Alfonso and T. P. Russell, "Kinetics of crystallization in semicrystalline/amorphous polymer mixtures," *Macromolecules,* vol. 19, no. 4, pp. 1143-1152, 1986/04/01 1986, doi: 10.1021/ma00158a036.

[156] G. C. Alfonso and T. P. Russell, "Crystallization and Melting Studies on Poly (Ethylene Oxide)/Poly (Methyl Methacrylate) Mixtures," in *Integration of Fundamental Polymer Science and Technology*, L. A. Kleintjens and P. J. Lemstra Eds. Dordrecht: Springer Netherlands, 1986, pp. 132-137.

[157] Y. L. Yap, A. H. You, and L. L. Teo, "Preparation and characterization studies of PMMA–PEO-blend solid polymer electrolytes with SiO2 filler and plasticizer for lithium ion battery," *Ionics,* vol. 25, no. 7, pp. 3087-3098, 2019, doi: 10.1007/s11581-019-02842-8.

[158] J. Straka, P. Schmidt, J. Dybal, B. Schneider, and J. Spěváček, "Blends of poly(ethylene oxide)/poly(methyl methacrylate). An i.r. and n.m.r. study," *Polymer,* vol. 36, no. 6, pp. 1147-1155, 1995/03/01/ 1995, doi: https://doi.org/10.1016/0032-3861(95)93916-A.

[159] D. Bhowmik *et al.*, "Investigation of a Nanocomposite of 75 wt % Poly(methyl methacrylate) Nanoparticles with 25 wt % Poly(ethylene oxide) Linear Chains: A Quasielatic Neutron Scattering, Calorimetric, and WAXS Study," *Macromolecules,* vol. 47, no. 9, pp. 3005-3016, 2014, doi: 10.1021/ma500215f.

[160] A. N. Gaikwad, E. R. Wood, T. Ngai, and T. P. Lodge, "Two Calorimetric Glass Transitions in Miscible Blends Containing Poly(ethylene oxide)," *Macromolecules,* vol. 41, no. 7, pp. 2502-2508, 2008/04/01 2008, doi: 10.1021/ma702429r.

[161] V. García Sakai, J. K. Maranas, I. Peral, and J. R. D. Copley, "Dynamics of PEO in Blends with PMMA: Study of the Effects of Blend Composition via Quasi-Elastic Neutron Scattering," *Macromolecules,* vol. 41, no. 10, pp. 3701-3710, 2008/05/01 2008, doi: 10.1021/ma0714870.

[162] Y. He, T. R. Lutz, and M. D. Ediger, "Segmental and terminal dynamics in miscible polymer mixtures: Tests of the Lodge–McLeish model," *The Journal of Chemical Physics,* vol. 119, no. 18, pp. 9956-9965, 2003, doi: 10.1063/1.1615963.

[163] K. Mpoukouvalas and G. Floudas, "Effect of Pressure on the Dynamic Heterogeneity in Miscible Blends of Poly(methyl methacrylate) with Poly(ethylene oxide)," *Macromolecules,* vol. 41, no. 4, pp. 1552-1559, 2008/02/01 2008, doi: 10.1021/ma702299n.

[164] I. M. Kalogeras and W. Brostow, "Glass transition temperatures in binary polymer blends," *Journal of Polymer Science Part B: Polymer Physics,* vol. 47, no. 1, pp. 80-95, 2009, doi: 10.1002/polb.21616.

[165] T. R. Lutz, Y. He, M. D. Ediger, H. Cao, G. Lin, and A. A. Jones, "Rapid Poly(ethylene oxide) Segmental Dynamics in Blends with Poly(methyl methacrylate)," *Macromolecules,* vol. 36, no. 5, pp. 1724-1730, 2003/03/01 2003, doi: 10.1021/ma021634o.

[166] R. Bergman, F. Alvarez, A. Alegría, and J. Colmenero, "The merging of the dielectric α- and β-relaxations in poly-(methyl methacrylate)," *The Journal of Chemical Physics,* vol. 109, no. 17, pp. 7546-7555, 1998, doi: 10.1063/1.477376.

[167] Y. Lin *et al.*, "Casting solvent effects on molecular dynamics of weak dynamic asymmetry polymer blend films via broadband dielectric spectroscopy," *Journal of Membrane Science,* vol. 439, pp. 20-27, 2013, doi: 10.1016/j.memsci.2013.03.033.

[168] S.-I. Hirota, Y. Tominaga, S. Asai, and M. Sumita, "Dielectric relaxation behavior of poly(methyl methacrylate) under high-pressure carbon dioxide," *Journal of Polymer*

Science Part B: Polymer Physics, vol. 43, no. 21, pp. 2951-2962, 2005, doi: https://doi.org/10.1002/polb.20592.

[169] Y. Seki, R. Kita, N. Shinyashiki, S. Yagihara, and M. Yoneyama, "Molecular dynamics of poly(methyl methacrylate) determined by dielectric relaxation spectroscopy," *AIP Conference Proceedings,* vol. 1518, no. 1, pp. 466-469, 2013, doi: 10.1063/1.4794618.

[170] V. G. Sakai, C. Chen, J. K. Maranas, and Z. Chowdhuri, "Effect of Blending with Poly(ethylene oxide) on the Dynamics of Poly(methyl methacrylate): A Quasi-Elastic Neutron Scattering Approach," *Macromolecules,* vol. 37, no. 26, pp. 9975-9983, 2004/12/01 2004, doi: 10.1021/ma0497355.

[171] A. Filippov, N. Azancheev, A. Gibaydullin, S. Bhattacharyya, O. N. Antzutkin, and F. U. Shah, "Dynamic properties of imidazolium orthoborate ionic liquids mixed with polyethylene glycol studied by NMR diffusometry and impedance spectroscopy," *Magnetic Resonance in Chemistry,* https://doi.org/10.1002/mrc.4636 vol. 56, no. 2, pp. 113-119, 2018/02/01 2018, doi: https://doi.org/10.1002/mrc.4636.

[172] S. B. Aziz, T. J. Woo, M. F. Z. Kadir, and H. M. Ahmed, "A conceptual review on polymer electrolytes and ion transport models," *Journal of Science: Advanced Materials and Devices,* vol. 3, no. 1, pp. 1-17, 2018/03/01/ 2018, doi: https://doi.org/10.1016/j.jsamd.2018.01.002.

[173] R. Buchner, "What can be learnt from dielectric relaxation spectroscopy about ion solvation and association?," *Pure and Applied Chemistry,* vol. 80, no. 6, pp. 1239-1252, 2008, doi: doi:10.1351/pac200880061239.

[174] R. J. Klein, S. Zhang, S. Dou, B. H. Jones, R. H. Colby, and J. Runt, "Modeling electrode polarization in dielectric spectroscopy: Ion mobility and mobile ion concentration of single-ion polymer electrolytes," *The Journal of Chemical Physics,* vol. 124, no. 14, p. 144903, 2006/04/14 2006, doi: 10.1063/1.2186638.

[175] H. Ericson, A. Brodin, B. Mattsson, L. Torell, H. Rinne, and F. Sundholm, "A Raman spectroscopic investigation of methoxyl end capped PPO doped with NaCF3SO3," *Electrochimica acta,* vol. 43, no. 10-11, pp. 1401-1405, 1998.

[176] A. Bernson, J. Lindgren, W. Huang, and R. Frech, "Coordination and conformation in PEO, PEGM and PEG systems containing lithium or lanthanum triflate," *Polymer,* vol. 36, no. 23, pp. 4471-4478, 1995/01/01/ 1995, doi: https://doi.org/10.1016/0032-3861(95)96855-3.

[177] H. T. Ahmed and O. G. Abdullah, "Structural and ionic conductivity characterization of PEO:MC-NH4I proton-conducting polymer blend electrolytes based films," *Results in Physics,* vol. 16, p. 102861, 2020/03/01/ 2020, doi: https://doi.org/10.1016/j.rinp.2019.102861.

[178] M. Unge, H. Gudla, C. Zhang, and D. Brandell, "Electronic conductivity of polymer electrolytes: electronic charge transport properties of LiTFSI-doped PEO," *Physical Chemistry Chemical Physics,* 10.1039/D0CP01130D vol. 22, no. 15, pp. 7680-7684, 2020, doi: 10.1039/D0CP01130D.

[179] T. P. L. a. T. C. B. McLeish, "Self-Concentrations and Effective Glass Transition Temperatures in Polymer Blends," 2000.

[180] E. Vijayakumar, A. Subramania, Z. Fei, and P. J. Dyson, "High-performance dye-sensitized solar cell based on an electrospun poly(vinylidene fluoride-co-hexafluoropropylene)/cobalt sulfide nanocomposite membrane electrolyte," *RSC Advances,* 10.1039/C5RA04944J vol. 5, no. 64, pp. 52026-52032, 2015, doi: 10.1039/C5RA04944J.

[181] P. Yao *et al.*, "Review on Polymer-Based Composite Electrolytes for Lithium Batteries," *Frontiers in Chemistry,* Review vol. 7, 2019. [Online]. Available: https://www.frontiersin.org/article/10.3389/fchem.2019.00522.

[182] L. A. Utracki and T. Sedlacek, "Free volume dependence of polymer viscosity," *Rheologica Acta,* vol. 46, no. 4, pp. 479-494, 2007/03/01 2007, doi: 10.1007/s00397-006-0133-z.

[183] R. P. White and J. E. G. Lipson, "Polymer Free Volume and Its Connection to the Glass Transition," *Macromolecules,* vol. 49, no. 11, pp. 3987-4007, 2016/06/14 2016, doi: 10.1021/acs.macromol.6b00215.

[184] V. Gregorio, N. García, and P. Tiemblo, "Ionic Conductivity Enhancement in UHMW PEO Gel Electrolytes Based on Room-Temperature Ionic Liquids and Deep Eutectic Solvents," *ACS Applied Polymer Materials,* vol. 4, no. 4, pp. 2860-2870, 2022/04/08 2022, doi: 10.1021/acsapm.2c00104.

[185] S. Gupta, P. K. Singh, and B. Bhattacharya, "Low-viscosity ionic liquid–doped solid polymer electrolytes: Electrical, dielectric, and ion transport studies," *High Performance Polymers,* vol. 30, no. 8, pp. 986-992, 2018/10/01 2018, doi: 10.1177/0954008318778763.

[186] D. Rosenbach, N. Mödl, M. Hahn, J. Petry, M. A. Danzer, and M. Thelakkat, "Synthesis and Comparative Studies of Solvent-Free Brush Polymer Electrolytes for Lithium Batteries," *ACS Applied Energy Materials,* vol. 2, no. 5, pp. 3373-3388, 2019/05/28 2019, doi: 10.1021/acsaem.9b00211.

[187] A. Khalyavina, L. Häußler, and A. Lederer, "Effect of the degree of branching on the glass transition temperature of polyesters," *Polymer,* vol. 53, no. 5, pp. 1049-1053, 2012/02/28/ 2012, doi: https://doi.org/10.1016/j.polymer.2012.01.020.

[188] K. L. Wooley, C. J. Hawker, J. M. Pochan, and J. M. J. Frechet, "Physical properties of dendritic macromolecules: a study of glass transition temperature," *Macromolecules,* vol. 26, no. 7, pp. 1514-1519, 1993/03/01 1993, doi: 10.1021/ma00059a006.

[189] M. Jayakannan and S. Ramakrishnan, "Synthesis and thermal analysis of branched and “kinked” poly(ethylene terephthalate)," *Journal of Polymer Science Part A: Polymer*

Chemistry, https://doi.org/10.1002/(SICI)1099-0518(19980130)36:2<309::AID-POLA14>3.0.CO;2-S vol. 36, no. 2, pp. 309-317, 1998/01/30 1998, doi: https://doi.org/10.1002/(SICI)1099-0518(19980130)36:2<309::AID-POLA14>3.0.CO;2-S.

[190] M. C. Righetti and A. Munari, "Influence of branching on melting behavior and isothermal crystallization of poly(butylene terephthalate)," *Macromolecular Chemistry and Physics,* https://doi.org/10.1002/macp.1997.021980212 vol. 198, no. 2, pp. 363-378, 1997/02/01 1997, doi: https://doi.org/10.1002/macp.1997.021980212.

[191] E. Q. Chen *et al.*, "Isothermal thickening and thinning processes in low molecular weight poly(ethylene oxide) fractions crystallized from the melt: 6. Configurational defects in molecules," *Polymer,* vol. 40, no. 16, pp. 4543-4551, 1999/07/01/ 1999, doi: https://doi.org/10.1016/S0032-3861(99)00069-5.

[192] T. A. Saleh, "Chapter 3 - Polymer science and polymerization methods toward hybrid materials," in *Polymer Hybrid Materials and Nanocomposites*, T. A. Saleh Ed.: William Andrew Publishing, 2021, pp. 59-103.

[193] S. J. Grabowski, "Hydrogen Bond and Other Lewis Acid–Lewis Base Interactions as Preliminary Stages of Chemical Reactions," *Molecules*, vol. 25, no. 20*,* doi: 10.3390/molecules25204668.

[194] L. Qiao *et al.*, "Anion π–π Stacking for Improved Lithium Transport in Polymer Electrolytes," *Journal of the American Chemical Society,* vol. 144, no. 22, pp. 9806-9816, 2022/06/08 2022, doi: 10.1021/jacs.2c02260.

[195] C. Lorthioir, F. o. Lauprêtre, J. Soulestin, and J. M. Lefebvre, "Segmental Dynamics of Poly(ethylene oxide) Chains in a Model Polymer/Clay Intercalated Phase: Solid-State NMR Investigation," (in English), *Macromolecules,* vol. 42, no. 1, pp. 218-230, 2009 2009, doi: 10.1021/ma801909s.

[196] R. Dockhorn *et al.*, "Polyolefins Formed by Chain Walking Catalysis-A Matter of Branching Density Only?," (in English), *Journal of the American Chemical Society,* vol. 141, no. 39, pp. 15586-15596, Oct 2 2019, doi: 10.1021/jacs.9b06785.

[197] A. L. Agapov and A. P. Sokolov, "Decoupling Ionic Conductivity from Structural Relaxation: A Way to Solid Polymer Electrolytes?," *Macromolecules,* vol. 44, no. 11, pp. 4410-4414, 2011/06/14 2011, doi: 10.1021/ma2001096.

[198] D. Golodnitsky, E. Strauss, E. Peled, and S. Greenbaum, "Review—On Order and Disorder in Polymer Electrolytes," *Journal of The Electrochemical Society,* vol. 162, no. 14, p. A2551, 2015/10/09 2015, doi: 10.1149/2.0161514jes.

[199] K. J. Johnson, E. Glynos, G. Sakellariou, and P. Green, "Dynamics of Star-Shaped Polystyrene Molecules: From Arm Retraction to Cooperativity," *Macromolecules,* vol. 49, no. 15, pp. 5669-5676, 2016/08/09 2016, doi: 10.1021/acs.macromol.6b00456.

[200] L. Fetters, D. Lohse, D. Richter, T. Witten, and A. Zirkel, "Connection between polymer molecular weight, density, chain dimensions, and melt viscoelastic properties," *Macromolecules,* vol. 27, no. 17, pp. 4639-4647, 1994.

[201] D. Ding, Y. Maeyoshi, M. Kubota, J. Wakasugi, K. Kanamura, and H. Abe, "Non-flammable super-concentrated polymer electrolyte with “solvated ionic liquid” for lithium-ion batteries," *Journal of Power Sources,* vol. 506, p. 230099, 2021/09/15/ 2021, doi: https://doi.org/10.1016/j.jpowsour.2021.230099.

[202] S. J. Wen, T. J. Richardson, D. I. Ghantous, K. A. Striebel, P. N. Ross, and E. J. Cairns, "FTIR characterization of PEO + LiN(CF3SO2)2 electrolytes," *Journal of Electroanalytical Chemistry,* vol. 408, no. 1, pp. 113-118, 1996/05/30/ 1996, doi: https://doi.org/10.1016/0022-0728(96)04536-6.

[203] K. Chrissopoulou *et al.*, "Crystallinity and Chain Conformation in PEO/Layered Silicate Nanocomposites," *Macromolecules,* vol. 44, no. 24, pp. 9710-9722, 2011/12/27 2011, doi: 10.1021/ma201711r.

[204] A. R. Polu and P. K. Singh, "Improved ion dissociation and amorphous region of PEO based solid polymer electrolyte by incorporating tetracyanoethylene," *Materials Today: Proceedings,* vol. 49, pp. 3093-3097, 2022/01/01/ 2022, doi: https://doi.org/10.1016/j.matpr.2020.10.950.

[205] L. Liu *et al.*, "Comprehensively-upgraded polymer electrolytes by multifunctional aramid nanofibers for stable all-solid-state Li-ion batteries," *Nano Energy,* vol. 69, p. 104398, 2020/03/01/ 2020, doi: https://doi.org/10.1016/j.nanoen.2019.104398.

[206] P. Chen *et al.*, "A ketone-containing all-solid-state polymer electrolyte with rapid Li-ion conduction for lithium metal batteries," *Chemical Engineering Journal,* vol. 427, p. 132025, 2022/01/01/ 2022, doi: https://doi.org/10.1016/j.cej.2021.132025.

[207] I. Rey, J. C. Lassègues, J. Grondin, and L. Servant, "Infrared and Raman study of the PEO-LiTFSI polymer electrolyte," *Electrochimica Acta,* vol. 43, no. 10, pp. 1505-1510, 1998/04/30/ 1998, doi: https://doi.org/10.1016/S0013-4686(97)10092-5.

[208] A. Bakker, S. Gejji, J. Lindgren, K. Hermansson, and M. M. Probst, "Contact ion pair formation and ether oxygen coordination in the polymer electrolytes M[N(CF3SO2)2]2PEOn for M = Mg, Ca, Sr and Ba," *Polymer,* vol. 36, no. 23, pp. 4371-4378, 1995/01/01/ 1995, doi: https://doi.org/10.1016/0032-3861(95)96841-U.

[209] T. Ikeda, "Poly(ionic liquid)s with branched side chains: polymer design for breaking the conventional record of ionic conductivity," *Polymer Chemistry,* 10.1039/D0PY01333A vol. 12, no. 5, pp. 711-718, 2021, doi: 10.1039/D0PY01333A.

[210] B. A. Abdulkadir *et al.*, "Optimization of the Electrochemical Performance of a Composite Polymer Electrolyte Based on PVA-K2CO3-SiO2 Composite," *Polymers*, vol. 13, no. 1*,* doi: 10.3390/polym13010092.

[211] M. Misheva, N. Djourelov, and E. T. Nedkov, "Gamma irradiation effect upon positron annihilation in ultra high molecular weight poly(ethylene oxide)," *Radiation Physics and*

Chemistry, vol. 62, no. 5, pp. 379-385, 2001/12/01/ 2001, doi: https://doi.org/10.1016/S0969-806X(01)00208-0.

[212] C. Wästlund and F. H. J. Maurer, "Positron Lifetime Distributions and Free Volume Parameters of PEO/PMMA Blends Determined with the Maximum Entropy Method," *Macromolecules,* vol. 30, no. 19, pp. 5870-5876, 1997/09/01 1997, doi: 10.1021/ma961604j.

[213] Y. Shibuya, R. Tatara, Y. Jiang, Y. Shao-Horn, and J. A. Johnson, "Brush-First ROMP of poly(ethylene oxide) macromonomers of varied length: impact of polymer architecture on thermal behavior and Li+ conductivity," *Journal of Polymer Science Part A: Polymer Chemistry,* https://doi.org/10.1002/pola.29242 vol. 57, no. 3, pp. 448-455, 2019/02/01 2019, doi: https://doi.org/10.1002/pola.29242.

[214] M. Iturrondobeitia, O. Akizu-Gardoki, O. Amondarain, R. Minguez, and E. Lizundia, "Environmental Impacts of Aqueous Zinc Ion Batteries Based on Life Cycle Assessment," *Advanced Sustainable Systems,* https://doi.org/10.1002/adsu.202100308 vol. 6, no. 1, p. 2100308, 2022/01/01 2022, doi: https://doi.org/10.1002/adsu.202100308.

[215] J. B. Goodenough and K.-S. Park, "The Li-Ion Rechargeable Battery: A Perspective," *Journal of the American Chemical Society,* vol. 135, no. 4, pp. 1167-1176, 2013/01/30 2013, doi: https://doi.org/10.1021/ja3091438.

[216] J. Feng, L. Wang, Y. Chen, P. Wang, H. Zhang, and X. He, "PEO based polymer-ceramic hybrid solid electrolytes: a review," *Nano Converg,* vol. 8, no. 1, p. 2, Jan 10 2021, doi: https://doi.org/10.1186/s40580-020-00252-5.

[217] S. Darvishi *et al.*, "Nonlinear Architectures Can Alter the Dynamics of Polymer–Nanoparticle Composites," *Macromolecules,* vol. 54, no. 21, pp. 10118-10125, 2021/11/09 2021, doi: https://doi.org/10.1021/acs.macromol.1c01382.

[218] I. Neamţu, A. P. Chiriac, L. E. Nita, G. Ghica, and V. Alley, "Characterization of poly(acrylamide) as temperature- sensitive hydrogel," *Journal of Optoelectronics and Advanced Materials,* vol. 8, pp. 1939-1943, 2006.

[219] Y. Park *et al.*, "Crosslinking effect on thermal conductivity of electrospun poly (acrylic acid) nanofibers," *Polymers,* vol. 11, no. 5, p. 858, 2019, doi: https://doi.org/10.3390/polym11050858.

[220] T. F. Freire *et al.*, "Thermal, mechanical and chemical analysis of poly (vinyl alcohol) multifilament and braided yarns," *Polymers,* vol. 13, no. 21, p. 3644, 2021, doi: https://doi.org/10.3390/polym13213644.

[221] P. S. Bass, L. Zhang, M. Tu, and Z. Cheng, "Enhancement of Biodegradable Poly(Ethylene Oxide) Ionic–Polymer Metallic Composite Actuators with Nanocrystalline Cellulose Fillers," *Actuators,* vol. 7, no. 4, p. 72, 2018, doi: https://doi.org/10.3390/act7040072.

[222] G. Gordon Cameron, M. D. Ingram, M. Younus Qureshi, H. M. Gearing, L. Costa, and G. Camino, "The thermal degradation of poly(ethylene oxide) and its complex with NaCNS," *European Polymer Journal,* vol. 25, no. 7, pp. 779-784, 1989/01/01/ 1989, doi: https://doi.org/10.1016/0014-3057(89)90044-X.

[223] H. Yang, S. Xu, L. Jiang, and Y. Dan, "Thermal decomposition behavior of poly (vinyl alcohol) with different hydroxyl content," *Journal of Macromolecular Science, Part B,* vol. 51, no. 3, pp. 464-480, 2012, doi: https://doi.org/10.1080/00222348.2011.597687.

[224] K. E. Strawhecker and E. Manias, "Structure and Properties of Poly(vinyl alcohol)/Na+ Montmorillonite Nanocomposites," *Chemistry of Materials,* vol. 12, no. 10, pp. 2943-2949, 2000/10/01 2000, doi: 10.1021/cm000506g.

[225] E.-Q. Chen *et al.*, "Isothermal Thickening and Thinning Processes in Low-Molecular-Weight Poly(ethylene oxide) Fractions Crystallized from the Melt. 8. Molecular Shape Dependence," *Macromolecules,* vol. 32, no. 15, pp. 4784-4793, 1999/07/27 1999, doi: https://doi.org/10.1021/ma9900176.

[226] D.-p. Wang, M.-q. Yang, Z.-x. Dong, S.-q. Bo, and X.-l. Ji, "Interaction between poly (ethylene oxide) and silica nanoparticles in dilute solutions," *Chinese Journal of Polymer Science,* vol. 31, no. 9, pp. 1290-1298, 2013/09/01 2013, doi: https://doi.org/10.1007/s10118-013-1321-9.

[227] C.-W. Nan, L. Fan, Y. Lin, and Q. Cai, "Enhanced Ionic Conductivity of Polymer Electrolytes Containing Nanocomposite SiO2 Particles," *Physical Review Letters,* vol. 91, no. 26, p. 266104, 12/31/ 2003, doi: https://doi.org/10.1103/PhysRevLett.91.266104.

[228] M. Soccio, N. Lotti, L. Finelli, M. Gazzano, and A. Munari, "Aliphatic poly(propylene dicarboxylate)s: Effect of chain length on thermal properties and crystallization kinetics," *Polymer,* vol. 48, no. 11, pp. 3125-3136, 2007/05/21/ 2007, doi: https://doi.org/10.1016/j.polymer.2007.04.007.

[229] G. P. Baeza *et al.*, "Network dynamics in nanofilled polymers," *Nature communications,* vol. 7, no. 1, pp. 1-6, 2016, doi: https://doi.org/10.1038/ncomms11368.

[230] Q. Chen, S. Gong, J. Moll, D. Zhao, S. K. Kumar, and R. H. Colby, "Mechanical reinforcement of polymer nanocomposites from percolation of a nanoparticle network," *ACS Macro Letters,* vol. 4, no. 4, pp. 398-402, 2015, doi: https://doi.org/10.1021/acsmacrolett.5b00002.

[231] A. Mayer, D. Steinle, S. Passerini, and D. Bresser, "Block copolymers as (single-ion conducting) lithium battery electrolytes," *Nanotechnology,* vol. 33, no. 6, p. 062002, 2021/11/15 2021, doi: 10.1088/1361-6528/ac2e21.

[232] W. Xiao, L. Xu, P. Liu, Y. Chen, J. Zhang, and J. Xu, "Hybrid Copolymerization of Ethylene Oxide and tert-Butyl Methacrylate with Organocatalyst," *Polymers,* vol. 13, no. 15, 2021, doi: 10.3390/polym13152546.

[233] S. Li, M. Tian, J. Wang, F. Du, L. Li, and Z. Xue, "Poly (Ethylene Oxide)-Based Block Copolymer Electrolytes Formed via Ligand-Free Iron-Mediated Atom Transfer Radical Polymerization," *Polymers,* vol. 12, no. 4, 2020, doi: 10.3390/polym12040763.

[234] X. Sun, H. Zhang, L. Zhang, X. Wang, and Q.-F. Zhou, "Synthesis of Amphiphilic Poly(ethylene oxide)-b-Poly(methyl methacrylate) Diblock Copolymers via Atom Transfer Radical Polymerization Utilizing Halide Exchange Technique," *Polymer Journal,* vol. 37, no. 2, pp. 102-108, 2005/02/01 2005, doi: 10.1295/polymj.37.102.

[235] X. G. Qiao, M. Lansalot, E. Bourgeat-Lami, and B. Charleux, "Nitroxide-Mediated Polymerization-Induced Self-Assembly of Poly(poly(ethylene oxide) methyl ether methacrylate-co-styrene)-b-poly(n-butyl methacrylate-co-styrene) Amphiphilic Block Copolymers," *Macromolecules,* vol. 46, no. 11, pp. 4285-4295, 2013/06/11 2013, doi: 10.1021/ma4003159.

[236] R. Yuan, A. A. Teran, I. Gurevitch, S. A. Mullin, N. S. Wanakule, and N. P. Balsara, "Ionic Conductivity of Low Molecular Weight Block Copolymer Electrolytes," *Macromolecules,* vol. 46, no. 3, pp. 914-921, 2013/02/12 2013, doi: 10.1021/ma3024552.

[237] W. Li, K. Min, K. Matyjaszewski, F. Stoffelbach, and B. Charleux, "PEO-Based Block Copolymers and Homopolymers as Reactive Surfactants for AGET ATRP of Butyl Acrylate in Miniemulsion," *Macromolecules,* vol. 41, no. 17, pp. 6387-6392, 2008/09/09 2008, doi: 10.1021/ma800892e.

[238] R. Bouchet *et al.*, "Charge Transport in Nanostructured PS–PEO–PS Triblock Copolymer Electrolytes," *Macromolecules,* vol. 47, no. 8, pp. 2659-2665, 2014/04/22 2014, doi: 10.1021/ma500420w.

[239] J. K. Oh, H. Dong, R. Zhang, K. Matyjaszewski, and H. Schlaad, "Preparation of nanoparticles of double-hydrophilic PEO-PHEMA block copolymers by AGET ATRP in inverse miniemulsion," *Journal of Polymer Science Part A: Polymer Chemistry,* https://doi.org/10.1002/pola.22230 vol. 45, no. 21, pp. 4764-4772, 2007/11/01 2007, doi: https://doi.org/10.1002/pola.22230.

[240] D. Jeong, J. Shim, H. Shin, and J.-C. Lee, "Sustainable Lignin-Derived Cross-Linked Graft Polymers as Electrolyte and Binder Materials for Lithium Metal Batteries,"

ChemSusChem, https://doi.org/10.1002/cssc.201903466 vol. 13, no. 10, pp. 2642-2649, 2020/05/22 2020, doi: https://doi.org/10.1002/cssc.201903466.

[241] A. Ghosh, C. Wang, and P. Kofinas, "Block Copolymer Solid Battery Electrolyte with High Li-Ion Transference Number," *Journal of The Electrochemical Society,* vol. 157, no. 7, p. A846, 2010, doi: 10.1149/1.3428710.

[242] A. J. Butzelaar *et al.*, "Styrene-Based Poly(ethylene oxide) Side-Chain Block Copolymers as Solid Polymer Electrolytes for High-Voltage Lithium-Metal Batteries," *ACS Applied Materials & Interfaces,* vol. 13, no. 33, pp. 39257-39270, 2021/08/25 2021, doi: 10.1021/acsami.1c08841.

[243] Y. Chen *et al.*, "Hyperbranched PEO-Based Hyperstar Solid Polymer Electrolytes with Simultaneous Improvement of Ion Transport and Mechanical Strength," *ACS Applied Energy Materials,* vol. 2, no. 3, pp. 1608-1615, 2019/03/25 2019, doi: 10.1021/acsaem.8b02188.

[244] S.-M. Hao *et al.*, "Lithium-Conducting Branched Polymers: New Paradigm of Solid-State Electrolytes for Batteries," *Nano Letters,* vol. 21, no. 18, pp. 7435-7447, 2021/09/22 2021, doi: 10.1021/acs.nanolett.1c02558.

[245] H. Xu and M. K. Mahanthappa, "Ionic Conductivities of Broad Dispersity Lithium Salt-Doped Polystyrene/Poly(ethylene oxide) Triblock Polymers," *Macromolecules,* vol. 54, no. 18, pp. 8798-8809, 2021/09/28 2021, doi: 10.1021/acs.macromol.1c01100.

[246] S. Q. Li *et al.*, "Molecular Brush with Dense PEG Side Chains: Design of a Well-Defined Polymer Electrolyte for Lithium-Ion Batteries," (in English), *Macromolecules,* vol. 52, no. 19, pp. 7234-7243, Oct 8 2019, doi: 10.1021/acs.macromol.9b01641.

[247] S. Li *et al.*, "Molecular Brush with Dense PEG Side Chains: Design of a Well-Defined Polymer Electrolyte for Lithium-Ion Batteries," *Macromolecules,* vol. 52, no. 19, pp. 7234-7243, 2019/10/08 2019, doi: 10.1021/acs.macromol.9b01641.

[248] S. A. Chopade, J. G. Au, Z. Li, P. W. Schmidt, M. A. Hillmyer, and T. P. Lodge, "Robust Polymer Electrolyte Membranes with High Ambient-Temperature Lithium-Ion Conductivity via Polymerization-Induced Microphase Separation," *ACS Applied Materials & Interfaces,* vol. 9, no. 17, pp. 14561-14565, 2017/05/03 2017, doi: 10.1021/acsami.7b02514.

[249] L. Chen, D. T. Hallinan, Y. A. Elabd, and M. A. Hillmyer, "Highly Selective Polymer Electrolyte Membranes from Reactive Block Polymers," *Macromolecules,* vol. 42, no. 16, pp. 6075-6085, 2009/08/25 2009, doi: 10.1021/ma901272s.

[250] I. Gitsov, A. Simonyan, and N. G. Vladimirov, "Synthesis of novel asymmetric dendritic-linear-dendritic block copolymers via “living” anionic polymerization of ethylene oxide initiated by dendritic macroinitiators," *Journal of Polymer Science Part A: Polymer Chemistry,* https://doi.org/10.1002/pola.22258 vol. 45, no. 22, pp. 5136-5148, 2007/11/15 2007, doi: https://doi.org/10.1002/pola.22258.

[251] X. He, L. Liang, M. Xie, Y. Zhang, S. Lin, and D. Yan, "Synthesis of Novel Linear PEO-b-PS-b-PCL Triblock Copolymers by the Combination of ATRP, ROP, and a Click Reaction," *Macromolecular Chemistry and Physics,* https://doi.org/10.1002/macp.200700153 vol. 208, no. 16, pp. 1797-1802, 2007/08/20 2007, doi: https://doi.org/10.1002/macp.200700153.

[252] A. Ghosh and P. Kofinas, "PEO based Block Copolymer as Solid State Lithium Battery Electrolyte," *ECS Transactions,* vol. 11, no. 29, pp. 131-137, 2008/05/16 2008, doi: 10.1149/1.2938916.

[253] S. Chaudhury, J. Gaalken, J. Meyer, and M. Ulbricht, "Calorimetric studies of PEO-b-PMMA and PEO-b-PiPMA diblock copolymers synthesized via atom transfer radical polymerization," *Polymer,* vol. 139, pp. 11-19, 2018/03/14/ 2018, doi: https://doi.org/10.1016/j.polymer.2018.01.082.

[254] M. T. Irwin, R. J. Hickey, S. Xie, S. So, F. S. Bates, and T. P. Lodge, "Structure–Conductivity Relationships in Ordered and Disordered Salt-Doped Diblock Copolymer/Homopolymer Blends," *Macromolecules,* vol. 49, no. 18, pp. 6928-6939, 2016/09/27 2016, doi: 10.1021/acs.macromol.6b01553.

[255] W. Zhang and X. M. Zhang, "Study on surface structure and properties of PMMA/PEG copolymer coatings," *Materials Research Innovations,* vol. 18, no. sup2, pp. S2-1028-S2-1033, 2014/05/01 2014, doi: 10.1179/1432891714Z.000000000474.

[256] G. Gorrasi, M. Stanzione, and L. Izzo, "Synthesis and characterization of novel star-like PEO–PMMA based copolymers," *Reactive and Functional Polymers,* vol. 71, no. 1, pp. 23-29, 2011/01/01/ 2011, doi: https://doi.org/10.1016/j.reactfunctpolym.2010.11.007.

[257] P. Chmielarz, A. Sobkowiak, and K. Matyjaszewski, "A simplified electrochemically mediated ATRP synthesis of PEO-b-PMMA copolymers," *Polymer,* vol. 77, pp. 266-271, 2015/10/23/ 2015, doi: https://doi.org/10.1016/j.polymer.2015.09.038.

[258] A. Wang *et al.*, "Electrochemical performances of a new solid composite polymer electrolyte based on hyperbranched star polymer and ionic liquid for lithium-ion batteries," *Journal of Solid State Electrochemistry,* vol. 21, no. 8, pp. 2355-2364, 2017/08/01 2017, doi: 10.1007/s10008-017-3582-7.

[259] A. Wang *et al.*, "A New All-Solid-State Hyperbranched Star Polymer Electrolyte for Lithium Ion Batteries: Synthesis and Electrochemical Properties," *Electrochimica Acta,* vol. 212, pp. 372-379, 2016/09/10/ 2016, doi: https://doi.org/10.1016/j.electacta.2016.07.003.

[260] E. Yilmaz, O. Yilmaz, and H. Caner, "Miscibility studies on polystyrene/poly(ethylene oxide) and polybutadiene-graft-polystyrene/poly(ethylene oxide) blends by dilute solution viscometry," *European Polymer Journal,* vol. 32, no. 8, pp. 927-933, 1996/08/01/ 1996, doi: https://doi.org/10.1016/0014-3057(96)00037-7.

[261] G. Hooftman, S. Herman, and E. Schacht, "Review: Poly(Ethylene Glycol)s with Reactive Endgroups. II. Practical Consideration for the Preparation of Protein-PEG Conjugates," *Journal of Bioactive and Compatible Polymers,* vol. 11, no. 2, pp. 135-159, 1996/04/01 1996, doi: 10.1177/088391159601100205.

[262] N. Sarier, R. Arat, Y. Menceloglu, E. Onder, E. C. Boz, and O. Oguz, "Production of PEG grafted PAN copolymers and their electrospun nanowebs as novel thermal energy storage materials," *Thermochimica Acta,* vol. 643, pp. 83-93, 2016/11/10/ 2016, doi: https://doi.org/10.1016/j.tca.2016.10.002.

[263] A. Asatekin, S. Kang, M. Elimelech, and A. M. Mayes, "Anti-fouling ultrafiltration membranes containing polyacrylonitrile-graft-poly(ethylene oxide) comb copolymer additives," *Journal of Membrane Science,* vol. 298, no. 1, pp. 136-146, 2007/07/20/ 2007, doi: https://doi.org/10.1016/j.memsci.2007.04.011.

[264] M. R. Ravindar, Subrahmanyama, A. R., Maheshwar, M. R., Kumarc, J. S., Kamalakerd, M., and Jaipal, M. R., "<X-RD, SEM, FT-IR, DSC Studies of Polymer Blend Films of PMMA and PEO.pdf>," 2016.

[265] Z. Osman, N. M. Ansor, K. W. Chew, and N. Kamarulzaman, "Infrared and conductivity studies on blends of PMMA/PEO based polymer electrolytes," *Ionics,* vol. 11, no. 5-6, pp. 431-435, 2005, doi: 10.1007/bf02430261.

[266] C. Alkan, E. Günther, S. Hiebler, Ö. F. Ensari, and D. Kahraman, "Polyurethanes as solid–solid phase change materials for thermal energy storage," *Solar Energy,* vol. 86, no. 6, pp. 1761-1769, 2012/06/01/ 2012, doi: https://doi.org/10.1016/j.solener.2012.03.012.

[267] M. R. Reddy, M. J. Reddy, and A. R. Subrahmanyam, "Structural, Thermal and Optical Properties of PMMA, PEO and PMMA/PEO/LiClO4 Polymer Electrolyte Blends," *Material Science Research India,* vol. 14, no. 2, pp. 123-127, 2017, doi: 10.13005/msri/140206.

[268] E. Aram, M. Ehsani, H. A. Khonakdar, S. H. Jafari, and N. R. Nouri, "Functionalization of graphene nanosheets and its dispersion in PMMA/PEO blend: Thermal, electrical,

morphological and rheological analyses," *Fibers and Polymers,* vol. 17, no. 2, pp. 174-180, 2016/02/01 2016, doi: 10.1007/s12221-016-5827-y.

[269] D. Imad Ud *et al.*, "Self-assembly and thermal behavior of amphiphilic di-block copolymers of poly(methyl methacrylate)-block-poly(ethylene oxide) (PMMA-b-PEO)," *Polymer Bulletin,* 2022/03/05 2022, doi: 10.1007/s00289-022-04148-8.

[270] T. Hirata, T. Kashiwagi, and J. E. Brown, "Thermal and oxidative degradation of poly(methyl methacrylate): weight loss," *Macromolecules,* vol. 18, no. 7, pp. 1410-1418, 1985/07/01 1985, doi: 10.1021/ma00149a010.

[271] A.-l. Zhang, F.-y. Cao, G.-z. Na, S. Wang, S.-x. Li, and J.-c. Liu, "A novel PEO-based blends solid polymer electrolytes doping liquid crystalline ionomers," *Ionics,* vol. 22, no. 11, pp. 2103-2112, 2016/11/01 2016, doi: 10.1007/s11581-016-1732-z.

[272] G. P. Baeza *et al.*, "Network dynamics in nanofilled polymers," *Nature Communications,* vol. 7, no. 1, p. 11368, 2016/04/25 2016, doi: 10.1038/ncomms11368.

[273] M. Huskić, E. Žagar, and M. Žigon, "The influence of a quaternary ammonium salt and MMT on the in situ intercalative polymerization of PMMA," *European Polymer Journal,* vol. 48, no. 9, pp. 1555-1560, 2012/09/01/ 2012, doi: https://doi.org/10.1016/j.eurpolymj.2012.06.010.

[274] Y. Hsu, M. Chuang, T. Hirano, and K. Ute, "Multivariate analysis of 13C NMR spectra to extract information about monomer sequences in poly(methyl methacrylate-co-benzyl methacrylate)s prepared by various polymer reactions," *Polymer Journal,* vol. 50, no. 5, pp. 355-363, 2018/05/01 2018, doi: 10.1038/s41428-018-0027-9.

[275] H. Momose, T. Maeda, K. Hattori, T. Hirano, and K. Ute, "Statistical determination of chemical composition and monomer sequence distribution of poly(methyl methacrylate-co-tert-butyl methacrylate)s by multivariate analysis of 13C NMR spectra," *Polymer Journal,* vol. 44, no. 8, pp. 808-814, 2012/08/01 2012, doi: 10.1038/pj.2012.110.